NATIONAL RESEARCH CENTRE
"KURCHATOV INSTITUTE"
PETERSBURG NUCLEAR PHYSICS INSTITUTE

PNPI Scientific Highlights

2014

Gatchina • 2015

Scientific editors:
Victor L. Aksenov
Svetlana V. Sarantseva

Editors:
Vladimir V. Voronin
Victor T. Kim
Andrey L. Konevega
Geliy F. Mikheev
Victor Yu. Petrov
Victor V. Sarantsev
Sergey R. Friedmann
Gleb V. Frolov
Yury P. Chernenkov

Redactors:
Alena M. Arkhipova
Elena Yu. Orobets
Maria A. Kamenskaya
Tatiana S. Zharova (translation)

Technical editing and design:
Tatiana A. Parfeeva

Layout composition:
Kristina D. Kashkovskaya
Anastasiya B. Kudryavtseva

Publisher:
Petersburg Nuclear Physics Institute
NRC "Kurchatov Institute"
Publishing Office

Orlova Roscha,
Gatchina, Leningrad District,
Russian Federation

PNPI Scientific Highlights 2014 (164 pages) contains a number of short overview reports of the main research results of PNPI NRC "Kurchatov Institute" achieved in 2014. The links for the leading Russian and foreign scientific journals containing the full versions of each paper are listed below each article.

Printed on Konica Minolta bizhub PRO C1060L

ISBN 978-5-86763-366-0

Copyright © 2015 PNPI NRC "Kurchatov Institute"

Table of contents

Preface

B.P. Konstantinov Petersburg Nuclear Physics Institute of National Research Centre "Kurchatov Institute" (PNPI) is a multidisciplinary research centre. It leads fundamental and applied research in fields of particle and high energy physics, nuclear physics, condensed matter physics, molecular and radiation biophysics.

Scientific works of PNPI researchers have been awarded with Lenin and State Prizes, National Awards of the Russian Federation Government, Academic Prizes. Since the establishment of the Institute, three PNPI employees were elected as full members and seven as corresponding members of the Russian Academy of Sciences. PNPI currently employs 1 912 employees, including 511 researchers, 76 full Doctors of Science and 263 first degree Doctors of Science (Candidates of Science). At the moment, one of its employees is a full member and two are corresponding members of the Russian Academy of Sciences.

In 2010, upon the initiative of Mikhail V. Kovalchuk, PNPI joined actions with several research institutions participating in the pilot project on creation of the National Research Centre "Kurchatov Institute" (Joint Research Programme). In September 2011, control over PNPI transited from the Russian Academy of Sciences to National Research Centre "Kurchatov Institute".

In the framework of the Joint Research Programme, PNPI carries out research in the following areas:

– Fundamental and applied research carried out with the use of neutrons (this area of research is coordinated by PNPI);
– Theoretical and mathematical physics;
– Fundamental interdisciplinary research in nano- and biosciences based on *X*-ray, synchrotron and neutron radiation;
– Fundamental and applied research carried out with the use of protons and ions; neutrino physics;
– Nuclear reactor and accelerator physics;
– Nuclear medicine (isotope production, beam therapy, nano- and biotechnologies for medical purposes).

There are five research divisions sharing a common infrastructure at PNPI:

– Theoretical Physics Division;
– Neutron Research Division;
– High Energy Physics Division;
– Molecular and Radiation Biophysics Division;
– Knowledge Transfer Division.

PNPI, as well as other NRC "Kurchatov Institute" institutes, takes an active part in various international projects and collaborates actively within its main research areas with largest international research centres:

– The European Organization for Nuclear Research (CERN, Switzerland);
– The European Centre for Neutron Science, The Institute Laue–Langevin (ILL, France);
– DESY Research Centre (Germany);
– Paul Scherrer Institute (PSI, Switzerland);
– Joint Institute for Nuclear Research (JINR, Russia)

and others.

PNPI possesses two main operating installations: WWR-M research reactor (first criticality reached in December 1959, power start-up in the end of 1961), and 1 GeV proton synchrocyclotron (power start-up in 1970).

Works on project development of a new reactor – the PIK reactor – have been launched in 1969. The construction started in 1976. After the Chernobyl nuclear accident, the reactor project was subject to a detailed revision and was to be modified with regard to the new safety standards until 1991. The construction was resumed but the funds were not allocated regularly, interruptions took place and the construction schedules were broken frequently. Nevertheless, thanks to the hard work of PNPI employees led by PNPI directors, academician Vladimir A. Nazarenko (1934–2006) from 1994 to 2006 and professor Vladimir M. Samsonov from 2006 to 2012, the PIK reactor complex had survived, but the prospects of the project completion were clouded.

The situation changed dramatically after the transition of control over PNPI from the Russian Academy of Sciences to National Research Centre "Kurchatov Institute". PNPI funding was stabilized through the provision of regular funds from the government of the Russian Federation allocated for the reactor facility construction and doubled by the programme of joined actions of institutions participating in the pilot project on creation of the National Research Centre "Kurchatov Institute". The construction of the second and the third PIK reactor start-up complexes was completed in December 2013. Works on adjustment, testing and accreditation of systems in accordance with atomic energy use standards will begin in 2015, as well as processing of a clearance for different stages of reactor power start-up and its launch into operation.

In November 2014, the RF State Expert Evaluation Department has approved two projects on modernization and reconstruction of engineering systems planned to be put into operation in 2014–2019. Within these projects, following actions are to be conducted: construction of a facility for isotope purification of heavy-water in the reflector, which is essential for the PIK reactor start-up; upgrading of constructed facilities, technological systems and engineering infrastructure of the PIK reactor complex in order to comply with increased safety requirements for nuclear installations; and preparation of the complex for exploitation. As a result, the power start-up of the reactor should take place in 2018 followed by it being put into operation with 12 operation experiential stations in 2019. Two stations will be transferred from the WWR-M reactor, seven stations were provided by Helmholtz Research Centre Geesthacht, Germany, in 2012 and now are in the stage of adjustment and adaptation. Three stations will be transferred from the European Centre for Neutron Science, Institut Laue–Langevin (ILL, Grenoble, France). The latter stations belong to PNPI NRC "Kurchatov Institute" and currently are being used to conduct experiments at the ILL reactor.

Furthermore, the project on equipping the PIK reactor complex with advanced research experimental stations started to be developed in 2014. 11 working groups consisting of NRC "Kurchatov Institute" employees and our colleagues from research centres of Russia and Europe were established in the framework of this project. More than 50 scientists took part in the conceptualization work. The topic of concept formation was discussed at 12 national and international workshops. In accordance with the general concept, working groups have provided conceptual and engineering recommendations

essential for the project work implementation, construction and creation of 20 experimental stations within the framework of investment project "Creation of the PIK reactor instrumentation".

The International Centre for Neutron Research (ICNR) is planned to be established on basis of the PIK reactor facility. Germany is PNPI strategic partner in establishment of ICNR. An agreement with Forschungszentrum Juelich, the research centre that coordinates the involvement of German research centres in ICNR establishment in Gatchina, was signed in 2014. The PIK reactor, as well as the ILL reactor and the ESS neutron spallation source being constructed at the moment in Sweden, is included as a research base in Strategic Plans for Development of Neutron Sciences in Europe. The PIK reactor research and instrumentation programmes are being built in cooperation with other neutron centres, first of all with JINR (Dubna), Forschungszentrum Jülich based on TU research reactor (München, Germany), ILL (Grenoble, France) and ESS (Lund, Sweden). We do expect participation of European physicists, from Germany and Hungary above all, in further concept development and subsequent project engineering and creation of experimental stations. In fact, the creation of PIK reactor experimental stations is the first step to ICNR establishment.

The International Advisory Committee on Photon and Neutron Research of NRC "Kurchatov Institute" will act as an international expert council, co-chaired by Professor H. Dosh (DESY, Germany), and the corresponding member of the Russian Academy of Sciences Mikhail V. Kovalchuk (NRC "Kurchatov Institute"). Professor S. Shmidt (FZ Jülich, Germany) was elected to be the Chairman of the Subcommittee on Neutron Sciences. The first meeting of the Subcommittee on Neutron Sciences is planned to be held in the beginning of March 2015.

Joint meeting of PNPI NRC "Kurchatov Institute" and "NIIEFA" JSC ("D.V. Efremov Institute of Electrophysical Apparatus" JSC) top management was held on December 23rd, 2014. The head of the PNPI Accelerator Department, Evgeny M. Ivanov, announced that 80 MeV Isochronous Cyclotron had reached the first criticality. Installation works were completed in November and physical testing was held in December. 80 MeV Cyclotron is being created in cooperation with "NIIEFA" JSC. The cyclotron project was planned for a long time already, but only the programme of joint actions of NRC "Kurchatov Institute" gave it a chance on implementation. It was actually launched only in 2011. A crucial phase of 80 MeV Cyclotron creation came to an end in 2014. 80 MeV Cyclotron is planned to become a base for an isotope facility for production of radionuclides and radiopharmaceuticals for medical purposes.

The most significant PNPI research findings of 2014 were summarized and presented in this volume. Each abstract contains not only a summary of research findings but also links to the articles of leading Russian and foreign scientific editions containing the full versions of the papers and describing the conducted work in detail. PNPI general description is presented in the conclusive part.

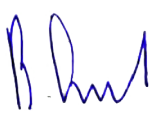

Director of PNPI NRC "Kurchatov Institute"
Corresponding member of the Russian Academy of Sciences
Victor L. Aksenov

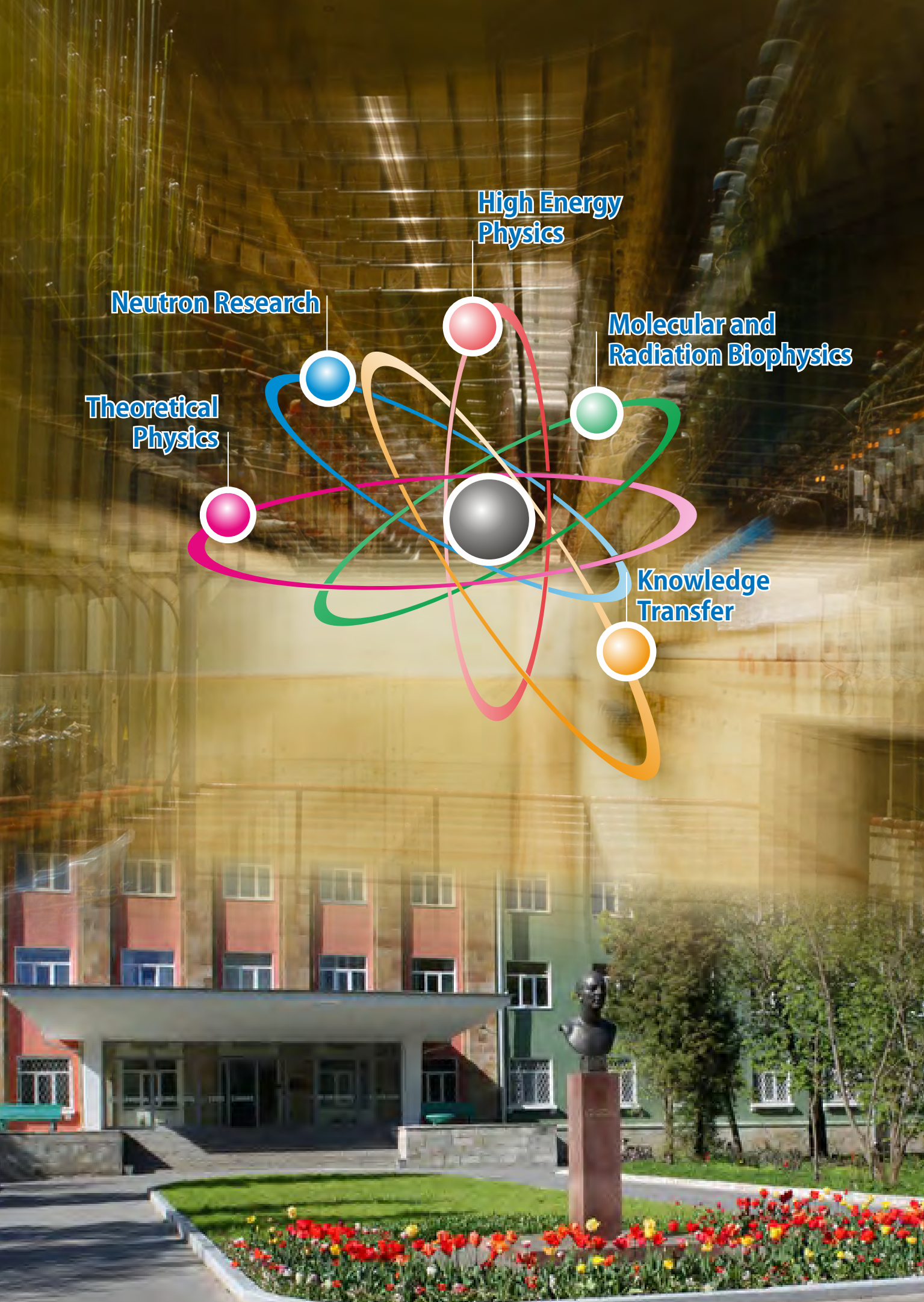
High Energy Physics
Neutron Research
Molecular and Radiation Biophysics
Theoretical Physics
Knowledge Transfer

Research Divisions

Theoretical Physics Division

Theoretical Physics Division (TPD) headed by Lev N. Lipatov (member of the Russian Academy of Sciences) consists of seven sectors (departments):

– Theory of Electroweak Interactions (headed by Dr. Gennady S. Danilov)**;**
– Theory of Strong Interactions (headed by Dr. Victor Yu. Petrov)**;**
– Quantum Field Theory (headed by Dr. Vyacheslav A. Kudryavtsev)**;**
– High Energy Theory (deputy head Dr. Victor Yu. Petrov)**;**
– Condensed Matter Theory (headed by Dr. Saul. L. Ginzburg)**;**
– Nuclear Theory (headed by Dr. Mikhail G. Ryskin)**;**
– Atomic Theory (headed by Dr. Alexander I. Mikhailov)**;**
and a Group of Physics of Nuclear Reactors (headed by Dr. Mikhail S. Onegin)**.**

TPD employs 68 research staff members (28 full Doctors of Science and 31 first degree Doctors of Science (Candidates of Science)).

Lev N. Lipatov
Member of the Russian Academy of Sciences,
Head of TPD

TPD research covers all branches of modern theoretical physics. Theory of high energy scattering is a traditional area of TPD research. It can be said that works of TPD researchers determine the frontier in this field. In 2014, the Green function of BFKL (Balitsky, Fadin, Kuraev, Lipatov) pomeron (i.e. the leading singularity presumably determining scattering at very high energies) was calculated for the first time in papers of L.N. Lipatov. The Green function is a basic object of Regge effective field theory, which should describe behavior of cross-sections at high energies. BFKL pomeron was also investigated for the processes with massive gluons. This is exactly the case of the Standard Model. In other words, results of L.N. Lipatov allow one to make conclusions about the asymptotic behavior of scattering amplitudes in this theory.

TPD is also one of the leaders in the field of so-called AdS/CFT duality (anti-de Sitter/conformal field theory), which is currently one of the hot topics in theoretical physics. Quite recently it was shown that some supersymmetric theories possess such a high symmetry that they (quite unexpectedly for d = 4 space-time) can be exactly solved. These field theories appear to be dual to a kind of superstring theory, which at certain limit reduces to the supergravity in specific metrics (anti-de Sitter space). In 2014, N.A. Gromov developed an exact theory of BFKL pomeron at arbitrary coupling constant within this theory. These works continue the previous studies of L.N. Lipatov, in which pomeron in AdS/CFT was considered in the weak and strong coupling limits. Thus, the behavior of the theory at high energies was completely determined. This result should be also useful for more realistic theories, such as Quantum Chromodynamics (QCD).

Investigation of nonperturbative effects in field theories is also in the centre of TPD attention. Quark confinement remains one of the most interesting and still unclear phenomena. It is still impossible to study it analytically, so simpler, more symmetrical theories are used to understand its mechanism. A.V. Yung has been studying the mechanism of confinement in supersymmetrical (SUSY) theories for many years. As a result, this mechanism is almost completely clarified in a number of theories. Unfortunately, it remains rather far from what we observe in nature. Nevertheless, A.V. Yung managed to discover a completely new phenomenon, so-called “instead-of-confinement mechanism”. In his papers, for the first time,

definite conclusions concerning the behavior of $N = 1$ SUSY Yang–Mills theories were made. Exact solution of this theory does not exist, and it still represents the last hope to discover a confinement of the type that is observed in nature. The research of A.V. Yung has an interesting by-product: a new type of duality between four-dimensional and two-dimensional SUSY-theories was found. This result is in line with other recent findings of the theory. It appeared that two-dimensional and four-dimensional theories are incredibly alike – the value of this similarity is still to be comprehended.

Lattice simulations are still the main tool to study QCD at $T > 0$. However, lattice data does not allow one to understand the nature of phenomena involved. A simple approach describing the data all the way down to the confinement-deconfinement phase transition was proposed in recent papers of V.Yu. Petrov. These papers deal with an effective potential for Polyakov's loop, which is an order parameter for phase transition. The effective potential was calculated under reliable approximations and a simple method to measure this quantity on the lattice was suggested.

M.G. Ryskin with co-authors studied the diffractive processes at Large Hadron Collider (LHC) energies. In their papers, the main points of V.N. Gribov theory were reconsidered in order to take into account a logarithmic growth of transverse momentum in QCD. Surprisingly, it makes the theory even simpler: using the modified theory, the authors managed to build a self-consistent model, which should presumably describe all diffractive phenomena at the LHC. Based on several examples, the authors prove that that is the case – a modified theory is in a good agreement with the data.

Works of V.N. Velizhanin reached the record accuracy in calculation of diagrams in perturbative theory. In 2013–2014, in a large series of papers, he calculated corrections to parameters of the Standard Model on the level of three loops (and better). Especially interesting is an effective potential for the Higgs field, which can be obtained from these calculations. Surprisingly, for the observed value of Higgs mass, the Standard Model seems to be out of the stability area. The precision of calculation still does not allow one to draw a final conclusion, but the danger of instability remains.

The works of M.I. Eides and co-authors reached a very high level of precision (three-loops and higher) as well. They concern another well-known theory – Quantum Electrodynamics (QED). Nowadays, the precision of experiments in QED is fantastic, so this accuracy of the theory is indeed necessary. In 2014, a superfine splitting in muonium was calculated.

The ideas concerning the origin of hierarchy of quark masses and the Kobayashi–Maskawa matrix itself draw specific attention. They were presented in works of I.T. Dyatlov in 2014. The author's considerations are based on the idea of mirror symmetry, which was suggested several years ago. Despite the fact that the idea seems far from reality, several coincidences pointed out by the author give one the food for consideration.

A.V. Sarantsev with his group continues to work on PWA (Partial Wave Analysis) of a series of reactions with mesons and baryons. This group (so called, Bonn – Gatchina) has already become the most recognized and reputable in the world: significant part of PDG (Particle Data Group) data is based on their results. The advantage of their analysis is that it is for the first time based on a single approach to all types of reactions. The data from different experiments complement each other. In 2014, a comprehensive overview of the methods used and achievements of the group was published in a large review article.

Works of TPD researchers have been widely represented in field of condensed matter physics as well. D.N. Aristov and co-authors have been developing the theory of quantum wires for many years. The properties of this theory appeared to be quite unusual: conductivity is equal either to zero or to the maximum value possible depending on the sign of electron-electron interaction. The theory of a junction of quantum wires (two, three or more) was suggested in papers of D.N. Aristov. This theory is essential for the future "quantum electrical technology". From the pure theoretical point of view, the theory of quantum wires reduces to beautiful conformal theories describing some critical behavior. In 2014, the authors developed a new field – the theory of nanowires out of thermodynamical equilibrium. One has to use completely new methods based on Keldysh technique in order to investigate such a theory.

TPD employee A.D. Mirlin has also chosen nanophysics to be the central topic of his research. He is one of the co-heads of a group that was awarded with a grant of the Russian Science Foundation (in cooperation with Landau Institute for Theoretical Physics).

Magnetics are the traditional topic of research in Condensed Matter Theory Department. A.V. Syromyatnikov with co-authors proposed a theory describing the low-temperature properties in magnetic field of a dimer spin-1/2 systems on a stacked triangular lattice with spatially anisotropic exchange interactions. The elementary excitations (triplon) spectrum and their interactions were obtained near the quantum critical point separating the paramagnetic phase and a magnetically ordered one. In addition, the dependencies of the critical field on the temperature and a transverse magnetization on the magnetic field were calculated. These calculations are in a good agreement with experimental data.

Gapped phases in two- and three-dimensional spin systems with a weak interaction of elementary boson excitations (both with long-range magnetic order and without it) and with bond disorder were considered. The elementary excitation spectrum and the density of states are calculated in the first order in defects concentration $c \ll 1$. These general results can be applied to describe low field and fully polarized paramagnetic gapped phases in dimer spin-1/2 systems and systems with integer spin and large single-ion easy-plane anisotropy.

S.L. Ginsburg and N.E. Savitskaya studied disordered systems in their works. They found conditions, under which a phase synchronization of some contact groups is possible in a superconducting metamaterial, which is a disordered lattice of Josephson junctions. The stability of this phenomenon under perturbations of contact parameters was also investigated. It was shown that the stability is realized on a significant part of the system phase diagram.

V.R. Shaginyan and co-authors have been developing the theory of strongly correlated Fermisystems for a number of years. It was proven that in many cases these systems can possess unusual properties. This is caused by the fact that effective mass of an elementary fermionic excitation becomes infinite if its momentum is close to the Fermi surface. A large number of phenomena observed in different systems of condensed matter physics could be explained by means of this theory. In 2014, Springer publishing company has published a book of V.R. Shagynian et al. devoted to their theory of strongly correlated fermions and its applications.

A significant part of TPD papers of 2014 was related to the theory of atoms and molecules, as well as traditional nuclear physics. In particular, the theory of multiple photonic atomic cascade transitions was suggested; an important contribution to the theory of internal conversion was made; the cross-sections of atom excitations by electrons and photons of high energies were calculated. Essential part of precise calculations in atomic physics in 2014 was aimed to be applied. Firstly, precise calculations of properties of a number of atoms and molecules were required by experiments on the stability of fundamental constants. Secondly, precise calculations were performed in connection with theoretical search for molecules, which can be used in experimental searches of electric dipole moment of the electron. Thirdly, one can mention the research needed for the purposes of the nuclear fusion reactor. For example, a precise study of properties of tungsten atoms (the material of the first wall of the nuclear reactor) was conducted within the latter topic in 2014.

Application of TPD works in field of nuclear reactor physics is also of a considerable practical importance. In 2014, specific fuel costs for the PIK reactor were calculated as a function of thickness of a fuel element blade. These calculations are rather important: the thinner is the fuel element blade, the less are the costs. Two applications for a patent were filed in 2014 and one patent has already been issued.

Practical issues of the PIK reactor exploitation were the topic of other TPD works as well. The reactivity of the PIK reactor was calculated and analyzed including the possible emergency situations. The full-scale modeling of the burn-up in the PIK reactor core after the power start-up was performed as well; the concept of the exploitation set of fuel assemblies for the PIK reactor was considered.

The following statistics demonstrates the results gained by TPD employees in the year 2014:

– 104 papers published in referred journals (including 98 papers published in foreign editions);
– Two patents received;
– One monography published;
– 30 papers presented at various international and Russian conferences and workshops;
– One doctoral thesis defended.

Neutron Research Division

Neutron Research Division (NRD) (deputy head Dr. Vladimir V. Voronin) consists of two research departments:

Neutron Physics Department (headed by Dr. Anatoly P. Serebrov) consists of four laboratories:

– Neutron Physics Laboratory (headed by Dr. Anatoly P. Serebrov)**;**
– *X*- and *g*-Ray Spectroscopy Laboratory (headed by Dr. Valery V. Fedorov)**;**
– Molecular Beam Laboratory (headed by Dr. Victor F. Ezhov)**;**
– Nuclear Spectroscopy Laboratory (headed by Dr. Ivan A. Mitropolsky)
and three groups:
– Nuclear Fission Physics Group (headed by Dr. Alexander S. Vorobyov)**;**
– Weak Interaction Research Group (headed by Dr. Alexandr N. Pirozhkov)**;**
– Research Group for Ultra-Cold Neutrons at WWR-M Reactor (headed by Dmitry V. Prudnikov)**.**

Condensed State Research Department (headed by Dr. Sergey V. Grigoryev) consists of four laboratories:

– Disordered State Physics Laboratory (headed by Dr. Vladimir V. Runov)**;**
– Crystal Physics Laboratory (headed by Dr. Yury P. Chernenkov)**;**
– Neutron Physical and Chemical Research Laboratory (headed by Dr. Vasily T. Lebedev)**;**
– Material Research Laboratory (headed by Dr. Alexander I. Kurbakov)
and two groups:
– Solid State Radiation Physics Group (headed by Dr. Sergey P. Belyaev)**;**
– Condensed Matter Electrodynamics Group (headed by Dr. Oleg V. Gerashchenko)**.**

NRD employs 153 research staff members (18 full Doctors of Science and 76 first degree Doctors of Science).

Dr. Vladimir V. Voronin
Deputy Head of NRD

Main directions of NRD research are Nuclear Physics, Particle Physics and Condensed Matter Physics. In 2014, new measurements of Neutron Electric Dipole Moment (EDM) were performed with the use of the PNPI double-chamber electric dipole moment spectrometer at ILL reactor (Grenoble, France). The double-chamber magnetic resonance spectrometer capable of holding the ultra-cold neutrons for a long time was used to carry out the experiments. The results obtained determine the upper limit of neutron EDM $|d_n| < 5.5 \cdot 10^{-26}\ e \cdot$ cm at 90% confidence level.

Investigations of the neutron optics close to the Bragg condition showed a resonance behavior of refraction index for neutrons moving in a perfect crystal at energies close to the Bragg ones. In this case, a small variation of the neutron energy by a value of an order of the Bragg (Darwin) width ($\Delta E / E \sim 10^{-5}$) leads to a significant (by a few tens percent) change of the neutron–crystal interaction potential.

Neutrino Laboratory was established at the SM-3 reactor. The first measurements were conducted on a prototype of a neutrino detector at the distance of 6–10 m from the reactor core.

A direct experimental evidence of the essential solar nuclear fusion reaction was obtained for the first time. In this reaction, a deuterium nucleus is produced by a fusion of two protons: $p + p \rightarrow d + e^+ + \nu$. This reaction (usually referenced as *pp*) is responsible for production of 99.8% of total solar energy, yet, until now, no direct observation of corresponding neutrino flux was performed. This work was published in *Nature* and included in the list of Physics Top Ten Breakthroughs of 2014.

A BGO bolometer cryogenically cooled down to several mK was for the first time used to perform

a search for axions. As a result, a new region of possible values of axion mass m_A and coupling constants g_{Ae} and $g_{AN}{}^3$ was excluded by a direct laboratory measurement. The new constraint is 20 times more stringent than the one obtained previously.

The study of the lifting of degeneracy of the chiral symmetry in the spin helix structure of Ho/Y superlattice induced by an in-plane applied magnetic field was performed as well. The original method was used in polarized neutrons scattering experiment, and it was discovered that the cooling in external magnetic field disturbs the balance between populations of the left- and right-handed helices of the spin structure of the sample. The results obtained can be explained by the appearance of Dzyaloshinsky–Moriya interactions between the layers of multilayered system. The results confirm the similarity of degeneracy of the chiral symmetry in multilayered systems with alternating magnetic and nonmagnetic layers on the basis of rare-earth metals.

The structure of metal Ni-based inverse opal-like crystals (IOLC) was studied on the mesoscopic and atomic scales. The mesoscopic structure of IOLC based on Ni repeats the structure of the original matrix of the artificial opal crystal completely with minor alteration of the lattice constant. Densely stacked hexagonal layers were aligned into Face-Centered Cubic Structure (FCC). The probability of FCC motif formation and the average structure lateral domain size do not depend on the number of layers, and it remains constant provided that the original matrix is the same for all the samples. When the number of layers increases, the number of reflections increases as well.

The structure and the function of β-mannosidase from *Trichoderma harzianum* was investigated. Currently, much attention is paid to alternative fuels. In this regard, a structural study of enzymes capable of converting renewable resources and waste into alternative fuels becomes important. As it has been shown previously, filamentous fungi of the genus Trichoderma secrete complex of enzymes hydrolyzing most abundant natural materials like cellulolignin and galactomannan – the most available natural renewable sources. One of important hydrolyzing enzymes of this complex is β mannosidase. Monsaccharides – glucose, mannose, galactose – produced as a result of hydrolysis can be used to produce biofuels. The three-dimensional structure of β-mannosidase from the fungus *Tri. harzianum* was built, and it was the first structure of a eukaryotic β-mannosidase from the second family of glycoside hydrolases. On the basis of the structure solved, the substrate-binding site – galactomannan – has been studied by methods of molecular dynamics, and the mechanism of action of the enzyme has been explored.

A new direction for development of neutron optics was suggested – a neutron spin manipulation optics based on quantum aspects of the neutron interaction with magnetically anisotropic layers. It signifies the transition from 1D (spin selection) to 3D (spin manipulation) in polarized neutron optics. Solutions that provide a high reflectivity and a weak dependence of the spin rotation angle on the neutron wavelength and on the glancing angle were suggested. As well they open up the new possibilities for creation of 3D-polarizers, spin manipulators, hyperpolarizers, quantum spin precessors and antiprecessors.

The technique of neutron activation analysis of scintillation ceramics Gd_2O_2S : Pr, Ce was developed. The concentrations of As, Ce, Co, Cr, Cs, Eu, Fe, La, Sc, Tb, Zn, Zr, Pr, Gd, Na in samples were measured in the range from $3 \cdot 10^{-8}$ to 2.0% of the mass. The detection thresholds of the elements were $(0.6–1.3) \cdot 10^{-8}$%. It was established that the relative light yield (λ_{max} = 513 nm) decreases with the increase of the content of Ce in scintillation ceramics. The maximum value of the relative light yield of ~ 40% is obtained when the Ce concentration reaches ~ 10^{-5}%. It is shown that alloying of ceramics Tb (~ 10^{-6}%) leads to the reduction of an afterglow.

The following statistics demonstrates the results gained by NRD employees in the year 2014:

– 85 research papers published in referred journals (including 39 papers published in foreign editions);

– 103 research reports presented at various international and Russian events;

– Two doctoral theses defended.

High Energy Physics Division

High Energy Physics Division (HEPD) headed by Prof. Alexey A. Vorobyov (corresponding member of the Russian Academy of Sciences) consists of 10 laboratories:

– Elementary Particle Physics Laboratory (headed by Prof. Georgiy D. Alkhazov)**;**
– Meson Physics of Condensed Matter Laboratory (headed by Dr. Sergey I. Vorobyev)**;**
– Relativistic Nuclear Physics Laboratory (headed by Prof. Vladimir M. Samsonov)**;**
– Short-Lived Nuclei Laboratory (headed by Dr. Vladimir N. Panteleev)**;**
– Meson Physics Laboratory (headed by Dr. Victorin V. Sumachev)**;**
– Few Body System Laboratory (headed by Prof. Stanislav L. Belostotski)**;**
– Hadron Physics Laboratory (headed by Dr. Oleg L. Fedin)**;**
– Physics of Exotic Nuclei Laboratory (headed by Prof. Yuri N. Novikov)**;**
– Crystal Optics of Charged Particles Laboratory (headed by Dr. Yuri M. Ivanov)**;**
– Cryogenic and Superconductive Techniques Laboratory (headed by Dr. Alexander A. Vasilyev)
and four technical departments:
– Radio Electronics Department (headed by Dr. Viktor L. Golovtsov)**;**
– Track Detectors Department (headed by Dr. Anatoly G. Krivshich)**;**
– Computing Systems Department (headed by Andrei Y. Shevel)**;**
– Muon Chambers Department (headed by Vladimir S. Kozlov)**.**

HEPD employs 134 research staff members (13 full Doctors of Science and 69 first degree Doctors of Science (Candidates of Science)).

Prof. Alexey A. Vorobyov
Corresponding member
of the Russian Academy
of Sciences,
Head of HEPD

HEP division activity is mainly aimed at the experimental research in the field of elementary particle physics and nuclear physics. Also, a solid state physics research with the use of the μSR-method is being performed. As in previous years, research works were conducted at PNPI facilities and at accelerators of the world's leading nuclear centres.

Charge radii and electromagnetic moments of several Bi isotopes and isomers have been measured at the mass separator complex IRIS at the PNPI synchrocyclotron with the method of resonance ionization spectroscopy. This method was also used to study the shape co-existence in neutron-deficient nuclei at the ISOLDE facility (CERN, Switzerland). The co-existence of two fission channels (symmetric and asymmetric) in At isotopes was discovered in these experiments.

A similar mass separator complex IRINA is planned to be constructed for investigations of neutron-excess nuclei that will be produced at the high flux neutron reactor PIK at PNPI.

The properties of the $Eu_{0.8}Ce_{0.2}Mn_2O_5$ multiferroic magnetics, such as phase transition and local magnetic field configuration, were investigated within the temperature range of 10–300 K using the μSR-installation in the muon channel of the PNPI synchrocyclotron. The μSR-method is also used to investigate the $Tb_{0.95}Bi_{0.05}MnO_3$ ceramics, the $TbMnO_3$ manganite, the ferromagnetic fluid based on $CoFe_2O_4$, and the samples of FeCr steel RUSFER-EK-181 and ChS-139.

Essential progress was achieved in preparations of the PolFusion experiment aimed at studies of the *dd*-fusion in collisions of polarized deuterons. The experiment will be performed at PNPI with participation of scientists from the Nuclear Physics Institute (Jülich, Germany) and from the University of Ferrara (Italy). In 2014, a source of deuteron ions with the energy up to 30 keV was constructed for this experiment.

Preparations are in progress for the production of the ^{82}Sr isotope for medical applications using a high current proton beam from the 80 MeV Proton Cyclotron (under construction at PNPI). An operating prototype of the target station was built for production of this isotope. The design of the RIC-80 radionuclide complex for mass production of radioisotopes for medicine has been completed at the new cyclotron.

The goal of the OLYMPUS experiment (DESY, Germany) is to solve the existing problems in studies of the nucleon EM form factor by comparative measurements of elastic scattering of electrons and positrons on the proton at the energy of 27 GeV. At present, the data taking is completed and the data analysis is on the way.

The high precision measurements of the muon capture rate on the proton and light nuclei is one of the major items in the HEPD scientific program. The experiments are carried out at the "meson factory" of the Paul Scherrer Institute (Switzerland) using the experimental method developed at PNPI. The measurement of the muon capture rate on the proton (experiment MuCap) made it for the first time possible to determine the nucleon pseudoscalar form factor: $g_p^{\text{MuCap}} = 8.06 \pm 0.5$. This experiment was included by the Phys. Rev. Lett. editors into the category of "outstanding research". The on-going experiment MuSun is aimed at high precision measurement of the muon capture rate on the deuteron. In 2014, a successful three-months physics run was performed.

The main efforts of the HEP division were concentrated on participation in the LHC experiments CMS, ATLAS, LHCb, and ALICE. PNPI participated in these experiments from the initial phase of design and construction of the collider detectors with essential contributions to the construction of various subsystems of these detectors. After the LHC start-up, HEPD physicists and engineers shared responsibilities in maintenance and operation of these detectors and took part in the analysis of the experimental data.

In 2014, the activities were focused on preparations for Run2 scheduled for 2015–2017. Also, the projects of essential upgrades of the CMS, ATLAS, LHCb, ALICE detectors were formulated to be realized during 2014–2017. HEPD takes part in these projects. In particular, in the framework of this programme, 76 new large muon chambers and a 2 500-channels high voltage system for the CMS detector have been produced and installed in 2014 with active participation of HEPD specialists.

The analysis of the experimental data collected in 2010–2012 yielded a great amount of new results crowned by the discovery of the Higgs boson. More than 200 papers were published in 2014. The list of authors in these publications includes 35 scientists from the PNPI HEP division, 21 of them being co-authors of the Higgs discovery. This volume presents some results obtained from the analyses with direct participation of HEPD physicists.

The LHCb and CMS Collaborations reported the first observation of the $B_s^0 \to \mu^+\mu^-$ decay. This decay is strongly suppressed in the Standard Model. On the other hand, it is predicted to be much more intensive by some models, such as the Minimal Supersymmetry Model, introducing "new physics" beyond the Standard Model. However, the experimental value for probability of this decay $\text{Br}(B_s^0 \to \mu^+\mu^-)\text{expt} = (3.2 \pm 0.7) \cdot 10^{-9}$ was found to be close to that predicted by the Standard Model: $\text{Br}(B_s^0 \to \mu^+\mu^-)\text{SM} = (3.66 \pm 0.23) \cdot 10^{-9}$, being a strong constraint on developments of "new physics" models. The importance of this result was discussed in a publication in *Nature*.

Several theories beyond the Standard Model predict the existence of heavy bosons. HEPD physicists participated in searches for such bosons (*W'* and *Z'*) with the data collected by the ATLAS experiment. As a result, the limits were set on production cross-sections of these bosons. It was shown that *W'*-bosons with the mass less than 3.3 TeV and *Z'*-bosons with the mass less than 2.8 TeV are not produced in proton-proton collisions at the centre-of-mass energy of 8 TeV.

A surprising result was obtained in the ALICE experiment. Previously, a strong suppression of charmonium yeilds in nucleus-nucleus collisions at the *NN* centre-of-mass energy of 200 GeV was observed in the PHENIX experiment (BNL, USA). This was explained by the formation of the quark-gluon matter in the nucleus-nucleus collisions. Charmonium suppression was expected to be similar or larger in kinematics of the ALICE experiment with significantly higher energy of colliding particles. However, the suppression effect in ALICE proved to be significantly weaker than that in PHENIX. This result is still to be explained theoretically.

The study of ultraperipheral collisions of protons with protons (LHCb experiment) and protons with heavy nuclei (ALICE experiment) allowed one to measure the gamma-proton scattering cross-sections at unprecedented high energies of up to $W_{\gamma p}$ = 1 000 GeV. This opened up the possibility to determine the gluon density in the nucleon at small x, down to $x = 10^{-5}$, thus extending the x-region investigated in the DESY experiments by an order of magnitude (x is a relative part of the nucleon momentum carried by the gluon).

First observation of the electroweak production of Z-boson in association with hadron jets was reported by the CMS and ATLAS Collaborations. The cross-section of this process was measured. This observation gives important information on the inter-boson interaction. Various "new physics" models predict much higher inter-boson interaction than that predicted by the Standard Model. The obtained experimental result agrees well with predictions of the Standard Model and disfavours other models.

Another rare process having high sensitivity to potential manifestation of "new physics" was observed at the Tevatron collider (FNAL, USA) in the CDF and D0 experiments (HEPD participates in the D0). This is the s-channel production of a single top quark at proton-antiproton collisions at the total energy of 1.96 TeV. The cross-section determined from the experimental data, σ_s = 1.29 ± 0.25 pb, proved to be in agreement with the Standard Model expectation σ_s = 1.05 ± 0.06 pb, thus showing no manifestation of "new physics".

The main results from the PHENIX experiment (BNL, USA) in 2014 are associated with measurements of the two particles correlations in $p + p$, d + Au, and ^{3}He + Au collisions at $\sqrt{s_{NN}}$ = 200 GeV. The observed collective behaviour quantified in terms of the hydrodynamical flows may indicate formation of the low-viscosity quark-gluon matter in all types of collisions studied in this experiment, including the pp-collisions. Note that HEPD physicists have been participating in the PHENIX experiment starting from its construction in 1991.

The crystal optics of high energy protons is a traditional research line at the HEP division. It was marked by various achievements, such as development of the elastic quasi-mosaisticity method for production of bent crystals, discovery of the volume capture into the channeling regime, discovery of the volume reflection, proton beam focusing and proton beam extraction from high energy accelerators. Since 2008, HEPD specialists have been participating in the UA9 experiment at CERN. The goal of this experiment is to use the bent crystals for collimation of the proton and heavy ion beams circulating inside the LHC. Extensive studies performed at the SPS accelerator at CERN demonstrated feasibility of this method. As a result, the CERN administration has approved a test experiment directly with the LHC beams. This experiment is scheduled for 2015–2017.

HEPD physicists participate in preparations for joint research at the accelerator complex FAIR, which is now under construction at Darmstadt (Germany). The FAIR facility will produce medium energy beams of protons, antiprotons, and stable heavy nuclei, as well as secondary beams of exotic nuclei with unique quality and high intensity. HEPD will take part in experiments CBM, PANDA, R3B, and MATS.

The following statistics demonstrates the scientific activity of the HEP Division in 2014:

– 211 research papers published in reviewed journals;

– 42 research reports presented at various international and Russian events.

Molecular and Radiation Biophysics Division

Molecular and Radiation Biophysics Division (MRBD) headed by Dr. Vladimir G. Korolev consists of 13 laboratories:

– Laboratory of Biophysics of Macromolecules (headed by Dr. Vladimir V. Isaev-Ivanov);
– Laboratory of Genetics of Eukaryotes (headed by Dr. Vladimir G. Korolev);
– Laboratory of Protein Biosynthesis (headed by Dr. Andrey L. Konevega);
– Laboratory of Molecular Genetics (headed by Dr. Valeriy N. Verbenko);
– Laboratory of Biopolymers (headed by Dr. Andrey L. Timkovskiy);
– Laboratory of Cell Biology (headed by Dr. Mikhail V. Filatov);
– Laboratory of Human Molecular Genetics (headed by Dr. Alexander L. Schvarzman);
– Enzymology Laboratory (headed by Dr. Anna A. Kulminskaya);
– Laboratory of Experimental and Applied Genetics (headed by Dr. Svetlana V. Sarantseva);
– Laboratory of Medical Biophysics (headed by Dr. Leonid A. Noskin);
– Laboratory of Medical and Bioorganic Chemistry (headed by Dr. Farid M. Ibatullin);
– Proteomics Laboratory (headed by Dr. Stanislav N. Naryzhny);
– Laboratory of Cryoastrobiology (headed by Dr. Sergey A. Bulat)
and a Sci-Tech Department of Bioelectronics (headed by Alexander P. Roganov).

MRBD employs 117 research staff members (16 full Doctors of Science and 62 first degree Doctors of Science (Candidates of Science)).

Dr. Vladimir G. Korolev
Head of MRBD

MRBD is actively involved in studies of macromolecular complexes with the use of methods of small-angle neutron scattering (SANS) and molecular simulation (Laboratory of Biophysics of Macromolecules headed by Dr. Vladimir V. Isaev-Ivanov). MRBD researchers developed a software for SANS spectra calculation based on the simulated full atomic trajectories of molecular dynamics, which allows one to take into account the protein mobility in interpreting SANS experiment. This approach was tested on the complexes of bacterial RecA and RecX proteins. SANS spectra for the protein complex RecX with ssDNA were in a good agreement with the double-sided "sandwich" model of the complex, while the spectra of RecX protein complex with the presynaptic RecA protein filament showed the best agreement with the calculated spectra for the full-atom molecular model with the stoichiometric ratio RecA : RecX of 4 : 1. An important implication of this work for structural biology is the possibility to obtain a full structure of multimolecular complexes of interest at atomic resolution under the native conditions by means of molecular dynamics simulations, while using low-resolution experimental methods, such as SAXS (small-angle X-ray scattering) or SANS, for its verification.

The study of molecular mechanisms of protein biosynthesis is a traditional field of MRBD research. Molecular mechanisms of translocation and rare events of translation, reading frame shifting and translational bypassing were investigated in works of researchers from the Laboratory of Protein Biosynthesis (since 2013 headed by Dr. Andrey L. Konevega). Apart from progressive movement of the ribosome along the messenger RNA (three nucleotides per one step), there are different translational recoding mechanisms, such as reading frame forward or backward shift. Realization of these processes allows one to increase the amount of information encoded in genome and exercise additional influence on gene expression regulation. In

their works, V.I. Katunin and his co-authors studied a mechanism of the programmed –1 frameshifting by means of a detailed review of ribosome movement along the specific region of mRNA that is characteristic for such frameshifting event. Two elements in the mRNA are prerequisites for the frameshifting: a "slippery sequence" that allows the ribosome to slide backward and a downstream secondary structure element – pseudoknot – that temporarily impedes the forward movement of the ribosome. The presence and work efficiency of these elements in a system created *in vitro* were validated *in vivo*. The paper reports the results of the analysis, including the kinetics of stepwise translation of the "slippery sequence", the kinetics of amino acid incorporation into translation products that correspond both to usual and shifted frames and the detailed kinetics of translocation reactions that govern programmed –1 frameshifting. A.L. Konevega and co-authors studied in their work another rare event – a translational bypassing. After translation of the first coding sequence (46 amino acids) of the gene product 60 of bacteriophage T4, the ribosome stops, 50 nucleotides of mRNA are pulled through the ribosome, and the synthesis resumes. Therefore, the polypeptide synthesis is being performed for two inconsequential reading frames. The work proved that the ability for translational bypassing is an internal property of the ribosome and all the signals required for such a rare event are encoded in the translated mRNA. This process is contributed significantly both by the amino acid sequence of nascent polypeptide chain and elements of a secondary structure of the mRNA, which, in particular, determine the place of the landing codon for the protein synthesis to be resumed. No auxiliary protein factors are needed for efficient bypassing. The third work of this laboratory proves that the rapid translocation catalyzed by EF-G and complemented by GTP hydrolysis appears simultaneously on 30S and 50S subunits of ribosomal complex. The use of antibiotics or EF-G mutants leads to desynchronization of translocation on 30S and 50S subunits. In this case, the translocation on 50S subunit goes through an extra intermediate state A/P2. In order to reach such a state, only the use of free binding energy of EF-G with the ribosome is needed, while the full translocation on 50S subunit and translocation on 30S subunit requires the GTP hydrolysis and a full-length EF-G factor.

Research on possible connection between Parkinson's disease (PD) and lysosomal storage diseases (LSDs) can be considered one of the most significant works of MRBD (Laboratory of Human Molecular Genetics headed by Dr. Alexander L. Schvarzman). About 10–15% of PD patients report the familial form of the disease. Currently, mutations in eight genes (*SNCA, LRRK2, PINK1, PARK2, PARK7, PLA2G6, FBX07, ATP13A2*) were identified to be the course of familial form of PD in rare cases. The most important for the PD prognosis are the *GBA*, *SMPD1* and *NPC1* genes that are the genes of high risk of PD development. Mutations in these genes increase the risk of PD development by up to 8-9 times, and their frequency in different populations is 0.5 – 5%. The most frequent are the mutations in the glucocerebrosidase (*GBA*) gene. In our population, each 250th citizen of the European part of Russia may be the carrier of those mutations and thus is exposed to a high risk of PD development. It was suggested that the mutations in genes of enzymes localized in lysosomes, cell compartments responsible for protein degradation, could affect the levels of alpha-synuclein and facilitate its oligomerization. This may lead to the formation of neurotoxic oligomeric alpha-synuclein protein species. It was known that half of cellular protein is degraded via lysosomes. In order to test the hypothesis, the researchers studied the level of oligomeric alpha-synuclein in plasma of 41 patients with Gaucher disease and 40 members of control groups. The study was the first one to show an increase of oligomeric alpha-synuclein levels in plasma of patients with mutations in LSDs genes linking together such different pathologies as LSDs and PD through alpha-synuclein aggregation. The data received opens a prospect for discussion of therapeutic strategies for treatment of such neurodegenerative disorder as PD (currently considered incurable).

Mechanisms of ATP hydrolysis in mkTIP49 proteins was studied in the work of M.G. Petukhov (Laboratory of Biophysics of Macromolecules headed by Dr. Vladimir V. Isaev-Ivanov). Researchers introduced a series of point mutations of amino acids in the active site of the protein and studied consequences of these mutations using theoretical and biochemical approaches. In particular, they proposed amino-acid substitution N326Q from the subunit neighboring

to the catalytic site that shifts the polar amino group closer to ATP compared to the wild-type protein. According to calculations, this rearrangement may lead to the appearance of a new hydrogen bond donor for water molecule in attacking position. Theoretically, it was predicted that this substitution would reorient the attacking water molecule and could interfere with Mg^{2+} ion coordination with D296 from Walker B motif. As predicted, ATPase activity of the mutant N326Q mkTIP49 was completely lost in course of biochemical experiments. These experimental results confirmed not only the calculations but also the correctness of a chosen mechanism of ATP hydrolysis in the proteins studied. They have also confirmed the correctness of the spatial arrangement of all the structural elements in the protein active site, as well as the arrangement of molecules participating in the ATP hydrolysis process, including a so far unknown structure of a hexameric complex of the protein studied.

The work devoted to the influence of chromatin structure on mutagenesis in yeast (Laboratory of Genetics of Eukaryotes headed by Dr. Vladimir G. Korolev) presented a study of the role of *SIN3* gene in this process. The product of *SIN3* gene is a RPD3 HDAC complex subunit and acts as a repressor for a considerable amount of genes in yeast *Saccharomyces cerevisiae*. Effects of *sin3* mutation on mutagenesis in *S. cerevisiae* yeast cell were subject to investigation. Single mutants on *SIN3* gene were constructed in the course of the study along with double mutants on *SIN3* gene and key genes of nucleotide excision repair (*RAD1* gene) and homologous recombination repair (*RAD52* gene) systems. Single *sin3*, *rad1* and double mutant *rad1sin3* analysis led to conclusion that *sin3* mutation leads to the increase in sensitivity of haploid cell upon higher UV irradiation doses. That fact is in accordance with the massive death of budding yeast cells. That may be interpreted as abnormalities in homologous recombination DNA repair mechanism. The inactivation of RPD3 complex in yeast cells leads to trespassing of the mutation process. The level of the UV-induced mutagenesis is decreased in *sin3* mutant. It means that Sin3p regulates a dNTP pool level negatively. Faults of that type of regulation result in induced mutagenesis reduction observed in our research. Similarly, *sin3* mutation affects both spontaneous replicative and reparative mutagenesis. Summarizing, we can conclude that *SIN3* gene plays a crucial role in dNTP pool level control both in DNA replication and in DNA repair mechanisms.

MRBD researchers work on the proteome profiling of malignancies (Proteomics Laboratory headed by Dr. Stanislav N. Naryzhny and Laboratory of Cell Biology headed by Dr. Mikhail V. Filatov). Separation of proteins by two-dimensional electrophoresis (2DE) followed by imaging, immunochemistry, spot picking, and mass-spectrometry allowed researchers to detect more than 600 protein spots and identify more than 130 of them. Proteome profiles in normal and glioblastoma cell lines are very similar, but levels of several proteins have prominent differences between the norm and the cancer. Proliferating Cell Nuclear Antigen (PCNA) and p53 (TP53) are among these proteins. Most interesting results obtained concerned the protein p53. Its level was dramatically upregulated and enriched by multiple additional isoforms. On the one hand, these results confirm the previously published data about several cancer marker proteins, both common and associated with glioblastoma; on the other hand, they indicate the possibility to use such known proteins as PCNA and p53 as biomarkers in glioblastoma assays.

The following statistics demonstrates the results gained by MRBD employees in the year 2014:

– 68 papers published in referred journals;
– 75 papers presented at international and Russian conferences and workshops;
– One doctoral thesis defended.

Molecular and Radiation Biophysics Division celebrates its 50th anniversary

The Laboratory of Radiation Genetics was established by the decision of the USSR Academy of Sciences of December 25th 1964, at the affiliated branch of the Ioffe Institute of Physics and Technology (currently PNPI NRC "Kurchatov Institute"). It was the first laboratory of Radiobiological Division (RBD). Initially, the division was created to study the effects of radiation on human health. The list of the most significant findings and achievements of RBD includes construction of an EPR spectrometer (V.N. Fomichev and co-authors, 1967), discovery of cytoduction in yeast (I.A. Zakharov and co-authors, 1969) and creation of the first inactivated influenza vaccine (S.E. Bresler and co-authors, 1971).

In 1970s, the amount of works on molecular biology, biophysics and genetics exceeded the one on radiobiology and in 1976, RBD was renamed as to Molecular and Radiation Biophysics Division (MRBD). Many fundamental and applied works were performed at MRBD during the years of its existence. Namely, significant advantages of catalyzers for sulphur filtration of oil developed in Gatchina were demonstrated in 1980 (G.A. Bagiyan and co-authors); in 1989, it was suggested to use the method of polymerase chain reaction for the diagnostics of human genetic diseases (E.I. Schwarz and co-authors); in 1992, a crystal structure of glucoamylase was obtained (L.M. Firsov and co-authors).

Currently, MRBD consists of 13 laboratories and employs over 190 staff members, 16 of which are Doctors of Science and 66 are first degree Doctors of Science (Candidates of Science). Since 1976, MRBD has been organizing Winter Biology Schools and since 2008 – S.E. Bresler conferences named "S.E. Bresler readings". MRBD is especially proud of the number of its young employees, which gives it a right to be considered the youngest division of the Institute.

MRBD cooperates with many research institutes and universities including the Ott Research Institute of Obstetrics and Gynecology; Department of Molecular, Genetic and Nanobiological Technologies of Pavlov First St. Petersburg State Medical University; Institute of Experimental Medicine; St. Petersburg Polytechnic University; Institute of Molecular Genetics of the Russian Academy of Sciences; Joint Institute for Nuclear Research; Research Institute for Genetics and Selection of Industrial Microorganisms; Ukrainian Radiobiological Society; Institute of Cell Biology and Genetic Engineering NASU, and many others. The Division made a great contribution to the scientific potential of the Russian Federation, promoted training and development of many brilliant scientists.

Knowledge Transfer Division

Knowledge Transfer Division (KTD) headed by Dr. Victor F. Ezhov, consists of three laboratories:

– Holographic Information and Measuring Systems Laboratory (HIMSLab) (headed by Dr. Boris G. Turukhano)**;**
– Radiative Physics Laboratory (headed by Dr. Nikolay A. Ivanov)**;**
– Quantum Chemistry Laboratory (headed by Dr. Anatoliy V. Titov)
and two departments:
– Accelerator Department (headed by Dr. Evgueny M. Ivanov)**;**
– Information Technologies Department (headed by Dr. German A. Riabov)**.**

KTD employs 43 research staff members (5 full Doctors of Science and 15 first degree Doctors of Science (Candidates of Science)).

Dr. Victor F. Ezhov
Head of KTD

The main function of Accelerator Department (AD) and Accelerator Physics and Technology Laboratory is the exploitation of 1 GeV synchrocyclotron (SC-1000), its use for the purposes of research and applied works, adjustment and optimization of 80 MeV cyclotron (C-80) systems.

Research complex at SC-1000 is used to conduct studies in fields of elementary particle physics, atomic nucleus structure, mechanism of nuclear reactions and solid state physics. It is also used for the purposes of applied physics and for the research purposes of nuclear medicine. In 2014, SC-1000 had been active for 2 784 hours.

Main fields of fundamental and applied works at accelerator are as follows: investigation of new materials by muon spin rotation technique (μSP-method) – 20%; investigation of short-lived isotopes (Short-Lived Nuclei Laboratory) – 14%; investigation of a nuclear matter on MAP spectrometer – 10%; proton channeling – 7%.

The system of one-turn deflection of a proton beam was upgraded in 2014. This work required new calculations and measurements of the installation construction. The transition to a new element base allowed one to have a required range of the pulse leading edge of 50–60 nsec at 120 kV pulse voltage amplitude. The upgrade of the system of one-turn deflection of a proton beam allowed one to make the system more reliable and its adjustment faster.

The upgrade project for synchrocyclotron systems was developed as well. The complex of proton therapy at 1 GeV beam is currently being modernized.

A significant work was performed in field of design and development of the complex for radiation testing of electronic component base (ECB) for aviation and space: two stands for ECB radiation testing were created on a neutron beam at the energy range of 1–1 000 MeV and on proton beams at the energy range of 200–1 000 MeV. A device for remote variation of the absorber length was designed for the transition from one beam energy to another. A beam profilometer, movement and temperature control equipment, two magnetometers for stabilization of SC-1000 and SP-40 magnetic fields were developed and manufactured as well.

The Centre of ECB Radiation Testing is currently being created. For the purpose of ECB testing, parameters of a new P2 path with an absorber made of copper were calculated and optimized at the energy range of 50, 100–1 000 MeV with one step equal to 100 MeV. Computer control over six lenses was introduced in cooperation with Neutron Research Division.

Eight contractual works on ECB radiation testing were realized on SC-1000 beams. ECB was tested for: JSC "ENGOsSPELS" (Moscow) – 1; JSC "Electronstandard

Russian Research Institute" (St. Petersburg) – 1; LLC "Granat" Research and Development Centre" (St. Petersburg) – 2; Research Institute of Space Instrument Engineering (Moscow) – 2; Obninsk – 1; Moscow Institute of Physics and Technology – 1.

In 2014, adjustment and optimization of C-80 systems were conducted at the Accelerator Department in order to obtain project parameters of the beam (in collaboration with D.V. Efremov Institute of Electrophysical Apparatus). This work led to C-80 start-up on December 5th, 2014. An accelerated beam of N^--ions with the radius of up to 30 cm, intensity of 30 μA and the energy of ~ 10 MeV was obtained. The work continues up to now.

The works within WLCG project continued in the Laboratory of Information and Measuring Systems (LIMS). These works included: a software upgrade (Grid FTR, DEPM, SRM) with the aim to increase the efficiency of data transfer on grid sites; development of a software for a distributed grid network used for experimental data processing at the Large Hadron Collider (LHC); the work at LHC clusters and maintenance support of experiments (more than 631 thousand tasks in the year 2014).

The following engineering developments were conducted in collaboration with High Energy Physics Division and Neutron Research Division: development and production of detectors on base of the thick gas electron multipliers (TGEM) and monolithic TGEM, production of printed circuit boards, electrodes for proportional chambers of LHCb CERN and others. It is reasonable to draw attention to the active participation of LIMS employees in joint programmes with HEPD and the LHC.

In Radiative Physics Laboratory (RPL), a virtual model of a proton beam formation was created for the purposes of ophthalmology. The calculation was made using Geant4 code. Several variants of formation schemes were calculated, and the optimal system of C-80 proton beam formation was suggested for ophthalmology.

The study on elastic scattering of protons was conducted, as well as the one on production of π-mesons in *pp*-interactions. The statistical data was gathered and the data from the bubble chamber processed.

The works on SC-1000 proton beam were conducted in collaboration with Accelerator Department in framework of the contract with Research and Development Institute of Cable Industry (VNIIKP). ECB was tested for the private JSC "Impuls" (St. Petersburg) and LLC Television Research Institute (St. Petersburg).

The influence of flux density of nucleons on the effectiveness of CCD-matrix was investigated, as well as the space and time distribution of spikes in matrices irradiated with protons or neutrons.

World class devices were developed at Holographic Information and Measuring Systems Laboratory (HIMSLab) on the basis of linear and radial holographic lattices. These devises were certified at the D.I. Mendeleyev Institute for Metrology (VNIIM). 3D nano universal measuring microscope UIM – 23 was designed for high-precision (0.6 μm) three-coordinate measurements (the resolution of all the coordinates is 10 nm). Ultra-precision micro-milling system with the resolution of 10 nm for the length of 1250 mm and 1 nm for the width of 150 mm was developed in collaboration with the companies "Rezus tochnosti" in Moscow, Tula, Noginsk.

Participation of HIMSLab and Dr. Boris G. Turukhano in XX International Exhibition-Congress "High Technologies. Innovation. Investments" was awarded with two diplomas and medals of the award winner.

The Quantum Chemistry Laboratory was occupied within its main fundamental research field – calculations for the estimation of electric dipole moment (EDM) of electron in molecules with "heavy atoms".

The following research results were also obtained by the Quantum Chemistry Laboratory.

The research on the periodical properties of superheavy elements was performed, chemical graphs were constructed; calculations for experiments on the search of *e*-EDM and Shiff momentum were performed; the highest actinide oxidation degrees (Pu, Am, Cm) were investigated; the values of chemical sifts of *X*-ray emission spectra were determined; HfF^+ cation spectra (HF-*d*-element) were identified.

The properties of super-heavy elements were simulated for their chemical identification. Experiments were conducted at JINR, GSI (Darmstadt), RIKEN (Wakō).

The following statistics demonstrates the results gained by MRBD employees in the year 2014:

- 14 papers published in referred journals;
- 18 papers presented at international and Russian conferences and workshops;
- One patent received.

Theoretical and Mathematical Physics

Conductance renormalization for junctions between interacting quantum wires

D.N. Aristov
Theoretical Physics Division, PNPI NRC "Kurchatov Institute"

My research activity is related to theoretical studies of contacts and junctions between quantum wires. The interest to this topic arises due to the fact that elements of modern electronic devices become smaller every few years. The development of nanotechnology leads to creation of objects on such a scale, on which quantum effects become essential.

Potentially useful gadgets have two basic quantum features. The first feature is so called size effects or quantum confinement. It turns out that the cross-section of a wire might be so small that electrons conducting the electric current would be transferred in this wire, in certain sense, "one by one". In this case, a second feature becomes important: any electronic device consists of various elements that are attached to each other by contacts and *Y*-junctions.

Usually contacts between different wires are only partly transparent for the electric current. This non-ideal transparency might depend not only on the contact itself, but also on the interaction between electrons in the wire. This interaction is rather weak for devices created on basis of traditional semiconductors. At the same time, new technological elements, such as carbon nanotubes (close relatives to now-famous graphene material), are very small in transverse direction, only a few nanometers, and the interaction in nanotubes is quite strong.

It was proven both in theory and experimentally that the conductance (transmission coefficient) of the contact is reduced by the repulsion between electrons. This quantum effect is called renormalization and is enhanced at lower temperatures and in longer wires. It explains the interest of researchers and engineers to seamless contacts between nanotubes.

The influence of the electronic interaction on the conductance of the wire with internal defects and the conductance of the contact between wires was theoretically discussed and studied for the first time

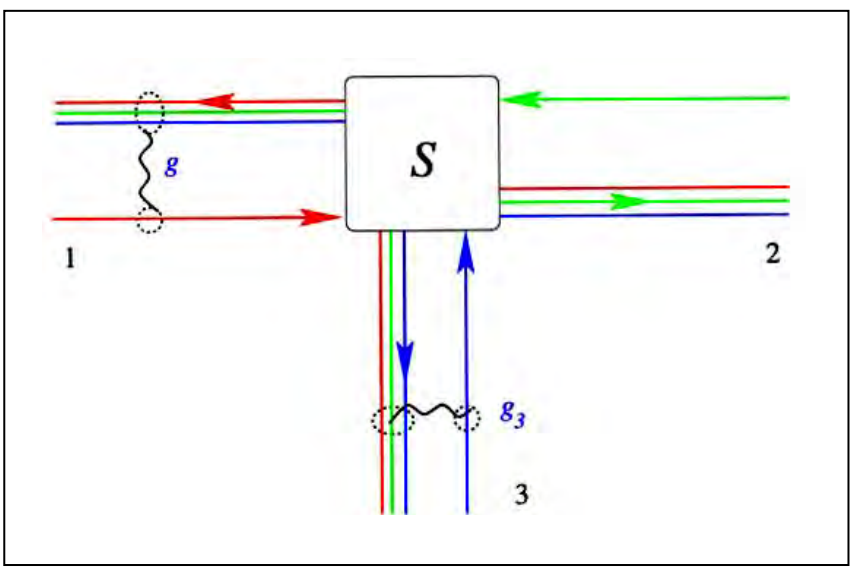

Fig. 1. *Y*-junction of three wires with interaction

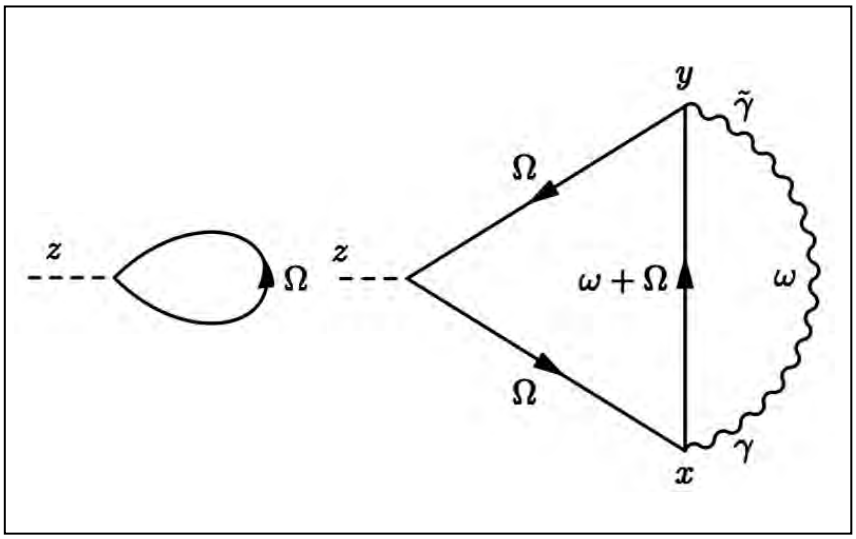

Fig. 2. First Feynman diagrams for electric current in Keldysh technique

in early 1990s. A junction of several wires (three and more) was discussed in theory in early 2000s. Effects of electronic interaction in quantum wires are usually quite essential and should be considered thoroughly. Rather sophisticated theoretical methods, developed in no connection with nanotechnologies in 1970s, were used to face this challenge. These methods, referred to earlier as "toys for theorists", became working instruments for description of quantum wires in 1990s.

The aim of our latest work was to describe the conductance renormalization of junctions of several wires, taking into account several model parameters. A few years ago, Prof. Peter Wölfle (KIT, Germany) and I developed a new method for the analysis of a single wire with an impurity. It appeared that we managed to reproduce exactly the key results obtained earlier by means of more sophisticated methods of conformal field theory.

This encouraged us to investigate a more complicated case of *Y*-junction of three wires. Compared to other existing methods, our technique is more flexible and provides more insight into physics. We have already finished a series of papers with rather exhaustive analysis of a problem of three-way junctions (Fig. 1), which includes a case of a wire tip touching the middle of a main wire.

The proposed way of analysis was generalized into a non-equilibrium situation. Initially, in order to elaborate the technique, we solved a simpler problem of an impurity in the middle of the wire, two edges of which were coupled to leads at different voltages. Instead of our usual instrument of Green's functions, we were forced to use matrix 2 × 2 functions in Keldysh formalism (Fig. 2). Currently we plan to extend our analysis towards *Y*-junction description.

The geometry of four-way *X*-junction of two wires touching in their middle is planned to be considered in the nearest future. This problem is more relevant to development of future applications, but more challenging technically.

This research was supported by the Russian Scientific Foundation (project 1422-00281).

1. *Aristov D.N.* // Phys. Rev. B. 2011. V. 83. P. 115446.
2. *Aristov D.N., Wölfle P.* // Phys. Rev. B. 2011. V. 84. P. 155426.
3. *Aristov D.N., Wölfle P.* // Phys. Rev. B. 2012. V. 86. P. 035137.
4. *Aristov D.N., Wölfle P.* // Phys. Rev. B. 2013. V. 88. P. 075131.
5. *Aristov D.N., Wölfle P.* arXiv:1408.4914.

Diffractive processes at the LHC: the role of transverse momenta of partons

M.G. Ryskin
Theoretical Physics Division, PNPI NRC "Kurchatov Institute"

Usually high-energy soft and diffractive interactions are described in the framework of the Reggeon Field Theory (RFT). The main element of interaction is the bare amplitude of high energy particle-particle scattering called the pomeron. Apart from that, multi-pomeron diagrams and interactions between the pomerons are accounted for this theory. Moreover, it was assumed that the pomeron is built of the partons, transverse momenta of which, kT, are limited and the vertices of multi-pomeron interaction are constant.

However, Quantum Chromodynamics (QCD) is a logarithmic theory with the dimensionless coupling. Therefore, in case of the BFKL pomeron, the transverse momentum of the parton may increase or decrease several times at each step of the evolution. Multi-pomeron diagrams that describe the absorptive corrections lead to a stronger absorption of low kT partons since the absorptive cross section $\sigma_{abs} \sim 1 / k_T^2$. As a result, a mean parton transverse momentum increases. This effect reveals itself strongly at high energies since the cross-section grows and thus

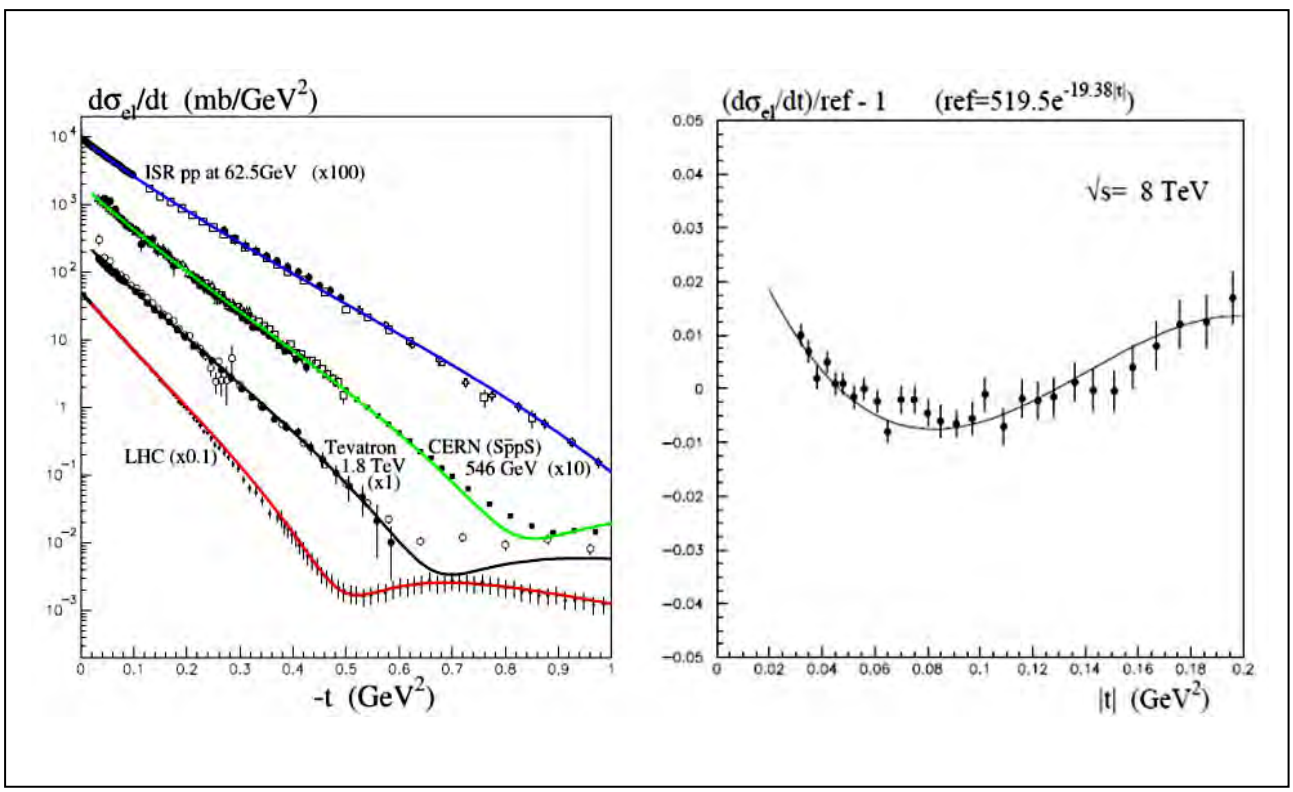

Fig. 1. Differential proton-proton cross section $d\sigma_{el} / dt$ as the function of the momentum transferred t (*left*); the deviation from the pure exponential behavior observed at $\sqrt{s} = 8$ TeV (*right*)

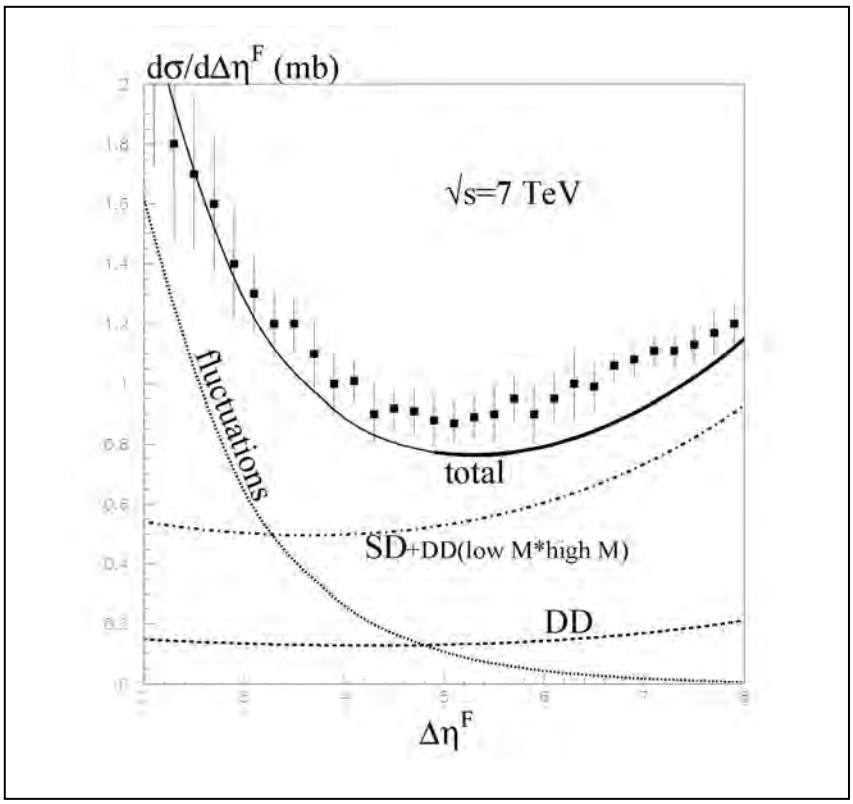

Fig. 2. Cross-section of the proton diffractive dissociation depending on the size of the Large Rapidity Gap $\Delta\eta^F$

the probability of the absorption of a low *kT* parton grows with it.

In other words, dynamics of "soft" interactions starts to be driven by the "hard" processes with larger *kT* at high energies and, due to this fact, can be described in terms of the perturbative QCD theory. Besides the increase of transverse momenta of secondaries, the growth of *kT* partons leads to diminishing of multi-pomeron vertices; these vertices are dimensionful and the value of a particular vertex is determined by the inverse value of *kT*. Correspondingly, the probability of diffractive proton dissociation diminishes.

Taking these effects into account, we succeeded to describe the behavior of total and elastic cross sections of *pp*-scattering in a broad energy interval (Fig. 1) and the probabilities of diffractive dissociation observed at the LHC both in a low- and in a high-mass region.

TOTEM Collaboration had observed an unexpectedly small cross-section ~ 2.6 +/– 2.2 mb in the case of a low mass dissociation with $M_X < 3.4$ GeV at $\sqrt{s} = 7$ TeV, which is close to the value observed at much lower CERN-ISR energies $\sqrt{s} = 30$–62 GeV. It should be noted that the elastic cross section increases in the same energy interval by about 3.5–4 times. Taking into account the energy dependence of transverse momenta *kT*, our model predicts 3.6 mb, which is in a good agreement with the experiment. The cross-section of diffractive dissociation in high-mass states are shown in Figure 2.

This research was supported by the Russian Scientific Foundation (project 1422-00281).

1. *Ryskin M.G. et al.* // Eur. Phys. J. C. 2011. V. 71. P. 1617; arXiv:1409.8451 [hep-ph].
2. *Khoze V.A. ..., Ryskin M. G.* // Eur. Phys. J. C. 2014. V. 74. P. 2756; arXiv:1402.2778 [hep-ph].

Radiative recombination and electron structure of tungsten ions in fusion and laser plasmas

M.B. Trzhaskovskaya
Theoretical Physics Division, PNPI NRC "Kurchatov Institute"

Tungsten is the main candidate for use as the plasma-facing material in International Thermonuclear Experimental Reactor ITER. The use of tungsten as a shield for the first wall is the reason for a considerable tungsten impurity in fusion plasmas. Due to its high radiative efficiency, the study of tungsten impurities is of a great importance for plasma analysis. Radiative recombination (RR) and photoionization are important mechanisms influencing the ionization equilibria and the thermal balance of fusion plasmas. In the framework of the International Atomic Energy Agency (IAEA) research project titled "Spectroscopic and Collisional Data for Tungsten from 1 eV to 20 keV", we developed a unified database, which included theoretical values of photoionization and RR cross-sections, RR rate coefficients and radiated power loss rate coefficients for all tungsten ions from W^{6+} to W^{74+}. These data are required for modeling and diagnostics of fusion plasmas.

The calculations are based on the fully relativistic treatment of photoionization and RR. All significant multipoles of the radiative field are taken into account. We used the Dirac–Fock method with the exact consideration of the electron exchange for calculations of the bound and continuum electron wave functions. The exact consideration of the electron exchange proved to be important in calculations of low-charged ions at low energies. On the contrary, relativistic and multipole effects are essential for highly-charged ions at high energies. In particular, the relativistic Maxwell–Jüttner distribution of continuum electrons used by us for the first time in the RR and radiated power loss rate calculations decreases the rates considerably at a high temperature as compared to the commonly used non-relativistic Maxwell–Boltzmann distribution.

Due to the fact that analytical expressions for the partial photoionization and RR cross-sections are convenient to use at plasma analysis, these values were approximated by a simple expression involving five fit parameters. The calculated fit parameters allow one to obtain the photoionization and RR cross-sections at any photon energy with the accuracy of no less than 2%. All the results were added to the IAEA electronic database ALADDIN.

We studied an electron structure of ions in the local thermodynamic equilibrium plasmas as well. The influence of plasma temperature and density on the energy spectrum and the level populations was considered. The PLASMASATOM code was designed on the basis of our computer program complex RAINE. Results obtained for the aluminum, iron and uranium laser plasmas were shown to correlate well with calculations performed with codes INFERNO (National Los Alamos Laboratory, 1982), PURGATORIO (Lawrence Livermore Laboratory, 2006), and PARADISIO (Atomic Energy Commissariat, CEA, France, 2009).

Our results were compared to calculations of the theoretical collaboration OPAC formed to prepare the LULI (Laboratoire pour L'Utilization des Lasers Intenses) 2010 experiments. Differences in the mean ionization stages $\langle q \rangle$ obviously imply the discrepancy between the frequency-dependent opacities (D. Gilles *et al.*, High Energy Dens. Phys. 7, 312 (2011)). These data are essential for investigation of the star atmosphere and evolution of stars in astrophysics. Mean ionization stages $\langle q \rangle$ associated with the opacity were obtained by OPAC with eleven codes using different approaches and methods. The results are demonstrated in Figure 1 for iron plasmas with the electron density $N_{el} = 3 \cdot 10^{19}$ cm^{-3} and temperature 15.3 eV $\leq kT \leq$ 38.5 eV. Our values of $\langle q \rangle$ are marked

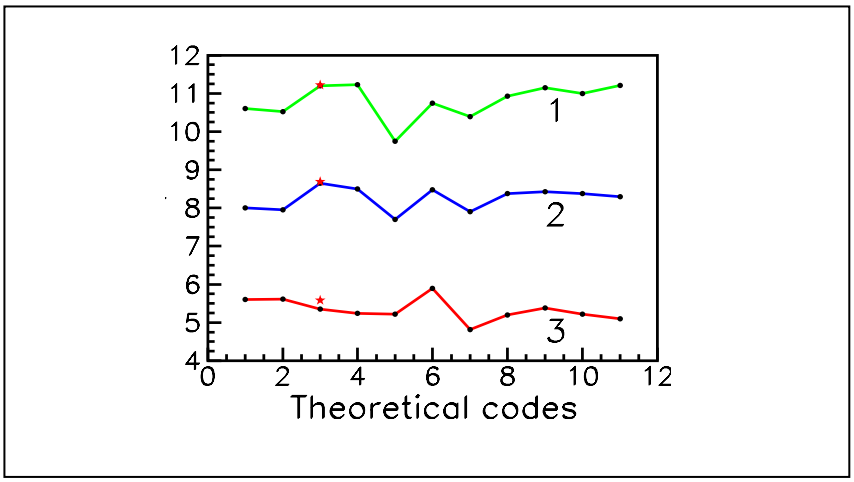

Fig. 1. Mean ionization stages <*q*> obtained by eleven various theoretical codes for iron ions in laser plasmas. 1: kT = 38.5 eV, 2: kT = 27.3 eV, 3: kT = 15.3 eV. Present calculations performed using our code PLASMASATOM are indicated with red asterisks

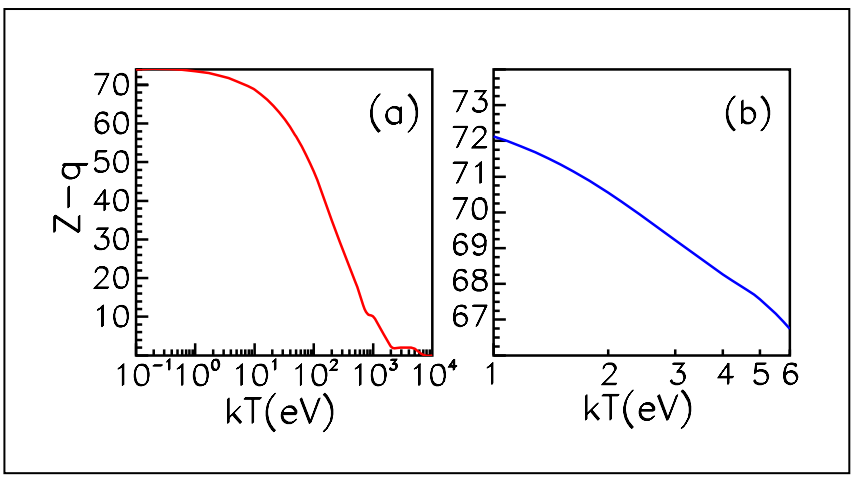

Fig. 2. A number of bound electrons of tungsten ions in laser plasmas with density $N_{ion} = 3 \cdot 10^{19}$ cm^{-3} (a) and impurity tungsten ions in fusion plasmas with density $N_{el} = 10^{14}$ cm^{-3} (b)

with red asterisks. It is evident that our results correlate well with previous calculations and practically coincide with the best results obtained with code 3 within the framework of the Opacity Project (http://cdsweb.u-strasbg.fr/topbase/). The largest difference is 4% at kT = 15.3 eV.

New calculations were performed for the dense tungsten plasmas with the ion density $N_{ion} = 3 \cdot 10^{19}$ cm^{-3} in the wide temperature range 0.1 eV ≤ kT ≤ 10 keV using the average-atom model, and for the impurity tungsten ion in fusion plasmas with electron density $N_{el} = 10^{14}$ cm^{-3} at low temperatures 1 eV ≤ kT ≤ 6 eV using the non-linear self-consistent field screening model. In Figure 2, the kT-dependence of the number of bound electrons Z–q for ions W^{q+} is presented for these two cases. The dependence demonstrates ions that are dominant at the specified plasmas temperature.

This research was supported by the Russian Scientific Foundation (project 1422-00281).

1. *Trzhaskovskaya M.B., Nikulin V.K. et al.* Horizons in World Physics. New York: Nova. 2012. V. 277. P 173–228.
2. *Trzhaskovskaya M.B., Nikulin V.K.* // At. Data Nucl. Data Tables. 2014. V. 100. P. 986–1058.
3. *Trzhaskovskaya M.B., Nikulin V.K.* // At. Data Nucl. Data Tables. 2014. V. 100. P. 1156–1188.
4. *Trzhaskovskaya M.B., Nikulin V.K.* Presentation at Final Research Coordination Meeting on project "Spectroscopic and Collisional Data for Tungsten in Plasma from 1 eV to 20 keV". Summary Report, Ed. by B.J. Braams et al., IAEA preprint No INDC(NDS)-0673. Vienna, Austria. 2014. P. 42–43.
5. *Trzhaskovskaya M.B., Nikulin V.K.* // Atoms, 2015. V. 3. P. 86–119.

Quark and lepton mixing matrices – manifestations of a violated mirror symmetry

I.T. Dyatlov
Theoretical Physics Division, PNPI NRC "Kurchatov Institute"

The invention of parity violation in weak interactions, which became the key element of the Standard Model (SM), gave a rise to a paradox that puzzled the discoverers Lee and Yang themselves. Nonconservation of parity means an absolute distinction of the left-handed (L) and right-handed (R) coordinate systems – that is an objectionable possibility of distinguishing them physically. Later, the problem became the subject of a number of subsequent studies. Lee and Yang proposed a solution of the above paradox by supplementing the observed particle system with a *mirror* system which consisted of heavier in masses particles, identical but with opposite weak properties.

The objective of the present studies is to prove that even well-known observed properties of quark and lepton systems could evidence in favor of the real existence of heavy mirror generations precisely of the type proposed by Lee and Yang. The cases in point concern the most important and at the same time the least understood SM parameters, namely observed qualitative structures of quark and lepton mass spectra and their weak mixing matrices.

In the mirror scenario, the formation mechanism for these quantities necessary includes very massive analogies of the SM fermions, which is associated with transitions through intermediate state (Fig.)

Such a simple picture is, in fact, an appropriate description of the approximate, in orders of SM mass hierarchies, complicated procedure of mass matrices diagonalization. The crucial point is the properties of the transition (q – Q) coefficients A (3 × 3 matrices in the space of generation indices)

$$A(up) = A(down),$$

"up" and "down" mean corresponding families of quarks and leptons. This equality is the necessary condition of the mirror mechanism, even its determination. The

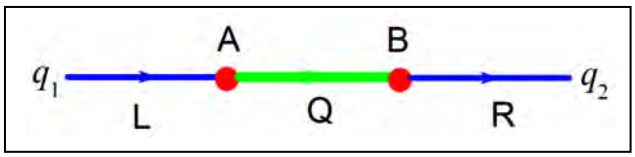

The L-R transition between SM fermions q_1 – q_2 of different generations through a very massive mirror state Q

equality is based on the invariance with respect to the weak isospin SU(2) – also the basic component of SM.

The immediate results of the analyses are the following:

1. The quark mixing matrix (CKM-matrix) acquires experimentally observed qualities: all diagonal elements are approximately close to unities, the hierarchy of nondiagonal elements with proper values appears. Such a matrix form is determined only by the SU(2) invariance and by the quark mass hierarchy. There is no need for any numerical adjustments.

2. All lepton mixing elements are of the same order in mass hierarchy perturbations. They do not depend on lepton masses in the lowest order. There is no theoretical explanation of hierarchy in elements. The lepton mixing matrix becomes completely dissimilar to the CKM-matrix. Such a behavior corresponds precisely to the properties observed in the experimental data.

3. Experimentally observed lepton properties induced by the mirror mechanism are only possible for Dirac-type neutrinos situated in the inverse mass hierarchy (two heavy neutrinos are close to each other, the light one – far enough). So we have here distinct predictions for both unanswered questions of the neutrino physics.

4. Tiny values of neutrino masses attain a new (with respect to the well-known see-saw mechanism) theoretical justification.

This research was supported by the Russian Scientific Foundation (project 1422-00281).

1. *Dyatlov I.T.* // Yad. Fiz. 2014. V. 77. P. 775; PAN 2014. V. 77. P. 793; arXiv:1312.4339 [hep-ph].
2. *Dyatlov I.T.* // Yad. Fiz. 2015. V. 78. P. 522; PAN 2015. V. 78. No. 6; arXiv:1502.01501 [hep-ph].

Computation of corrections to parameters of the Standard Model

V.N. Velizhanin – Theoretical Physics Division, PNPI NRC "Kurchatov Institute", Gatchina
A.V. Bednyakov, A.F. Pikelner – Joint Institute for Nuclear Research, Dubna

An increase of the precision of experiments requires improvement of the precision of theoretical computations. The exceptional importance of precise calculations arises due to research at the Large Hadron Collider (LHC). A recently discovered Higgs boson, being a main object of research at LHC, raises new questions that can be clarified by means of computations in the higher order of perturbative theory. One type of such calculations is the calculations of renormalization group quantities in framework of the Standard Model of the Fundamental Interactions, which were performed in collaboration with the colleagues from BLTP JINR at the third order of perturbative theory. This kind of calculations is rather cumbersome since one has to deal with an enormous number of Feynman diagrams. In order to obtain a self-coupling beta-function, one needs to evaluate about ten million Feynman integrals corresponding to different diagrams. It should be noted that it is impossible to deal with such a number of diagrams without the use of modern computers.

The most interesting application of the results obtained was found in the study of vacuum stability of the Standard Model. It is known that in the Standard Model elementary particle masses appear due to spontaneous electroweak symmetry breaking. As a result, the scalar Higgs field acquires a non-zero vacuum expectation value, which leads to generation of masses. The effective Higgs potential used for a theoretical description of this phenomenon has a minimum for certain value (Fig. 1a). This minimum is the closest to the origin of the coordinates. However, with increase of the energy, the Higgs potential may have other minimums (Fig. 1b, c) that are even deeper compared to the value of current vacuum of the Standard Model (Fig. 1c). Then the question arises whether this vacuum state is stable or whether there is a possibility of the transition of the current vacuum expectation value to other possible value. Increase of the accuracy of theoretical calculations allows us to improve our understanding of behavior of the Higgs potential.

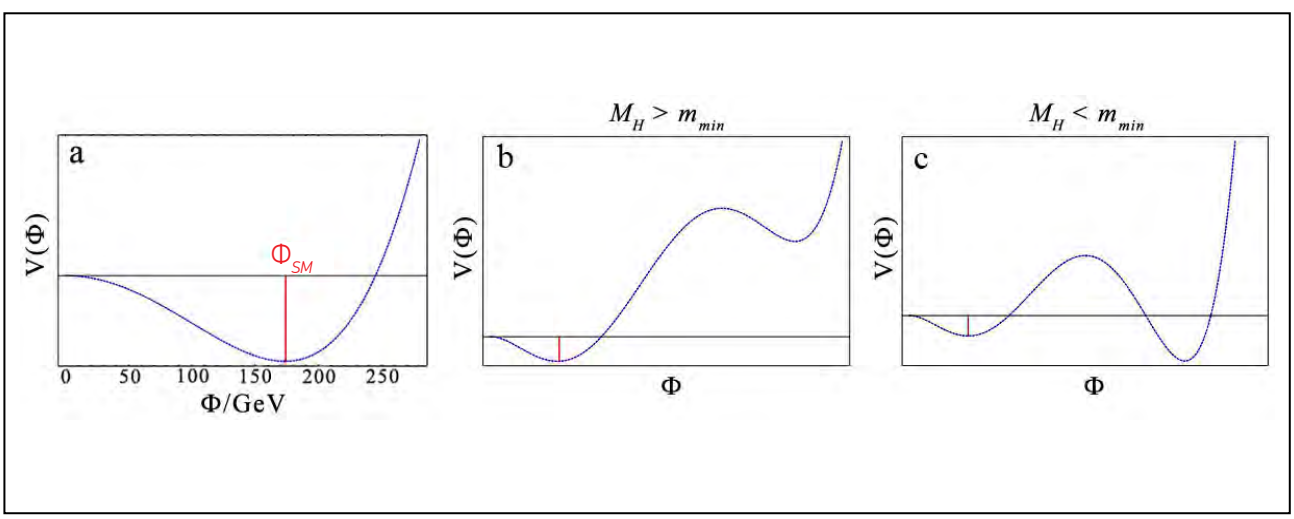

Fig. 1. The Higgs potential: minimum realized in the Standard Model (a); local minimum at large scales is higher than the current value (b); local minimum at large scales is deeper than the current value, which may lead to instability of vacuum (c)

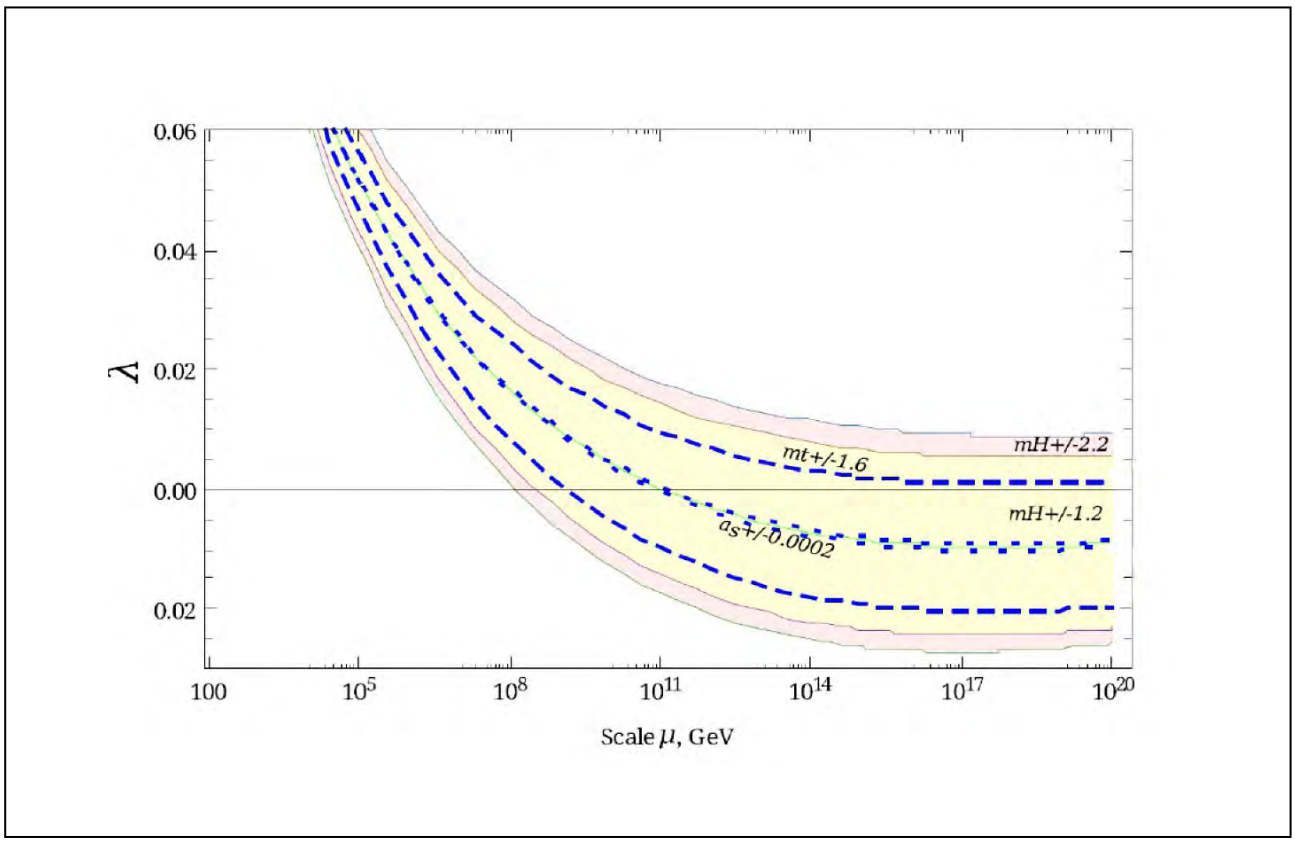

Fig. 2. Renormalisation group analysis of the evolution of the Higgs self-coupling. The change of the sign is interpreted as a possible instability of electroweak vacuum (an existence of another minimum in the Higgs potential)

The results of analysis performed with the use of our computations show that the Higgs potential indeed may change the sign at a very high energy (Fig. 2). However, at the moment the precision of theoretical computations is significantly higher than the precision of experimental data (uncertainty of the top-quark mass first of all) and we can not specify the possibility that is realized in nature.

This research was supported by RFBR grant (project 12-02-00412-a).

1. *Bezrukov F., Kalmykov M.Y., Kniehl B.A., Shaposhnikov M.* // JHEP. 2012. V. 1210. P. 140.
2. *Bednyakov A.V., Pikelner A.V., Velizhanin V. N.* // JHEP. 2013. V. 1301. P. 017.
3. *Bednyakov A.V., Pikelner A.V., Velizhanin V. N.* // Phys. Lett. B. 2013. V. 722. P. 336.
4. *Bednyakov A.V., Pikelner A.V., Velizhanin V. N.* // Nucl. Phys. B. 2013. V. 875. P. 552.

Theory of heavy-fermion compounds – theory of strongly correlated Fermi-systems

V.R. Shaginyan
Theoretical Physics Division, PNPI NRC "Kurchatov Institute"

The theory of Fermion condensation of strongly correlated Fermi-systems is stated in the book "Theory of Heavy-Fermion Compounds" (Amusia M.Ya., Popov K.G., Shaginyan V.R., Stephanowich W.A. Berlin: Springer, 2014. V. 182. 359 p.). This theory became a basis for explanations of numerous important experimental facts collected in modern physics of strongly correlated Fermi-systems that attracts interest of modern scientists. Heavy-fermion (HF) compounds are represented by such strongly correlated Fermi-systems as HF metals, high-temperature superconductors, quantum spin liquids, quasicrystals, and two-dimensional Fermi-systems. With regard to experimental facts observed in physics of theory of strongly correlated systems, it is necessary to revise many sections of physics of solid state and liquids. At the same time there are effects that are absent in usual physics of solid state. For example, violation of the particle-hole symmetry, or violation of the Wiedemann–Franz law, *etc*. One might say that the physics of HF compounds represents a new edition of the condensed matter physics, as the observed behavior is quite unique; though, the edition is still not complete. Therefore, the problem of presenting a theory of HF compounds is both arduous and of a great importance.

Having studied the book, the reader will find that the most various strongly correlated Fermi-systems have the identical universal scaling behavior other than the observed behavior in usual metals and Fermi-liquids. Such behavior, revealed within the original theory of strongly correlated Fermi-systems formulated in the book, allowed the authors to draw a conclusion that a new state of matter possessing unique properties is realized in these systems.

In particular, this new state is realized, perhaps, in quantum spin liquids, which, as recent pilot and theoretical studies show, belong to strongly correlated Fermi-systems. Exotic quantum spin liquid consists of spinons, which are quasiparticles with spin of 1/2 and of zero electrical charge. Recent experiments on magnetic insulators with almost flat bands containing spinons shed light on the nature of the quantum spin liquid made of spinons.

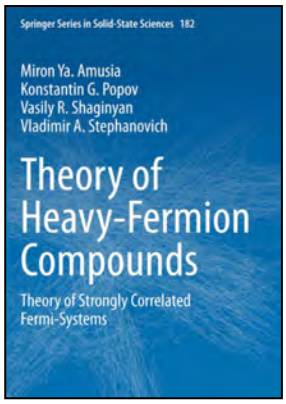

The theory of thermodynamic, relaxation and transport properties characteristic for HF compounds, including quantum spin liquid, is presented in the book. It offers the explanation for modern experimental data. Particularly, it is shown there that magnetic insulators behave as strongly correlated metals, the low-temperature thermodynamics, transport and relaxation properties of which are defined by strongly correlated quantum spin liquid. Thus, recently opened magnetic insulators of a new type possess all properties of strongly correlated metals with one exception: they do not conduct electric current. However, they can support spin current responsible for the heat conductivity at low temperatures.

For convenience of the reader, the analysis of strongly correlated Fermi-systems is carried out on the basis of characteristic and significant experimental facts. Numerous calculations of thermodynamic, relaxation and transport properties of strongly correlated Fermi-systems, being in good consent with experimental facts, help the reader to grasp both the theory, and its numerous appendices. Various experiments analyzed in detail, as a rule, do not find explanations within the other existing theories of strongly correlated Fermi-systems. The main content of the book is based on the original papers of its authors published in the best international scientific journals. The book demonstrates that the theories of fermion condensation offer an unexpectedly simple and at the same time complete description of strongly correlated Fermi-systems.

This research was supported by the Russian Scientific Foundation (project 1422-00281).

BFKL pomeron and the vacuum structure in QCD

L.N. Lipatov
Theoretical Physics Division, PNPI NRC "Kurchatov Institute"

The equation of Balitsky, Fadin, Kuraev and Lipatov (BFKL) for the pomeron wave function at the vanishing momentum transfer q in the leading logarithmic approximation (LLA) can be written as follows (taking into account the asymptotic freedom in QCD):

$$\omega f_\omega(t) = \frac{1}{\beta_0 t}\chi(\hat{\nu}) f_\omega(t),$$

where $j = 1 + \omega$ is a complex spin of the pomeron responsible for the growth of hadron cross-sections; $k_\perp^2$ – are virtualities of two reggeized gluons inside the pomeron. The following notations were used as well:

$$t = \ln\frac{k_\perp^2}{\Lambda_{QCD}^2};\ \hat{\nu} = -i\partial_t;\ \beta_0 = \frac{11}{12} - \frac{n_f}{18};$$

$$\chi(\nu) = 2\psi(1) - 2\Re\psi(\frac{1}{2} + i\nu).$$

Further in the paper, we will discuss an influence of the strong coupling region with $k_\perp^2 \sim \Lambda_{QCD}^2$ on the pomeron spectrum in LLA. A simple solution of the BFKL equation has the following form:

$$f_\omega(t) = \int_{-\infty}^{\infty} d\nu e^{it\nu} g_\omega(\nu);$$

$$g_\omega(\nu) = \left(\frac{\Gamma(\frac{1}{2} + i\nu)}{\Gamma(\frac{1}{2} - i\nu)} e^{-2i\nu\psi(1)}\right)^{\frac{1}{\beta_0\omega}}.$$

Analogously, one can construct a particular solution for the Green function:

$$G_\omega^0(t,t') = -\frac{it'}{\omega}\int_{-\infty}^{\infty}\frac{d\nu}{2\pi}e^{it\nu}g_\omega(\nu)\int_{-\infty}^{\infty}\frac{d\nu'}{2}\varepsilon(\nu +$$

$$+\nu')e^{it'\nu'}g_\omega(\nu');\ \varepsilon(x) = x/|x|.$$

The general solution G_ω compatible with boundary conditions at $\omega > 0$ is given below

$$G_\omega(t,t') = G_\omega^0(t,t') + \frac{t'}{4\pi\omega}\cot\phi(\omega) f_\omega(t) f_\omega(t').$$

Non-perturbative effects at $|k_\perp^2| \sim \Lambda_{QCD}^2$ are taken into account in the function $\phi(\omega)$. It is equal to the difference of phases $\delta_\omega^{np}(t)$ and $\delta_\omega^{p}(t)$ of wave functions evolved from a small and large t, respectively. For example, one can consider the case of gluons obtaining a non-perturbative mass $m \approx 2.7\ \Lambda_{QCD}$ in QCD and pomeron wave functions going to zero at $t = 0$ in accordance with numerical estimates of the phase $\delta_\omega^{np}(t)$ at the Higgs model. In quasi-classical approximation $\phi(\omega) \approx 1/4 + 0.40862/\omega$ and, therefore, the pomeron spectrum is defined approximately by the simple expression

$$\omega_k \approx \frac{0,40862}{k + 3/4},\quad \text{at}\quad k = 0, 1, 2...$$

This result coincides with the exact spectrum obtained from the quantization condition $f_\omega(0) = 0$.

One can construct pomeron wave functions for an arbitrary momentum transfer q using the conformal invariance of the BFKL equation. These functions are expressed in terms of the following simple solution with an integer conformal spin n at $q = 0$:

$$f_\omega(t,\theta,n) = e^{i\theta\nu}\int_{-\infty}^{\infty} d\nu e^{it\nu} g_\omega(\nu,n);$$

$$g_\omega(\nu,n) = \left(\frac{\Gamma(\frac{1}{2}+i\nu+\frac{|n|}{2})}{\Gamma(\frac{1}{2}-i\nu+\frac{|n|}{2})} e^{-2i\nu\psi(1)}\right)^{\frac{1}{\beta_0\omega}}.$$

In a similar way, one can find a particular solution for the Green function:

$$G^0_\omega(t,\theta,t',\theta') =$$

$$= -\frac{it'}{\omega}\sum_{n=-\infty}^{\infty}\frac{e^{in(\theta-\theta')}}{2\pi}\int_{-\infty}^{\infty}\frac{d\nu}{2\pi}e^{it\nu}g_\omega(\nu,n)\int_{-\infty}^{\infty}\frac{d\nu'}{2}\,\varepsilon(\nu+$$

$$+\nu')e^{it'\nu'}g_\omega(\nu',n).$$

The physical Green function

$$G_\omega(t,\theta,t',\theta',q) = G^0_\omega(t,\theta,t',\theta') +$$

$$+\frac{t'}{4\pi\omega}\sum_{n=-\infty}^{\infty}\frac{e^{in(\theta-\theta')}}{2\pi}\cot\phi_\omega(n,q)f_\omega(t,n)f_\omega(t',n)$$

depends on the parameter $\phi\omega(n, q)$ equal to the difference of phases $\delta^{np}_\omega(t,n,q)$ and $\delta^{p}_\omega(t,n)$ for the pomeron wave function in its evolution from large and small t, respectively. The spectrum of the Regge trajectories $\omega_k(n, q)$ can be found from the equation $\varphi_{\omega_k}(n, q) = \pi k$ taking into account that the phase δ^{np} generally depends on q / Λ_{QCD} due to the fact that the running QCD coupling constant freezes at $k_\perp \sim q$. An example of such dependence was constructed in the paper of de Vega et al. where the BFKL pomeron was considered at a thermostat with $T \neq 0$. Physically, it corresponds to the model, in which the two-dimensional space of impact parameters $\vec{\rho}$ has a topology of the surface of a cylinder with the symmetry axes directed along $\vec{q}$ and the radius $R = 2\pi / T \sim 1 / \Lambda_{QCD}$. As it is commonly believed, the physical vacuum in QCD appears as a result of the monopole condensation generating the dual Meissner effect of repulsing the chromo-electric field created by quarks and gluons. As a consequence of it, each hadron (including the pomeron) contains a drop (or a bag) of the bare vacuum, which leads to the confinement of quarks and gluons. Indeed, initially, the intercept of the BFKL pomeron increases with growing T, which is explained by an additional attraction between two reggeized gluons due to a string produced as a result of the dual Meissner effect. In order to consider the influence of the vacuum structure in QCD on the pomeron spectrum in more detail, one should construct (and solve) the BFKL equation on compact Riemann surfaces containing several additional parameters.

This research was supported by the Russian Scientific Foundation (project 1422-00281).

1. *Kowalski H., Lipatov L. et al.* // Phys. Part. Nucl. 2013. V. 44. P. 547; arXiv:1401.6298[hep-ph].
2. *De Vega H., Lipatov L.N.* // Phys. Part. Nucl. 2013. V. 44. P. 515.
3. *Levin E.M., Lipatov L.N. et al.* // Phys. Rev. D. 2014. V. 89. P. 074002.

The search for *P*- and *T*, *P*-odd effects in diatomic molecules

L.V. Skripnikov, A.N. Petrov, A.D. Kudashov, N.S. Mosyagin, A.V. Titov
Knowledge Transfer Division, PNPI NRC "Kurchatov Institute"

The existence of nonzero permanent electric dipole moment (EDM) of elementary particles (in case of charged particles, it is the shift of the centre of charge from the centre of mass multiplied by the charge of the particle; the shift direction is collinear to the particle spin) refers to the existence and manifestation of fundamental interactions that violate not only the spatial parity (*P*), but also the temporal invariance (*T*). The nature of interactions that violate *T*-invariance (in accordance with the *CPT*-theorem, a violation of *T*-invariance also means violation of *CP*-invariance, where the operation C is the charge conjugation) is still unclear. It cannot be explained within the framework of the Standard Model, which combines strong, electromagnetic and weak (which violates *P*) interactions. The discovery of the EDM of elementary particles may shed light on the mechanism of manifestation of "ultra-weak" (*CP*- and *T*-odd) interactions. The search of EDM of an elementary particle is regarded as one of the most urgent problems of modern physics, in the context of understanding the mechanism of *CP*-violation and existence of supersymmetry and other extensions of the Standard Model in nature.

In 70th–80th of the last century, it was shown that the experiments aimed at the measurement of the electron EDM on molecules or solids containing heavy atoms, are very promising. In such compounds, one can achieve an extremely strong internal effective electric field E_{eff}, affecting the electron EDM, which leads to appearance of the measurable energy of interaction of E_{eff} with electron EDM (see Fig.). However, the magnitude of E_{eff}, required for "extraction" of the electric dipole moment from the experimental data may be obtained only on the basis of theoretical calculations. Our group has developed a two-step method for calculating these and other characteristics required for the experiment. The two-step approach avoids major obstacles encountered in the case of direct relativistic calculation.

At the end of 2013, using the experimental restriction to the frequency of precession of the magnetic moment of ThO molecule in a metastable $H^3\Delta_1$ state in an external electric field and the value of the effective electric field, the new most rigid restriction to the electric dipole moment of the electron was obtained. A remarkable achievement of these two studies is that the new resulting restriction, $d_e < 8.7 \cdot 10^{-29}$ $e \cdot$ cm, is more than an order of magnitude greater than the previously obtained constraints on the YbF molecule ($d_e < 1.05 \cdot 10^{-27}$ $e \cdot$ cm, 2011) and thallium atoms ($d_e < 1.6 \cdot 10^{-27}$ $e \cdot$ cm, 2002). The new restriction to the electric dipole moment of the electron is by itself a serious challenge for popular extensions of the Standard Model, primarily supersymmetry which predicts the existence of the electron EDM at the level of $d_e \sim 10^{-26}$–10^{-29} $e \cdot$ cm. It should be noted that the observation of the electric dipole moment of an electron at the level significantly greater than 10^{-38} $e \cdot$ cm (prediction of the Standard Model) will indicate the presence of a New physics beyond the Standard Model (popular extensions of the Standard Model predict the electron EDM level of 10^{-27}–10^{-30} $e \cdot$ cm). This result also demonstrates unique possibilities of not only modern molecular experiments but also theoretical methods (precision *ab initio* relativistic calculations of the electronic structure of molecules with heavy atoms), developed by our group previously. This result is at least as significant as "potential opportunities" of experiments aimed at the study of *CP*-invariance of the Large Hadron Collider at CERN.

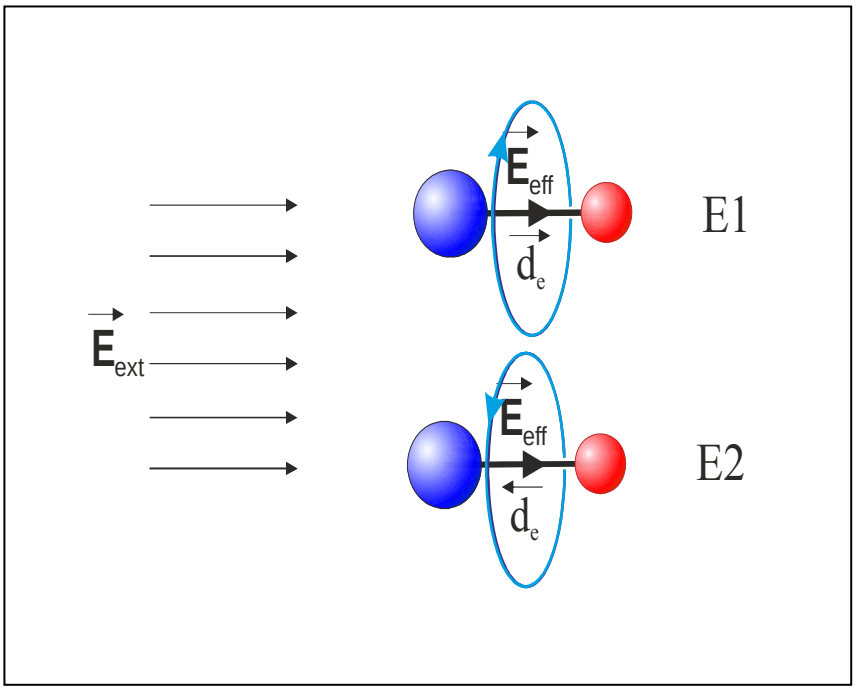

Measurement of the interaction energy ($E1$, $E2$) of the internal effective field (E_{eff}) and the electric dipole moment of an electron (d_e) with opposite directions of projection of the total angular momentum to the molecular axis, taking into account that $|E1 - E2| = 2|d_e \cdot E_{eff}|$

In 2013, only the first series of experiments on the ThO molecule was completed. At present, a new series of experiments is being prepared; in these experiments, one expects to improve the sensitivity by an order of magnitude. In 2014, in collaboration with ACME, we analyzed the ability to perform experiments on the second rotational sublevel of ThO molecules instead of the first one, as it was done in the experiment of 2013. As it is shown in the paper, it will reduce the number of systematic errors, i.e. one will be able to carry out the experiment more accurately.

In addition to ThO molecule, our group considered other systems, which could be used to carry out experiments aimed at the search for effects of spatial and temporal symmetry in fundamental interactions in the future. One of such systems is the molecular radical RaF. We performed a theoretical study of this system. It is shown that the effective electric field in it is about 50 GV/cm, which is very large. In addition, it is suggested that it will be possible to use RaF in order to search for other effects, in particular the so-called anapole and nuclear Shiff moments.

1. *ACME Collaboration* // Science. 2013. V. 343. No. 6168. P. 269–272.
2. *Skripnikov L.V., Petrov A.N., Titov A.V.* // JCP Communication. 2013. V. 139. P. 221103.
3. *Petrov A.N., Skripnikov L.V., Titov A.V. et al.* // Phys. Rev. A. 2014. V. 89. P. 062505.
4. *Kudashov A.D., Petrov A.N., Skripnikov L.V., Mosyagin N.S., Isaev T.A. ..., Titov A.V.* // Phys. Rev. A. 2014. V. 90. P. 052513.

Chemistry of elements from the island of stability

A.V. Zaitsevskii, Yu.A. Demidov
Knowledge Transfer Division, PNPI NRC "Kurchatov institute"

The existence of long-living superheavy nuclides, which appear on the map in the coordinates "atomic number Z – number of neutrons N" as an island surrounded by the sea of unstable nuclides, had been predicted several decades ago. The peaks on this island corresponding to the nuclei with lifetimes comparable to the age of the Earth are presumably located at Z = 114 and 126 and N = 184. Several isotopes of nuclei with Z = 112–117 (i.e. in the range that is characteristic for the island of stability) have been successfully synthetized in Flerov Laboratory of Nuclear Reactions (JINR, Dubna). Being still quite far from the peaks of stability because of their neutron deficiency, these nuclei have lifetimes long enough (seconds and even dozens of seconds) to turn to neutral atoms and to enable the studies of the chemical reactions of the latter. At present, the yield of superheavy elements is very small, about one atom per week (atom-at-a-time regime), and up to now, gas thermochrogratography remains the only experimental technique successfully applied to investigate the chemistry of elements with Z = 112 and more. The only physical / chemical property that can be determined this way is the adsorption energy. Its values have been found with reasonable accuracy for E 112 (Cn) and E 114 (Fl) on the surface of gold; there are also rough estimates of adsorption energy of element 113 on the same adsorbent.

Electronic structure modeling of superheavy element compounds is a much more universal source of information on physical and chemical properties of the elements from the island of stability, offering the possibility to predict various characteristics of their compounds. This is necessary both in order to search for the superheavy elements in nature and to plan experimental studies of their chemistry.

One should not underestimate the difficulties of the first principle based modeling of superheavy element chemistry. The speed of electrons in the vicinity of superheavy nuclei is huge, and non-relativistic description of electron subsystems of chemical compounds becomes senseless and cannot be used even as a zero-order approximation. Spin symmetry widely used for reducing the computational work in "normal" quantum chemistry is completely broken. Spatial shell structure in superheavy atoms is blurred, complicating the correlation treatment and the conventional separation of electronic shells into core and valence subsets. Nevertheless, significant progress in first principle based modeling has been achieved.

New electronic structure modeling technologies developed in the Laboratory of Quantum Chemistry of PNPI have enabled us to build models yielding superheavy element adsorption energies in a quantitative agreement with the available experimental data (Fig. 1). The striking difference of Fl (eka-Pb) chemical properties from those of Pb and a certain analogy between Fl and heavy rare gases have been confirmed. The results of thermochromatographic experiments for some other elements from the island of stability have been predicted. Systematical calculations of simple compounds of these elements with common light elements provided insight into specific manifestations of the periodic law related to the unprecedented role of the effects of relativity. One can note, for instance, the subperiodic structure of the seventh period and striking differences between Cn and Fl and their homologues (Fig. 2). In contrast, the changes of properties in passing from "normal" heavy elements to the elements of the island of stability in groups 1 and 2 are regular, so that elements 119 and 120 are alkaline and alkaline earth metals respectively.

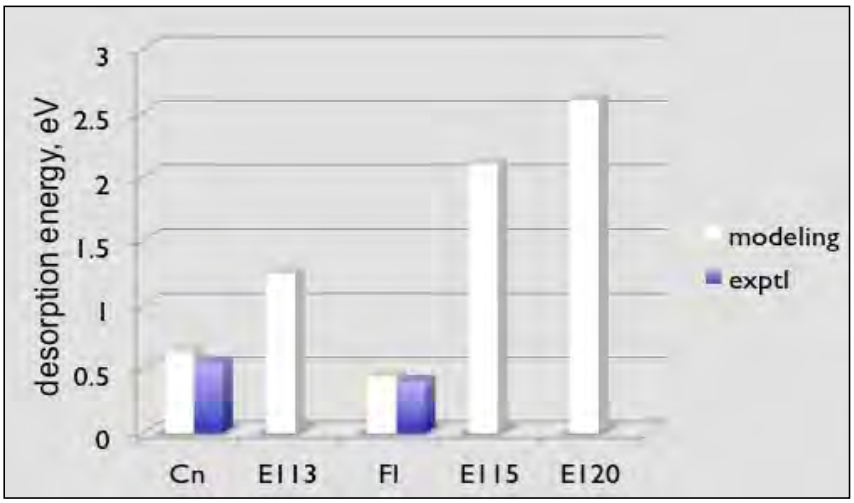

Fig. 1. Calculated and experimental values of desorption energy from the gold surface for some elements from the island of stability

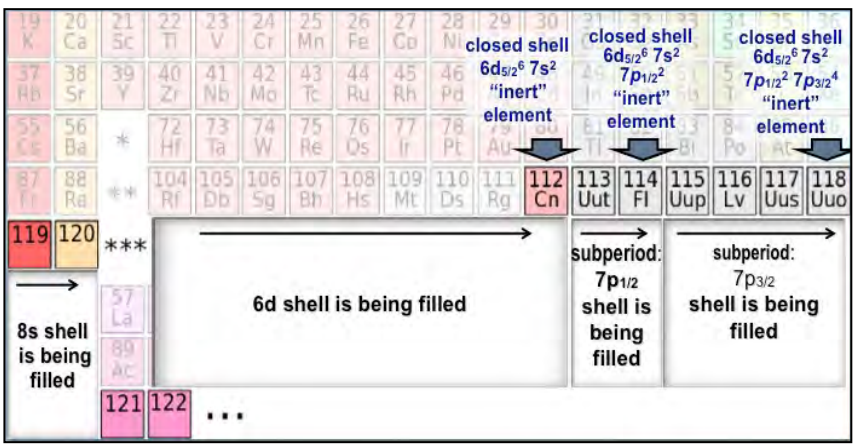

Fig. 2. Subperiodic structure of the seventh row of the periodic table caused by the extremely strong relativistic stabilization of 6*s* и $7p_{1/2}$ shells

Nowadays both experimental and theoretical studies are focused on the chemistry of element 113, the only non-inert element of the unique short subperiod composed of this element and flerovium. Its atomic configuration, a single *p* electron outside of the stable (in a sense, rare-gas-like) closed shell, has no analogs in the periodic table. We have already shown that its chemistry should be radically different from that of its formal homologue, thallium. Furthermore, the hydroxide of E 113 has good chances of becoming the first experimentally detected gas-phase compound of an element from the island of stability, and we had obtained very accurate estimates for various properties of this compound.

1. *Demidov Yu.A., Zaitsevskii A.V. et al.* // Phys. Chem. Chem. Phys. 2014. V. 16. P. 2268.
2. *Demidov Yu.A., Zaitsevskii A.V.* // Russ. Chem. Bull. 2014. No. 8. P. 1647 (Russ. pag.).

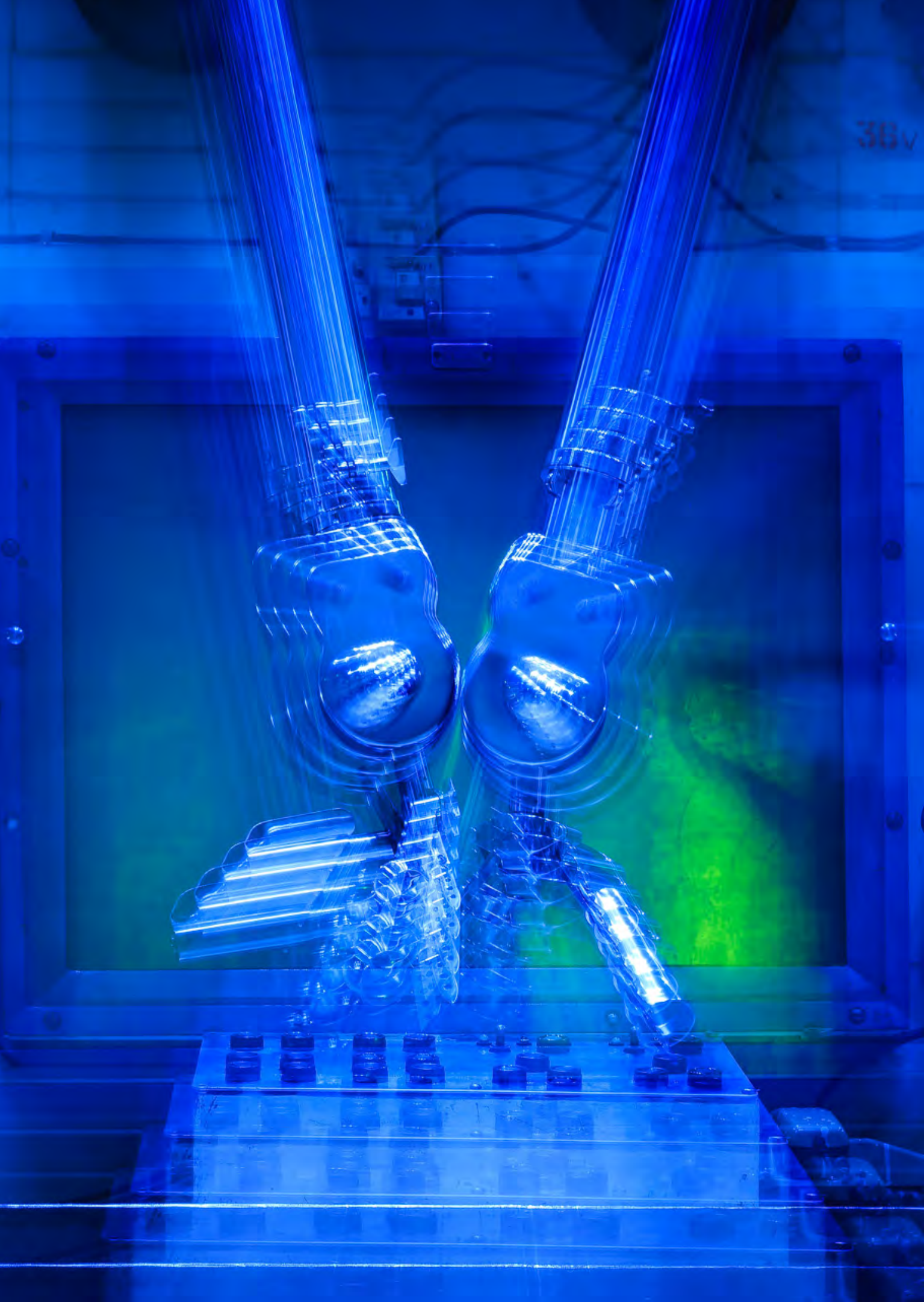

Research Based on the Use of Neutrons, Synchrotron Radiation and Muons

New measurements of the neutron electric dipole moment with the use of the PNPI Double-Chamber Electric Dipole Moment Spectrometer

A.P. Serebrov
Neutron Research Division, PNPI NRC "Kurchatov Institute"

Search for the neutron electric dipole moment (EDM) in low energy physics is an alternative to the search for new particles in high energy physics at hadron colliders. The value or a new limit of the value of neutron EDM is a very sensitive test for a choice of the theory with *CP* violation. This work presents the results of measurements of neutron EDM carried out at ILL reactor (Grenoble, France) on the PNPI experimental installation. The double-chamber magnetic resonance spectrometer capable of holding the ultracold neutrons for a long time was used to carry out the experiments. The results obtained determine the upper limit for neutron EDM $|d_n| < 5.5 \cdot 10^{-26}\ e \cdot$ cm at 90% confidence level. This accuracy of measurements corresponds to the level of a modern experimental limit for the neutron EDM value. The possibility to obtain a new result and the confirmation of the existing limit in independent experiment on other installation is essentially important for this fundamental problem.

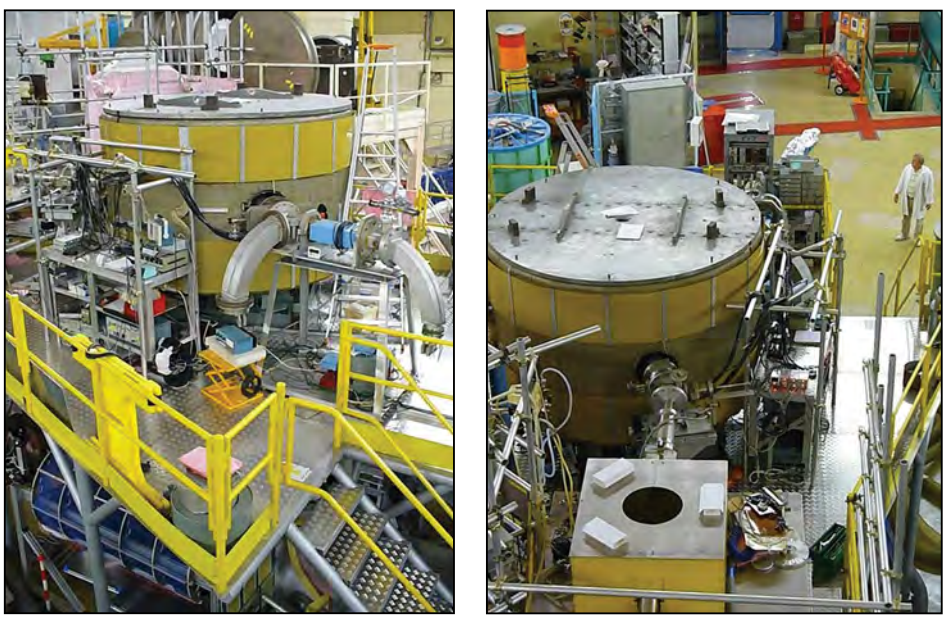

PNPI spectrometer used for the neutron electric dipole moment search at the ultracold neutron beam of the Institute Laue–Langevin

1. *Serebrov A.P., Kolomenskiy E.A., Pirozhkov A.N. et al.* // JETP Letters. 2014. V. 99(1). P. 7–11.
2. *Serebrov A.P., Kolomenskiy E.A., Pirozhkov A.N. et al.* // PNPI preprint 2956. Gatchina, 2014. P. 43.
3. *Serebrov A.P., Kolomenskiy E.A., Pirozhkov A.N. et al.* // Physics of Particles and Nuclei Letters. 2015. V. 12(2). P. 286–296.

Resonance behavior of refraction index for neutrons moving in a perfect crystal close to the Bragg condition

V.V. Fedorov
Neutron Research Division, PNPI NRC "Kurchatov Institute"

A new phenomenon was found for neutrons, moving through a perfect crystal close to the Bragg condition. Dispersive (resonant) behavior of refraction index for neutrons is observed when the neutron energy approaches the Bragg one. It is shown that in this case a small variation of the neutron energy by a value of an order of the Bragg (Darwin) width ($\Delta E/E \sim 10^{-5}$) leads to significant (by a few tens percent) change of the neutron–crystal interaction potential.

This resonant energy dependence of neutron refraction index leads to the discovery of another new effect – a neutron acceleration found experimentally for neutrons passing through the accelerated perfect crystal for neutron energies close to the Bragg ones. The effect is caused by the change of the parameter of deviation from the exact Bragg condition during the neutron time-of-flight through the accelerated crystal (Fig. 1). As a result, the refraction index changes as well and so does the velocity of outgoing neutron (Fig. 2).

One should take this phenomenon into account in precise neutron optical experiments, because the neutron refraction index is determined not only by an averaged crystal potential, but also by its harmonics which have the same order of value as the average potential itself.

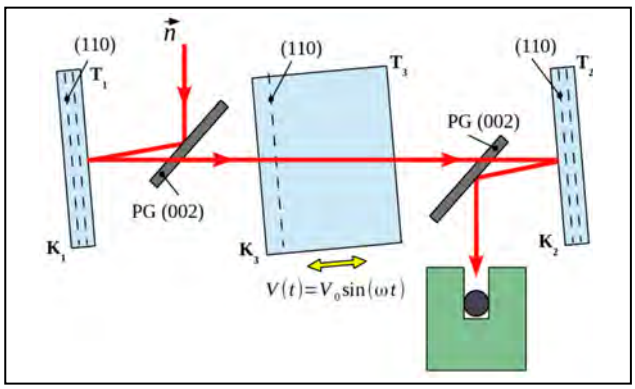

Fig. 1. Scheme of the experiment

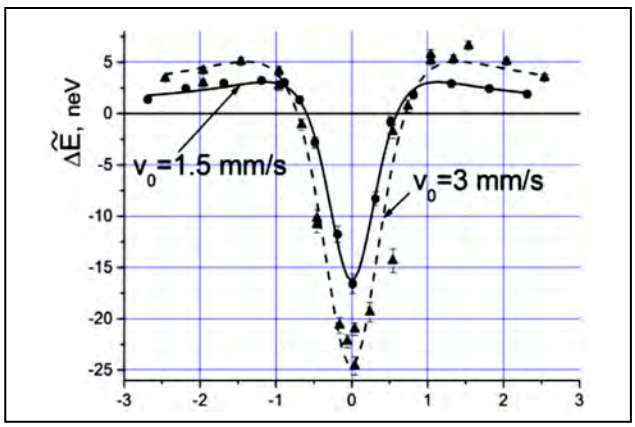

Fig. 2. Neutron acceleration effect for neutrons passing through the accelerated crystal

Voronin V.V., Berdnikov Ya.A., Berdnikov A.Ya., Braginetz Yu.P., Vezhlev E.O., Kuznetsov I.A., Lasitsa M.V., Semenikhin S.Yu., Fedorov V.V. // JETP Letters. 2014. V. 100. No. 8. P. 497–502.

Neutron channeling in layered Cu/Ti/Cu structures

V.L. Aksenov – Petersburg Nuclear Physics Institute NRC "Kurchatov Institute", Gatchina
Yu.V. Nikitenko – Joint Institute for Nuclear Research, Dubna
V.V. Proglyado – Institute of Metal Physics Ural Branch of RAS, Yekaterinburg

The phenomenon of particle channeling in solids is quite known. The channeling phenomenon is considered to be an enhancement of emission of particles during their propagation along a channel singled out in a medium. In a layered structure, the structure layers play a role of such singled out channels for neutrons. There is a very important condition that must be fulfilled for channeling: near the interface between the layer and the environment, the neutron–medium interaction must make the neutron return to the layer. Obviously, for such a reflection the particle potential energy must exceed its kinetic energy in the direction perpendicular to the layer boundary. At channeling, the irradiation cross-section in the direction along the channel, as a rule, is less than in other directions. The interest in the study of the phenomenon of neutron channeling is caused by the relevant phenomenon of multiple interactions between neutrons and boundary layers or the inhomogeneous layer structure. In this context, it should be expected that the accuracy of measurements can be increased and highly collimated and monochromatic neutron beams can be obtained in the case of channeling. Moreover, it was shown recently that the formation of enhanced standing neutron waves is related to the channeling phenomenon. In this relation, measurements of neutron channeling length (NCL) became important.

We performed measurements of the NCL for a Cu (33 nm)/Ti (350 nm)/Cu (150 nm)/ glass (5 mm) structure that was prepared at PNPI NRC "Kurchatov Institute". A substrate made of a glass with the thickness of 5 mm had dimensions of 6 cm (width) × 8 cm (length). Glass and cadmium plates with 3 mm thickness each were placed on Cu (33 nm) layer.

Experiments were performed at ILL (Grenoble) with ADAM reflectometer, neutron wavelength was λ = 4.4 Å. Only neutrons exiting from the layer ends were recorded in this study. Grazing angle varied in the range of 0.05–0.038°, which corresponds to variation in the neutron wave vector in the range $k_z = 1.25 \cdot 10^{-4} – 9.5 \cdot 10^{-3}$ Å^{-1}.

The Figure below shows that the experimental data corresponds more to channeling in Cu layer. At small values of $k_z < 0{,}004$ Å^{-1} the channeling process is going in both Cu and Ti layers with equal probability.

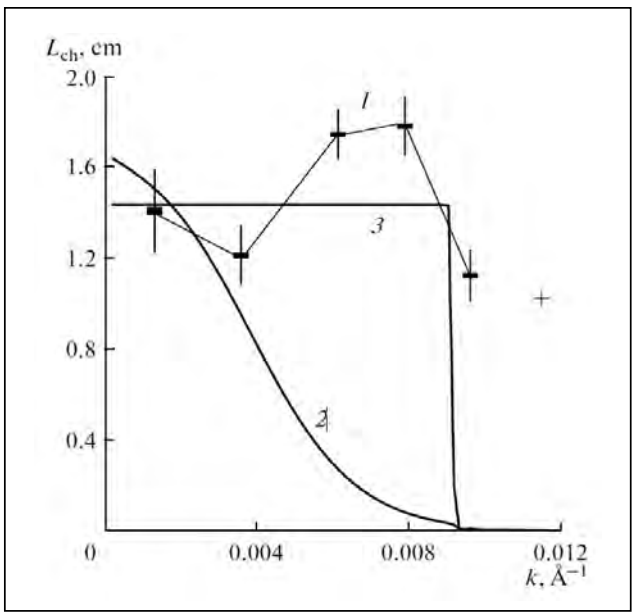

Dependence of NCL (L, cm) on k_z(Å^{-1}); 1 – experimental data; 2 – calculations for the Ti layer; 3 – calculations for the Cu layer

Nikitenko Yu.V., Proglyado V.V., Aksenov V.L. // Journal of Surface Investigaton. *X*-ray, Synchrotron and Neutron Techniques. 2014. V. 8. No. 5. P. 961–966.

Antisymmetrical exchange in RMn$_2$O$_5$ multiferroics

I.A. Zobkalo, S.V. Gavrilov
Neutron Research Division, PNPI NRC "Kurchatov Institute"

The family of rare-earth manganates RMn$_2$O$_5$ (R – rare-earth element) was causing a great interest recently due to impressive magnetoelectric effects that take place in its compounds.

Various models were considered in order to identify the mechanism (-s) of origin of a magnetoelectric interaction in RMn$_2$O$_5$ multiferroics. These theories are mainly based on two types of exchange interaction: the symmetric Heisenberg exchange described by a scalar product of spins of interacting ions ($\mathbf{S}_1 \cdot \mathbf{S}_2$), and the antisymmetric exchange of Dzyaloshinsky–Moriya, described by vector product [$\mathbf{S}_1 \times \mathbf{S}_2$].

For the purposes of clarification of microscopic mechanisms of magnetoelectric interactions in RMn$_2$O$_5$, a neutron research was performed on single crystals of multiferroics TbMn$_2$O$_5$, Tb$_{1-x}$Ce$_x$Mn$_2$O$_5$, and non-ferroelectric counterpart NdMn$_2$O$_5$. A difference in number of the "right" and "left" spirals was determined by means of the technique of the diffraction of polarized neutrons.

Dependence of the scattering intensity on the direction of polarization was observed in compounds of multiferroics TbMn$_2$O$_5$, Tb$_{1-x}$Ce$_x$Mn$_2$O$_5$. This fact confirms the difference in population of the domains with "right" and "left" spirals (~ 50%) which remained a constant for all magnetic phases (Fig.). Such dependence is not observed for any magnetic satellites in the non-ferroelectric isostructural crystal of NdMn$_2$O$_5$ at all temperatures of magnetic ordering.

It is known that antisymmetric interaction defines the primary direction of rotation of spirals in helical magnetic structures. Consequently, existence of an antisymmetric exchange is a necessary condition for emergence of ferroelectricity in RMn$_2$O$_5$. Dzyaloshinsky–Moriya interaction can be regarded in the commensurate magnetic phase as an indirect cause of enhancement of electric polarization.

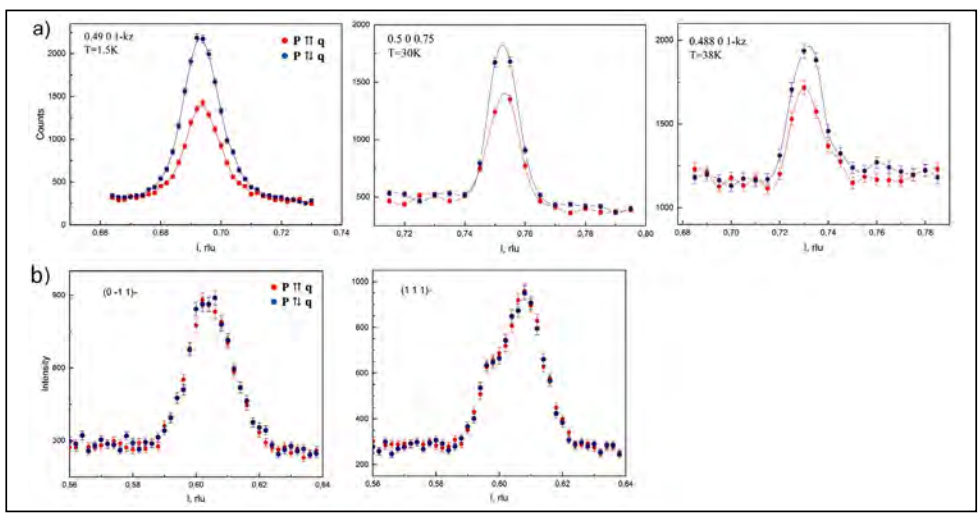

Results of scans of magnetic satellites at two polarization **P** – directions – along and against scattering vector **q**: TbMn$_2$O$_5$ (a); NdMn$_2$O$_5$ (b)

1. *Zobkalo I.A., Gavrilov S.V. et al.* // Physics of the Solid State. 2014. V. 56, No. 1. P. 51–56.
2. *Zobkalo I.A., Gavrilov S.V. et al.* // J. Magn. Magn. Mater. 2014. V. 354. P. 85.
3. *Zobkalo I.A., Gavrilov S.V. et al.* // Journal of Surface Investigation. *X*-ray, Synchrotron and Neutron Techniques. 2015. V. 9. No. 3. P. 550–554.

Mesostructure and fractal properties of novel transparent glasses based on zirconium dioxide

G.P. Kopitsa, N.N. Gubanova, K.V. Ezdakova – PNPI NRC "Kurchatov Institute", Gatchina, Russia
A.E. Baranchikov, V.K. Ivanov – Kurnakov Institute of General and Inorganic Chemistry of RAS, Moscow, Russia
A. Feoktistov, V. Pipich – Forschungszentrum Jülich GmbH (JCNS), Outstation at MLZ, Garching, Germany
B. Angelov – Institute of Macromolecular Chemistry (ASCR), Prague, Czech Republic

Transparent glasses based on amorphous zirconium dioxide are considered to be promising materials for the development of photochromic devices, catalytic systems, chemical sensors, etc. Moreover, these materials are promising matrices for heat resistant luminescent nanocomposites and nonlinear optical devices, such as laser systems.

In the present work, transparent porous glasses based on zirconium dioxide were prepared for the first time without the use of any glass-forming additives such as SiO_2. Glasses were synthesized by the sol-gel approach from organic solutions of zirconium propylate using nitric and acetic acids as gelation agents.

The structure and properties of zirconia glasses were studied using small-angle and ultra small-angle neutron scattering, *X*-ray small-angle scattering, *X*-ray diffraction scanning electron microscopy, thermal analysis and low-temperature nitrogen adsorption.

Joint analysis of experimental data obtained using these complementary methods has shown that:

1. All the glasses are *X*-ray amorphous and possess high specific surface areas up to 250 m^2/g.

2. Zirconia glasses obtained using nitric acid as a gelation agent possess three-level hierarchic structure. The first level consist of primary 1 nm sized zirconia particles that form the second structural level – fractal 24÷52 nm sized clusters. The third level corresponds to relatively large ($d_3 \approx 2$ μm) aggregates with diffuse surface.

3. Zirconia glasses obtained using acetic acid as a gelation agent possess perfectly different structure. It consists of two structural levels, where the first one includes short-range ordered primary 1 nm ZrO_2 particles. These particles form the large aggregates with diffuse surface of the second structural level.

4. Both the temperature of synthesis and H_2O concentration in starting solution sufficiently affect the structural parameters of glasses in different structural levels.

Gubanova N.N., Kopitsa G.P., Ezdakova K.V. et al. // Journal of Surface Investigation. *X*-ray, Synchrotron and Neutron Techniques. 2014. V. 8. No. 5. P. 963–971.

Studies of the structure and conformations of star-shaped polymers with fullerene branching centres functionalized by carbonyl groups

V.T. Lebedev
Neutron Research Division, PNPI NRC "Kurchatov Institute"

Hybrid structures with polymers and fullerenes were synthesized for the first time and studied by small-angle neutron scattering. These new substances seem to be very promising materials for electronics, biology and molecular medicine since fullerenes play a role of active centres which are able, for instance, to induce catalytic processes at their surface screened by polymeric shell composed of attached arms (nanoreactors). This work presents the results obtained at PNPI (Laboratory for Neutron Physical and Chemical Research, Head of the Laboratory Dr. of Physical and Mathematical Sciences V.T. Lebedev and Research Associate D.N. Orlova) in cooperation with the Institute of Macromolecular Compounds of RAS (Leading Researcher Dr. of Chemical Sciences L.V. Vinogradova) and the Budapest Neutron Centre (Dr. Gy. Török).

These star-shaped polystyrenes $(PS)_6C_{60}$ have been prepared with the use of anionic polymerization. In this way the parameters of polymeric shell around C_{60} were regulated by varying the molecular mass of the arms and grafting C=O groups to fullerene surface. It allowed one to polarize differently the π-electrons on carbon cage, which demonstrated a specific influence on the attached polymeric arms. In order to find a relationship between the structural features of $(PS)_6C_{60}$ molecules and the state of fullerene surface (C=O groups, number n = 1–3), the polymers in

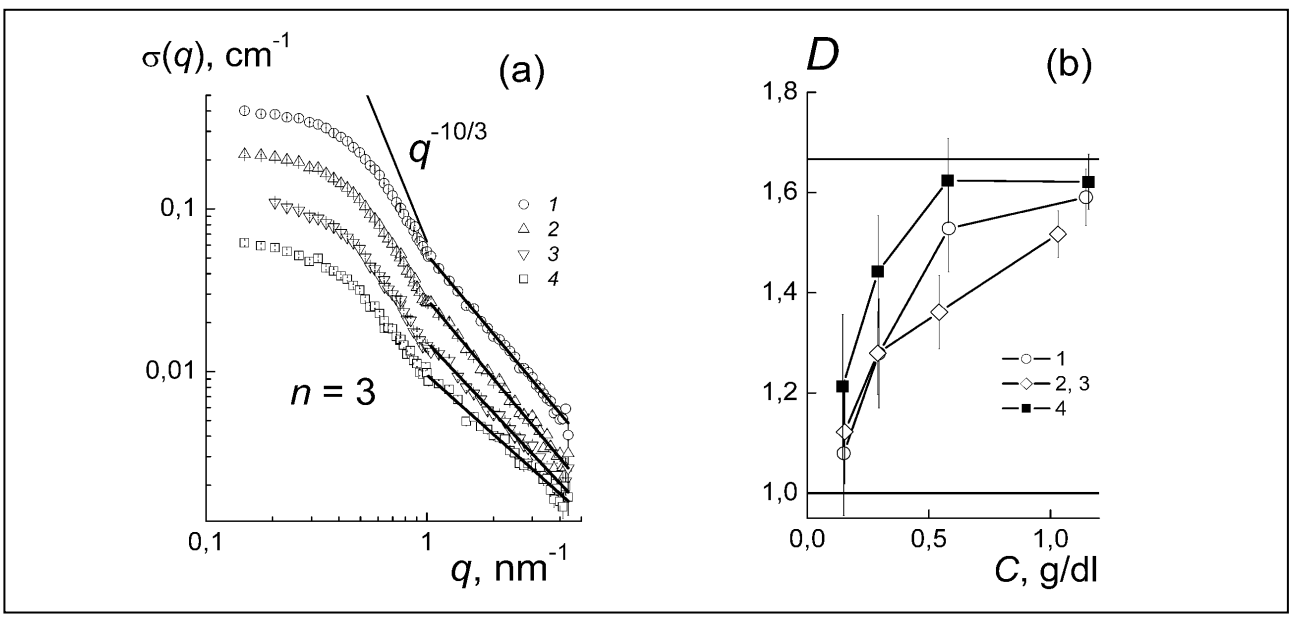

Fig. 1. Cross-sections σ(q) for the solutions of stars (a) with three carbonyl groups linked to fullerenes vs. momentum transfer at the initial polymer content C ~ 1 g/dl (1) and at lower concentrations (two-; four-; eight-fold dilution, data 2–4). The lines represent fitting functions J/q^D with the parameters $J(C, n)$, $D(C, n)$. The calculated model function σ(q) ~ $q^{-10/3}$ is shown as well. The exponents $D(C, n)$ are plotted for different polymer concentrations (b): 1 – data for the stars without carbonyl groups; 2, 3 – averaged data for group's numbers n = 1 and 2; 4 – data for n = 3

deuterated toluene have been studied at different concentrations. The measured scattering cross-sections $\Sigma(q) = \sigma(q) + B$ included the incoherent background $B \approx$ const and the coherent $\sigma(q)$ parts. Magnitudes of the latter increased proportionally to the concentration, which indicated the absence of aggregation in molecular solutions (Fig. 1a).

The data for the total cross-section $\Sigma(q)$ at $q \geq 1$ nm^{-1} was fitted by the function $\Sigma(q) = J/q^D + B$ with the factor $J(C, n)$ proportional to the amount of polymer in solution. The exponent $D(C, n)$ characterizes the conformation of polymers at different scales from the size of a monomer unit to the dimension of a chain segment. The values of this exponent are defined by the concentration (C) and the number of carbonyl groups (n) at fullerene surface.

Initially, at the concentration $C \sim 1$ g/dl, it was found that the parameter $D \sim 1.5–1.6$ is close to Flory exponent $D_F = 5/3$ for flexible chains in good solution. Subsequent dilution led to the decrease of exponent approaching its lower limit $D \to 1$ for stretched chains. This reflects a mutual repulsion of the arms due to the solvent ordering near C_{60} surface via stacking into the columns providing a radial arrangement of the arms (Fig. 2).

When polymer concentration decreased (1.0 → 0.1 g/dl), a transition from coiled to stretched arms was observed (Fig. 1b). The conformational changes were revealed to be stronger in the presence of 1–2 carbonyl groups at fullerene surface. However, three groups caused an opposite effect when the arms were more coiled. The latter could be a result of non-uniform electric polarization of fullerene and side phenyl rings in polystyrene arms by C=O groups having dipolar moments.

The gyration radii of stars $R_G \sim 3.3–3.4$ nm have exceeded by ~ 30% the dimension of star-shaped macromolecules estimated by Benoit model with Gaussian conformation of the arms. This finding is explained by the increase of statistical segment length in half as compared to the one of linear polystyrene. Along with it, the Daoud-Cotton model considering the stars of high functionality as gradient structures, with the arms aligned radially, can be applied to these objects only qualitatively since the model predicts the asymptotic behavior $\sigma(q) \sim q^{-10/3}$ but does not describe the experimental data (Fig. 1a).

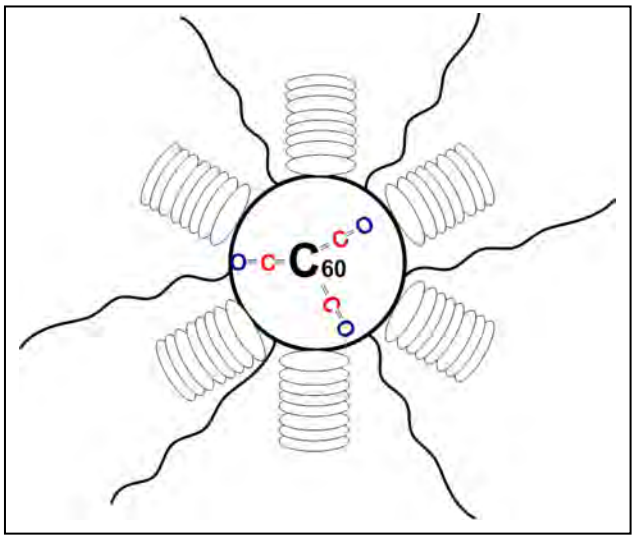

Fig. 2. Star-shaped polymers $(PS)_6C_{60}$ with C=O groups grafted to C_{60}-centre. The polymeric arms and columnar structures of solvent molecules near fullerene are shown

By means of neutron scattering method, it was observed that polymeric stars have unusual behavior at a transition to diluted solutions when C_{60}-centres in stars induce solvent structuring, which stabilizes stretched conformations of the arms at segmental scale. Grafting polar C=O groups to fullerenes might intensify or damp these trends depending on the amount of groups. The results obtained really demonstrated new possibilities to regulate the conformations of polymers using the fullerenes as active centres with a variation of amount of functional groups grafted.

Magnetic structure and phase transitions in the "green phase" $^{160}Gd_2BaCuO_5$. Neutron diffraction study

I.V. Golosovsky, A.K. Ovsyanikov
Neutron Research Division, PNPI NRC "Kurchatov Institute"

The cuprates with the general formula R_2BaCuO_5 (R – stands for a rare-earth element), known as the "green phases", first attracted attention of researchers when they were observed as impurities in the early synthesis of high-temperature superconducting oxides. Soon, these compounds became a subject of intense research since the structure of the copper sublattice was similar to the structure of copper in high-temperature superconductors. Later it was realized that these compounds are also excellent objects for the study of magnetic interactions between 3*d*- and 4*f*-sublattices.

Physical properties of the compounds with different rare-earth elements appeared to be very diverse. Unlike other "green phases", specific heat and magnetic susceptibility measurements in Gd_2BaCuO_5 show a single magnetic transition instead of two magnetic transitions, which usually corresponds to the establishment of order in the 3*d*- and 4*f*-sublattices. Therefore, a question arose about the real magnetic structure and its temperature evolution.

The magnetic order was studied by neutron diffraction method using isotope-substituted sample $^{160}Gd_2BaCuO_5$ because the natural Gd has a very large absorption of neutrons. Below the Néel temperature of about 12 K, the incommensurate magnetic structure with wave vector **k** = [0 0 1/2–δ] was discovered. However, at a temperature of 5 K a new transition to a commensurate structure with the wave vector **k** = [0 0 1/2] was observed, which was previously "invisible" in the magnetic measurements. It turned out that this so-called "lock-in" transition was accompanied by a reorientation of the magnetic moments in the rare-earth sublattice and transformation of the atomic structure. Basing on the temperature dependences of the magnetic moments, one can conclude that the compound $^{160}Gd_2BaCuO_5$ is a low-dimensional magnet, which is typical for rare-earth cuprates (Fig. below).

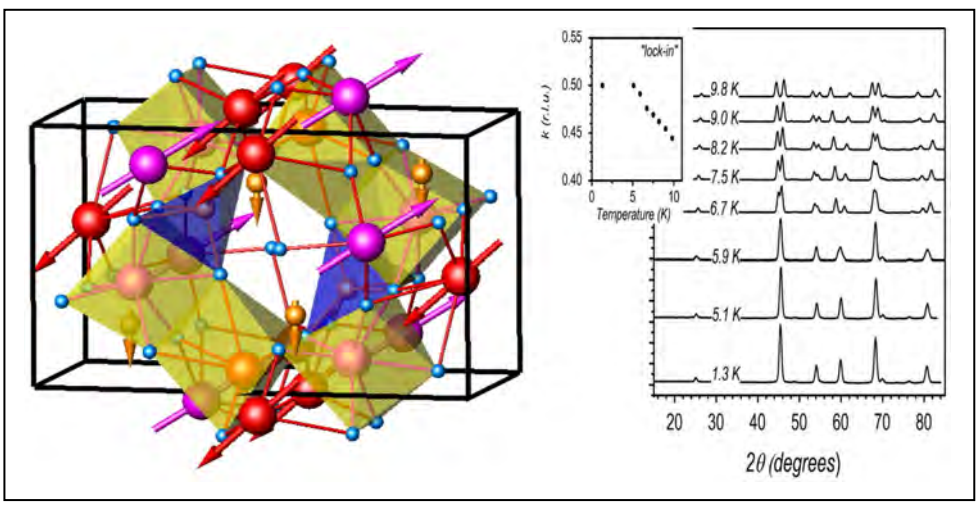

Left panel: magnetic structure of $^{160}Gd_2BaCuO_5$ at temperature T = 1.3 K with the wavevector **k** = [0 0 1/2] Gd atoms in different positions and Cu atoms are shown in magenta, red and orange, respectively. Neutron diffraction patterns are measured at different temperatures.
Right panel: the temperature dependence of the wavevector is shown in inset

Ovsyanikov A.K., Golosovsky I.V., Zobkalo I.A., Mirebeau I. // J. Magn. Magn. Mater. 2014. V. 353. P. 71–75.

Neutron spin manipulation optics

N.K. Pleshanov
Neutron Research Division, PNPI NRC "Kurchatov Institute"

A new direction for development of neutron optics was suggested. The introduction of the neutron spin manipulation optics is based on quantum aspects of the neutron interaction with magnetically anisotropic layers and signifies the transition from 1D (spin selection) to 3D (spin manipulation) in polarized neutron optics.

Solutions that provide a high reflectivity ($R \sim 1$) and a weak dependence of the spin rotation angle on the neutron wavelength and on the glancing angle were suggested. They open new possibilities for spin manipulations. Neutron spin-turning reflectors (particularly, $\pi/2$-turners and π-turners, see Fig. below) may be either directly used or combined to build 3D-polarizers, 3D-analyzers, 3D-rotators (spin manipulators), hyperpolarizers, quantum spin precessors and antiprecessors.

Polarizers of a new type, hyperpolarizers in which spin-flipping reflectors are used, were suggested. A hyperpolarizer not only separates neutrons with the opposite spins, but also flips the "wrong" spins, thus polarizing up to 100% of neutrons (with the increase either in the angular divergence or in the width of the beam, in accordance with the Liouville theorem). Quantum precessors based on spin-splitting layered structures are counterparts of the conventional precession coils and also provide large precession angles. In addition, there appears the possibility of designing precessors with "non-classical" dependence of the precession angle on the neutron wavelength; the very sign of the spin precession can be made opposite to that of the Larmor precession (antiprecessors).

Neutron spin manipulation optics (NSMO) is directly applicable to the development of such neutron techniques as reflectometry with 3D-polarimetry, Neutron Optical Spin Echo including compact and TOF schemes. There may also appear the possibility of developing polarimetry with VCN and even UCN, which is an equivalent of ellipsometry, but with extremely high sensitivity to surface magnetism.

In conclusion, it should be noted that the first flipper based on reflection from a multilayer was built and its flipping efficiency was found to be 98%, as reported at the Muromets-2014 workshop (18–19 September 2014, Gatchina, Russia). It may be regarded as the confirmation of concepts developed for NSMO.

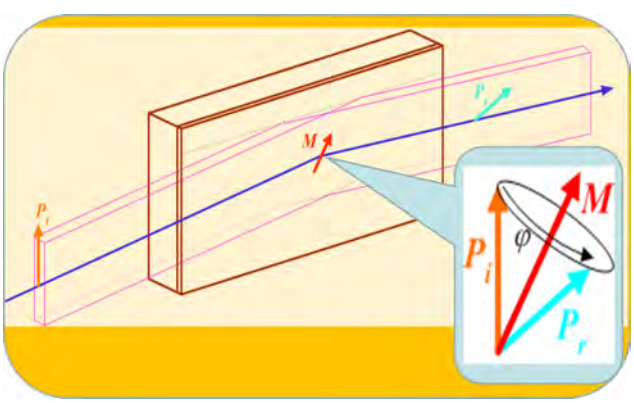

Spin turners, including $\pi/2$-turners and π-turners (flippers), can be built with mirrors on the basis of magnetically anisotropic layers and multilayers. For a practical use, the reflectivity should be close to 1 and the angle φ of the spin rotation under reflection should but weakly depend on the neutron wavelength and on the glancing angle. $\mathbf{P}_i$ и $\mathbf{P}_r$ – are the incident and reflected neutron polarization vectors, respectively

1. *Pleshanov N.K.* // J. Phys.: Conf. Ser. 2014. V. 528. P. 012023.
2. *Pleshanov N.K.* // Journal of Surface Investigation. *X*-ray, Synchrotron and Neutron Techniques. 2015. V. 9. P. 24.

Nuclear-magnetic interference effects in small-angle scattering of polarized neutrons

V.V. Runov
Neutron Research Division, PNPI NRC "Kurchatov Institute"

Scattering of polarized neutrons has a very important advantage in comparison with the scattering of non-polarized ones, as in this case it is possible to allocate the part determined by the magnetic nuclear interference scattering, i.e. to measure the product of the nuclear scattering amplitude (*A*) on magnetic amplitude (*B*), (*AB*). As shown in this report, the allocation in SAPNS (Small-Angle Scattering of Polarized Neutrons) method is highly efficient for the solution of some specific problems. This efficiency is based on the possibility to study nuclear-magnetic scattering in contrast to the general, much more powerful magnetic or nuclear (or both) small-angle scattering. Performing this task is like looking for a needle in a haystack. Nevertheless, it can be solved due to the mutual magnetic-nuclear contrast enhancement of scattering. The interference scattering $\Delta(q)$ is measured as the difference in the intensity of scattering with polarized neutrons up/down the magnetic field applied to the sample, that is, $\Delta(q) = I^{+}(q) - I^{-}(q) \approx P\,(AB)$, where P is the neutron polarization through the sample. Thus, the effect of the interference is measured at zero background in absence of interference.

The results presented in this report were obtained at PNPI after the upgrade of the "Vector" installation: 1) the study of ferromagnetic correlations caused by impurities in nonmagnetic material (CuZn (20) with 1% of Ni) using the method of small-angle scattering of polarized neutrons, (Fig. 1); 2) detection and evolution of magnetic-nuclear contrasting fraction in the magnetic alloy P91 during the heat treatment (Fig. 2).

Based on the results of the experiment, the type of cross-correlation function was determined and the value of the characteristic correlation radius of impurities was calculated.

The interference scattering data determined characteristic dimensions evolved during the heat treatment phases, which increased from 150 to 450 Å with the increase of the temperature and time of annealing, which is consistent with the decrease of hardness of the alloy.

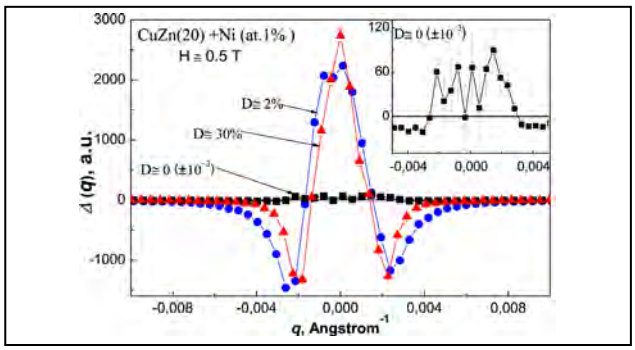

Fig. 1. Dependence of nuclear-magnetic interference $D(q) = I^{+}(q) - I^{-}(q)$ versus the wave vector transfer in samples CuZn(20) (Ni – 1 at. %) in $H \approx 0.5$ T at different heat treatment of samples. D – depolarization in the sample

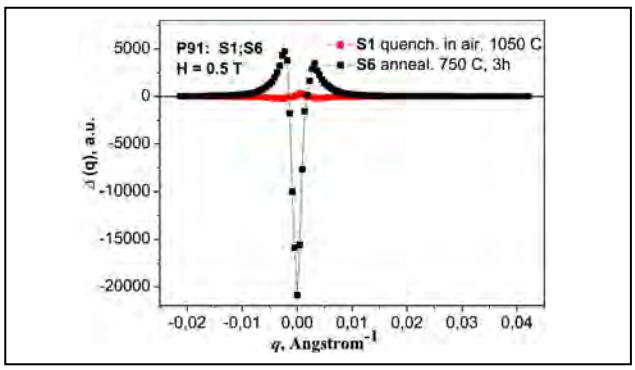

Fig. 2. Dependence of the nuclear-magnetic interference $\Delta(q) = I^{+}(q) - I^{-}(q)$ versus the wave vector transfer in the samples P91 in the $H \approx 0{,}5$ T at different heat treatment of the samples. It is visible as essential is the difference of interference scattering for quenched and annealed samples. There were two stages of heat treatment: 1) quenching and 2) annealing, in which the sign of the scattering of the interference changed, which is caused by the change of the sign of nuclear contrast, associated with the formation of *V* or *V*(*C*) phase during quenching and metal carbide phases during annealing

1. *Runov V.V., Ilyn D.S., Runova M.K., Radzhabov A.K.* // JETP Letters. 2012. V. 95. No. 9. P. 467–470.
2. *Runov V.V., Skorobogatykh V.N., Runova M.K., Sumin V.V.* // Physics of the Solid State. 2014. V. 56. No. 1. P. 62–67.

Field-induced chirality in the helix structure of Ho/Y multilayers

V.V. Tarnavich, S.V. Grigoriev – PNPI NRC "Kurchatov Institute", Gatchina, Russia
D. Lott – Helmholtz-Zentrum Geesthacht, Geesthacht, Germany
S. Mattauch – Forschungszentrum Jülich (JCNS), Garching, Germany
A. Oleshkevych, V. Kapaklis – Uppsala University, Uppsala, Sweden
S.V. Grigoriev – Saint Petersburg State University, Saint Petersburg, Russia

We focused on the study of the net chirality in the spin helix structure of Ho/Y multilayers induced by an in-plane applied magnetic field. The lifting of degeneracy of the chiral symmetry was revealed by means of polarized neutron reflectometry. Superlattice consists of alternating layers of magnetic Ho and non-magnetic Y. The samples of different thicknesses of Ho and Y layers were grown with the use of molecular-beam-epitaxy techniques: [$Ho_{45Å}/Y_{30Å}$], [$Ho_{25Å}/Y_{20Å}$], [$Ho_{20Å}/Y_{30Å}$]. The chiral states are degenerated upon zero field cooling below the critical temperature *TN*, the lifting of degeneracy cancels by the cooling in external magnetic field below TN (FC procedure). The average chirality, which is proportional to the difference in the population of the left- and right-handed helices, was measured as the polarization-dependent asymmetric part of the magnetic neutron-scattering cross-section. We measured the chirality parameter $\gamma = (I^+ - I^-) / (I^+ + I^-)$ of the multilayers as a function of the temperature and magnetic field, where $I^{+/-}$ is the integrated intensity of the helical peak with up (+) and down (–) neutrons. Figure 1 shows reflectivity profiles, $I(+P_0)$ and $I(-P_0)$, for the sample $Ho_{25Å}/Y_{20Å}$ after the ZeroFC procedure and FC procedure at H = 1 T cooled down to T = 30 K.

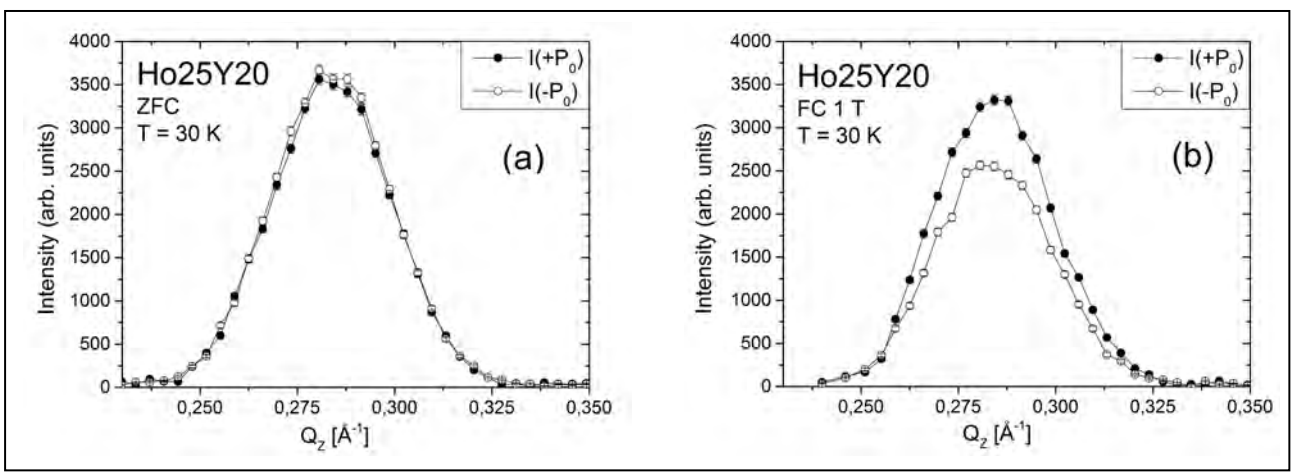

Fig. 1. The *Q* dependence of the neutron-scattering intensity (reflectivity profile) for the samples $Ho_{25Å}/Y_{20Å}$, taken for two polarizations of the incident beam at T = 30 K after the ZFC procedure (a) and FC procedure at an applied field H = 1 T (b)

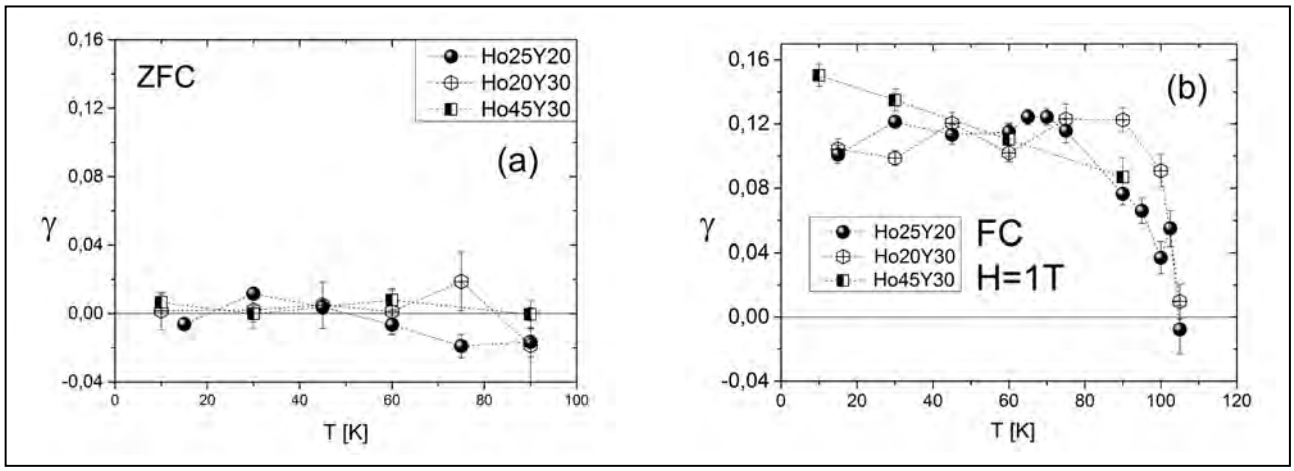

Fig. 2. The chirality for the samples $Ho_{45Å}/Y_{30Å}$, $Ho_{25Å}/Y_{20Å}$ and $Ho_{20Å}/Y_{30Å}$ in dependence on temperature prehistory: *T* dependence after ZFC (a) and *T* dependence after FC under an applied field *H* = 1 T (b)

Figure 2 shows the value of γ for the samples Ho25Y20, Ho20Y30, and Ho45Y30 in dependence of the temperature after ZFC and FC procedures, respectively. After the ZFC procedure shown in Figure 2(a), the chirality γ is close to zero within the error bars over the complete temperature range for all three samples. This observation can be easily understood considering the RKKY interaction as the dominant interaction for formation of the helical structures. In this case, the right- and left-handed helices are energetically equivalent to each other and both states will be occupied in equal measures. The value of chirality γ measured after the FC procedure in a magnetic field of 1 T, on the other hand, clearly shows nonzero values of up to 12%, suggesting strongly that the degeneracy of the chiral symmetry is now lifted. The value of γ drops sharply to zero when the temperature approaches *TN*, indicating that the introduction of the chirality in systems predominantly occurs in a very limited temperature range close to the transition temperature for all three samples.

While the samples are subject to cooling in magnetic field, the resulting chirality of Ho layers is established according to the minimum of the energy of the DMI at the interfaces and the main spin component directed along the field (sin-structure). Yet the sin-structure is destroyed when the field is switched off. However, the RKKY interaction forces a formation of a simple helix with previously chosen handedness. The chirality parameter γ rises during the field cooling procedure in the field range from 0 to 1 T and saturates at a value of 0.12 ± 0.01. The phenomenon is explained by the interplay between exchange interactions (the RKKY and the Dzyaloshinsky–Moriya interactions), an external magnetic field and a special confinement of magnetic constituents.

Tarnavich V., Lott D., Mattauch S. et al. // Phys. Rev. B. 2014. V. 89. P. 054406.

The structure periodic order and defects in Ni-based inverse opal-like crystals on the mesoscopic and atomic scale

A.V. Chumakova, A.A. Mistonov, V.A. Dyadkin, S.V. Grigoriev
Neutron Research Division, PNPI NRC "Kurchatov Institute"

The structure of inverse opal crystals based on nickel was probed on the mesoscopic and atomic levels by a set of complementary techniques such as scanning electron microscopy and synchrotron microradian and wide-angle diffraction.

The IOLC films based on nickel were prepared using a templated electrodeposition. The use of the electrochemical technique for metal deposition into the matrix voids enables us to control the level of filling coulometrically and to stop the deposition at a desired depth. Thereby, one can obtain a sample with predesigned thickness. In particular, for the present study a number of films with gradually increasing thickness were obtained, that is, the samples with 3.5, 8, 17, and 26 layers (corresponding to the layers of the initial opal templates).

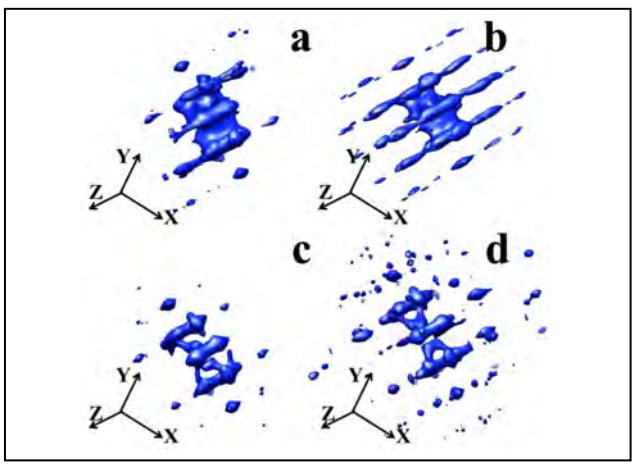

The 3D visualization of reciprocal space of inverse opal-like crystals $Ni_{3,5}$ (a), Ni_8 (b), Ni_{17} (c), Ni_{26} (d)

The microradian *X*-ray diffraction study results led to the following conclusions. (i) The mesoscopic structure of IOLC based on Ni completely repeats the structure of the original matrix of the artificial opal crystal with minor alteration of the lattice constant. The structure formed is primary fcc (the probability of fcc motif formation, $\alpha \sim 0.7$) and its lattice constant is equal to 750 ± 10 nm. (ii) Additional features observed in the diffraction pattern are the diffuse Bragg rods, which are clearly seen by 3D visualization of the reciprocal space (Fig. 1).

These diffuse Bragg rods are situated not only along [111], which corresponds to substrate normal, but also along other <111> directions in the IOLC, the [111] direction being the dominant one. These findings suggest the presence of stacking faults, not only along the direction orthogonal to the sample surface. (iii) The probability of fcc motif formation, α and the average structure lateral domain size being about 5 μm, does not depend on the number of layers and it remains constant provided that original matrix is the same for all the samples. However, when the number of layers increases above 20 then the number of reflections increases and the number of stacking faults decreases.

The results of wide-angle *X*-ray diffraction study can be summarized as follows. The IOLC samples contain Ni possessing fcc crystal structure with the lattice parameter of about 3.52 Å. The Debye temperature in a reasonable agreement with the literature values as for single crystals and for powder. The thermal expansion coefficient for thick IOLC is higher than that for bulk Ni. The IOLC samples contain dislocations with the density higher than $1 \cdot 10^{15}$ m^{-2} as well as stacking faults of the atomic structure. The dislocation density is high but in a reasonable agreement with the values reported for powders and nanocrystalline thin films. The concentration of twin stacking faults (~ 0.01) is higher than that of deformation type stacking faults (0.003 ± 0.002). The size of the coherent scattering region is ~ 50 nm, being a good lower-bound estimate of average crystallite aggregates size, which is ~ 100 nm according to the SEM data. Larger crystallites were found in thinner inverted opal-like crystals (with fewer layers).

Chumakova A.V., Valkovskiy G.A., Mistonov A.A., Dyadkin V.A., Grigoryeva N.A., Sapoletova N.A., Napolskii K.S., Eliseev A.A., Petukhov A.V., Grigoriev S.V. // Phys. Rev. B. 2014. V. 90. P. 144103.

Investigation of the $Eu_{0.8}Ce_{0.2}Mn_2O_5$ multiferroic by the μSR-method

S.I. Vorobyev, A.L. Getalov, E.N. Komarov, S.A. Kotov, G.V. Shcherbakov
High Energy Physics Division, PNPI NRC "Kurchatov Institute"

$Eu_{0.8}Ce_{0.2}Mn_2O_5$ multiferroic magnetic properties were investigated within the temperature range of 10–300 K using the μSR-method on the μSR-installation on the muon channel of the PNPI synchrocyclotron.

Measurement results demonstrated significant loss of polarization within the temperature range of 15–40 K (Fig. 1). Moreover, the polarization loss is determined by the cooling mode used for the sample. Maximum discrepancy in a_s asymmetry loss between different sample's cooling modes is observed within the temperature range of 25–40 K (incommensurate phase zone). No peculiarities are detected within the temperature range of 40–290 K. When the temperature reaches 40 K one can observe the transition from the paramagnetic state to magnetically ordered (AFM) state.

Behavior pattern of λ polarization relaxation rate depending on the temperature change in $Eu_{0.8}Ce_{0.2}Mn_2O_5$ sample (blue dots in the Figures below) perfectly corresponds to the one in $EuMn_2O_5$ sample (red dots in the Figures) and demonstrates almost no dependence on the cooling mode (Fig. 2). No peculiarities of λ parameter temperature dependence are observed within the temperature range of 80–290 K. Significant growth of λ parameter is detected upon the approach to the temperature of the sample's transition to magnetically ordered state. Monotonic decrease of λ relaxation rate is observed upon the sample's temperature fall in the range of $T < T_N$ (where T_N is the temperature of transition).

Therefore, one can observe that the cerium (Ce) doping of $EuMn_2O_5$ sample did not have a significant effect on the behavior of indicated a_s and λ parameters. If the previously discovered effect of asymmetry loss is connected to the appearance of ferromagnetic pairs in a sample, then the later was not caused by doping, but by tunneling of e_g-electrons between planes. Such pairs are equally distributed throughout the whole volume of the sample, but the modified doped volume is very low.

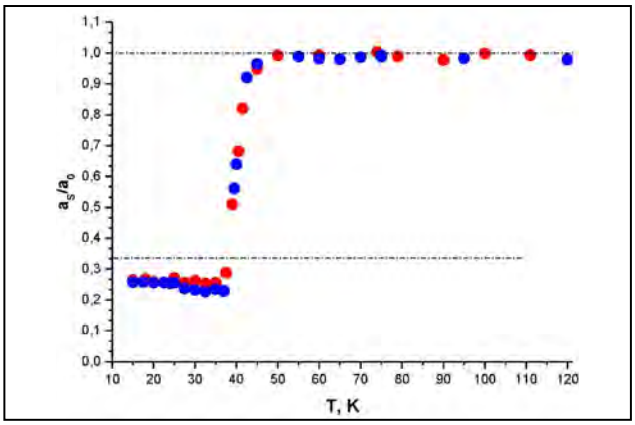

Fig. 1. Temperature dependence of residual asymmetry a_s normalized against total asymmetry a_0: $Eu_{0.8}Ce_{0.2}Mn_2O_5$ sample – blue dots; $EuMn_2O_5$ sample – red dots. The levels of normalized asymmetry $a_s/a_0 = 1/3$ ($T < T_N$) and $a_s/a_0 = 1$ ($T > T_N$) are identified by dot-and-dash lines

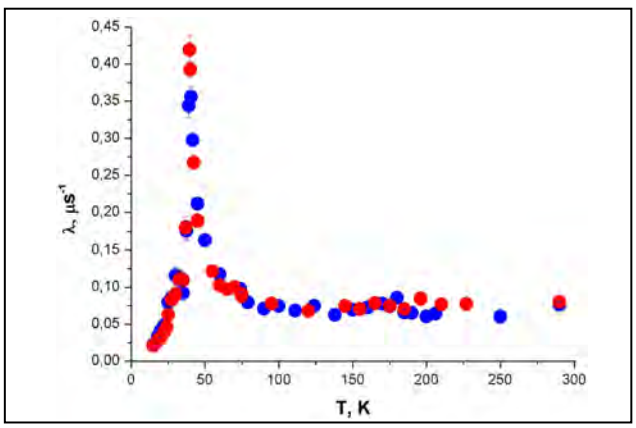

Fig. 2. Temperature dependence of the dynamic relaxation rate λ: $Eu_{0.8}Ce_{0.2}Mn_2O_5$ sample – blue dots; $EuMn_2O_5$ sample – red dots

1. *Vorobyev S.I., Getalov A.L., Goloventchits E.I., Komarov E.N., Kotov S.A., Pavlova I.I., Moroslip A.E., Sanina V.A., Shcherbakov G.V.* // Proc. of the VI Intern. Conf. on "Actual Problems of Solid State Physics". Minsk. 2013. V. 1. P. 227–229.
2. *Vorobyev S.I., Getalov A.L., Goloventchits E.I., Komarov E.N., Koptev V.P., Kotov S.A., Pavlova I.I., Sanina V.A., Shcherbakov G.V.* // Physics of the Solid State. 2013. V. 55. No. 3. P. 466.

Research Based on the Use of Protons and Ions. Neutrino Physics

Higgs-boson properties from CMS and ATLAS experiments at the LHC

CMS and ATLAS Collaborations

V.L. Golovtsov, V.T. Grachev, O.G. Grebenyuk, A.E. Ezhilov, O.L. Fedin, Yu.M. Ivanov, V.T. Kim, P.M. Levchenko, M.P. Levchenko, V.P. Maleev, V.A. Murzin, V.A. Oreshkin, V.A. Schegelsky, I.B. Smirnov, V.M. Solovyev, V.V. Sulimov, L.N. Uvarov, S.A. Vavilov, A.A. Vorobyev, An.A. Vorobyev
High Energy Physics Division, PNPI NRC "Kurchatov Institute"

CMS and ATLAS experiments, the most ambitious projects in high energy physics, demonstrated unique capabilities of extending the human knowledge in field of fundamental elementary particle physics. The main result of the two major experiments is the discovery of the Higgs-boson made in 2012. In the Standard Model, the Higgs-boson is the quantum of the fundamental scalar vacuum field responsible for spontaneous electroweak symmetry breaking and origin of mass. In 2014, the CMS and ATLAS collaborations presented the results of final data analysis based on the data collected in 2010–2012 and devoted to clarification of the Higgs-boson properties. In both experiments, the Higgs-boson was observed in all basic branching modes predicted by the Standard Model both in bosonic and fermionic decays: into two Z-bosons, into two photons, into two W-bosons, into b-quarks, and via τ-leptons. The measured invariant mass distributions for the $H \to \gamma\gamma$ and for the $H \to ZZ^* \to 4l$ channels are shown in Figure 1.

The mass of the Higgs-boson measured in ATLAS: m_H = 125.36 ± 0.37 (stat.) ± 0.18 (syst.) GeV is in good agreement with the result of the CMS: m_H = 125.03 ± 0.26 (stat.) ± 0.14 (syst.) GeV.

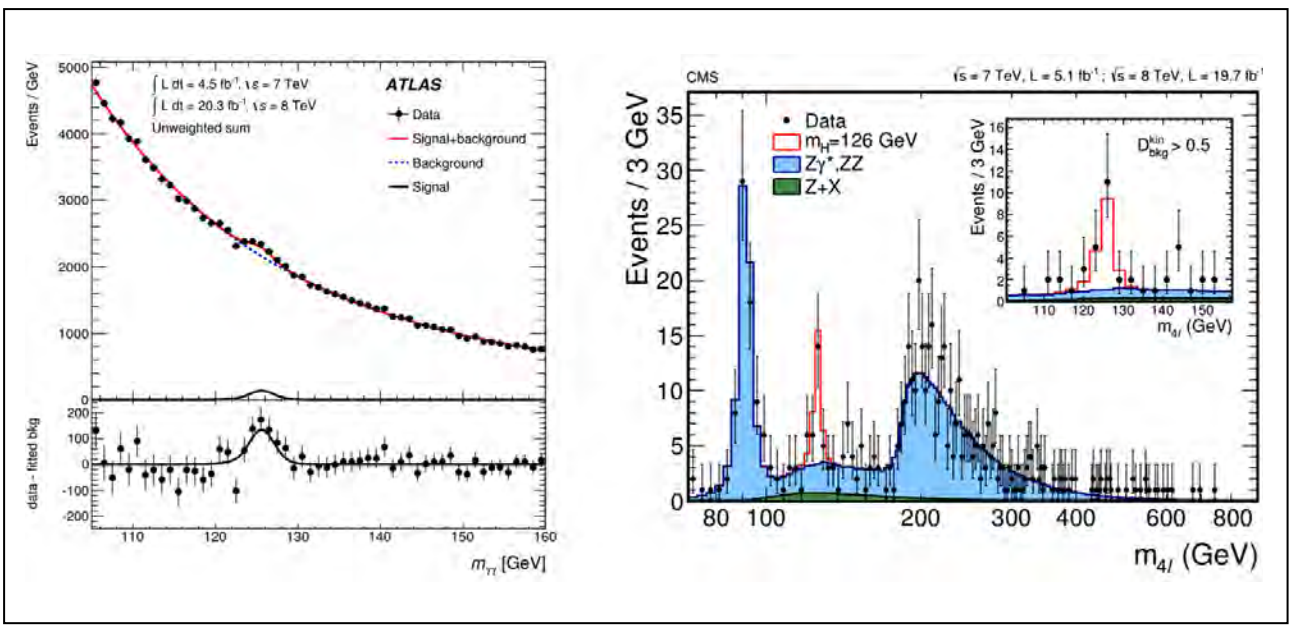

Fig. 1. The two-photon invariant mass distribution from the ATLAS experiment (*left*) and the four-lepton invariant mass distribution from the CMS (*right*). The observed peaks at 125 GeV correspond to the Higgs boson

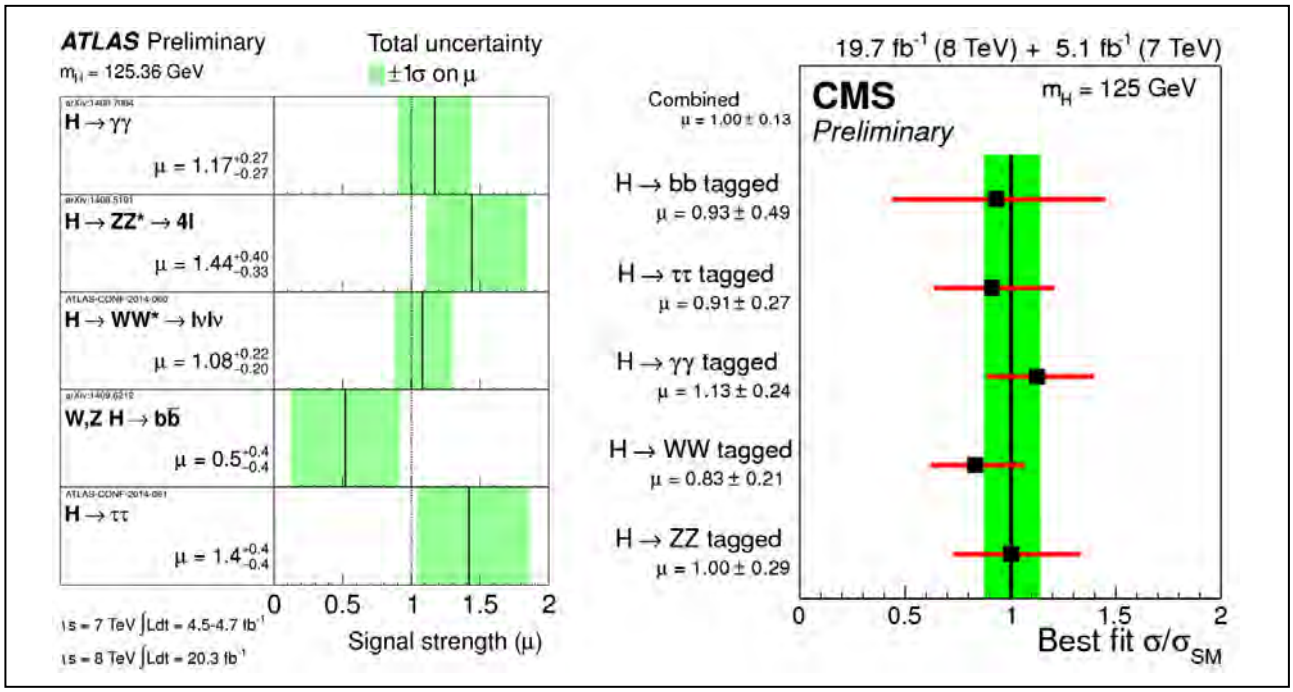

Fig. 2. Ratio of the signal magnitudes to those expected in the Standard Model for various decay channels of the Higgs-boson. Data from the ATLAS (*left*) and from the CMS (*right*) experiments

Figure 2 shows the ratio of the measured cross-sections for various Higgs-boson decay channels to those predicted by the Standard Model. It was found to be $1.30^{+0.18}_{-0.17}$ for ATLAS and $1.00^{+0.13}_{-0.13}$ for the CMS, which demonstrates good agreement between the experimental values and the Standard Model predictions. The parity and spin analysis result is compatible with the hypothesis of spin-zero particle and positive parity. Thus, the studies of the newly found boson properties lead to consistency with the Higgs-boson properties predicted by the Standard Model.

PNPI NRC "Kurchatov institute" team made substantial contributions to the construction and maintenance of the CMS endcap Muon system (the EMU system) and the ATLAS central tracker (the TRT system), which in their turn played an important role in the discovery of the Higgs-boson and determination of its properties.

1. *CMS Collaboration* // Phys. Rev. D. 2014. V. 89. P. 092007.
2. *CMS Collaboration* // Eur. Phys. J. C. 2014. V. 74. P. 3076.
3. *CMS Collaboration* // JHEP. 2014. V. 1401. P. 096.
4. *CMS Collaboration* // JHEP. 2014. V. 1405. P. 104.
5. *CMS Collaboration* // Phys. Lett. B. 2014. V. 736. P. 64.
6. *ATLAS Collaboration* // Phys. Rev. D. 2014. V. 90. P. 052004.
7. *ATLAS Collaboration* // Phys. Lett. B. 2014. V. 726. P. 120.

First observation of the rare $B_s^0 \to \mu^+\mu^-$ decay. LHCb experiment

LHCb, CMS Collaborations

N.F. Bondar, A.A. Dzyuba, O.E. Maev, N.R. Sagidova, Yu.A. Scheglov, A.A. Vorobyev
High Energy Physics Division, PNPI NRC "Kurchatov Institute"

The Standard Model of particle physics describes strong, electromagnetic, and weak interactions of fundamental particles. The Standard Model has a strong predictive power, and it can be tested experimentally. Such kind of measurements constitutes an essential part of the LHC experimental program. Rare decays of particles containing *c*- and *b*-quarks are of particular interest. In the framework of the Standard Model, it is possible to predict branching fractions of the B_s^0 and B^0 rare decays into the $\mu^+\mu^-$ channel. According to these predictions, approximately four of such decays occur for every billion of B_s^0 mesons produced, and only one decay for every ten billion of B^0 mesons. Many theories beyond the Standard Model predict large deviations of these observables from the Standard Model prediction. Thus, precise measurement of these branching fractions is a powerful tool for searching evidence for so-called "new physics".

In 2013, the LHCb collaboration reported on the first evidence for the decay $B_s^0 \to \mu^+\mu^-$ with the measured branching fraction $\mathrm{Br}(B_s^0 \to \mu^+\mu^-) = (3.2^{+1.5}_{-1.2}) \cdot 10^{-9}$. Later this result was confirmed by the CMS collaboration. Then in November 2014, the LHCb and CMS experiments submitted to Nature journal the result of a combined analysis of all experimental data collected during the LHC Run I period. The Figure below presents the distribution of selected candidate events as a function of the $\mu^+\mu^-$ invariant mass. The blue line indicates the overall fit to the spectrum, which includes contributions of the studied decays (shaded peaks) and the background contributions (specified in the Fig.). The best fit to the data claims that the decay $B_s^0 \to \mu^+\mu^-$ is observed with the statistical significance of 6.2σ. Moreover, the data suggests the evidence of the decay $B_s^0 \to \mu^+\mu^-$ at the 3σ confidence level. The measured branching fractions are:

$$\mathrm{Br}(B_s^0 \to \mu^+\mu^-) = (2.8^{+0.7}_{-0.6}) \cdot 10^{-9} \text{ and}$$
$$\mathrm{Br}(B^0 \to \mu^+\mu^-) = (3.9^{+1.6}_{-1.4}) \cdot 10^{-9}.$$

These results are in agreement with the Standard Model predictions:

$$\mathrm{Br}(B_s^0 \to \mu^+\mu^-)_{SM} = (3.66 \pm 0.23) \cdot 10^{-9} \text{ and}$$
$$\mathrm{Br}(B^0 \to \mu^+\mu^-)_{SM} = (1.06 \pm 0.09) \cdot 10^{-9}.$$

The obtained result is an unprecedented test of the Standard Model validity, and it sets strong constraints for developements of "new physics" models (such as the Minimal Super Symmetry Model).

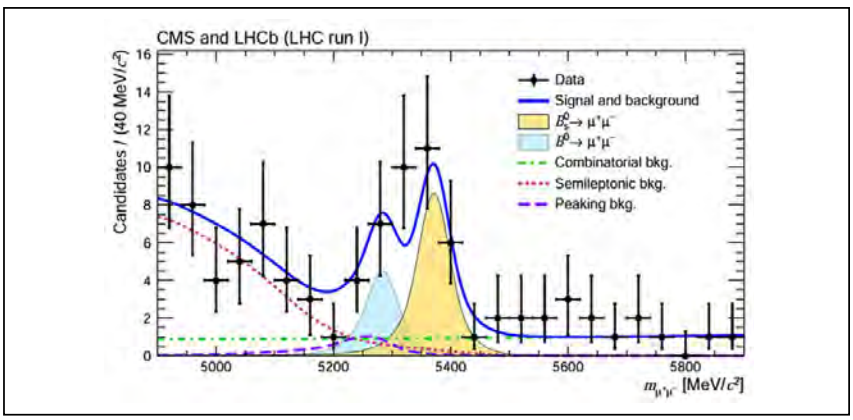

Invariant mass distribution of selected cadididate events

LHCb and CMS Collaborations// LHCb and CMS Collaborations // Nature. 2015. V. 522. P. 68–72.

The first observation of the electroweak *Z*-boson production by the CMS and ATLAS experiments at the LHC

CMS and ATLAS Collaborations

V.L. Golovtsov, V.T. Grachev, O.G. Grebenyuk, A.E. Ezhilov, O.L. Fedin, Yu.M. Ivanov, V.T. Kim, P.M. Levchenko, M.P. Levchenko, V.P. Maleev, V.A. Murzin, V.A. Oreshkin, V.A. Schegelsky, I.B. Smirnov, V.M. Solovyev, V.V. Sulimov, L.N. Uvarov, S.A. Vavilov, A.A. Vorobyev, An.A. Vorobyev
High Energy Physics Division, PNPI NRC "Kurchatov Institute"

The CMS and ATLAS experiments reported on the first observation of the electroweak production of *Z*-boson in association with hadron jets at the LHC. The *Z*-boson production via two *W*-bosons fusion (left diagram in the Fig. below) provides crucial information on the vector-boson self-coupling related to the non-abelian nature of the Standard Model (SM) electroweak interaction, since many beyond-SM models predict anomalously large vector boson coupling.

The cross-sections of the electroweak production of *Z*-boson in association with two hadron jets measured in CMS:

$$\sigma = 154 \pm 24\ (\text{stat.}) \pm 46\ (\text{syst.}) \pm 26\ (\text{th.}) \pm 3\ (\text{lumi.})\ \text{fb}$$
$$\text{at } m_{JJ} > 120\ \text{GeV, 7 TeV;}$$
$$\sigma = 174 \pm 15\ (\text{stat.}) \pm 40\ (\text{syst.})\ \text{fb}$$
$$\text{at } m_{JJ} > 120\ \text{GeV, 8 TeV}$$

and in ATLAS:

$$\sigma = 10.7 \pm 0.9\ (\text{stat.}) \pm 1.9\ (\text{syst.}) \pm 1.9\ (\text{lumi.})\ \text{fb}$$
$$\text{at } m_{JJ} > 1\,000\ \text{GeV, 8 TeV}$$

are in reasonable agreement (within uncertainties) with the SM predictions.

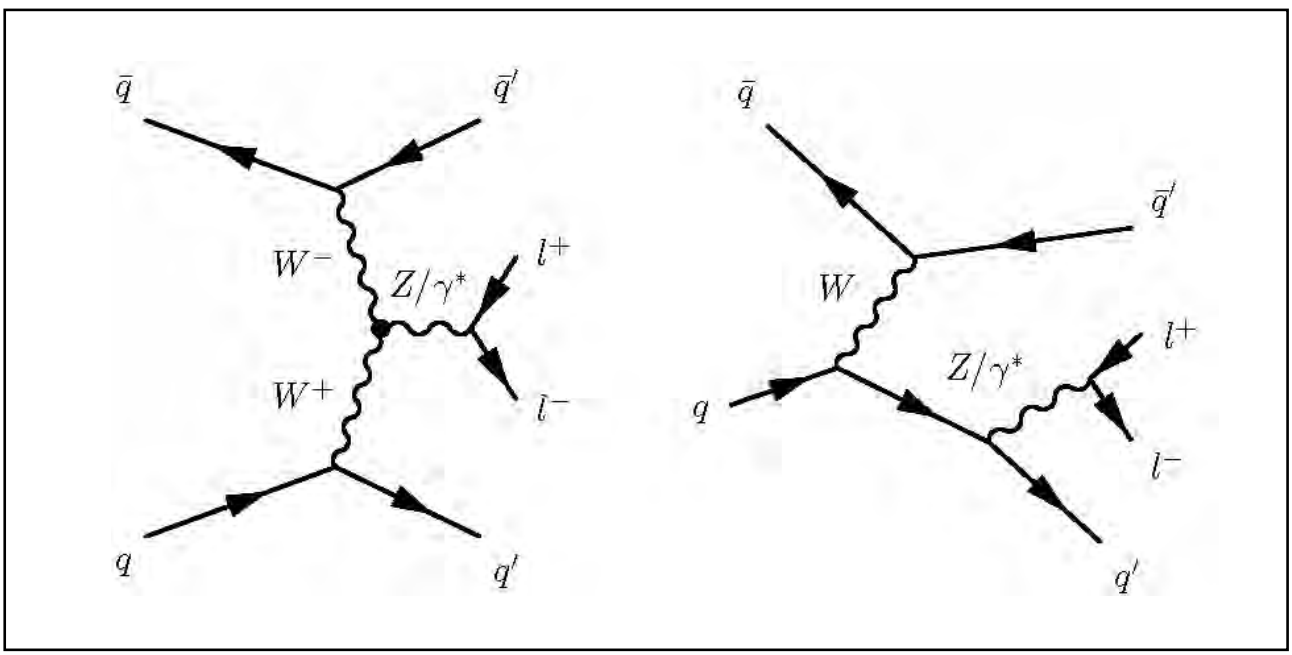

The electroweak *Z*-boson production at the LHC: *W*-boson fusion (*left*) and bremsstrahlung (*right*)

1. *CMS Collaboration* // JHEP. 2013. V. 1310. P. 062.
2. *CMS Collaboration* // Eur. Phys. J. C. 2015 V. 75. P. 66.
3. *ATLAS Collaboration* // JHEP. 2014. V. 1404. P. 031.

First observation of single top quark production in the *s*-channel. D0 Experiment

D0 Collaboration

G.D. Alkhazov, A.A. Lobodenko, P.V. Neustroev, Yu.A. Scheglov, L.N. Uvarov, S.L. Uvarov
High Energy Physics Division, PNPI NRC "Kurchatov Institute"

PNPI NRC "Kurchatov Institute" participates in the international experiment D0 carried out at the proton-antiproton collider "Tevatron" at the Fermi National Accelerator Laboratory (FNAL, USA) with the world's highest energy (1 TeV) of colliding beams of accelerated protons and antiprotons. The Figure below presents a schematic view of the D0 experiment set-up.

The High Energy Physics Division (HEPD) was involved in the D0 project in 1996 through the design and construction of readout electronics for mini-drift tubes (50 000 channels) and operation of the Forward Muon System. In addition, HEPD physicists took part in the data analysis. The data acquisition was finished in 2011. However, the data analysis continued through 2012–2014, and new results have been reported. Here, we present one of these results obtained in 2014. In the combined data analysis performed in the experiments D0 and CDF, the *s*-channel production of single top quark has been observed for the first time. The cross-section σ_s of this process is very small, and it has high sensitivity to potential contributions from the fourth generation of quarks, as well as from flavour-changing neutral currents, anomalous top-quark couplings, heavy *W'*-bosons, supersymmetric charged Higgs-bosons, or other new phenomena. The cross-section σ_s determined from the experimental data, $\sigma_s = 1.29 \pm 0.25$ pb, proved to be in agreement with the Standard Model expectation, $\sigma_s = 1.05 \pm 0.06$ pb, thus showing no manifestation of "new physics" beyond the Standard Model.

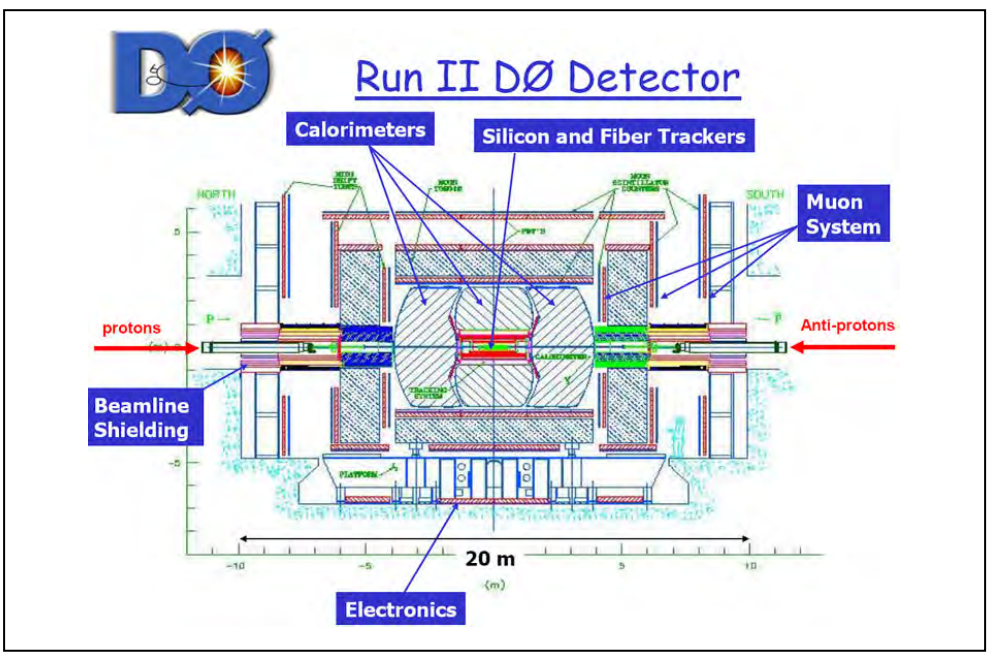

Schematic view of the D0 detector

Aaltonen T.A. ..., et al. // Phys. Rev. Lett. 2014. V. 112. P. 231803.

The search for high mass resonances in the ATLAS experiment

ATLAS Collaborations

V.T. Grachev, O.G. Grebenyuk, A.E. Ezhilov, O.L. Fedin, M.P. Levchenko, V.P. Maleev, V.A. Schegelsky, V.M. Solovyev
High Energy Physics Division, PNPI NRC "Kurchatov Institute"

Despite the great success of the Standard Model (SM) in the description of the particle interactions, there are still questions that the SM might not be able to answer. In particular, the SM does not predict existence of the Dark Matter (DM), does not contain any quantum model of the gravity, does not explain neutrino oscillations, etc. These questions are left to theories Beyond the Standard Model (BSM), and many of them predict new heavy resonances at the TeV scale. For example, various Grand Unification Theories (GUT), devoted to unification of the electroweak and strong interactions, contain additional gauge groups and predict new spin-1 particles usually denoted as *Z'* (for a neutral gauge boson) or *W'* (for a charged gauge boson). Other BSM theories, seeking to answer questions such as so called "hierarchy problem" or trying to propagate the quantum gravity from the Plank scale to the weak scale through extra spatial dimensions, involve a new spin-2 boson attributed to the Graviton (*G**). There is also a model suggested by Russian physicists that addresses the hierarchy problem and predicts existence of a doublet of chiral spin-1 bosons named *Z** and *W**.

HEPD physicists participated in searches of both neutral and charged high mass resonances in lepton channels with the data collected by the ATLAS experiment in proton-proton collisions at the centre-of-mass energy of 8 TeV. No evidence of new particles was found in the 2012 data corresponding to the integrated luminosity of 20 fb^{-1}. In the absence of the signal manifestation, the exclusion limits were set on the cross-section times branching ratio of the signal process for a number of models. Figure 1 demonstrates the 95% CL exclusion limits on the mass of the *Z'*- and *W'*-bosons predicted by the Sequential Standard Model (SSM). The SSM is used as a benchmark model for

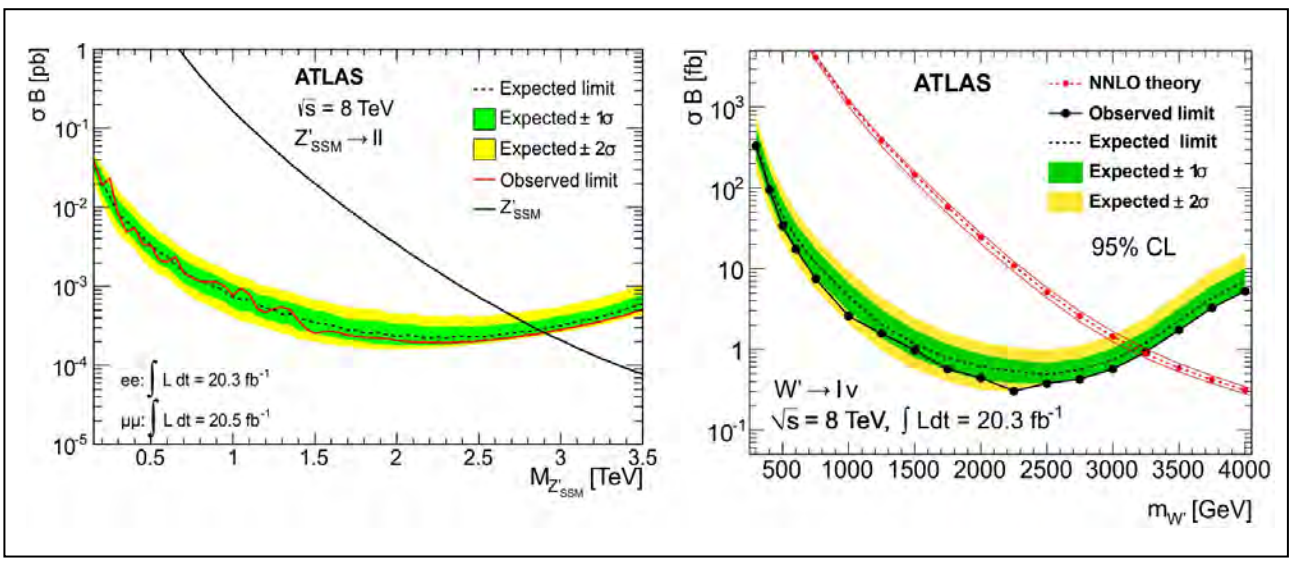

Fig. 1. Median expected (dashed line) and observed (solid red line) 95% CL upper limits on cross-section times branching ratio (σB) in combined (electron plus muon) channel, along with predicted σB for Z'_{SSM} (*left*) and W'_{SSM} (*right*)

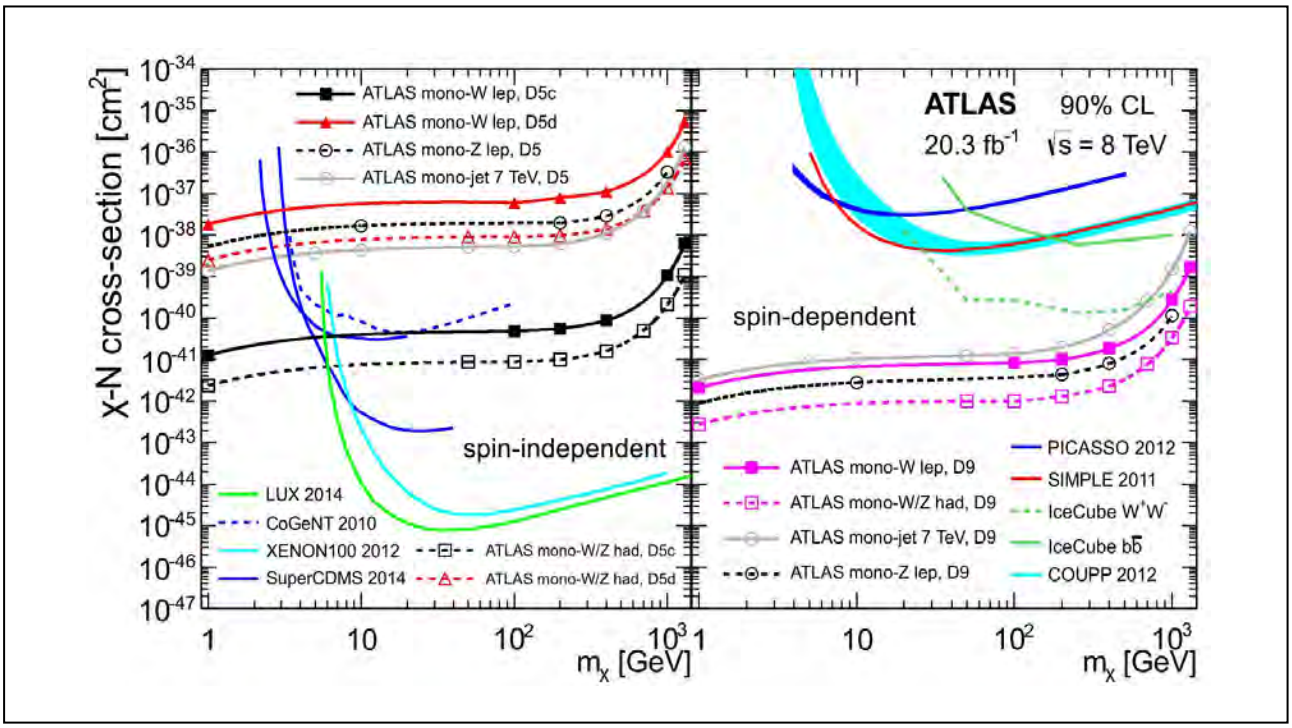

Fig. 2. Observed limits on the DM-nucleon scattering cross-section as a function of m_x at the 90% CL for spin-independent (*left*) and spin-dependent (*right*) operators in the EFT. Results are compared with the results of previous ATLAS searches and with direct DM detection experiments

heavy gauge bosons, its main feature being prediction of the same coupling of the new heavy gauge bosons to the SM fermions as coupling of the gauge bosons of the SM. As demonstrated in Fig. 1, the possibility of existence of the *Z'*-boson is excluded on the 95% CL up to 2.85 TeV, while *W'* is excluded up to 3.2 TeV.

The results of the search for charged heavy bosons were re-interpreted in the framework of the search for dark matter (DM) pair production in association with a leptonically decaying *W*-boson, the so-called mono-*W* search. The obtained limits on the dark matter-nucleon scattering cross-section for spin-independent (left) and spin-dependent (right) operators in the Effective Field Theory (EFT) are shown in Fig. 2 together with the limits established in direct DM detection experiments. One can see that the ATLAS results improve considerably the existing limits both for the case of spin-dependent interaction (in a wide mass range of DM particles) and for spin-independent interaction (in the mass range less than 10 GeV).

1. *Atlas Collaboration* // Phys. Rev. D. 2014. V. 90. P. 052005. arXiv:1405.4123.
2. *Atlas Collaboration* // JHEP. 2014. V. 09. P. 037.

Measurement of the muon capture rate on the proton and determination of the pseudoscalar coupling g_P. MuCap experiment

MuCap Collaboration

V.A. Andreev, V.A. Ganzha, P.A. Kravtsov, A.G. Krivshich, M.P. Levchenko, E.M. Maev, O.E. Maev, G.E. Petrov, G.N. Schapkin, G.G. Semenchuk, M.A. Soroka, A.A. Vasilyev, A.A. Vorobyov, M.E. Vznuzdaev
High Energy Physics Division, PNPI NRC "Kurchatov Institute"

The goal of the MuCap experiment was to determine with 1% precision the capture rate Λ_S of the muon in the singlet state of the μp-atom improving precision of the previously existing data by an order of magnitude. This gives a possibility to determine the unknown nucleon pseudoscalar form factor g_P. The MuCap experiment was carried out by international collaboration of scientists from Russia, Switzerland, USA, and Belgium. The experiment was performed in the high intensity muon beam at the Paul Scherrer Institute (PSI, Switzerland) using the experimental method developed at PNPI NRC "Kurchatov institute". The basic element of the experimental technique is a Time Projection Chamber (TPC) filled with extremely pure hydrogen at 10 atm. gas pressure. The TPC is the target for the muon beam and the muon detector, simultaneously (Fig.). The muon track in the TPC and the muon stop 3D-coordinates can be reconstructed from the TPC signals. This makes it possible to select muon stops in hydrogen gas inside the TPC far enough from all TPC materials. The TPC is surrounded by two cylindrical proportional wire chambers ePC1 and ePC2 and by a segmented cylindrical scintillation counter eSC. These detectors provide information on trajectories of the muon decay electrons so that the muon decay vertex in the TPC can be reconstructed. The incident muon is registered by a proportional wire chamber μPC and by a scintillation counter μSC, which provides the start signal for the muon lifetime measurements, while the stop signal is determined by detection of the muon decay electron in the eSC. The muon capture rate Λ_S is evaluated from the difference

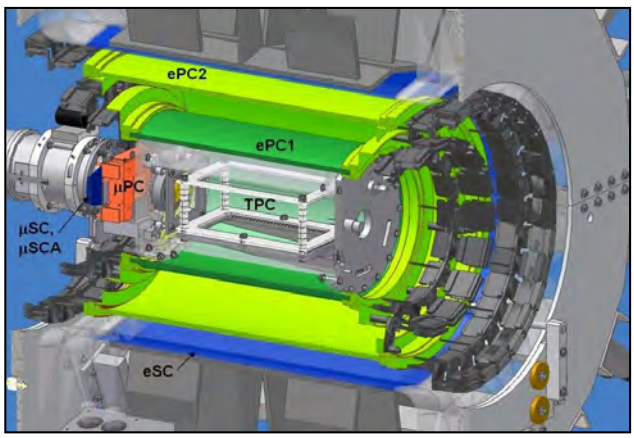

MuCap detector layout

between the measured μ^- decay rate in hydrogen and the decay rate of free μ^+ muons known at present with high precision. Extremely high chemical purity (~ $1 \cdot 10^{-8}$ content for overall chemical impurities) and isotopic purity (~ $6 \cdot 10^{-9}$ content for HD molecules) are provided by a gas circulation purification system and by a cryogenic isotopic purification system both developed at PNPI.

In the experiment, $1.2 \cdot 10^{10}$ muon stops were registered in the TPC, and the muon capture rate was measured to be $\Lambda_S = (714.9 \pm 5.4_{stat.} \pm 5.1_{syst.})\ s^{-1}$. This allowed one to determine for the first time the nucleon pseudo scalar form factor with high precision:

$$g_P(q_0^2 = -0.88 m_\mu^2) = 8.06 \pm 0.55,$$

this value being a critical test of the Heavy Baryon Chiral Perturbation Theory.

Andreev V. A. et al. // Phys. Rev. Lett. 2013. V. 110. P. 012504.

Charmonium photoproduction in proton–nucleus ultraperipheral collisions at the Large Hadron Collider

ALICE Collaboration

V.A. Guzey, V.V. Ivanov, E.L. Kryshen, A.V. Khanzadeev, M.V. Malaev, V.N. Nikulin, V.G. Riabov, Yu.G. Riabov, V.M. Samsonov, M.B. Zhalov
High Energy Physics Division, PNPI NRC "Kurchatov Institute"

Coherent charmonium photoproduction on a proton is a unique source of information on the gluon density in the proton. To the leading order of perturbative Quantum Chromodynamics (QCD), the $\gamma + p \to p + J/\psi$ cross-section at high energies is proportional to the square of the proton gluon density, $g_p(x = \frac{M^2_{J/\psi}}{W^2_{\gamma p}}, \mu^2)$, where x is the fraction of the proton momentum carried by the gluon and μ is the resolution scale determined by the charm quark mass and its characteristic transverse momentum in J/ψ. While $g_p(x, \mu^2)$ is known at small x with the significant uncertainty, this fundamental quantity is required for the description and predictions of cross-sections of hard processes with protons and nuclei, studies of formation and evolution of quark-gluon plasma in collisions of ultrarelativistic ions and searches of new physics beyond the Standard Model.

Currently the only experimental method to study photon-proton and photon-nucleus processes at high energies is provided by ion ultraperipheral collisions (UPCs) at colliders. In such collisions, relativistic ions serve as intensive sources of quasi-real photons of a wide energy spectrum, which allows one to study charmonium photoproduction on a proton in *pA* collisions at unprecedentedly large energies at the LHC.

The ALICE Collaboration at the LHC has for the first time measured exclusive photoproduction of J/ψ mesons in proton-nucleus collisions at the energy of $\sqrt{s_{NN}} = 5.02$ TeV. The J/ψ mesons were reconstructed through their decay into a muon pair using the muon spectrometer; PNPI significantly contributed to its construction. The requirement of absence of any other hadronic activity guaranteed the condition of exclusivity and ultraperipheral mechanism of reaction. In the course of data acquisition, directions of proton and lead beams were reversed allowing one to measure the cross section at the large positive ($2.5 < y < 4$) and the large negative ($-3.6 < y < -2.6$) J/ψ rapidities corresponding to the following values of the photon-proton invariant energy $W_{\gamma p}$: $21 < W_{\gamma p} < 45$ GeV and $577 < W_{\gamma p} < 952$ GeV. Thus, the ALICE measurement gives one the possibility to determine the behavior of $g_p(x, \mu^2)$ in a wide range of small x, $0.00002 < x < 0.02$, and to check whether a transition to the new regime of the saturated gluon density in a proton occurs in this region of x. One should point out that the minimal value of $x \approx 0.00002$ is five times smaller than that achieved within the measurements of the $\gamma + p \to p + J/\psi$ cross-section at the electron-proton collider HERA by the H1 and ZEUS Collaborations.

The left panel of the Figure below presents the comparison of data on J/ψ photoproduction on the proton obtained by the ALICE, H1 and ZEUS Collaborations with theoretical predictions of the leading order (JMRTLO) and next-to-leading order (JMRTNLO) perturbative QCD and the color dipole model (b-Sat). The solid line with the shaded area represents the result of a one-parameter fit to the H1 and ZEUS data in form of $\sigma \propto W^{\delta}_{\gamma p}$ where $\delta = 0.69 \pm 0.02$ (stat.) ± 0.03 (syst.). As shown in the Figure below, theoretical models (except for the b-Sat dipole model) describe the data well.

Photoproduction of J/ψ on the proton was also measured in proton-proton UPCs by the LHCb Collaboration at the LHC. In this case, the extracted values of the $\gamma + p \to p + J/\psi$ cross-section have somewhat larger errors due to the uncertainty in the separation

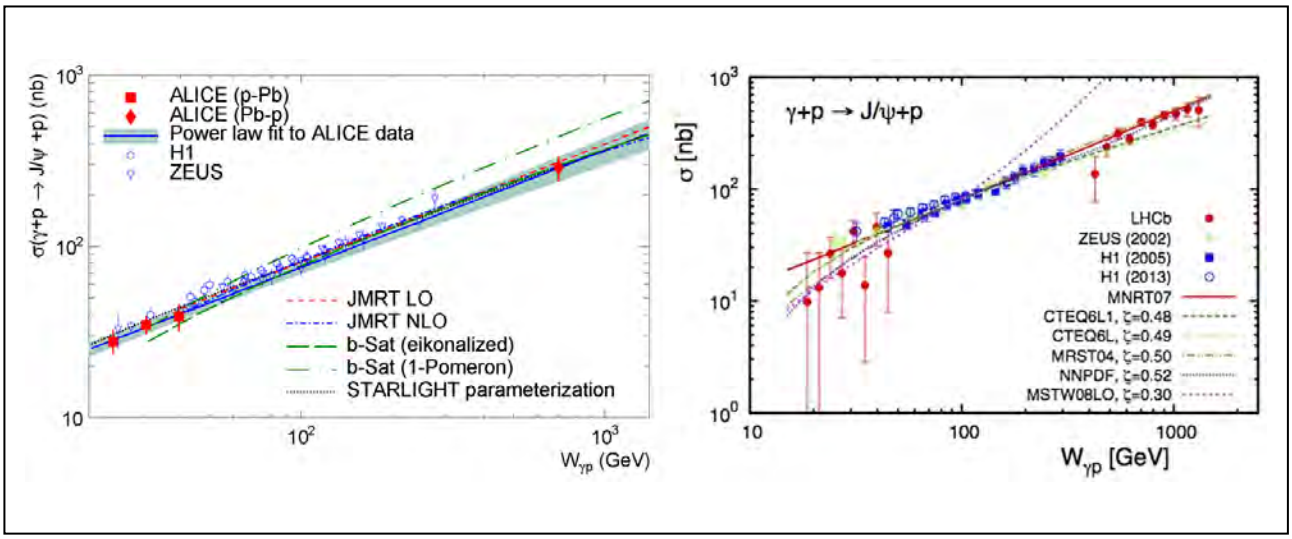

Left panel: the $\gamma + p \to p + J/\psi$ cross-section as a function of $W_{\gamma p}$. ALICE, H1 and ZEUS experimental values vs. theoretical predictions of perturbative QCD and the color dipole model.
Right panel: LHCb, H1 and ZEUS experimental values vs. theoretical predictions of leading order perturbative QCD using various parameterizations of the gluon density in the proton

of the contributions of photons with high and low energies and the necessity to take into account *pp* interactions in the initial and final states. Within experimental errors, the ALICE and LHCb results agree.

The right panel of the figure shows the comparison of the $\gamma + p \to p + J/\psi$ cross-section measured by H1, ZEUS and LHCb collaborations with the theoretical calculations in the framework of leading order perturbative QCD using various parameterizations of the gluon density in the proton. Many modern gluon distributions (CTEQ6L, CTEQ6L1, MRST, NNPDF) describe the $W_{\gamma p}$ dependence of the cross-section well, but require the additional 50% normalization (the factor of $\xi \approx 0.5$). At the same time, the MSTW08LO gluon distribution predicts a too steep $W_{\gamma p}$ dependence, which contradicts the data.

In conclusion, it is important to emphasize that the power-like fit to $W_{\gamma p}$ dependence of the $\gamma + p \to p + J/\psi$ cross-section measured at HERA describes very well the ALICE and the LHCb data. This indicates the absence of significant effects associated with the saturation of the proton gluon density down to $x \approx 0.00001$ at $\mu 2$ of the order of a few GeV^2.

1. *ALICE Collaboration* // Phys. Rev. Lett. 113 (2014) 23, 232504; CERN Courier, Oct. 27, 2014, http://cerncourier.com/cws/article/cern/58915; arXiv:1406.7819 [hep-ex].
2. *LHCb Collaboration* // J. Phys. G: Nucl. Part. Phys. 2014. V. 41. P. 055002.
3. *Guzey V., Zhalov M.* // JHEP. 2013.

New effects in inclusive charmonium production in nucleus-nucleus collisions at the Large Hadron Collider

ALICE Collaboration

M.B. Zhalov, V.V Ivanov, E.L. Kryshen, M.V. Malaev, V.N. Nikulin, V.G. Riabov, Yu.G. Riabov, V.M. Samsonov, A.V. Khanzadeev
High Energy Physics Division, PNPI NRC "Kurchatov Institute"

The ALICE Collaboration at the Large Hadron Collider (LHC) has measured inclusive charmonium production in proton-proton (*pp*), proton-nucleus (*pA*) and nucleus-nucleus (*AA*) collisions. These measurements were performed using the muon spectrometer; PNPI significantly contributed to its construction. The goal of these measurements is a detailed study of the influence of the medium created in the interaction of ultrarelativistic nuclei on the process of charmonium production. A natural quantity characterizing this influence is the factor of nuclear modification

$$R_{AA}^{J/\psi} = \frac{Y_{AA}^{J/\psi}}{N_{\text{coll}} Y_{pp}^{J/\psi}},$$

which is defined by the ratio of inclusive yields $Y_{AA}^{J/\psi}$ and $Y_{pp}^{J/\psi}$, scaled by the number of binary nucleon-nucleon collisions N_{coll}.

Suppression of the quarkonium yield (quarkonium is a quark–antiquark bound state) in ultrarelativistic nucleus collisions was expected due to several reasons. Firstly, heavy quarks and antiquarks are created in hard parton-parton interactions at the initial stage of the collision and, hence, nuclear shadowing of nuclear parton distributions and the final-state rescattering in the hadronic medium should lead to $R_{AA}^{J/\psi} < 1$. These so-called "cold nuclear matter effects" can be studied in proton-nucleus and peripheral nucleus-nucleus scattering. Secondly, another interesting phenomenon was predicted (Matsui & Satz): if a hot quark-gluon plasma (QGP) is formed in the interaction volume of ultrarelativistic nuclei, then, by analogy with the Debye screening in classical plasma, color charges of heavy quarks should be screened. As a result, bound quark-antiquark states either cannot be formed or, if they do, they dissociate as soon as the Debye radius becomes smaller than the quarkonium radius as the medium temperature increases. In this case, one expects the "anomalous" $R_{AA}^{J/\psi} << 1$ suppression.

Suppression of the charmonium yield in high hadron multiplicity events in ultrarelativistic nucleus collisions at the energy of $\sqrt{s_{NN}} \approx 18$ GeV was for the first time discovered at the SPS accelerator at CERN. This result was interpreted as one of the most dramatic signals of the QGP formation. However, a detailed analysis showed that the observed $R_{AA}^{J/\psi}$ and its dependence on the atomic numbers of colliding nuclei can be explained by cold nuclear matter effects and the fact that approximately 40% of J/ψ originate from decays of weakly-bound excited charmonium states, which dissociate at the temperatures below or near to the temperature of the phase transition, $T_к \approx 160$–170 MeV.

The interest to the studies of suppression of the J/ψ yield renewed when the experiments at the Relativistic Heavy Ion Collider (RHIC) at the collision energy of $\sqrt{s_{NN}} \approx 200$ GeV have obtained the unambiguous evidence of formation of the quark-gluon matter with properties of an almost ideal liquid with the temperature exceeding 200 MeV in the initial stage of its evolution. It also turned out that $R_{AA}^{J/\psi}$ is almost the same at RHIC and SPS. Therefore, either the dependence of the suppression effect on the temperature of the medium created in the interaction zone is absent or a new effect of J/ψ production compensating the suppression increase appears at RHIC energies

From this point of view, the measurement of $R_{AA}^{J/\psi}$ in collisions of lead nuclei at the energy of $\sqrt{s_{NN}} \approx 2.76$ TeV at the LHC was undoubtedly interesting. The data analysis leading to determination of R_{AA} implied the selection of central nucleus scattering events characterized by large hadron multiplicities.

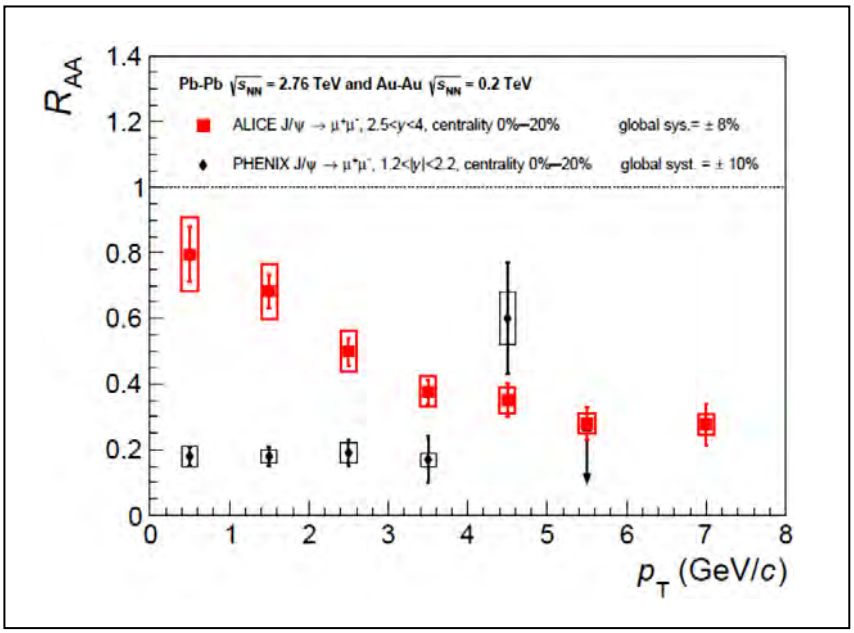

Dependence of $R_{AA}^{J/\psi}$ on the transverse J/ψ momentum obtained by the ALICE Collaboration at the LHC and by the PHENIX Collaboration at RHIC

The signs of formation of the dense and hot quark-gluon matter with the temperature of $T > 300$ MeV in the interaction region were found in this class of events (suppression of the yield of light hadrons, jet quenching, elliptic flows of different particles and the effect of the quark scaling of the elliptic flows, and the yield of direct photons).

The Figure above shows the comparison of the results for the dependence of $R_{AA}^{J/\psi}$ on the transverse J/ψ momentum obtained by the ALICE Collaboration in the J/ψ rapidity interval of $2.5 < y < 4$ at the LHC and by the PHENIX Collaboration in the interval of $1.2 < |y| < 2.2$ at RHIC. Despite the expectation based on the observation that the medium temperature increases by the factor of more than 1.5, suppression of the J/ψ yield turned out to be smaller at the LHC energies.

The intriguing dependence of $R_{AA}^{J/\psi}$ on the transverse momentum can be possibly explained (Andronic et al.) by the manifestation of a new mechanism of J/ψ production, which constitutes of recombination of thermalized charm quark and antiquark at the late stage of QGP evolution. At this stage, the temperature of the quark-gluon matter is 160–170 MeV, which is close to the boundary of the phase transition. The argument supporting this interpretation is an almost ten-fold increase in the number of produced charm quarks and antiquarks at the LHC compared to that at RHIC resulting from a rapid increase of cross-sections of hard processes with an increase of the collision energy. As a result, the probability of statistical hadronization increases and the presence of the dense quark-gluon matter facilitates heavy quark thermalization.

ALICE Collaboration // Phys. Lett. B. 2014. V. 734. P. 31.

Detection of solar *pp*-neutrinos within the BOREXINO experiment

A.V. Derbin
Neutron Research Division, PNPI NRC "Kurchatov Institute"

A direct experimental evidence of essential solar thermonuclear reaction was obtained for the first time. In this reaction, a deuterium nucleus is produced by fusion of two protons: $p + p \rightarrow d + e^+ + \nu$ (see left Figure). This reaction (usually referenced as *pp*) is responsible for production of 99.8% of total solar energy, yet, until now, no direct observation of corresponding neutrino flux was performed. The reaction produces neutrinos with threshold energy of 420 keV, which were detected within the BOREXINO experiment. The detection of *pp*-neutrinos is an extremely difficult task due to their low energy (the lowest among the solar neutrinos, actually), which overlaps with the region of high-rate natural background (see right Figure).

Previously, BOREXINO Collaboration published the results of neutrino flux measurements for secondary solar reactions that occur downstream of the *pp*-reaction and create relatively minor contribution to the total amount of solar energy. The comparison of BOREXINO results with the value of the solar radiation power confirms the stability of solar energy output on the time scale of several hundred thousand years.

The results were obtained with the valuable contribution from Russian researchers from PNPI NRC "Kurchatov Institute" (Low Background Measurements Laboratory: A.V. Derbin, V.N. Muratova), JINR, NRC "Kurchatov Institute" and SINP MSU.

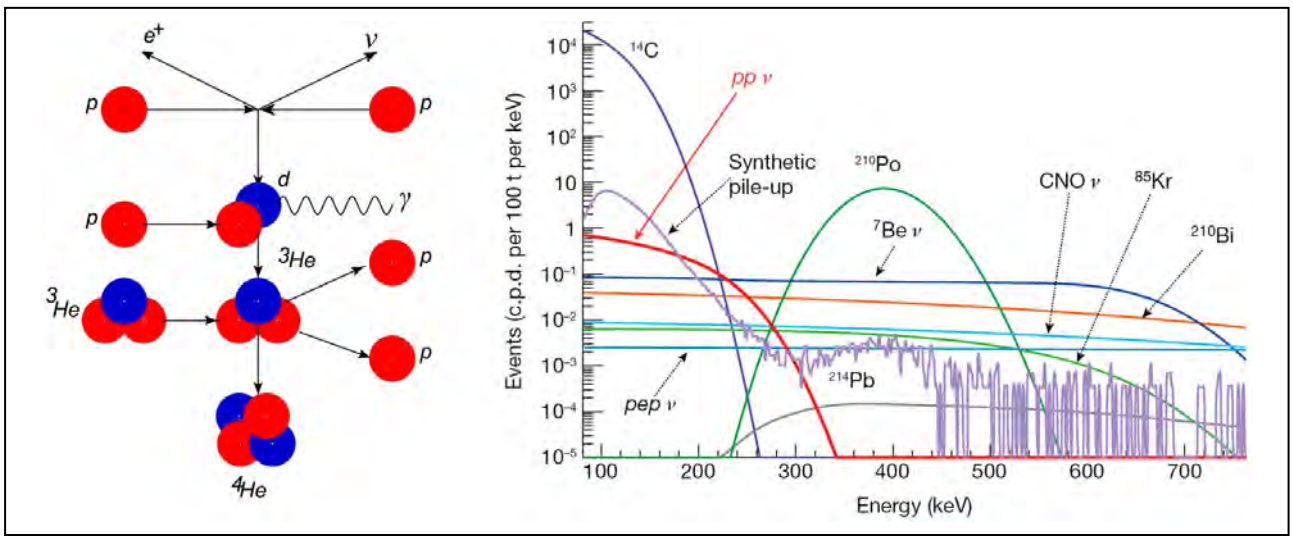

Left: the main sequence of nuclear reactions that transform four protons into the ^{4}He nucleus. It starts with the fusion of two protons producing deuterium nucleus, positron and *pp*-neutrino. *Right*: the energy spectrum (150–600 keV) measured by BOREXINO detector and its main components determined by the analysis. The solid red line indicates the *pp*-neutrino contribution

Borexino Collaboration (Bellini G. et al.) // Nature. 2014. V. 512. P. 383.

The search for solar axions produced by $p(d,^3\mathrm{He})A$ reaction using the scintillating BGO bolometer

A.V. Derbin
Neutron Research Division, PNPI NRC "Kurchatov Institute"

An axion is a hypothetical particle that was introduced to the theoretical framework in order to solve the strong *CP*-problem. Due to its assumed properties, this particle became a viable dark matter candidate. The sun should be a powerful source of axion production, provided the given particle does actually exist.

A search for axioelectric effect (similar to the photoelectric effect) on bismuth atoms was conducted at the Low Background Measurement Laboratory of PNPI NRC "Kurchatov Institute" (head of laboratory: A.V. Derbin) and Gran Sasso National Laboratory. Solar axions with 5.5 MeV energy can be produced by the proton capture: $p + d \rightarrow {}^3\mathrm{He} + A$. Since the value of axiolelectric effect cross-section depends on Z^5, bismuth ($Z = 83$) appears to be a viable target material. A cryogenically cooled scintillating BGO bolometer was for the first time used to perform a search for axions (see left Figure).

As a result, a new region of possible values of axion mass m_A and coupling constants g_{Ae} and g_{AN^3} was excluded by a direct laboratory measurement (see right Figure). The new limit is 20 times more stringent than the one obtained by conventional scintillation BGO detector.

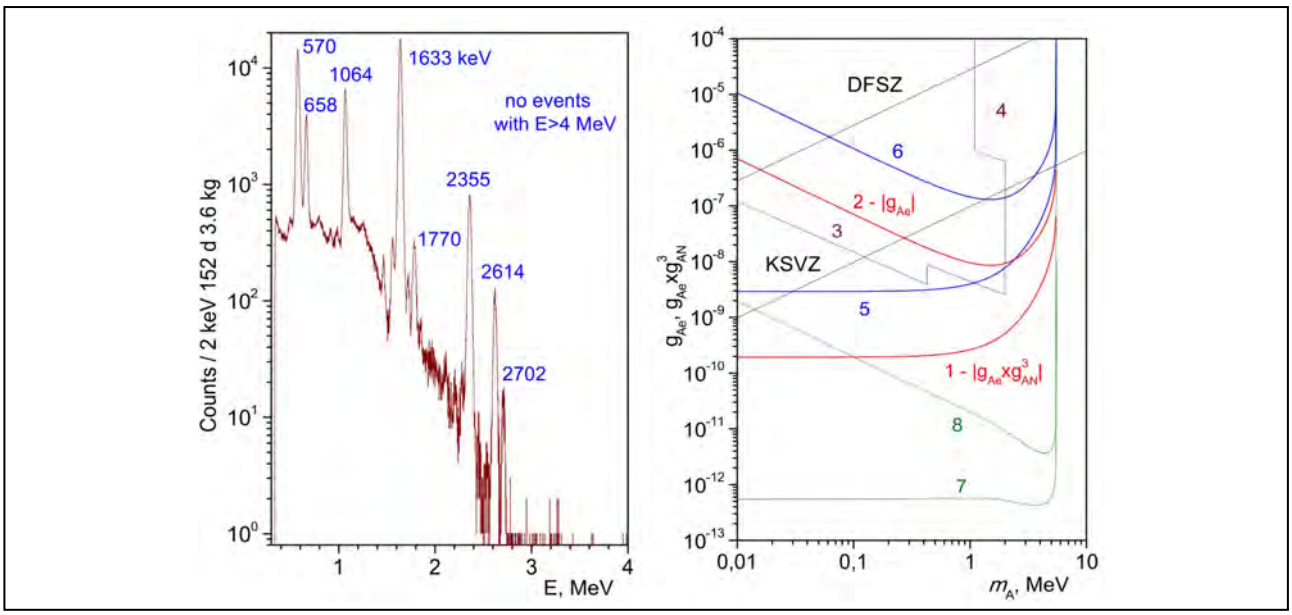

Left: the spectrum of β- and γ-events measured by scintillating BGO bolometer for 152 days. The spectrum does not contain any events above 4 MeV. *Right:* regions of excluded axion mass and values of coupling constants (above the lines) obtained by various experiments: 1, 2 – our limits for $|g_{Ae} \times g_{AN^3}|$ and $|g_{Ae}|$ values respectively; 3 – reactor experiments; 4 – beam-dump accelerator experiments; 5, 6 – limits for $|g_{Ae} \times g_{AN^3}|$ and $|g_{Ae}|$ obtained with conventional BGO detector; 7, 8 – BOREXINO limits obtained from the Compton conversion

1. *Derbin A.V., Bakhlanov S.V., Dratchnev I.S., Kayunov A.S., Muratova V.N.* // Eur. Phys. J. C. 2013. V. 73. P. 2490.
2. *Derbin A.V., Gironi L., Nagorny S.S., Pattavina L. ..., Drachnev I.S. ..., Kayunov A.S. ..., Muratova V.N. ..., Semenov D.A., Unzhakov E.V.* // Eur. Phys. J. C. 2014. V. 74. P. 3035.

The influence of flux density of nucleons on the effectiveness of CCD-matrix damage

K.N. Ermakov, N.A. Ivanov, O.V. Lobanov, V.V. Pashuk, E.V. Mitin, M.O. Prigunov
Knowledge Transfer Division, PNPI NRC "Kurchatov Institute"

At present, "single event effects" are observed in modern integrated circuits: soft errors and destructive failures in the work of microelectronic products caused by the action of individual protons, cosmic radiation ions and neutrons in the near atmosphere. Radiation resistance of components of electronic equipment used for aerospace purposes is tested usually with the use of accelerators of protons and ions. Since the density of a particle flux exceeds in this case significantly (by several orders of magnitude) the flux density of particles of outer space, the question arises whether the results of ground testing correspond to results of the work of electronics in space.

We studied the impact of protons with energy of 1 000 MeV and atmospheric neutron spectrum with a maximum energy of 1 000 MeV on image sensors based on charge-coupled devices (CCD). The effect of individual particles is caused by structural abnormalities in the sensitive volume generated by products of nuclear reactions of nucleons with nuclei of silicon atoms, and is manifested in the occurrence of spikes with dark currents IDC of significantly higher values than the average.

Time distribution of pixels with high dark current value was investigated in a CCD matrices irradiated by nucleons with fluences in range of 10^9–10^{10} cm^{-2}. The brightness of matrix pixels was regularly measured during the period of one month. Dark currents in pixels of the matrix were determined by the degree of their brightness in integer relative units (r. u.) in the range of 0 (black) to 255 (white).

As a result, we obtained time dependences of the number of spikes in irradiated matrices, dark currents of which differed from the values in non-irradiated matrices by 10÷30, 31÷60, 61÷100, and 101÷250 r. u. presented in Figure 1. The cross-sections of the spike generation by nucleons calculated for these groups from the experimental data were $1.1 \cdot 10^{-6}$, $2.7 \cdot 10^{-7}$, $3.6 \cdot 10^{-8}$ and $4.3 \cdot 10^{-9}$ cm^{-2}, respectively. Figure 1 shows that after irradiation the number of spikes decreased over

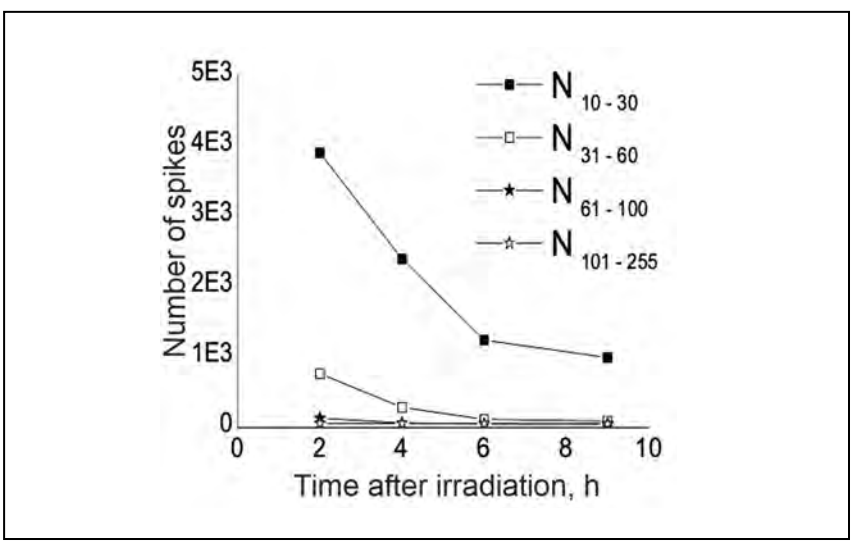

Fig. 1. Time dependence of the number of spikes

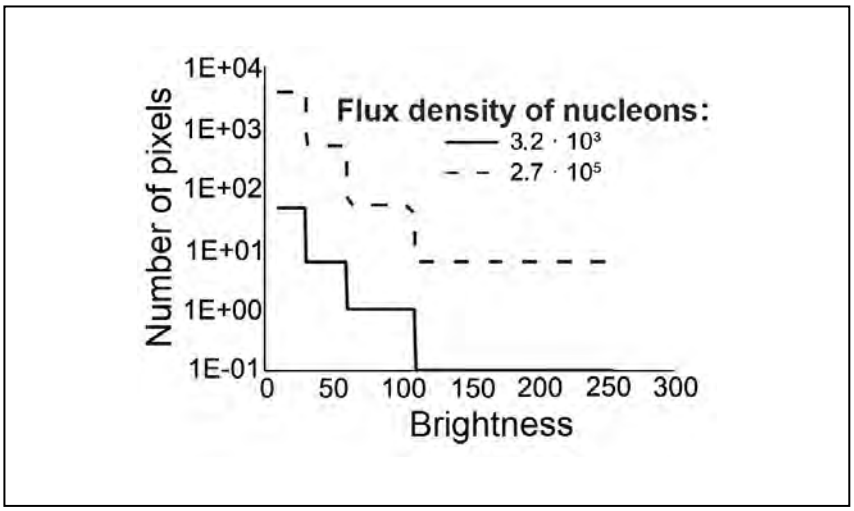

Fig. 2. The equilibrium distribution of number of spikes by brightness

time. Time dependence of the number of spikes was approximated by the exponential function: $N \sim \exp(t/\tau_i)$ separately for pixels of each group of brightness. As a result of approximation, relaxation times were obtained for spikes of different brightness equal to: $\tau_{10\div30} = 6 \cdot 10^4$, $\tau_{31\div60} = 4 \cdot 10^4$, $\tau_{61\div100} = 3.5 \cdot 10^4$ и $\tau_{101\div255} = 3.5 \cdot 10^4$ s.

The decrease in the number of spikes is caused by the annealing of radiation defects in irradiated products. Due to this fact, prolonged irradiation by nucleons with a flux density of particles φ in CCD matrix will lead to creation of equilibrium distribution of spikes on dark current $N_{eq.}(I_{dc})$, which is determined from the following condition: the rate of formation of new spikes $\varphi \cdot \sigma$ is equal to the speed of annealing – $N_{eq.}/\tau$ where σ, τ is a cross-section of generation and the average lifetime of spikes with dark currents I_{dc} respectively. Then $N_{eq.} = \varphi \cdot \sigma \cdot \tau$.

Consequently, the equilibrium distribution of spikes with prolonged irradiation of CCD-matrix by nucleons and ions of cosmic radiation with different flux densities will also be different. Figure 2 demonstrates the histogram distribution of pixel brightness obtained after irradiation by nucleons with a flux density of $2.7 \cdot 10^5$ cm$^{-2} \cdot$ s^{-1} and calculated by the formula $\varphi_{cr} = 3.2 \cdot 10^3$ cm$^{-2} \cdot$ s^{-1}. The Figure shows that the equilibrium distribution of spikes according to their brightness at the flux density of particles typical for cosmic radiation is significantly different from the distribution obtained at a higher flux density of particles in course of accelerator experiments.

Thus, this study shows a significant effect of particle flux density distribution of simulating installation on the distribution of the dark current in pixels of the CCD matrix, which requires consideration when predicting effects from exposure to individual particles of cosmic radiation.

This research was supported by the Russian Scientific Foundation (project 1429-09240).

1. *Ivanov N.A., Lobanov O.V., Mitin E.V., Pashuk V.V., Tverskoy M.G.* // JETP Letters. 2013. V. 39. Iss. 17. P. 35–43.
2. *Ivanov N.A., Lobanov O.V., Pashuk V.V., Mitin E.V., Prigunov M.O., Bogdanov V.P., Osadchy I.S., Treschchalin A.P.* // Voprosi atomnoy nauki I techniki. 2014. Iss. 1. P. 49–51.

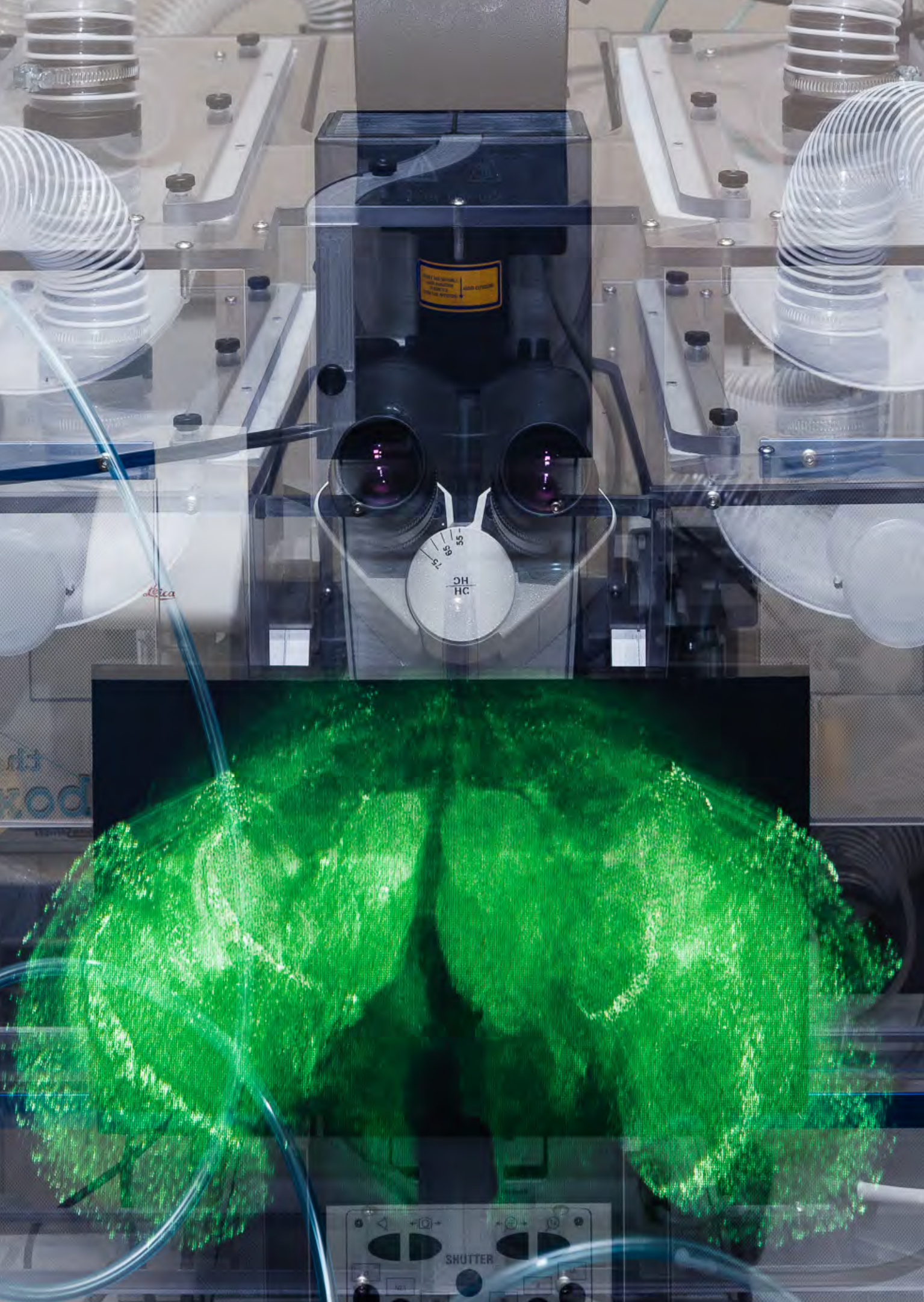
55
65
75
HC
SHUTTER

Molecular and Radiation Biophysics

Structure and function of β-mannosidase from *Trichoderma harzianum*

A.M. Golubev
Neutron Research Division, PNPI NRC "Kurchatov Institute"

In economically developed countries, much attention is paid to alternative fuels (ethanol, biodiesel, biopropanol). In this regard, structural study of enzymes capable of converting renewable resources and waste into alternative fuels becomes important. As it has been shown previously, filamentous fungi of the genus *Trichoderma* secrete complex of enzymes hydrolyzing most abundant natural materials like cellulolignin and galactomannan into monosaccharides that can be used to produce biofuels. One of the important hydrolyzing enzymes of this complex is β-mannosidase.

We managed to solve the 3-dimensional structure of β-mannosidase from the fungus *Trichoderma harzianum*. It is the first structure of a eukaryotic β-mannosidase from the 2nd family of glycoside hydrolases. On the basis of the structure solved, the substrate-binding site has been studied by methods of molecular dynamics and the mechanism of action of the enzyme has been explored.

The crystals of β-mannosidase – glycoprotein with a molecular weight of 105 kDa – were obtained previously and *X*-ray data have been collected using synchrotron radiation for two crystal forms: orthorhombic and tetragonal. The best crystallographic resolution achieved was 1.9 Å. The structure of the protein has been solved using the anomalous scattering of cadmium atoms incorporated into the crystals of the protein during growth.

One of the limitations of the *X*-ray analysis is the fact that a constructed model is static. In order to study the dynamic behavior of the protein molecule, the comparison of two models based on data from different crystalline forms was carried out. In this case, the presence of two crystal forms enabled us to evaluate the conformational mobility and flexibility of the protein molecule. The molecule of β-mannosidase consists of five well-defined domains (Fig.). A comparison with the structures of other glycoside hydrolases of 2nd family allowed us to determine the position of the catalytic domain in the molecule. The molecular dynamics method has been used to detect the galactomannan-binding site. These enabled us to estimate precisely the free energy of the enzyme-substrate complex and localize amino acid residues involved in catalysis.

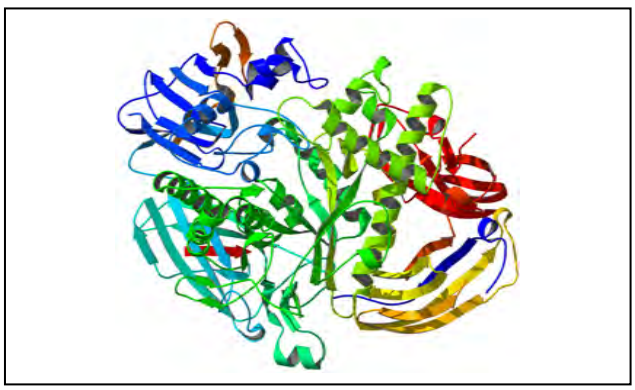

General view of the β-mannosidase molecule – ribbon diagram

1. *Horta M.A., Vicentini R., Delabona P.A.S., Laborda P., Crucello A., Freitas S., Kuroshu R.M., Polikarpov I., Pradella J.G., Souza A.P.* // PLoS One. 2014. V. 9. P. e88689.
2. *Nascimento A.S., Muniz J.R., Aparício R., Golubev A.M., Polikarpov I.* // FEBS J. 2014. V. 281. P. 4165–4178.

Increased level of plasma oligomeric alpha-synuclein in patients with lysosomal storage diseases

S.N. Pchelina, E.P. Nuzhnyi, A.K. Emelyanov, T.M. Boukina, T.S. Usenko, M.A. Nikolaev, G.N. Salogub, A.F. Yakimovskii, E.Yu. Zakharova
Molecular and Radiation Biophysics Division, PNPI NRC "Kurchatov Institute"

In 2014 we conducted a study on levels of oligomeric alpha-synuclein in plasma of patients with lysosomal storage diseases (LSDs). Alpha-synuclein oligomerization is believed to be the major neurotoxic event in neurodegenerative process in common neurodegenerative disorder, Parkinson's disease (PD). About 10–15% of PD patients report the familial form of the disease. Currently, mutations in several genes (*SNCA*, *LRRK2*, *PINK1*, *PARK2*, *PARK7*, *PLA2G6*, *FBXO7*, *ATP13A2*) were identified to be the course of PD in rare cases. The most important for the PD prognosis are the *GBA*, *SMPD1* and *NPC1* genes that are the genes of high risk of PD development. Mutations in these genes increase the risk of PD development by up to 8–9 times, and their frequency in different populations is 0.5–5% (Fig.). The most frequent are the mutations in the glucocerebrosidase (*GBA*) gene. In our population, each 250th citizen of the European part of Russia may be the carrier of those mutations and thus is exposed to a high risk of PD development.

How to explain such a high risk for PD development in carriers of mutations in *GBA*, *SMPD1* and *NPC1*

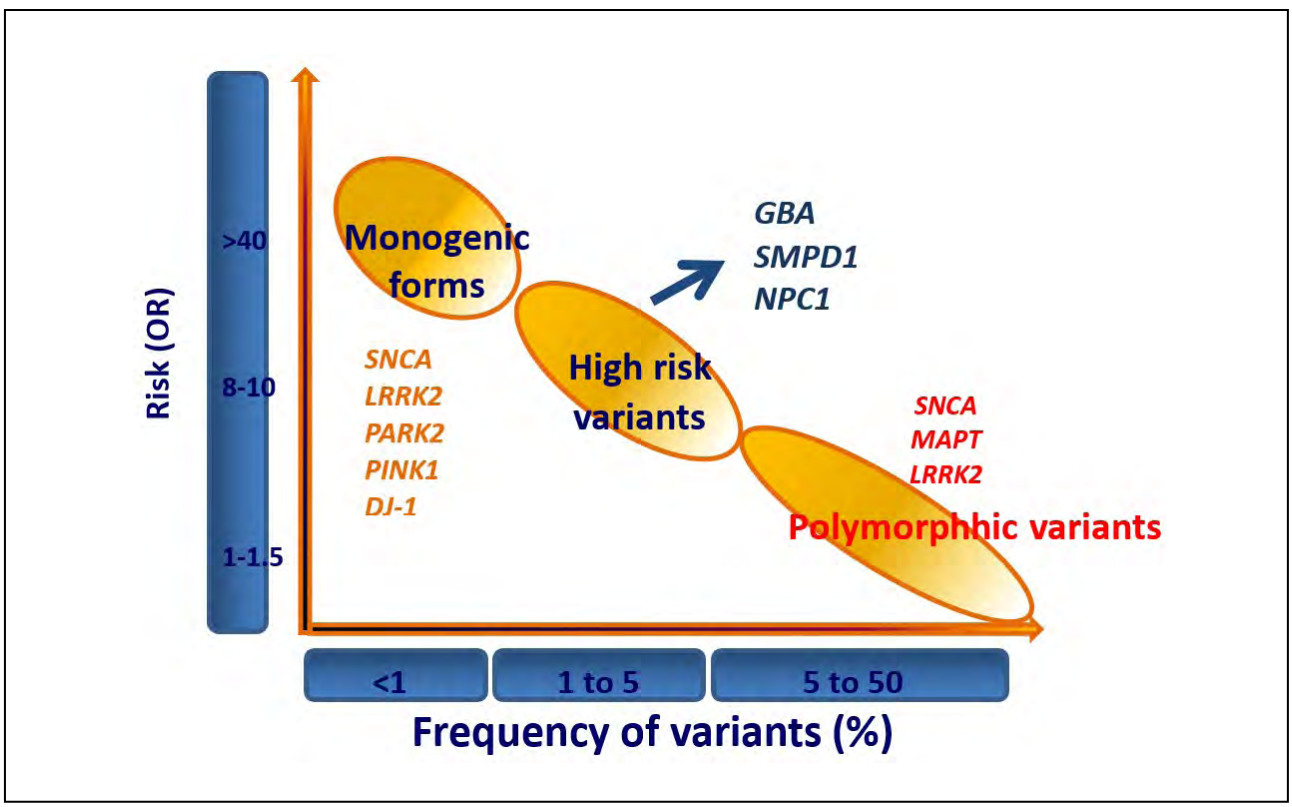

Genetic risk factors for Parkinson's disease development. An arrow indicates the genes that, if subjected to mutations, increase the risk of PD development by 8–9 times

genes? It was proven that all these genes encode the enzymes localized in lysosomes, cell compartments responsible for protein degradation. One mutant allele in the *GBA*, *SMPD1* and *NPC1* genes leads to increased risk of PD. Mutation in both alleles are the course of rare inherited diseases linked to lysosomal disfunction, LSDs. The most frequent disorder among LSDs is Gaucher disease caused by mutations in the *GBA* gene. We hypothesized that lysosomal dysfunctions observed in LSDs could affect the levels of alpha-synuclein as half of cellular protein is degraded via lysosomes, and facilitate its oligomerization in patients bearing mutations in LSDs causative genes. This may lead to the formation of neurotoxic oligomeric alpha-synuclein protein species that are thought to cause the neurodegeneration in PD.

We studied the level of oligomeric alpha-synuclein in plasma of 41 patients with Gaucher disease and 40 members of control groups by means of ELISA with recently introduced oligomeric alpha-synuclein antibodies. The level of oligomeric alpha-synuclein form, associated with PD development, was significantly increased in plasma of patients with Gaucher compared to the plasma of control group members ($p < 0.0001$). Moreover, levels of alpha-synuclein oligomers in plasma is also higher in patients with other LSDs (Niemann-Pick type C, Krabbe disease, Wolman disease) compared to the mean value in control group members. Our study was the first to show an increase of oligomeric alpha-synuclein levels in plasma of patients with mutations in LSDs genes linking together such different pathologies as LSDs and PD through alpha-synuclein aggregation. Furthermore, alpha-synuclein levels were increased only in patients who did not receive an enzyme replacement therapy (ERT) or received it for less than 5 years. Alpfa-synuclein levels in plasma of Gaucher disease patients receiving ERT for more than 5 years did not differ from the same level in control groups. Thus, the present study supports the notion of insufficiency in GBA activity being able to influence alpha-synuclein oligomerization and suggests that therapeutic strategies argumenting GBA activity might be potentially helpful for treatment of *GBA*-associated PD.

This research was supported by the Russian Foundation for Basic Research (projects No. 13-04-01510 and No.14-04-31665).

1. *Pchelina S.N., Nuzhnyi E.P., Emelyanov A.K., Boukina T.M., Usenko T.S., Nikolaev M.A., Salogub G.N., Yakimovskii A.F., Zakharova E.Y.* // Neurosci. Lett. 2014. V. 583. P. 188–193.
2. *Deng H., Xiu X., Jankovic J.* // Mol. Neurobiol. 2014. Aug. 7 [Epub ahead of print].
3. *Kovacs G.G., Wagner U., Dumont B., Pikkarainen M., Osman A.A., Streichenberger N., Leisser I., Verchère J., Baron T., Alafuzoff I., Budka H., Perret-Liaudet A., Lachmann I.* // Acta Neuropathol. 2012. V. 124. P. 37–50.

Sin3 histone deacetylase controls level of spontaneous and UV-induced mutagenesis in yeast *Saccharomyces cerevisiae*

V.G. Korolev, A.Yu. Chernenkov, I.Yu. Lebovka, T.N. Kozhina, I.V. Fedorova, V.T. Peshekhonov, T.A. Evstyukhina
Molecular and Radiation Biophysics Division, PNPI NRC "Kurchatov Institute"

Genetic regulation of chromatin assembly and modifications is the most important and rapidly developing directions of up-to-date biology and medical research. The exceeding amount of data obtained recently in a field of chromatin affects upon the DNA repair. However, there are only several published investigations concerning modified chromatin effects on mutation process. The properties of chromatin forming structural subunits – histones and nucleosomes – could be modified under the influence of special chemical improvements such as acetyl, methyl or phosphate groups addition, that controls DNA transcription, replication and repair processes occurring in the living cell. Each member of wide variety of histone modifying enzymes is definitely specific with regard to the sites of modifications. Manifold histone variants act in cell resistance to the DNA damaging agents and at the same time provide signaling and DNA repair regulation.

Histone acetylation, realized by histone acetyltransferases (HAT), and deacetylation, accomplished by histone deacetylases (HDAC), are the patterns used by a cell to modify the chromatin structure. HAT and HDAC manifest the antagonistic behavior affecting the genes expression: acetylation induces gene expression and deacetylation causes repression. Main function of HDAC is the acetyl group's elimination from chromatin structure, which makes chromatin inaccessible for DNA transcription complexes. Chromatin modifying exists with the combined HAT and HDAC action: HAT executes the improvements over all genome and HDAC selectively recognizes those marks in special DNA sites to realize deacetylation for peculiar acetylation pattern to be established.

The product of *SIN3* gene is a RPD3 HDAC complex subunit and acts as a repressor for a considerable amount of genes in yeast *S. cerevisiae.* Sin3p is capable of interaction with other DNA-binding proteins for the purpose of aiming the RPD3 complex on specific promotors in order to regulate DNA transcription. The deoxyribonucleotide (dNTP) pool increase after the massive DNA damage is regulated by ribonucleotide reductase (RNR) activity and is crucial for DNA replication and cell survival. RNR catalyzes rate-limited synthesis reaction of all four dNTP species, which are required for mitochondrial and nuclear DNA synthesis.

We examined the effects of *sin3* mutation on mutagenesis in *S. cerevisiae* yeast cell. Standard yeast growth medium was used in our investigation. Cell cultures were treated by canavanine (spontaneous mutation rate registration), hydroxyurea (inhibition of RNR) and UV irradiation (induced mutation rate registration). Single mutants on *SIN3* gene were constructed along with double mutants on *SIN3* gene and key genes of nucleotide excision repair (*RAD1* gene) and homologous recombination repair (*RAD52* gene) systems.

Single *sin3*, *rad1* and double mutant *rad1 sin3* analysis let us conclude that *sin3* mutation leads to the increase in sensitivity of haploid cell upon higher UV irradiation doses. That fact is in accordance with the massive budding yeast cells death (Fig. 1). That may be interpreted as abnormalities in homologous recombination DNA repair mechanism and conformed with previously published data.

Homologous recombination DNA repair pathway is blocked in *sin3rad52* double mutant, and all DNA lesions are mended using post-replicative DNA repair mechanism, which is less effective by reason of low dNTP concentration caused by the presence of *sin3* mutation. As a result, total cell death will increase and the level of spontaneous mutations emerged in error-prone DNA repair pathway will reduce (Fig. 2).

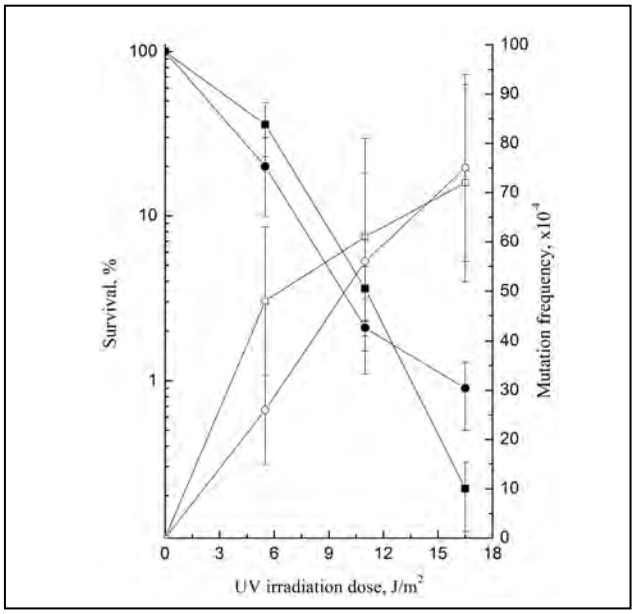

Fig. 1. Survival of (-■-) – *rad1*, (-●-) – *sin3rad1* and mutagenesis of (-□-) – *rad1*, (-○-) – *sin3rad1* under UV-light irradiation

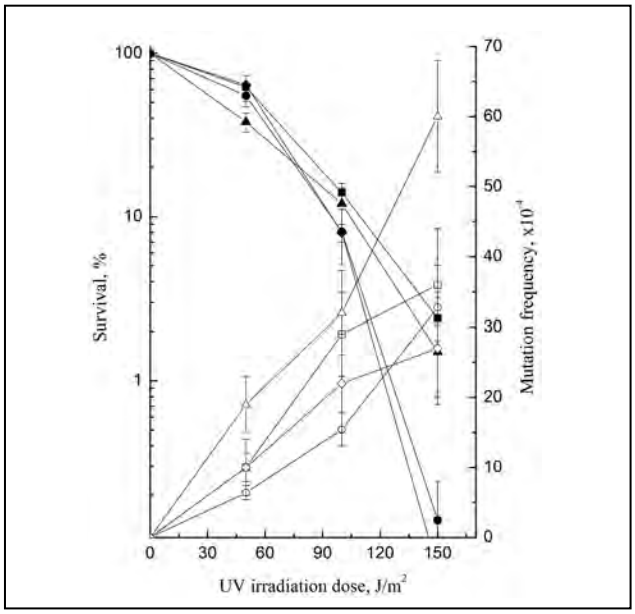

Fig. 2. Survival of (-■-) – wild type, (-●-) – *sin3*, (▲) – *rad52*, (♦) – *sin3rad52* and mutagenesis of (-□-) – wild type, (-○-) – *sin3*, (-△-) – *rad52*, (◊) – *sin3rad52* under UV-light irradiation

The expansion of dNTP synthesis occurs in the living cell directly prior to DNA replication. The second reason is the RNR activation in response to DNA damage. Using UV irradiation as an inductor of DNA lesion's appearance leads to 6–8 fold rise of dNTP concentration, which correlates with cell resistance to DNA damage. At the same time, higher tolerance is connected with the increased mutation rate, which is caused by more effective error-prone DNA repair synthesis.

The inactivation of RPD3 complex in yeast cells leads to mutation process trespassing. The level of the UV-induced mutagenesis is decreased in *sin3* mutant (Fig. 2). That means Sin3p regulates dNTP pool level negatively. Faults of that type of regulation result in induced mutagenesis reduction observed in our research.

Similarly, *sin3* mutation affects both spontaneous replicative and reparative mutagenesis. The decrease of levels of both types of spontaneous mutagenesis could be explained by the fact that due to the *sin3* mutation the required raise of dNTP pool does not occur during DNA replication, but the lower dNTP concentration induces sluggish DNA synthesis and error-prone DNA polymerases block. As a result, we observed replicative spontaneous mutagenesis rate deceleration. In case of reparative spontaneous mutagenesis, dNTP pool level is not raised as well, which leads to lower amount of DNA repair mistakes.

Summarizing, we can conclude that *SIN3* gene plays a crucial role in dNTP pool level control both in DNA replication and in DNA repair mechanisms.

Lebovka I.Yu., Kozhina T.N., Fedorova I.V., Peshekhonov V.T., Evstyukhina T.A., Chernenkov A.Yu., Korolev V.G. //
Russian Journal of Genetics. 2014. V. 50. No. 1. P. 1–6.

Investigation of mechanisms of ATP hydrolysis in the DNA dependent ATPases mkTIP49 of hyperthermophilic archeabacteria *Methanopyrus kandleri*

M.G. Petukhov, A.S. Afanasyeva
Molecular and Radiation Biophysics Division, PNPI NRC "Kurchatov Institute"

In this project, we studied essential for eukaryotic cells and archea proteins DNA-dependent ATPases TIP49, belonging to the AAA+ superfamily. Being a part of complexes of chromatin remodeling TIP60, SWR1 and INO80, they play an important role in most metabolic processes of cells, such as transcription, DNA repair, mitosis and apoptosis. It has recently been shown that these proteins play a key role in cancerogenesis, and that selective inhibitors of the ATPase activity of these proteins are prospective drugs against several types of human cancer.

The objective of this project is an investigation of mechanisms of DNA-dependent ATPase activity of TIP49 proteins with the use of a combination of theoretical methods, molecular modeling, molecular dynamics in periodic water box and modern experimental molecular biological and biochemical methods. The mechanism of ATP hydrolysis in proteins can proceed in several alternative ways. In this paper, we have examined one of the most probable variants, so-called associative mechanism, which imply that the attacking water molecule is preliminary activated by means of the polar or negatively charged side chains of ATPase accepting a water proton. The object of our research is the TIP49 ortholog from hyperthermophilic organism *Methanopyrus kandleri* (mkTIP49; UniProtKB ID: Q8TZC3_METKA), which has a sufficiently high level of homology to human TIP49a/b proteins (45% and 42%, respectively), and due to its high thermostability, these proteins are easily subjected to separation, purification, and biochemical study.

In present work, we used various theoretical (molecular dynamics) and experimental approaches (molecular biological and biochemical) in a single combined study of mechanisms of ATP hydrolysis. In particular, we developed new methods for analysis of the dynamics of activated water molecules in the vicinity of their target groups. Spatial structure of mkTIP49 hexameric complexes was built with the use of homology modeling based on known crystal structures of TIP49a, TIP49b and TIP49ab complexes. Calculations of molecular dynamics of hexameric complex were performed on a multiprocessor high performance computing complex NRC "Kurchatov Institute" HPC2 using the software package GROMACS 4.5.5 in AMBER99SB force field. The ATPase activity of the wild-type protein and its mutant forms was considered to be corresponding to the availability of ATP for the attacking water molecule in correct orientation towards the γ-phosphate group of ATP. The value of a latter was calculated as cumulative probability of the presence of water molecule within the limited volume located in the center in front of the γ-phosphate group of ATP. This volume, containing only one water molecule at a time, was defined as a sphere radius of 1.4 Å at a distance of 2.5 Å from the γ-phosphate group. The probability of water presence was calculated as the proportion of time, during which the water molecule is present in this volume. Since ATP hydrolysis requires the activation of water molecules by surrounding functional groups of the protein that are able to accept a proton of water, we calculated the probability of formation of hydrogen bonds between the lytic water molecule and several negatively charged residues of the protein (E297, D346 and D349) as well. This way we characterized the probability of a correct orientation of a water molecule in attacking position. The calculations were performed with the reference to all known steric constraints of the formation of appropriate hydrogen bonds. Separation, purification and experimental study of the ATPase activity of the investigated proteins were performed with the use of standard biochemical methods.

In our work, we investigated the mechanisms of ATP hydrolysis of the proteins mkTIP49. We introduced a series of point mutations of amino acids in

the active site of the protein and studied consequences of these mutations using theoretical and biochemical approaches. In particular, we proposed amino acid substitution N326Q from the subunit neighboring to the catalytic site that shifts the polar amino group closer to ATP compared to the wild-type protein and, according to our calculations, this rearrangement may lead to the appearance of a new hydrogen bond donor for water molecule in attacking position (Fig.).

Theoretically, we predicted that this substitution would reorient the attacking water molecule and could interfere with Mg^{2+} ion coordination with D296 from Walker B. motif. As predicted, ATPase activity of the mutant N326Q mkTIP49 was completely lost in course of biochemical experiments. These experimental results confirmed our calculations and correctness of a chosen mechanism of ATP hydrolysis in the proteins studied. This way we have also confirmed the correctness of the spatial arrangement of all the structural elements in the protein active site, as well as the arrangement of molecules participating in the ATP hydrolysis process, including so far unknown structure of a hexameric complex of the protein studied.

In addition, the suggested mutant can be used to protect ATP from hydrolysis in studies of different biological functions of these proteins in cellular processes. These results show that the ATP hydrolysis in active sites of TIP49 family proteins, both in archea and in human cells, occur according to the associative mechanism and based on a complex network of hydrogen bonds and coordination bonds of the protein, ions, Mg^{2+} and lytic water. This approach of monitoring of lytic water molecules in the ATPase active site discovers new possibilities for research on the enzymatic activity of other proteins using the methods of molecular modeling and molecular dynamics.

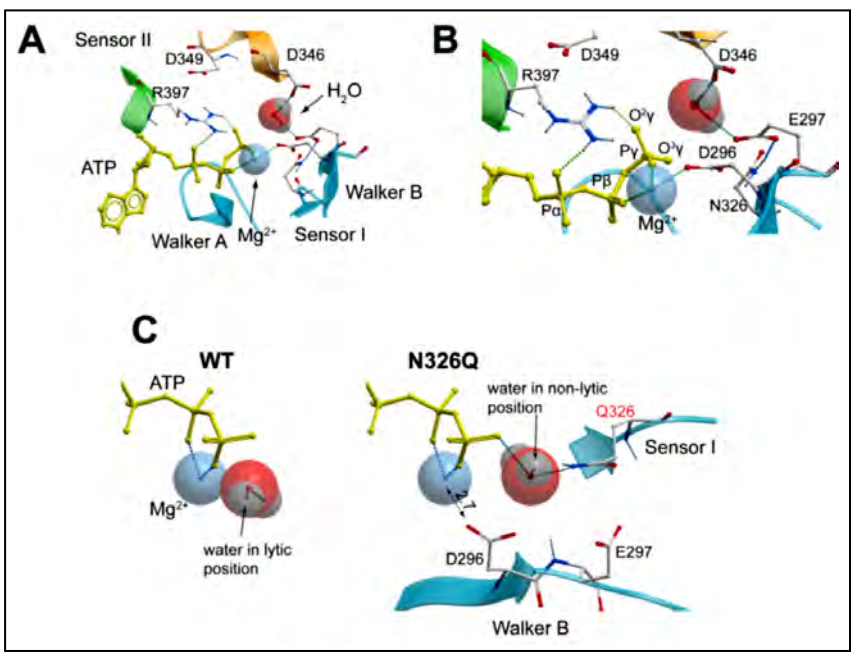

Structure of the active site of mkTIP49 protein and the proposed mechanism of ATP hydrolysis. General view of the active site (A) and surroundings of the γ-phosphate group of ATP (B), shown in yellow, Mg^{2+} ion, and the attacking water molecule. (C) Position of the attacking water molecules in wild-type mkTIP49 (*left*) and in mutant N326Q (*right*) proteins

Afanasyeva A. ..., Petukhov M. et al. // Structure. 2014. V. 22. P. 549–559.

Molecular modeling and neutron spectroscopy of macromolecular assemblies of RecA protein

A.V. Shvetsov, D.V. Lebedev, D.M. Baitin, V.V. Isaev-Ivanov
Molecular and Radiation Biophysics Division, PNPI NRC "Kurchatov Institute"

Up to now, an atomic scale resolution structure of biological macromolecules came almost exclusively from two experimental methods – *X*-ray crystallography and nuclear magnetic resonance (NMR). *X*-ray crystallography is the main source of information about the protein structure, but obtaining crystals of large multimolecular complexes comprising various biomacromolecular machines is nearly impossible. Besides, this method yields the structure of the "frozen" states of a macromolecule, thus ignoring an often significant conformational flexibility of the functioning enzyme or multimolecular complexes. NMR, on the other hand, while providing the structure of macromolecules in solution, is usually limited in the size of the resolvable structure to a mere 30 kDa.

Small-angle *X*-ray and neutron scattering methods have practically no limitations on the size of the macromolecular system and allow one to study its structure in the functional state in solution. However, by themselves those two techniques provide only limited information and have rather low resolution.

Another approach to study biological systems in solution is the use of theoretical methods, such as a molecular modeling and dynamics simulations. The main challenge of the theoretical approach is to verify whether or not the complex biomolecular system really behaves as predicted by the model. Combination of it with the small-angle scattering could allow one to create and verify all-atom models even for a large and complex molecular system. We used this approach on such multicomponent biological systems as RecA::ssDNA and RecA::RecX::ssDNA complexes.

RecA protein plays a key role in homology recombination reaction in a bacterial cell and has functional analogs in all living cells, including archea and eucariotes. It works by forming a right-handed filament structure on ssDNA. RecA searches homology region between two DNA molecules – ssDNA inside RecA filament and dsDNA outside of it – and then it does a strand exchange reaction between this two homology regions. RecX, a small bacterial protein, is known as a negative regulator of RecA, which is the essential part of the DNA reparation machinery in bacteria. RecX has been shown to bind to RecA filament and inhibit its activity of the homologous strand exchange. An ability of RecX to form a filament by binding to the grove on RecA::ssDNA presynaptic complex have been implied in the earlier cryo-EM studies.

To investigate the structural basis for RecA protein function, we have built atomic-scale models of the presynaptic complex of RecA from *Escherichia coli* and *Deinococcus radiodurans* with single stranded (ss)DNA and ATP, and RecX complexes with ssDNA and with the RecA complex above. The obtained structures underwent molecular dynamics simulations in the periodic water box with 100 ns trajectory length. A method of calculation of SANS curves from MD trajectories that we developed and implemented as analysis modules for molecular dynamics software package GROMACS was applied to this set of MD simulations.

The small-angle neutron scattering experiment together with the molecular modeling showed that RecX in solution could form filaments on ssDNA. SANS allowed us to discriminate between the possible models of such filaments, strongly favoring the specific sandwich-like structure of the complex. We have also seen that RecX can bind to RecA::ssDNA::ATP complex without destroying its filament structure. Based on the analysis of the

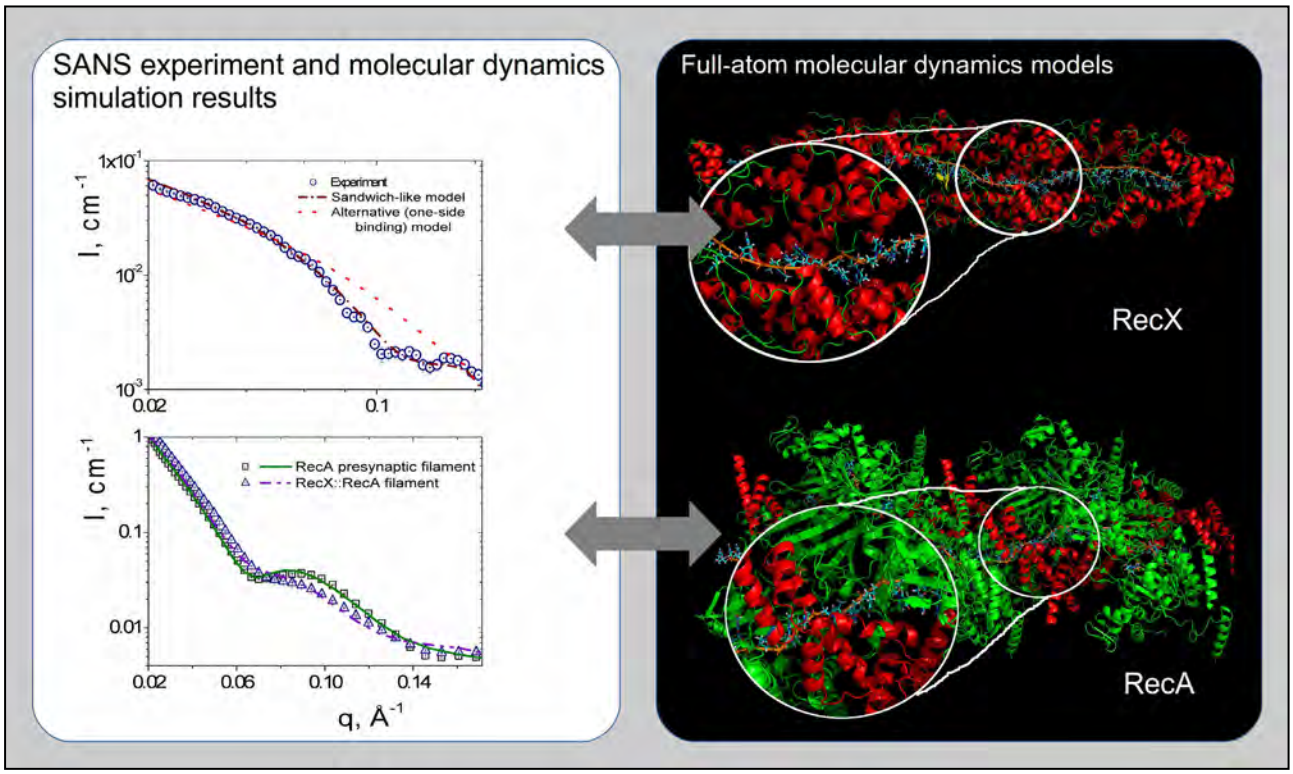

Full-atom molecular models and small-angle neutron scattering

experimental and modeling data, we were able to come up with a molecular model for RecX complex with RecA presynaptic filament where RecX protein binds in the filament groove (see Fig. above). The model implies RecX binding mainly via Coulomb interactions between RecX and ssDNA inside the filament, similar to ssDNA-RecX interactions.

An important implication of this work is the possibility to obtain a full structure of a functional multimolecular complex at atomic resolution as well as its fast conformational dynamics in solution using the combination of advanced molecular modeling techniques and low-resolution experimental methods such as SAXS or SANS.

Shvetsov A., Lebedev D., Chervyakova D., Bakhlanova I., Radulescu A., Kuklin A., Yung I., Baitin D., Isaev-Ivanov V. // FEBS Letters. 2014. V. 588. No. 6. P. 948–955.

Development of barcode and proteome profiling of glioblastoma

S.N. Naryzhny, N.L. Ronzhina, N.V. Belyakova, R.A. Pantina, M.V. Filatov – Molecular and Radiation Biophysics Division, PNPI NRC "Kurchatov Institute", Gatchina
M.A. Maynskova – Orekhovich Institute of Biomedical Chemistry, Moscow

High grade glioma (glioblastoma) is the most common brain tumor. Its malignancy makes it the fourth biggest cause of cancer death. In our experiments, we used several glioblastoma cell lines to obtain proteomics information specific for this disease. Separation by two-dimensional electrophoresis (2DE) followed by imaging, immunochemistry, spot picking, and mass-spectrometry allowed us to detect more than 600 protein spots and identify more than 130 of them (Fig. 1). Proteome profiles in normal and glioblastoma cell lines are very similar, but levels of several proteins have prominent differences between the norm and the cancer. Among these proteins are PCNA (PCNA_HUMAN), p53(TP53_HUMAN) (Fig. 2) and others. Most interesting results obtained concerned the protein p53. Its level was dramatically upregulated and enriched by multiple additional isoforms in all glioblastoma cell lines (Fig. 3). An immunological analysis (Western blot) of three hub proteins (p53, 14-3-3, PCNA) allowed us to create a minimal barcode of glioblastoma cell lines (table). It can be pointed out from these preliminary data that this barcode is a promising diagnostic tool to be used to test biological fluids of patients.

The development of proteomics causes high expectations connected to the introduction of new approaches for diagnosis of various diseases and the development of new drug compounds. As for neurooncology, the application of proteomics is in its development stage but gains popularity extremely fast. It is assumed that the production of protein profiles will give an opportunity to combine efforts in various areas and will have a significant effect on the study and treatment of gliomas. On the one hand, our results confirm the previously published

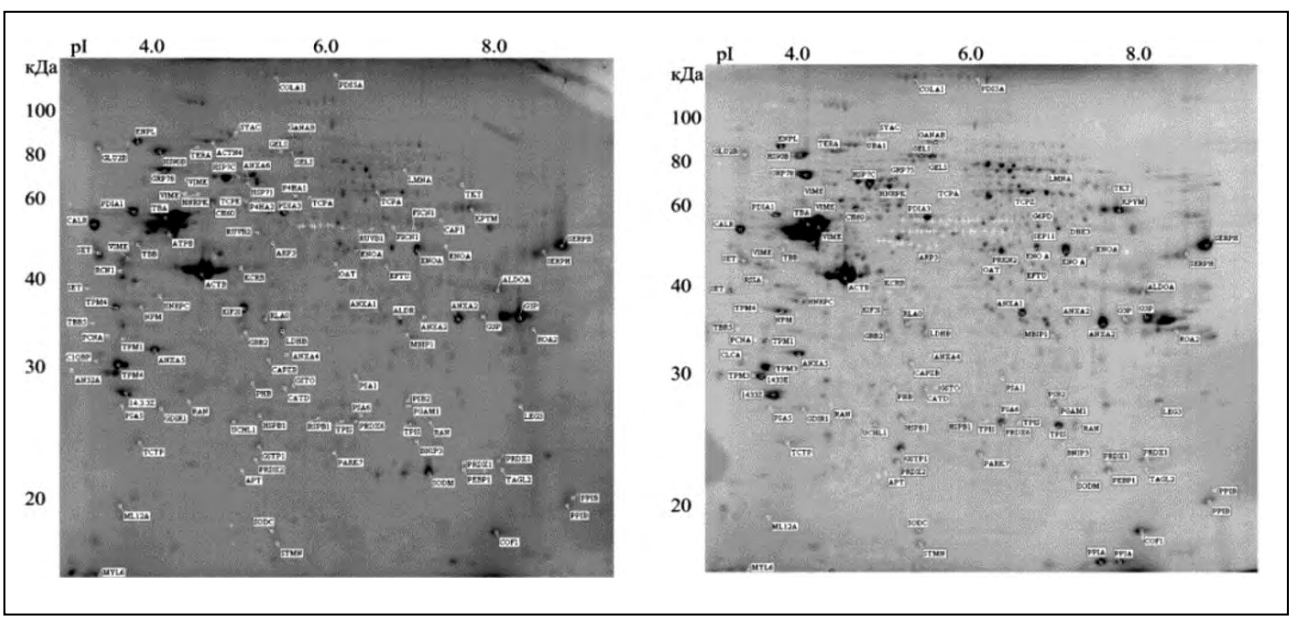

Fig. 1. Protein separation by 2DE followed by image analysis, spot picking and protein identification. *Left panel* – the norm, FLEH; *right panel* – glioblastoma (L). Forms of p53 are marked with crosses

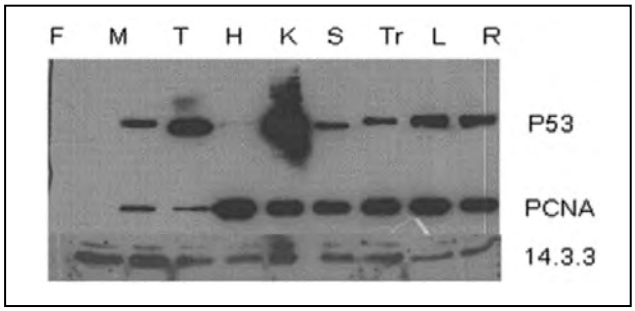

Fig. 2. Levels of p53, PCNA, and 14_3_3 detected by Western blot in seven different glioblastoma cell lines. The glioblastoma cell lines M, T, K, S, Tr, L, R and cervical cancer line HeLa (H) were tested. The line of human embryonic lung fibroblasts (FLEH, F) and normal brain tissue (*not shown*) were used as a control

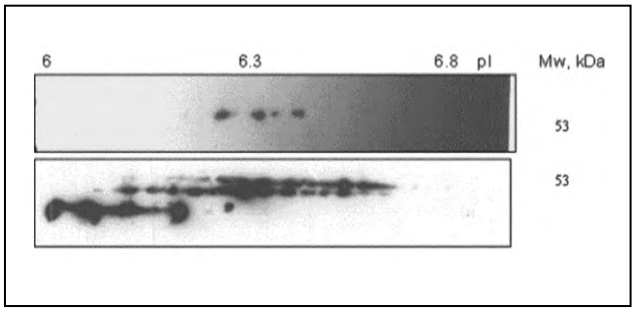

Fig. 3. Immunodetection of protein p53 in normal and glioblastoma cells after 2DE (2DE Western blot). *Top* – the norm (F), *below* – glioblastoma (T)

Table. The list of identified proteins upregulated in glioblastoma cell lines

№	UniProtKB / Swiss-Prot	Name of the protein	pI / MW[1]	FLEH, % V	Glioblastoma / FLEH
1	P53_HUMAN	Cellular tumor antigen p53	6.33 / 43 653	< 0.05	19 ± 18[3]
2	PCNA_HUMAN	PCNA, proliferating cell nuclear antigen	4.57 / 28 769	< 0.05	14 ± 6[3]
3	COF1_HUMAN	Cofilin-1	8.22 / 18 502	0.58	4.0 ± 2.3
4	KPYM_HUMAN	Pyruvate kinase PKM	7.96 / 57 936	0.34	3.2 ± 1.1
5	ANXA1_HUMAN	Annexin A1	6.57 / 38 714	0.16	3.1 ± 0.2
6	TPIS_HUMAN	Triosephosphate isomerase	5.65 / 30 791	0.20	2.8 ± 1.0
7	NPM_HUMAN	Nucleophosmin	4.64 / 32 575	0.19	2.8 ± 0.7
8	VIME_HUMAN	Vimentin	5.05 / 53 651	0.04	2.5 ± 0.9
9	ANXA2_HUMAN	Annexin A2	7.57 / 38 604	0.10	2.5 ± 0.8
10	TERA_HUMAN	Transitional endoplasmic reticulum ATPase	5.14 / 89 321	0.08	2.3 ± 0.9
11	ENOA_HUMAN	Alpha-enolase	7.01 / 47 168	0.20	2.2 ± 1.0
12	PRDX1_HUMAN	Peroxiredoxin-1	8.27 / 22 110	0.07	2.2 ± 0.7
13	SYAC_HUMAN	Alanine-tRN Aligase, cytoplasmic	5.34 / 106 810	0.05	2.2 ± 0.5
14	TCTP_HUMAN	Translationally-controlled tumor protein	4.84 / 19 595	0.15	2.1 ± 0.6

[1] – pI and Mw of the canonical form of the protein were taken from UniProtKB/SwissProt.

data about several cancer marker proteins, both common and associated with glioblastoma, on the other hand, they indicate the possibility to use such known proteins as PCNA and p53 as biomarkers in glioblastoma assays. Therefore, the minimum barcode for glioblastoma could have the form shown in Fig. 1. Moreover, we have shown the extremely high heterogeneity of protein p53 forms in glioblastomas, which itself requires a special attention and analysis.

1. *Naryzhny S.N., Ronzhina N.L., Maynskova M.A., Belyakova N.V., Pantina R.A., Filatov M.V.* // Biomeditsinskaya Khimiya. 2014. V. 60. Ed. 3. P. 308–321.
2. *Naryzhny S.N., Ronzhina N.L., Maynskova M.A., Belyakova N.V., Pantina R.A., Filatov M.V.* // Biochemistry (Moscow) Suppl. Ser. B: Biomedical Chemistry. 2014. V. 8. Ed. 3. P. 243–251.
3. *Moskaleva N.E., Zgoda V.G.* // Biomeditsinskaya Khimiya. 2012. V. 58. Ed. 6. P. 617–634.
4. *Kalinina J., Peng J., Ritchie J.C., Van Meir E.G.* // Neuro-Oncology. 2011. V. 13. P. 926–942.

Synchronization of tRNA translocation on small and large ribosomal subunits

A.L. Konevega
Molecular and Radiation Biophysics Division, PNPI NRC "Kurchatov Institute"

Many aspects of the molecular mechanism of protein biosynthesis remain unclear, despite the titanic efforts of researchers. Among them – the molecular mechanism of translocation: the movement of native ribosome substrates (tRNA and mRNA) within the ribosomal intersubunit space with high speed and accuracy. In this paper, utilizing a new system of fluorescent labels, we were able to show that in some

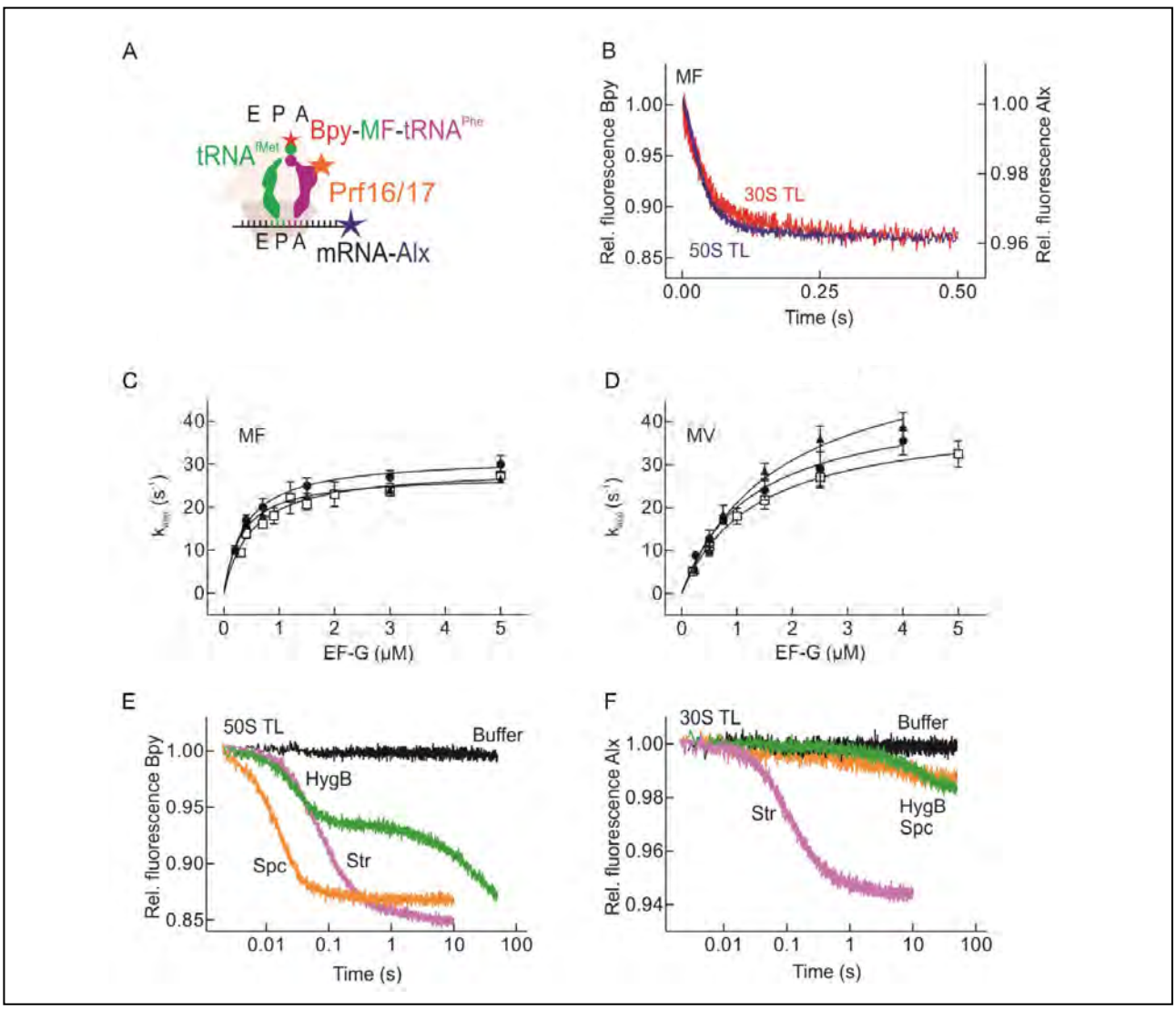

Positions of fluorescence reporters on the ribosomal complex (A); synchronous translocation on the 30S and 50S subunits catalyzed by elongation factor EF-G-GTP (B–D); desynchronization of translocation on small and large subunits in the presence of antibiotics: streptomycin, spectinomycin, hygromycin B (E, F)

cases the translocation on 50S and 30S subunits does not occur simultaneously. In particular, certain antibiotics lead to selective slowdown of the translocation on the 30S subunit. In addition, substitution of the native EF-G with mutants, including those unable to hydrolyze GTP, leads to slowing down and desynchronization of translocation.

In order to study the kinetics of translocation of $tRNA_2$-mRNA complex catalyzed by EF-G, we used a combination of fluorophores located at the 3'-end of the mRNA and peptidyl-tRNA allowing one to observe the mRNA and tRNA translocation in a single experiment (Fig. above). It was shown that only the full-length EF-G factor and GTP hydrolysis lead to a rapid and simultaneous translocation of the tRNA on 30S and 50S subunits. Antibiotics viomycin, spectinomycin, hygromycin B lead to a desynchronization of translocation: a partial translocation on the 50S subunit in the presence of EF-G-GTP occurs relatively fast, whereas translocations of the tRNA anticodon and mRNA on the 30S subunit are strongly delayed.

At saturating concentrations of EF-G-GTP, velocities of translocation measured by fluorophores in the peptidyl moiety of peptidyl-tRNA(BPY), mRNA (Flu, Alx405) and the D-loop of tRNA (Prf, proflavin) coincide (28–30 s^{-1}). In addition, correspondence of velocities of translocation occurred for two systems (fMet-Phe and fMetVal), very dissimilar in the differences of the free energies of pre- and post-translocation states. The results of this work support the existing model of translocation and convincingly demonstrate an additional mechanism of action of antibiotics known to inhibit protein biosynthesis.

Holtkamp W., Cunha C., Peske F., Konevega A.L., Wintermeyer W. and Rodnina M.V. // EMBO J. 2014. V. 33. P. 1073-85.

Translational bypassing: omission of non-coding mRNA sequence during translation

A.L. Konevega
Molecular and Radiation Biophysics Division, PNPI NRC "Kurchatov Institute"

The majority of proteins are synthetized by progressive movement of the ribosome along the messenger RNA (mRNA). However, for the synthesis of DNA topoisomerase subunit (the gene product *60* of bacteriophage T4) the ribosome uses a unique mechanism: bypassing of a non-coding mRNA region of 50 nucleotides located between the two coding sequences. After translation of the first coding sequence, the ribosome stops at positioning of the stop codon in the A site, codon-anticodon interaction in the P site weakens, 50 nucleotides of mRNA are pulled through the ribosome, and polypeptide synthesis resumes.

The aim of this work was to disclose the mechanism of the ribosome movement and identify the minimum set of signals required for bypassing. To address these questions, we have studied bypassing *in vitro*

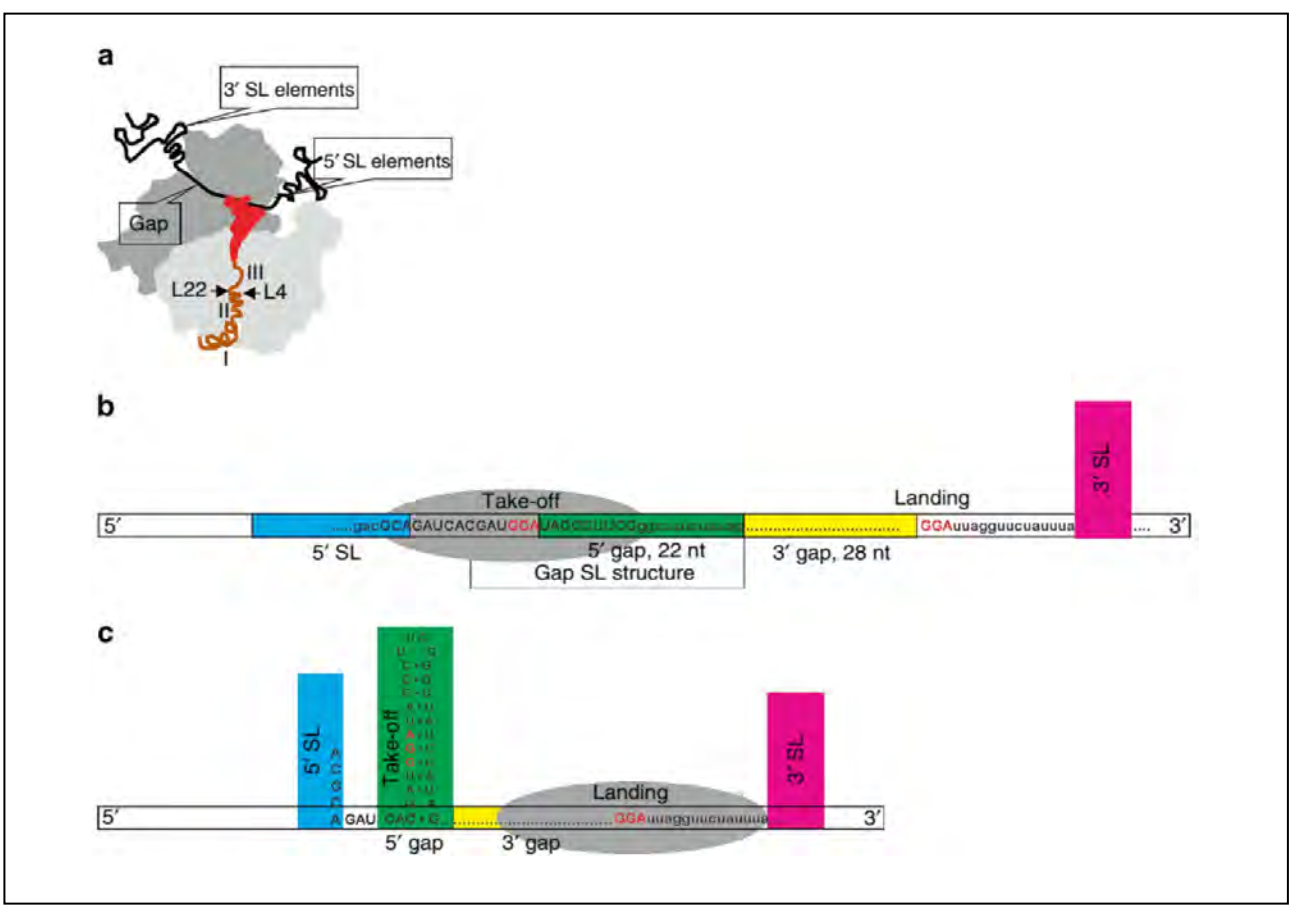

Schematic image of the ribosome with putative mRNA secondary structures upstream of the gap (5'SL), the gap region and putative structures downstream of the gap (3'SL) at the moment of bypassing initiation (a). The position of the ribosome (grey oval) at the onset of bypassing (b). The position of the ribosome at the resume of translation (c)

in a fully reconstituted translation system consisting of purified, biochemically characterized components. The main elements of the mRNA that encode non-linear translation were characterized using a unique method of *in vitro* translation of polypeptides with a fluorescently labeled N-terminal amino acid. It was shown that the presence of certain elements of the mRNA in untranslated region, as well as in 5' and 3' adjacent areas, is sufficient for translational bypassing (Fig.). Here we recapitulate efficient and accurate bypassing in a minimum translation system in the absence of any auxiliary factors, indicating that the signals crucial for bypassing are encoded by the gene *60* mRNA sequence itself. Thus, non-linear translation is an internal property of translational system and does not require any additional factors. Systematic analysis of the mRNA suggests an unexpected contribution of a secondary structure of the mRNA as well as an amino acid sequence of nascent polypeptide chain. During bypassing, ribosome glides forward along the mRNA track in a progressive way until it reaches the landing codon in order to resume protein synthesis. This gliding may have a role not only for gene product *60* synthesis, but also during the regular mRNA translation for reading frame selection in course of initiation or during the tRNA translocation. Translational bypassing in process of the decoding of mRNA of bacteriophage T4 gene *60* is the first example of a riboswitch with regulatory elements in the coding region. Studies of molecular mechanisms of the bacterial ribosome functioning, including rare events of translation, are necessary for a subsequent application in biotechnological systems, synthetic biology, and development of new specific inhibitors of protein biosynthesis to be used as antibiotics.

Samatova E., Konevega A.L., Wills N.M., Atkins J.F. and Rodnina M.V. // Nature Communications. 2014. V. 5. P. 4459.

Kinetic mechanism of the programmed –1 frameshifting

V.I. Katunin
Molecular and Radiation Biophysics Division, PNPI NRC "Kurchatov Institute"

Translation of genetic information encoded in messenger RNA (mRNA) down to an amino acid sequence can be achieved either by progressive movement of the ribosome along the mRNA or by various mechanisms of translational recoding, for example, by a shift of the reading frame forward or backward. In this paper, we studied the mechanism of programmed –1 frameshifting with a detailed review of ribosome movement along the specific region of mRNA that is characteristic for frameshifting event mentioned above. Two elements in the mRNA are prerequisites for the frameshifting: a "slippery sequence" that allows the ribosome to slide backward and a downstream secondary structure element – pseudoknot – that temporarily impedes the forward movement of the ribosome.

Here, we report the results of the analysis, including the kinetics of stepwise translation of the "slippery sequence", the kinetics of amino acid incorporation into translation products that correspond both to usual and shifted frames and the detailed kinetics of translocation reactions that govern programmed –1 frameshifting.

Frameshifting occurs at a late stage of translocation when the two transfer RNAs are bound to adjacent slippery sequence codons of the mRNA (Fig. below). The downstream pseudoknot in the mRNA impairs the closing movement of the small ribosomal subunit head, the dissociation of EF-G, and the release of the transfer RNA from the ribosome. The slippage of the ribosome into the –1 frame accelerates the completion of translocation, thereby favoring a further translation in the new reading frame.

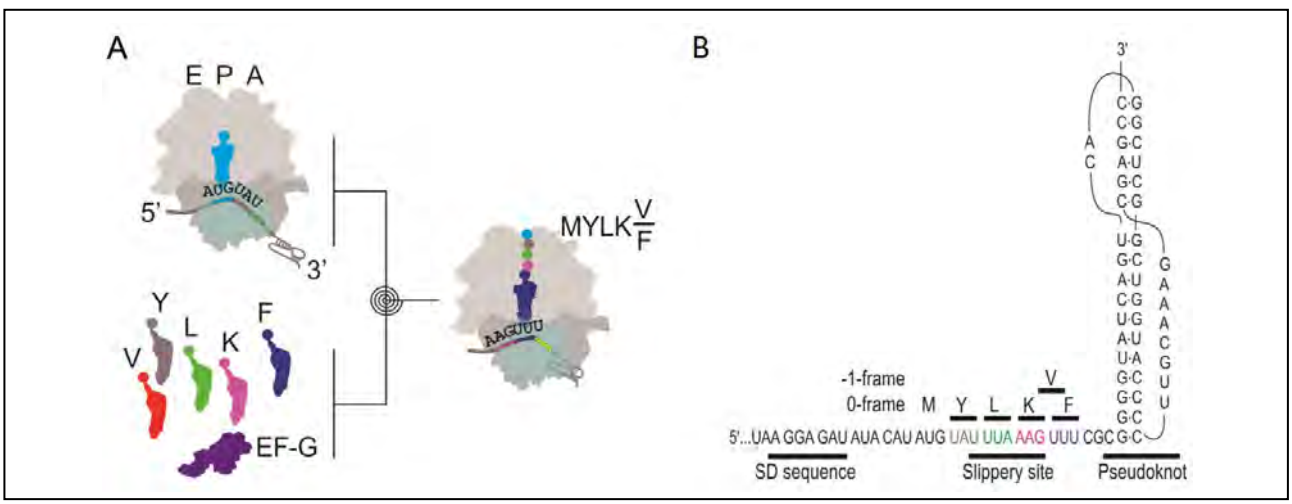

Schematic image of the experiment: ribosomal complexes were mixed with elongation factor EF-G and set of aa-tRNA·EF-Tu·GTP ternary complexes (A); schematic image of the frameshifting mRNA. Structural elements crucial for the efficient frameshifting are underlined (B)

Caliskan N., Katunin V.I., Belardinelli R., Peske F., Rodnina M.V. // Cell. 2014. V. 157. P. 1619–1631.

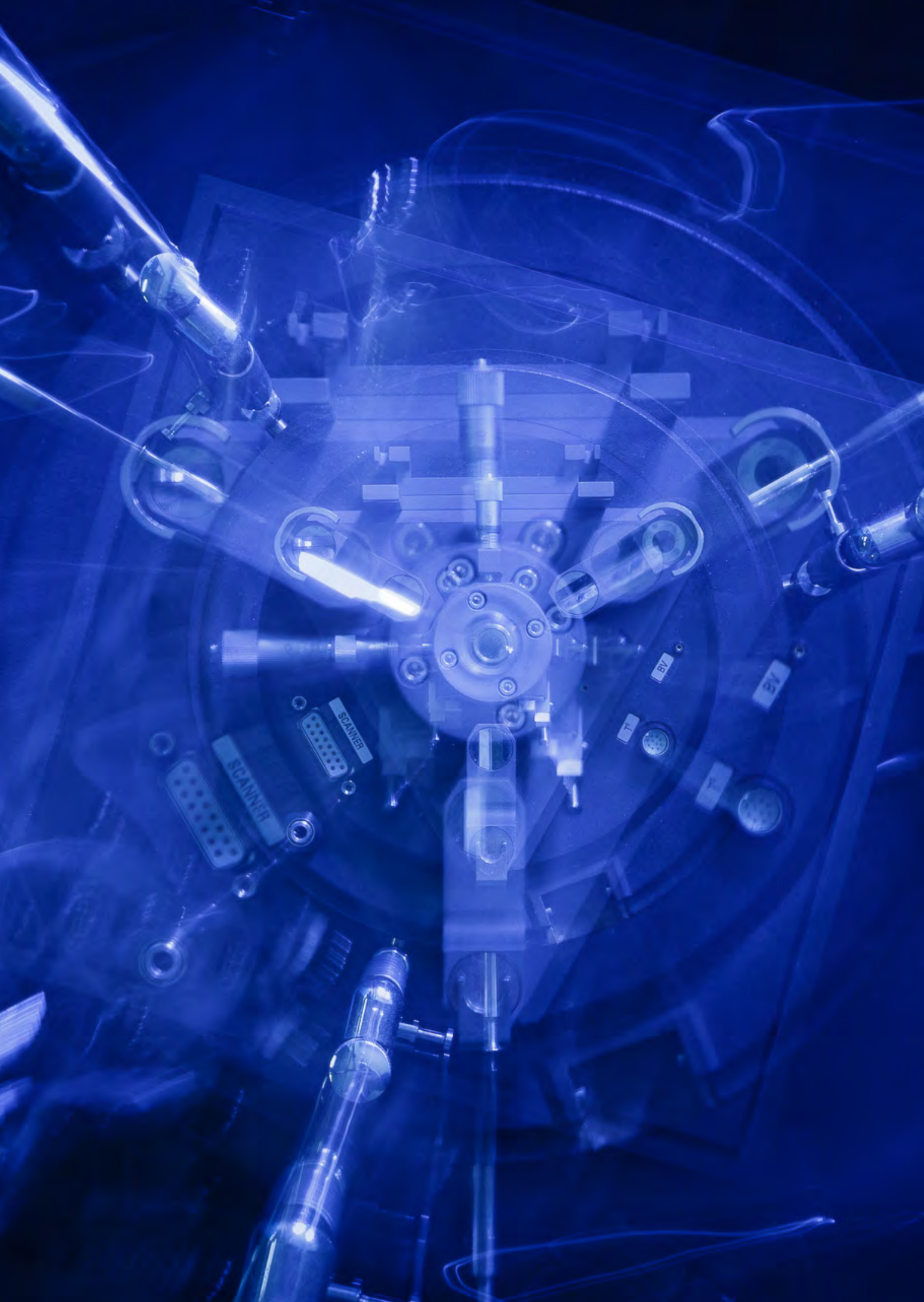
SCANNER
SCANNER
BV

Nuclear Medicine (Isotope Production, Beam Therapy, Nano- and Biotechnologies for Medical Purposes)

Multimodal beta-delayed fission of $^{194, 196}$At, ^{202}Fr

A.E. Barzakh, D.V. Fedorov, P.L. Molkanov, M.D. Seliverstov
High Energy Physics Division, PNPI NRC "Kurchatov Institute"

A recent discovery of a new region of asymmetric β-delayed fission (βDF) near the nuclei $^{178, 180}$Hg initiated a number of theoretical papers applying new dynamical approaches to the analysis of low-energy fission. This approaches give a satisfactory description of an asymmetric distribution of $^{178, 180}$Tl fission-fragments. A graduate transition from asymmetric to symmetric fission with the decreasing mass split between heavy and light fission-fragments was predicted in the same papers. In contrast to these predictions, it was found in our recent experiments that a complex multimodal fission occurs with triple-hampered mass distribution for the nuclei in this transitional region ($^{194, 196}$At, ^{202}Fr) (see Fig.). It means that there is a probability of β-delayed fission with both asymmetric and symmetric fragment mass distribution for these nuclei. At the same time the mass split between heavy and light fission-fragments is nearly constant and the probability of the asymmetric mode of fission decreases when one approaches the region of symmetric fission (near ^{204}Fr). As mentioned above, these new experimental results contradict the recent theoretical models and require the refinement of theoretical approaches. The similar co-existence of asymmetric and symmetric βDF modes with corresponding triple-hampered mass distribution was found previously only for a few nuclei near ^{226}Th. Our results along with the previously obtained information, point out that the multimodal fission is the common mechanism of the transition between two main fission modes.

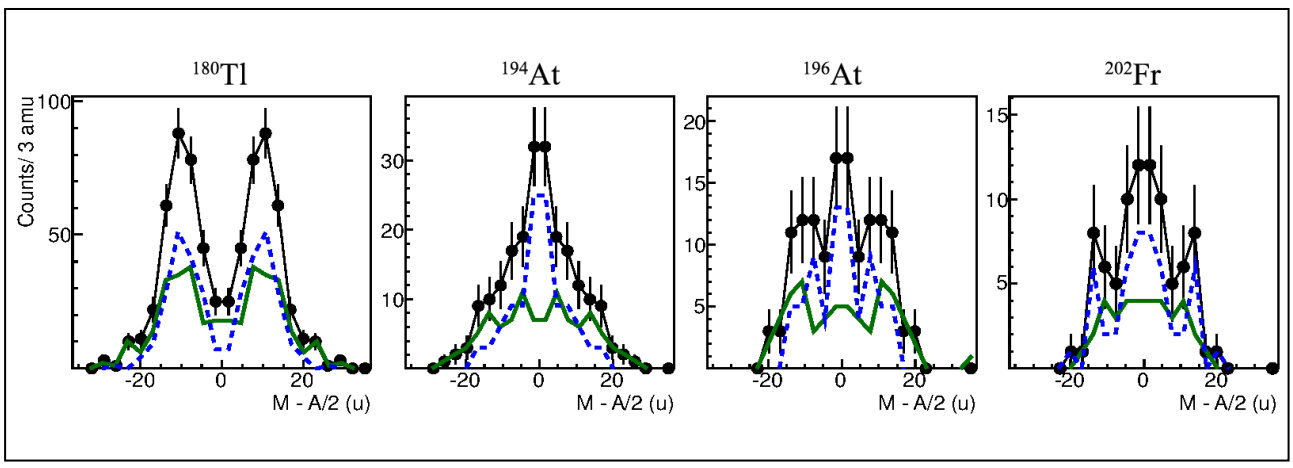

Mass distribution of the fission-fragments for ^{180}Tl (asymmetric fission), $^{194, 196}$At, ^{202}Fr (multimodal fission)

1. *Andreyev A.N., Barzakh A., Fedorov D., Seliverstov M. et al.* // Phys. Rev. Lett. 2010. V. 105. P. 252502; *Elseviers J., Barzakh A., Fedorov D., Seliverstov M. et al.* // Phys. Rev. C. 2013. V. 88. P. 044321; *Liberati V., Barzakh A., Fedorov D., Molkanov P., Seliverstov M. et al.* // Phys. Rev. C. 2013. V. 88. P. 044322.
2. *Ghys L., Barzakh A., Fedorov D., Seliverstov M. et al.* // Phys. Rev. C. 2014. V. 90. P. 041301(R).

Investigation of shape co-existence in polonium isotopes

A.E. Barzakh, D.V. Fedorov, P.L. Molkanov, M.D. Seliverstov
High Energy Physics Division, PNPI NRC "Kurchatov Institute"

Investigations of the shape co-existence and the shape evolution in polonium isotopes continued in 2014. Dipole magnetic (μ) and electric quadrupole (*Q*) moments for the Po isotope chain A = 193–211 were measured. Significant deviation of electromagnetic moment values at $N < 113$ as compared to almost constant values for heavier isotopes was discovered (see Fig.). The "early" onset of deformation was found during the previous study of changes in mean-square charge radii ($\delta \langle r^2 \rangle$) in polonium: a deformation developed earlier (at $N < 113$) than it was expected and predicted.

The deviation of polonium isotope magnetic moments from the systematic trend (at $N < 113$) as well as their quadrupole moments behavior were explained with reference to the Coriolis interaction at a moderate deformation and by mixing spherical and deformed configurations. Thus, the data on changes in mean-square charge radii and the behavior of the polonium electromagnetic moment were explained in the framework of a single consistent approach.

Measurements of $\delta \langle r^2 \rangle$, μ and *Q* for neutron-rich polonium isotopes (N = 132–134) were carried out as well. The "inverse odd-even effect" in mean-square charge radii was found earlier in this range of nuclides (Fr, Ra, Rn isotopes with the same neutron numbers). The "normal odd-even effect" means that the radius of the odd-neutron-number nuclide is less than the mean value of the radii of its even-neutron neighbors. The inverse situation takes place for Fr, Ra, Rn at N = 133: the radius of the odd-neutron-number nuclide is bigger than the mean value of the radii of its even-neutron neighbors. This effect was explained by the supposition of the presence of an octupole deformation for these nuclei. This phenomenon was confirmed later by the different nuclear-spectroscopy evidences. Our measurements have demonstrated the conservation of "normal odd-even effect" for polonium nuclides at N = 133. Thus, the border of the octupole deformation area have been established. The magnetic moment of ^{217}Po measured in our experiments presents an additional evidence of the absence of octupole deformation in this nucleus. The experimental value of this magnetic moment is in a good agreement with the simple shell-model estimations and does not reqire the octupole-deformed nucleus model for its theoretical description.

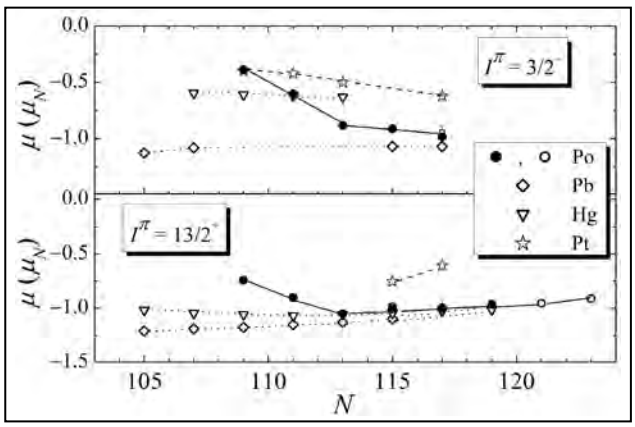

Dipole magnetic moments of Po isotopes as compared to Pb, Hg and Pt isotopes

1. *Seliverstov M.D., Barzakh A., Fedorov D., Molkanov P. et al.* // Phys. Rev C. 2014. V. 89. P. 034323.
2. *Cocolios T.E., Barzakh A., Fedorov D., Molkanov P., Seliverstov M. et al.* // Phys. Rev. Lett. 2011. V. 106. P. 052503; *Seliverstov M.D., Barzakh A., Fedorov D., Molkanov P. et al.* // Phys. Lett. B. 2013. V. 719. P. 362.
3. *Fink D., Barzakh A., Fedorov D., Molkanov P., Seliverstov M. et al.* // Phys. Rev. X. 2015. V. 5. P. 011018.

Formation of a proton beam to be used in ophthalmology

N.A. Ivanov, Zh.S. Lebedeva
Knowledge Transfer Division, PNPI NRC "Kurchatov Institute"

Proton therapy is becoming a widespread method of radiotherapy. A sharp increase of ionization loses at the end of the range gives one the opportunity to deliver a high dose to the target tissue and reduce the dose in the health tissue. This is a reason of the proton therapy gaining so much popularity as a method of radiotherapy in ophthalmology.

The C-80 cyclotron is currently under construction at PNPI NRC "Kurchatov Iinstitute". The goal of this study is a Monte-Carlo simulation of a beam formation system. The calculation was made using Geant4 code.

Proton beam should be formed in such a way that it can cover a tumor of a linear size of around 1–3 cm. Traditionally, the scattering system consisted of one or two tantalum or brass foils and collimators. Proton beam profiles and distribution of Bragg peak curve calculated using this method are illustrated in the Figure below. This method helps to spread a "pencil beam" (2–3 mm in diameter) to the required size, but more than 90% of protons are lost during the formation. Up to 10% of these protons produce secondary particles and radionuclides due to interactions with constructive materials. For that reason the calculation was made using the "wide beam" (spot size is about several cm). As the spot size of the beam is equal or close to the diameter of the target, it is more effective to use such a beam.

If we define the effectiveness of the beam – ε as a ratio of the number of protons transferred to the target to number of protons that entered the treatment room we will find that for the "pencil beam" $\varepsilon_{pen} = 0.06$, and for the "wide beam" $\varepsilon_{wide} = 0.17$. The rest of protons interact with constructive materials. The ratio of the number of such protons η for the "wide beam" and the "pencil beam":

$$\eta = (\varepsilon_{wide} / \varepsilon_{pen}) \cdot [(1 - \varepsilon_{pen}) / (1 - \varepsilon_{wide})].$$

The result proves that the use of the "wide beam" allows one to get an advantage in effectiveness of the beam. In addition, the formation system gets a little bit less complicated.

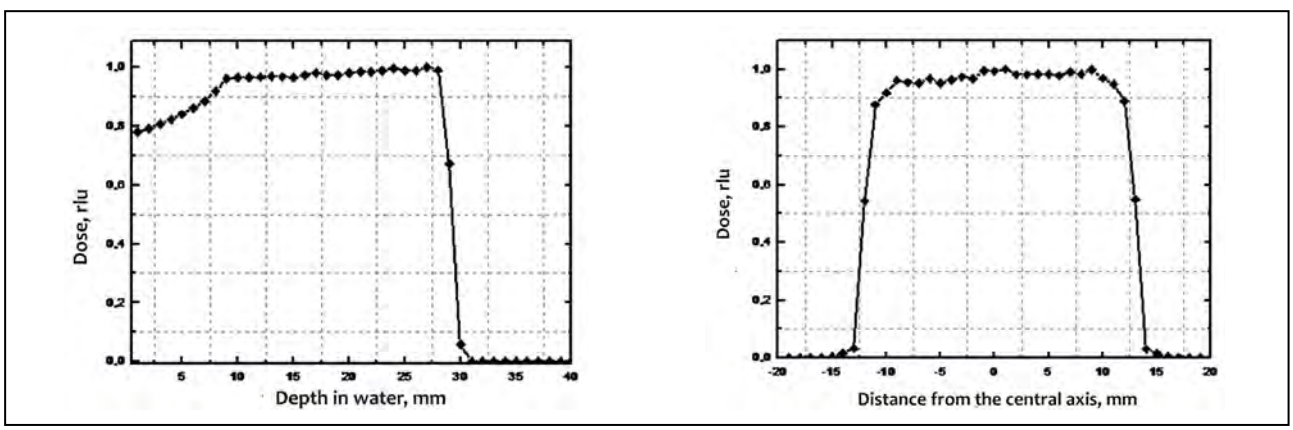

Proton beam profiles and distribution of Bragg peak curve in water: SOBP on the 90% isodose level is 20.7 mm; beam profile width is 25 mm; penumbra (20–80%) is 3.0 mm; beam efficiency is 17%

Moyers M.F., Vatnitsky S.M. Practical Implementation of Light Ion Beam Treatments. Madison: Med. Phys. Pub. 2012. P. 580.

New endometallofullerenes encapsulating iron atoms

V.P. Sedov, A.A. Szhogina, V.T. Lebedev, Yu.P. Chernenkov, V.L. Aksenov
Neutron Research Division, PNPI NRC "Kurchatov Institute"
M.V. Kovalchuk – NRC "Kurchatov Institute"

Behavior of a new endohedral structure in aqueous solutions has been studied by small-angle neutron scattering due to its expected application in biomedicine (Fig. 1). Basing on the results of the studies, it was concluded that these $Fe@C_{60}(OH)_x$ (x ~ 30) molecules are organized in aqueous solutions (concentrations C > 1% wt.) into stable globular structures with correlation radius R_c ~ 10–12 nm and aggregation numbers N_c ~ 10^4. Such a transition has a reversible character but demonstrates some hysteresis by a dilution of the system when cluster's size and aggregation numbers return to their initial magnitudes but at lower concentrations. Thus, nontoxic endometallofullerenes (Fig. 2) were obtained for the first time. Their properties in NMR-experiments (influence on surrounding proton's relaxivity in water) have been tested at the State Research Institute of Highly Pure Biopreparations of Federal Medical-Biological Agency (Saint Petersburg). Fullerenols $Fe@C_{60}(OH)_x$ may serve as safe MRI-contrasting agents since they contain only Fe, C, O, H.

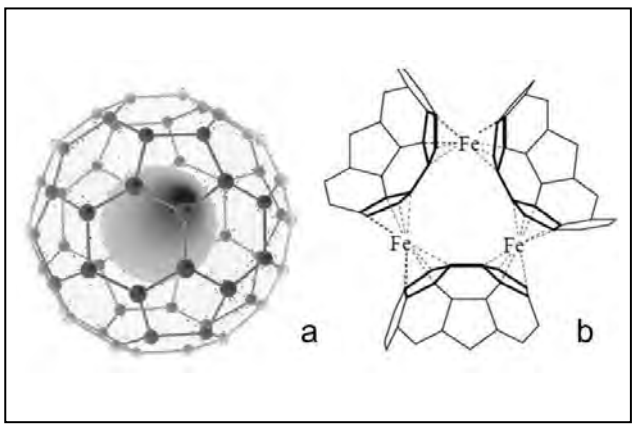

Fig. 1. Endometallofullerene $Fe@C_{60}$ synthesized for the first time; the developed method of its transformation into water-soluble form $Fe@C_{60}(OH)_x$ (x ~ 30) (a);
exohedral complexes – the only ones known earlier (b)

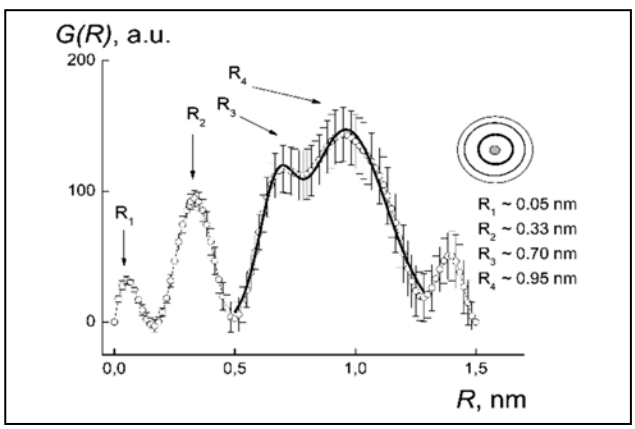

Fig. 2. Correlation function $G(R) = R^2\gamma(R)$ vs. radius R. Concentric arrangement of atoms (radii R_1–R_4) around the central iron atom

Sedov V.P., Szhogina A.A., Lebedev V.T., Chernenkov Yu.P., Aksenov V.L., Kovalchuk M. V. // PNPI preprint 2963. Gatchina, 2014. P. 12

Structure and toxicity of aqueous fullerene C_{60} solutions

V.L. Aksenov – PNPI NRC "Kurchatov Institute", Gatchina, Russia
E.A. Kyzyma, A.A. Tomchuk, V.I. Petrenko, M.V. Avdeyev – Frank Laboratory of Neutron Physics, Joint Institute for Nuclear Research, Dubna, Russia
E.A. Kyzyma, L.A. Bulavin, V.I. Petrenko – Taras Shevchenko National University of Kyiv, Ukraine
L. Almasy - Institute for Solid Physics and Optics Wigner Research Centre for Physics, Budapest, Hungary
M.V. Korobov, D.S. Volkov, I.V. Mikheev – Moscow State University, Russia
I.V. Koshlan, N.A. Koshlan, P. Bláha – Laboratory of Radiation Biology, Joint Institute for Nuclear Research, Dubna, Russia
P. Bláha – Faculty of Nuclear Sciences and Physical Engineering, Czech Technical University, Prague, Czech Republic

Today, the issues of nanotoxicology and biosafety promising nanomaterials and those already in use are important problems. Modern carbon nanomaterials (fullerenes, nanodiamonds, nanotubes, etc.) are being increasingly tested in the development of systems for drug delivery, as well as a basis for anticancer, antibacterial, and other pharmaceutical preparations. In this regard, various methods for preparing aqueous solutions of carbon nanostructures, including fullerene, have attracted much interest. Solutions of fullerene C_{60}, including both solutions of modified C_{60} (solubilization, complexes with polymers) and those prepared without stabilizers (condensation, solvent-exchange method), are among the most prospective. The issue of the toxicity of such systems has not been completely studied. To some extent, this is due to differences in the preparation methods of aqueous solutions of C_{60}, which leads to different structural parameters of solutions from the viewpoint of their colloidal organization. However, it is believed that the presence of clusters in aqueous C_{60} solutions may be responsible for the formation of superoxide anions, which lead to the destruction of cell membranes. Therefore, efforts are underway to improve existing and to develop new methods for the preparation of aqueous nontoxic solutions of C_{60} with significant membrane-trophic activity due to low polydispersity and smaller clusters, in the ideal case, solutions of individual C_{60} molecules. Thus, the association between the structural parameters and the toxicity of C_{60} solutions determines the need for a detailed structural description of the synthesized systems.

An additional factor that contributes to interest in finding ways to synthesize C_{60} solutions in water, close to molecular solutions, is that the biological activity of C_{60} increases with approaching the molecular state.

It should also be noted that all of the existing methods for preparing aqueous solutions of fullerene C_{60} yield colloidal dispersions, where the fullerene is completely in the cluster state. It was shown recently that the use of N-methylpyrrolidone (NMP) as a primary solvent with subsequent mixing with water reduces the size of aggregates in the final mixture. Individual unaggregated fullerenes are observed in the mixture. Due to the good miscibility of rather toxic NMP with water, its extraction from a mixture is a fairly difficult task. However, the fact of the formation of a solution with single fullerene molecules and the ability to decrease the cluster size motivate the study of mixed (NMP – water) solutions and their comparison with purely aqueous fullerene solutions. A natural way to decrease toxicity in this case is strong dilution with water, while maintaining significant, from a biological point of view, concentrations of fullerene in the mixture.

In this paper, we investigate an aqueous solution of fullerene C_{60} (VDF-60), prepared by the solvent-exchange method, and a solution of C_{60}/H_2O (NMP) with a low content of NMP. The structure of VDF-60 at the nanoscale level (up to 100 nm) is analyzed by a small-angle neutron scattering (SANS) and compared with published data on similar systems and mixed solutions of C_{60}/H_2O/(NMP). In order to assess the prospects of using these solutions in biology,

Table. Survival rate of Chinese-hamster V-79 cells in the presence of aqueous C_{60} solutions

Concentration of C_{60} in the system	Survival rate				
	4th day	7th day	9th day	11th day	13th day
VDF-60					
0.05 μg/mL	95%	98%	98%	94%	88%
0.5 μg/mL	85%	95%	92%	–	92%
5 μg/mL	90%	94%	99%	85%	–
C_{60}/H_2O (NMP)					
0.05 μg/mL	90%	95%	92%	90%	–
Control/H_2O					
0	92%	97%	–	92%	–

we investigated their toxicity to Chinese-hamster V-79 cells; among other things, the effect of the NMP concentration in mixed solutions on their toxicity is studied.

Structural studies of fullerene solutions prepared by different methods showed a double difference in the fullerene cluster size. The radius of gyration for a solution of VDF-60 is 18.8 ± 0.2 nm, compared to 8 ± 1 nm for a solution of C_{60}/H_2O (NMP). Regardless of the method of preparation and size of clusters in a solution of C_{60} in water, both the investigated systems of C_{60}/H_2O (NMP) and VDF-60 showed no toxicity in *in vitro* experiments on Chinese-hamster V-79 cells in the investigated concentration range of C_{60} of 0.05–5 μg/mL. The fact that N-methylpyrrolidone does not show high toxicity at these fullerene concentrations in a solution indicates that it can be considered as a base solvent in further attempts to produce biocompatible aqueous solutions of monomer C_{60} molecules under condition of further purification of the systems.

The toxicity of solutions VDF-60 and C_{60}/H_2O (NMP) was studied in the concentration range of 0.05–5 μg/mL and 0.05 μg/mL in accordance with the range of concentrations of aqueous solutions of C_{60} reported earlier in the publications. Preliminarily, the toxicity of primary solvent NMP was studied at high concentrations in the mixture and its maximum possible nontoxic concentration in a solution was determined to be 0.1 vol %. This, in turn, determined the selection of the maximum fullerene concentration in experiments on the toxicity of C_{60}/H_2O (NMP), which amounted to 0.05 μg/mL, with a content of NMP in the medium with cells of 0.005%. The cells grew for 13 days. Regardless of the method of preparation and the concentration of fullerene C_{60}, a high survival rate of cells was observed, more than 85% in all samples.

As it is seen from the table, the survival ratio of cells is comparable in all cases with the control sample. Despite the fact that the cited studies for similar concentrations of fullerene in aqueous solutions reported its toxic properties, the studied aqueous solutions of VDF-60, prepared by solvent exchange, showed no toxicity in experiments *in vitro*, even for high fullerene concentrations (up to 5 μg/mL). This may be due to a rather long (23 days) procedure of evaporation of the organic components (toluene) of the solution.

Kyzyma E.A., Tomchuk A.A., Bulavin L.A. et al. // Journal of Surface Investigation. *X*-ray, Synchrotron and Neutron Techniques. 2015. No. 1. P. 1–5.

Nuclear Reactor and Accelerator Physics

Neutron fluxes in the low-temperature channel of WWR-M reactor

A.S. Poltavsky, A.A. Zakharov, P.A. Sushkov, V.A. Chekanov
Department of Nuclear and Radiation Safety, Neutron Research Division
and Department of Reactor Physics and Technology, PNPI NRC "Kurchatov Institute"

The work was executed as part of a bigger task aimed at the resumption of the low-temperature channel at WWR-M reactor. In 1993, a low-temperature channel was set in the B-13 vertical channel in order to study properties of high-temperature superconducting materials when subjected to radiation at cryogenic temperatures. In 1997, the channel was replaced. The new channel had a central pipe with a bigger diameter for loading specimens. Currently, the channel is not used at low temperatures due to the physical wear and dismounting of the cooling system. The list of tasks that are aimed at the resumption of the channel work at cryogenic temperatures includes the research on neutronic characteristics of the channel. With the aim to fulfill this task, calculations of neutronic characteristics of the channel and measurements of neutron fluxes along the height of the channel were performed.

For the purpose of investigation on neutronic characteristics of the low-temperature channel, neutron detectors were placed in 16 points along the height of the channel. The location of detectors is demonstrated in the Figure below. In, Ni, Au and Au into Cd detectors were used for experimental determination of fluxes of fast and thermal neutrons along the height of the channel. They were mounted on a flexible tape with a weight below. Detectors were packed and placed with the use of the method that permits to locate them as close to the central axis of the channel as possible, minimize their size and exclude their mutual influence.

CANBERRA spectrometer with GC2020 detector and DSA-1000 multichannel analyzer were used to measure the gamma-ray spectrum of neutron detectors. Data processing was carried out using programs of data center of PNPI NRC "Kurchatov Institute". Total error of neutron flux doesn't exceed 15%, which includes errors of the monitor data determination (weight, size, etc.), experimental measurement's error, errors of spectrometer calibration and errors of nuclear-spectroscopy constants.

The estimate of neutron fluxes at the low-temperature channel was carried out via WWR-M reactor computer model created with the use of MCNP certified program. Error of estimation values of neutron fluxes in accordance with MCNP passport for WWR-M reactor is 15%. The comparison of experimental and calculated values of neutron fluxes was performed for different energy intervals: less than 0.5 eV, more than 1.2 MeV and more than 2.3 MeV. All values coincided within the errors.

Additionally, the distribution of neutron flux along the height of the low-temperature channel was calculated for the following energy intervals: less than 0.5 eV, more than 0.1 MeV, more than 0.5 MeV and more than 1.0 MeV. The resultant values of neutron fluxes inside the low-temperature channel normalized to 17 MW power level are demonstrated in the Figure below. This data allows one to determine resulting neutron fluence for different energy intervals depending on the position of loading specimens in the channel.

Fast neutron flux in the low-temperature channel of WWR-M reactor at 17 MW power level is equal to $1.1 \cdot 10^{13}$ $cm^{-2} \cdot s^{-1}$ ($E > 1.0$ MeV). Currently the channel has no cryogenic cooling.

In comparison with the operating low-temperature channels (for example, on Japanese JMTR and KUR

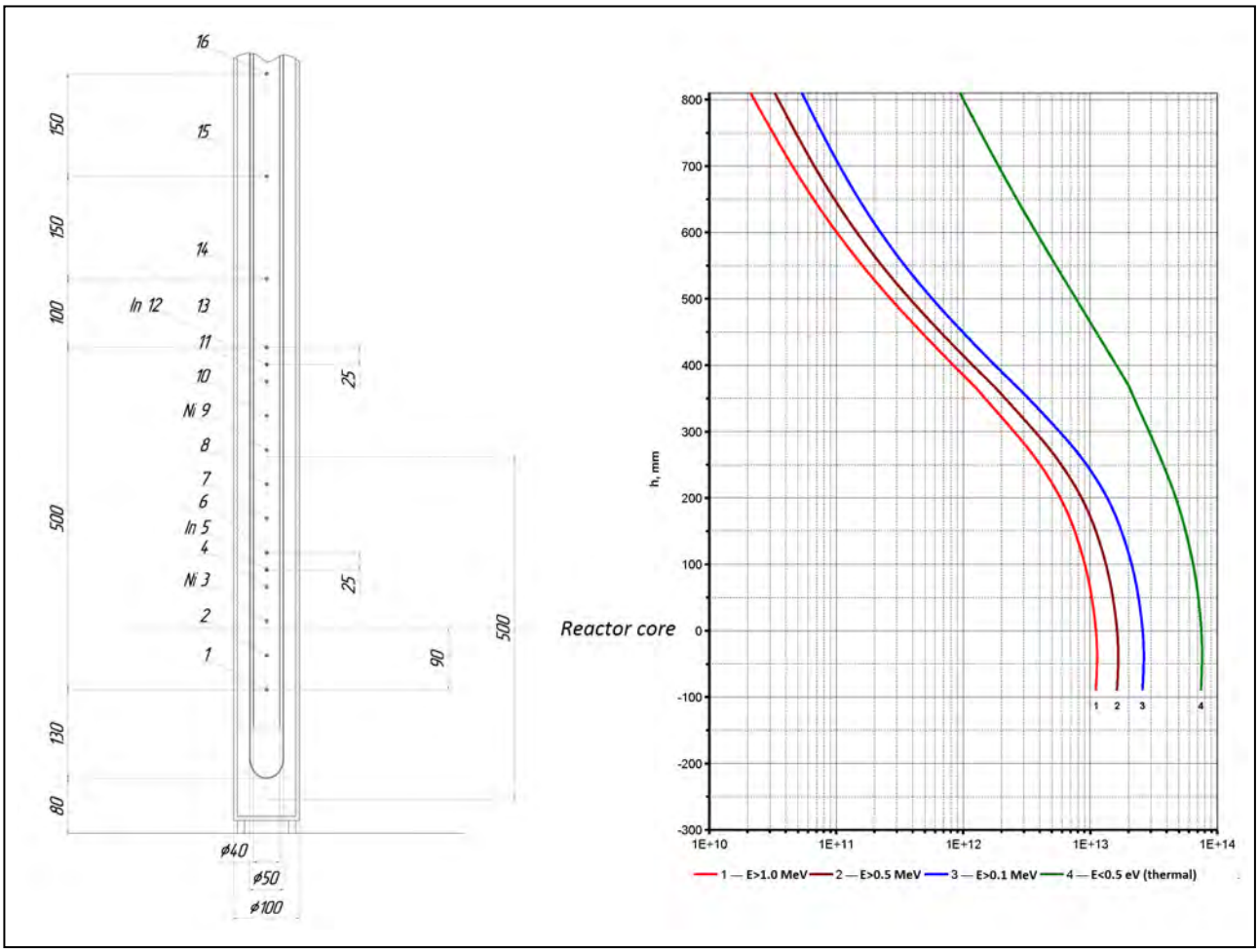

Location of detectors and distribution of neutron flux along the height of the low-temperature channel of WWR-M reactor at 17 MW power

reactors), neutronic characteristics of the WWR-M reactor channel seem to be more effective. Equipping the channel with the cryogenic cooling system will mean creating the unique world-scale research tool for radiation physics of solid state and low-temperature radiation materials science.

Zakharov A.A., Poltavsky A.S., Sushkov P.A., Chekanov V.A. // PNPI preprint 2951. Gatchina, 2014. P. 16.

Calculation of reactivity effects of the PIK reactor with the use of MCU and MCNP codes for analysis of accidents

A.S. Poltavsky, S.L. Smolsky, A.N. Erykalov, A.S. Zakharov, K.A. Konoplev, A.V. Korotynsky, M.S. Onegin, A.P. Malkov, M.V. Voronov, V.N. Tishchenko – PNPI NRC "Kurchatov Institute", Gatchina
A.A. Baligin, E.V. Burlakov, L.V. Bidulya, I.N. Geraskin, G.B. Davydova, A.M. Degtyarev, L.N. Zakharova, A.A. Ivanov, A.V. Krayushkin, A.A. Myasnikov, O.N. Saltykova, Yu.M. Semchenkov, T.E. Trofimova – Kurchatov Nuclear Technology Complex, NRC "Kurchatov Institute", Moscow

The work was performed in the framework of NRC "Kurchatov Institute" R&D on "Safety justification of the PIK reactor operation".

The purpose of the work is to develop computational models of the PIK reactor using the MCNP and MCU software, to verify the models and use them to define reactor neutronic characteristics required for reactor emergency modes and safety analysis.

Verification of computational models was carried out by means of comparison with experimental data obtained in the process of physical start-up of the PIK reactor and through comparative calculation of data acquired with the use of MCNP computer model developed in PNPI NRC "Kurchatov Institute" and certified for this reactor (Figs. 1 and 2).

A set of characteristics that give the fullest overview of special physical aspects of the reactor and are in need of justification of correctness of their calculation was subjected to consideration. These characteristics include the following: effectiveness of Control and Protection System (CPS) regulators; effects of reactivity in process of water heating and its loss in separate circuits of the reactor; field of energy release. Furthermore, a cross-check of MCU and MCNP-ORI codes developed at NRC "Kurchatov Institute" was carried out through simulation of the campaign of uniform lattice of fuel rods. It was done due to the necessity to analyze states of the reactor with burnt fuel.

The results show that the calculated error of the MCU program during the criticality analysis of states of the reactor at the moment of physical start-up doesn't go beyond the declared error of the program equal to about 0.5%. Deviation from the MCNP code

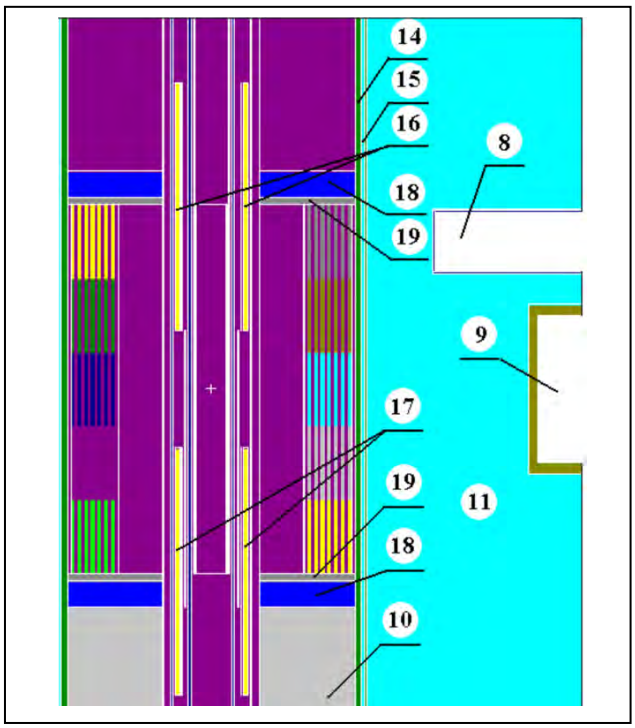

Fig. 1. Longitudinal section of the MCNP model of the PIK reactor core: 8 – horizontal experimental channel No. 1 (HEC1); 9 – HEC2; 10 – core support grid; 11 – heavy water (D_2O); 14 – vessel; 15 – vessel casing; 16 – top shutter (CPS regulator); 17 – bottom shutter (CPS regulator); 18 – bottom nozzle; 19 – top nozzle

for a wide range of relevant states of the reactor with fresh fuel does not exceed 0.2%, with burnt fuel (by the end of the campaign) – 1%.

According to calculations of effectiveness of CPS regulators and temperature and void reactivity effects, discrepancies between MCNP and MCU codes lie within the statistical error range. General reactivity effects related to the change of states in the core

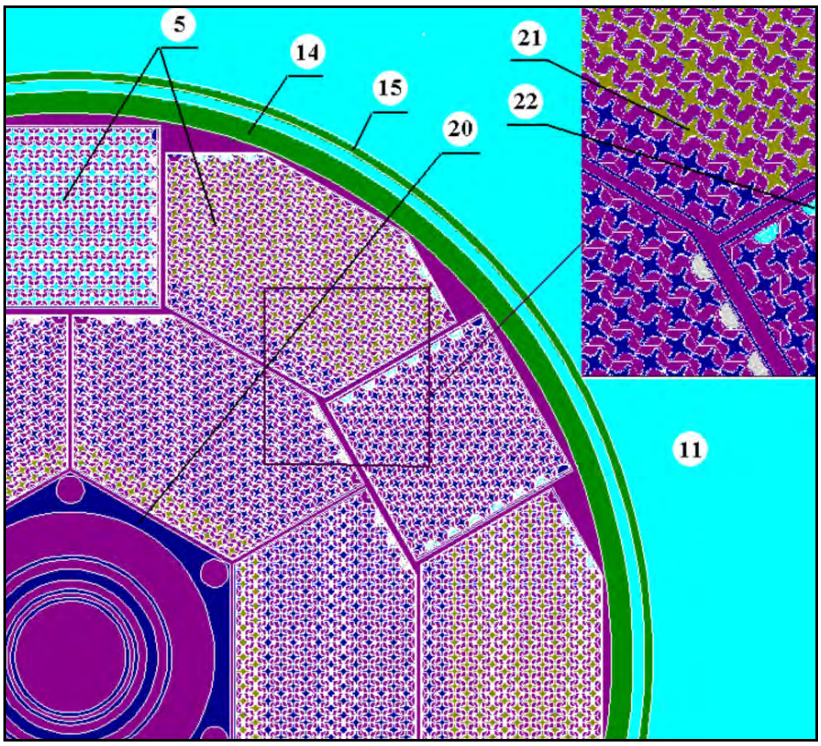

Fig. 2. Cross-section of MCNP model of the PIK reactor (with a fragment zoomed in):
5 – fuel assembly;
11 – heavy water (D_2O);
14 – vessel;
15 – vessel casing;
20 – guide of neutron trap;
21 – fuel elements (rods);
22 – semicylindrical displacers

(temperature and void effects) have a stable negative value in the PIK reactor.

In order to use results of experiments correctly when comparing them with results of calculation of MCU and MCNP codes (that have a stationary function), it is necessary to conduct a preliminary analysis of experiments based on their direct computational modeling and estimation of the role of spatial effects. It is possible to be done only by means of the model of spatial neutron kinetics. Such a three-dimensional computational model describing the PIK reactor in five-energy groups diffusive approximation, has been prepared as part of this work with the use of STEPAN code certified and used to analyze accidents in high-power channel-type (RBMK) reactors. The model and methods of calculation were subjected to initial testing.

This model can be used to analyze reactivity accidents and results of experiments on determination of reactivity effects.

Further challenges for the model development are:

– development of the library of neutron cross-sections with their dependencies on the main parameters determining the feedbacks;

– inclusion of delayed neutrons from (γ, n) reaction of deuterium in the model and evaluation of the contribution of this reaction with beryllium;

– development of a thermal-hydraulic model for description of feedbacks.

Computational models developed for the PIK reactor and the results of calculation of reactivity effects will be used to face priority challenges of safety justification and to continue works on the preparation of the reactor for the power start-up.

Baligin A.A., Burlakov E.V., Bidulya L.V., Geraskin I.N., Davydova G.B., Degtyarev A.M., Zakharova L.N., Ivanov A.A., Krayushkin A.V., Myasnikov A.A., Saltykova O.N., Semchenkov Yu.M., Trofimova T.E. (Kurchatov Nuclear Technology Complex, NRC "Kurchatov Institute"), *Voronov M.V., Erykalov A.N., Zakharov A.S., Konoplev K.A., Korotynsky A.V., Malkov A.P., Onegin M.S., Poltavsky A.S., Smolsky S.L., Tishchenko V.N.* (PNPI NRC "Kurchatov Institute"). Calculation of reactivity effects of the PIK reactor with the use of MCU and MCNP codes for analysis of accidents. R&D report No. 211-14/14-45. Moscow – Gatchina. 2014. P. 101.

Modelling of the fuel burnup in the PIK reactor core during the power start-up

A.S. Zakharov, K.A. Konoplev, M.S. Onegin, A.S. Poltavsky
Department of Nuclear Reactor Physics and Engineering, Department of Nuclear and Radiation Safety, Theoretical Physics Division, PNPI NRC "Kurchatov Institute"

The goal of this research is to test MonteBurns and ORIGEN codes used for the fuel burnup calculation combined with MCNP code through simulation of the PIK reactor power start-up.

A preliminary verification was based on comparison of calculation results obtained by MonteBurns method with similar calculations of MCU REA code that contains an embedded program for the fuel burnup calculation.

Power start-up of the PIK reactor is planned to be performed with the use of an original set of fuel assemblies. This set of fuel assemblies was already used for experiments in reaching first criticality in 2011. Fifteen fuel assemblies are used in an active core for the power start-up. Three aluminum displacers are loaded instead of three tetrahedral fuel assemblies (FA), which allows reactivity excess to be decreased so that standard subcriticality will be guaranteed by inserted control rods in case of the reactor shutdown (Fig. 1).

Safe transition to full number of 18 fuel assemblies is a significant challenge of the power start-up procedure. The power start-up concept is based on the power limitation and refueling minimization while the core is incomplete. Testing equipment on a single core configuration investigated in details during critical experiments provides more reliable measurement data for verification and validation of software used for calculation of neutronic parameters.

It is planed to load 18 fuel assemblies after generation of sufficient quantity of fission products during a single reactor campaign without intermediate refueling.

MCU and MCNP computational models with fresh fuel were validated in advance during the PIK reactor mock-up experiments and at the reactor itself in the process of attaining first criticality. The model with specified depletion zones for burnup calculations is presented in Figure 2.

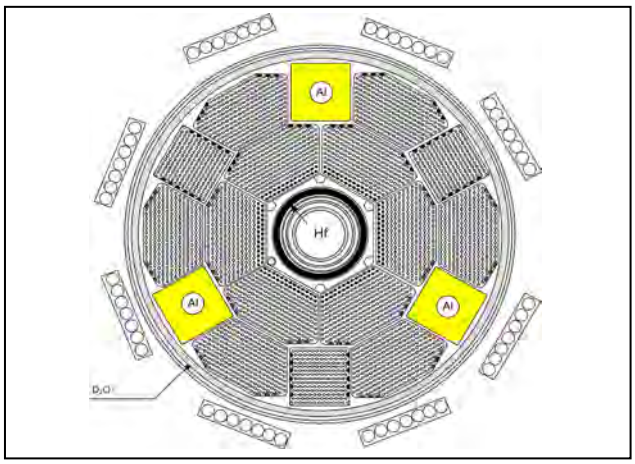

Fig. 1. Starting core for the power start-up

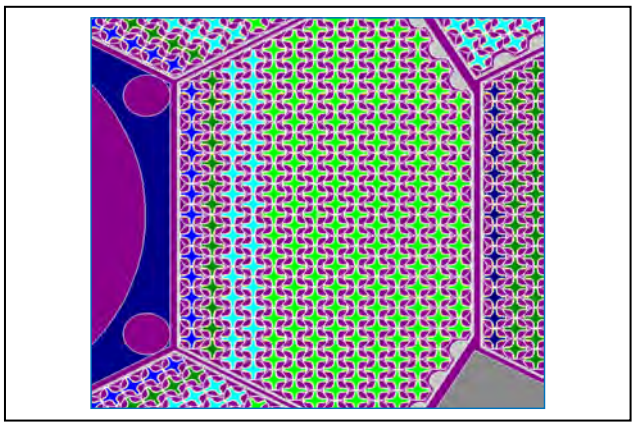

Fig. 2. Computational model of hexagon fuel assembly in central plan

MonteBurns + ORIGEN + MCNP computational package can be recommended for the PIK reactor fuel burnup calculations. The local reactivity deviation between MCU REA and MonteBurns results does not exceed 0.22% of reactivity for the change curve of Keff against operation time. Average rates of reactivity loss during a reactor cycle agree in limits of 5% (Fig. 3).

The computational simulation of the reactor power start-up with incomplete number of 15 fuel assemblies

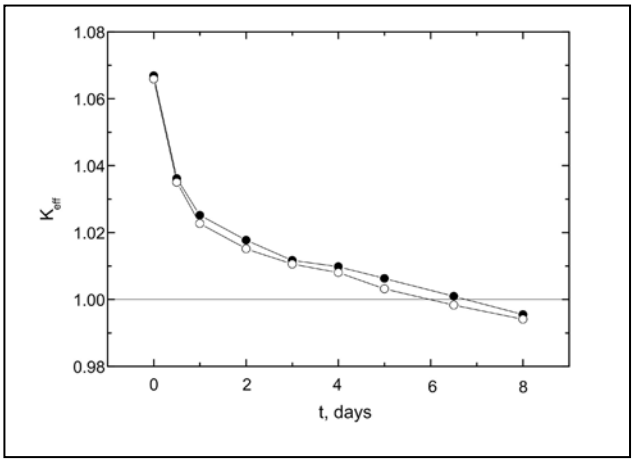

Fig. 3. Change of K_{eff} as a function of time of the reactor operation with the load of 15 FA (100 MW).
Dark markers – MonteBurns calculations,
White markers – MCU REA calculations

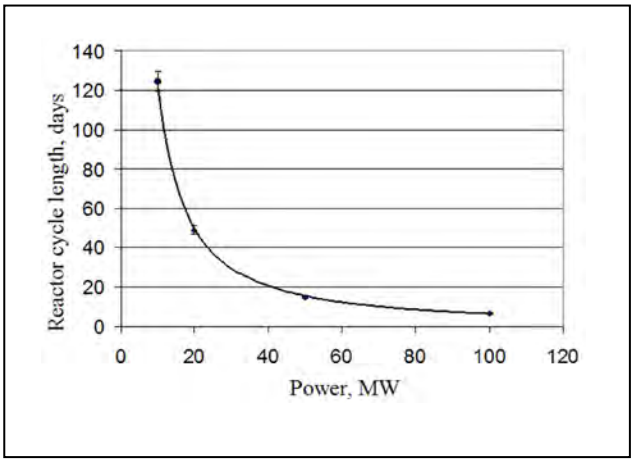

Fig. 4. Dependence of the first rector cycle duration on reactor power

in the core was carried out. Reactivity effect of an additional charge of the core up to a full number of 18 fuel assemblies was calculated for the case of the fuel burnup after the reactor cycle maximal power of 10 MW is reached.

Changes of reactivity worth of central absorbing rods (shutters) and a coefficient of nonuniformity of power distribution were estimated too.

The calculations of K_{eff} changes were performed for the reactor cycle at the power of 10 MW, 20 MW, and 100 MW. Xenon and samarium poisoning effects were determined for different power levels. Duration of the reactor cycle was estimated as a function of reactor power (Fig. 4). Simultaneously, it was confirmed that simple analytical dependences of reactivity calculation could be used to describe transient processes.

An optimal variant of the power start-up performed with the use of one complete set of fuel assemblies has been suggested basing on the calculations performed. The initial stage of the reactor power start-up is equipment testing with 15 FA loaded. The testing is performed in seven short cycles no less than two days long with interruptions for ^{135}Xe decay. At this stage, the power is limited by the value of no more than ≈ 50 MW. Further on, the average power has to be lowered to ≈ 10 MW for additional accumulation of fission products and lowering the reactivity excess in order to ensure safe conditions for core loading up to 18 FA. At this stage a power decrease can be used to start testing experimental facilities at the neutron beams and checking the reactor biological shielding. Demonstration of 100 MW full-power operation of the reactor during a single reactor campaign will be performed after the transition to a full number of 18 FA.

The solutions found can be applied to perform the power start-up even when different types of fuel are used. Demonstration of the reactor operation with upgraded fuel assemblies (complete operational set) is planed at the final stage of the power start-up.

Preliminary calculations proved that safety conditions of loading to full number of 18 FA could be provided by additional power reduction up to 10 MW. Additional energy release value at minimum power depends on a selected reactor power during the first rector cycle, and its prolongation is possible due to reduced power and xenon effect. Total energy release of ~ 2 100 MW-days scheduled under the power start-up program can be provided with the use of one complete set of FA if necessary power decrease is taken into account after the first phase of operation with incomplete number of FA. The full time of the power start-up including the operation at nominal power could take about 100 calendar days.

1. *Zakharov A.S., Konoplev K.A., Onegin M.S., Poltavsky A.S.* // PNPI preprint 2954. Gatchina, 2014. P. 31.
2. *Aksenov V.L., Kovalchuk M.V.* // Intern. conf. "Nuclear power innovation projects and technologies". 2014. NIKIET. Moscow. October 7th–10th. V. 1. P. 103–113.

The concept of the exploitation set of fuel assemblies for the PIK reactor

A.S. Zakharov, A.N. Erykalov, K.A. Konoplev, M.S. Onegin, A.S. Poltavsky, S.L. Smolsky, S.R. Friedmann, I.M. Kosolapov, V.L. Aksenov – Department of Nuclear Reactor Physics and Engineering, Theoretical Physics Division, Department of Nuclear and Radiation Safety, PNPI NRC "Kurchatov Institute", Gatchina
M.V. Kovalchuk – NRC "Kurchatov Institute", Moscow

The PIK reactor project is based on the use of SM-2 reactor fuel elements with active length extended to 500 mm. The first complete sets of fuel elements (FE) and fuel assemblies (FA) of the PIK reactor were investigated in detail. The start-up set was used for the PIK reactor start-up in 2011 under the first criticality program.

Provision of safe and effective operation of the PIK reactor at nominal reactor power of 100 MW depends on the organization of production of improved PIK-2 fuel assemblies that meet current requirements on the operating cycle duration and arrangement of surveillance specimens of tested irradiated materials.

For these purposes, a reference variant of PIK-2 fuel implied manufacturing zirconium casings and embodying burnable poison rods (BPR) instead of steel displacers in the fuel assembly structure. A variant of replacement of some fuel elements with BPR is possible too. In order to place irradiated surveillance specimens in a square-type fuel assembly, three rows of fuel elements should be extracted (Fig. 1).

According to the computation of different BPR variants of the PIK reactor operating cycle and irradiation tests of developed BPR at the WWR-M reactor, the PIK reactor operating cycle length can be increased from ≈ 15 days to 25–30 days (Figs. 2 and 3). The Gd_2O_3 + ZrO_2 composition was selected as the burnable absorber material.

The pilot factory-made variants of fuel assemblies with zirconium casings and burnable poison rods were produced for adjustment of the fabrication technology and tested at "the PIK reactor mock–up" critical facility. Additional researches and calculations have revealed a necessity for additional increase of the fuel loading as the number of consumed fuel assemblies remains

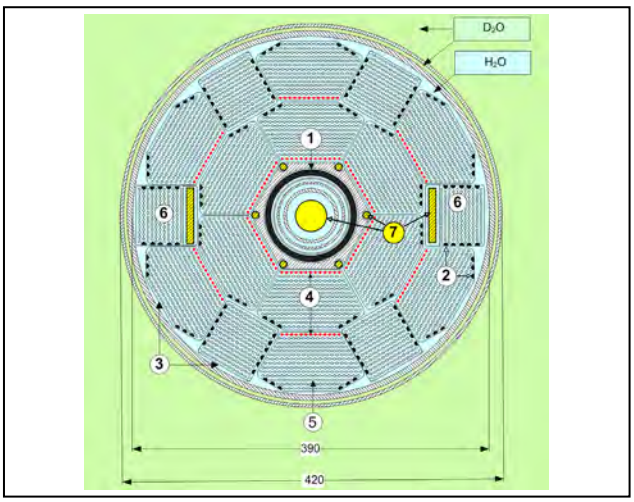

Fig. 1. The PIK reactor core: 1 – Hafnium absorbing shutters; 2 – Burnable poison rods, Gd_2O_3 + ZrO_2; 3 – Zirconium casing of fuel assemblies; 4 – Fuel elements with the reduced fuel content (0.48 of nominal value); 5 – Fuel elements with the nominal fuel content; 6 – Fuel assemblies with the surveillance specimens; 7 – Irradiated samples

at a rather high level for the most preferable refueling regime with replacement of ½ part of a core.

In order to reduce R&D expenses for PIK-2 fuel assemblies (Fig. 4), its design should be based on a proven variant of serial SM type fuel element with the fuel content increased by 20%, which will provide an essential economy of fuel consumption. The PIK reactor cycle calculations demonstrated the possibility of 30% increase in energy release, so the number of consumed fuel assemblies would be reduced to the same degree (with the mass of consumed uranium reduced only by 9%). These possibilities might be used to prolong a reactor operating cycle until 25–30 days taking into account a reactivity loss for performance of the irradiation program. It is possible to decrease the mass of consumed uranium by 20% by means of

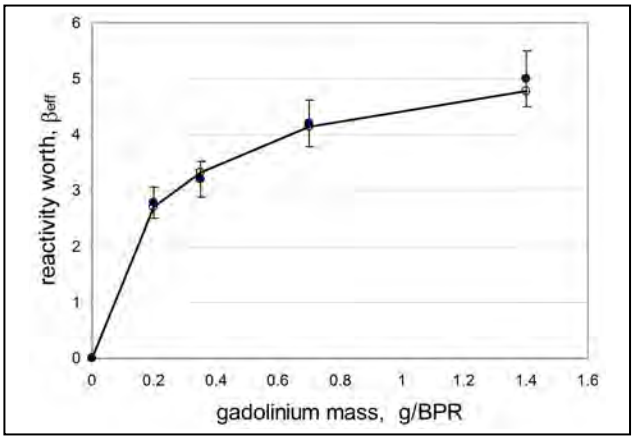

Fig. 2. The curve of reactivity worth of 144 burnable poison rods against gadolinium mass (with all control rods removed). Dark markers – experiment, Light markers – MCNP calculation

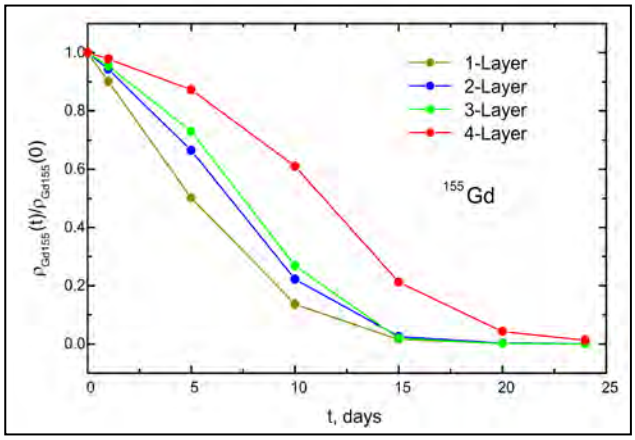

Fig. 3. Temporal dynamics of the ^{155}Gd concentration change in different layers of burnable poison rods

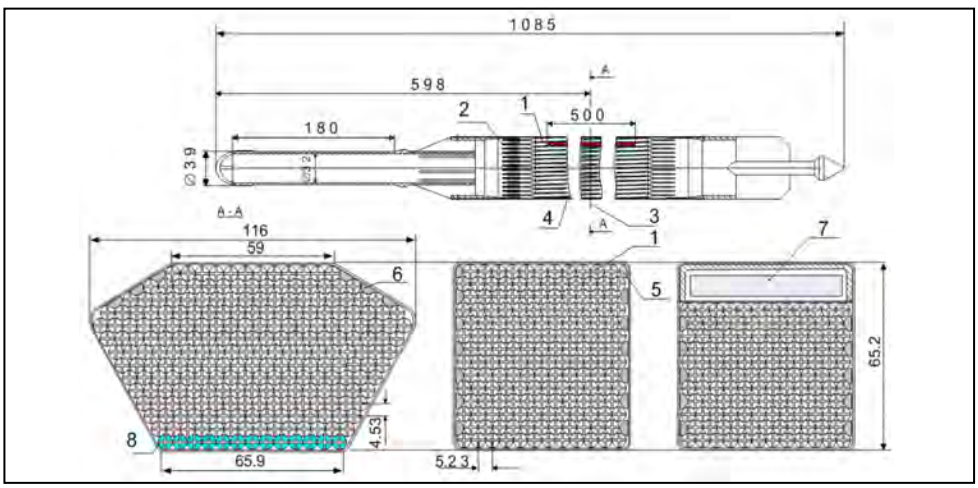

Fig. 4. The exploitation set of PIK-2 fuel assemblies (the concept): 1 – Fuel elements; 2 – Bottom spacer grid; 3 – Center of fuel; 4 – Casing (E-125 or E-110); 5 – Angular displacer; 6 – Burnable poison rod; 7 – Ampoule with surveillance specimens; 8 – Fuel elements with "0.48 of nominal" reduced fuel content

more energy-conserving refueling with reactor cycle length of around 20 days.

Values of the key parameters defining safety of reactor operation remain invariable. The increase of fuel content causes insignificant changes of K_V peak volume factor of power distribution. Mainly, local power density increase in fuel elements placed close to the neutron trap, where the fuel content is reduced to prevent a power growth in these elements.

The typical value of $K_V \approx 3.0$ is provided also by shuffling between inner and outer hexagon fuel assemblies with different fuel burnup, which is possible due to their identical design (Fig. 1).

In order to realize new capabilities, the exploitation set of PIK-2 (Fig. 4) fuel assemblies must embody the following design changes of the start-up set:

– installation of burnable poison rods;

– replacement of stainless steel casings for fuel assemblies with zirconium ones;

– use of the optimal fuel profiling;

– increase of the nominal content of ^{235}U in the fuel element from 7.14 g to 8.57 g.

The modification of a fuel assembly with a cavity for irradiation of constructive materials must be embodied in the structure of the exploitation set of the fuel assemblies.

Different variants of design of improved cavities for irradiated surveillance specimens were investigated at the critical facility.

Kovalchuk M.V., Aksenov V.L., Erykalov A.N., Zakharov A.S., Konoplev K.A., Kosolapov I.M., Onegin M.S., Poltavsky A.S., Smolsky S.L., Fridman S.R. // Intern. conf. "Nuclear power innovation projects and technologies". NIKIET. Moscow, October 7th–10th. 2014. V. 1. P. 339–347.

Creation of an additional security system for the PIK reactor based on an industrial FT-NIR spectrometer

T.V. Voronina, I.V. Zapitetskaya
Department of Nuclear and Radiation Safety, PNPI NRC "Kurchatov Institute"

Detection of the reactor vessel disruption on its early stage is a relevant task to be solved at any operating reactor. Today, the Leak-Before-Break Concept is a basic approach to assurance of safe operation of the reactor equipment. Such an approach demands a sure fixation of a leak for registration of through defects. It is impossible to organize an operating inspection of reactor vessel defects on the base of standard pressure and level detectors for the research heavy-water reactor PIK since the detection time for it is no less than one hour.

However, it is possible to offer a more sensitive inspection method for the PIK reactor vessel integrity. The liquid regulation cooling circuit (LRCC) of the PIK reactor has no analogues in other operating reactors. It is an annular cavity (4 mm thick) surrounding the reactor vessel where concentrated heavy water ($a_D \geq 96\%$) circulates in slot gaps.

This design feature allows one to inspect the reactor vessel integrity based on the decrease of deuterium content in heavy water of the LRCC that occurs at appearance of light water leakage in the primary cooling circuit. For this purpose, it is necessary to create a system of precise remote monitoring of the protium content in heavy water of the LRCC based on an on-line analyzer. At present, the system of continuous measurement of heavy water concentration in the LRCC is included in the PIK reactor project. Analyzer 12 is switched on by a bypass between the downstream and upstream lines of the LRCC pumps, as shown in Figure.

It was shown earlier that it is possible to solve this problem by means of infrared (IR) spectrometry method (based on the FT-NIR spectrometer). However, such an approach has essential disadvantages. 1. Due to the significant absorption, it is necessary to use "thin" sample cells (< 1 mm) for measurement, but such cells are difficult to work with in the LRCC conditions (pressure of 13–16 atm.). Moreover, it is necessary to use sapphire to make cell optical windows, which makes such cells very expensive. 2. A sample cell section is an integral part of the FT-NIR spectrometer, therefore, the device should be placed in the LRCC line directly. 3. Optical fiber for the middle IR band is still under development. Such optical fiber considerably weakens a signal, therefore, one cannot use more than 2 m.

This work covers a possible application of the FT-NIR spectrometer (spectroscopy) in such system of continuous measurement of heavy water concentration for exact and reproducible analysis. The NIR band (12 500 to 4000 cm^{-1}) consists of overtones and compound molecular vibrations of water, absorption coefficients of which are 20–50 times weaker than absorption coefficients of main molecular vibrations (MIR band). It allows one to increase thickness of an on-line sample cell (up to 5 mm). Moreover, it is possible to use cheap cell optical windows made of quartz. Special quartz optical fiber is developed for NIR and its use reduces a signal only slightly. Due to the use of quartz optics, the FT-NIR spectrometers are more reliable, adapted for long work in difficult industrial conditions. Such a device (MATRIX-F) has been already developed and is used for on-line control in petrochemical industry.

The research was carried out on a laboratory FT-NIR spectrometer MPA. To avoid dilution of heavy water, an experimental hermetic on-line scheme was assembled and parameters and conditions of heavy water spectrum measurement were determined. As a result, calibration models were designed in two concentration ranges: for concentrated heavy water (99.0–99.9%) and in the wide range of concentration. For concentrated heavy water, a graduation

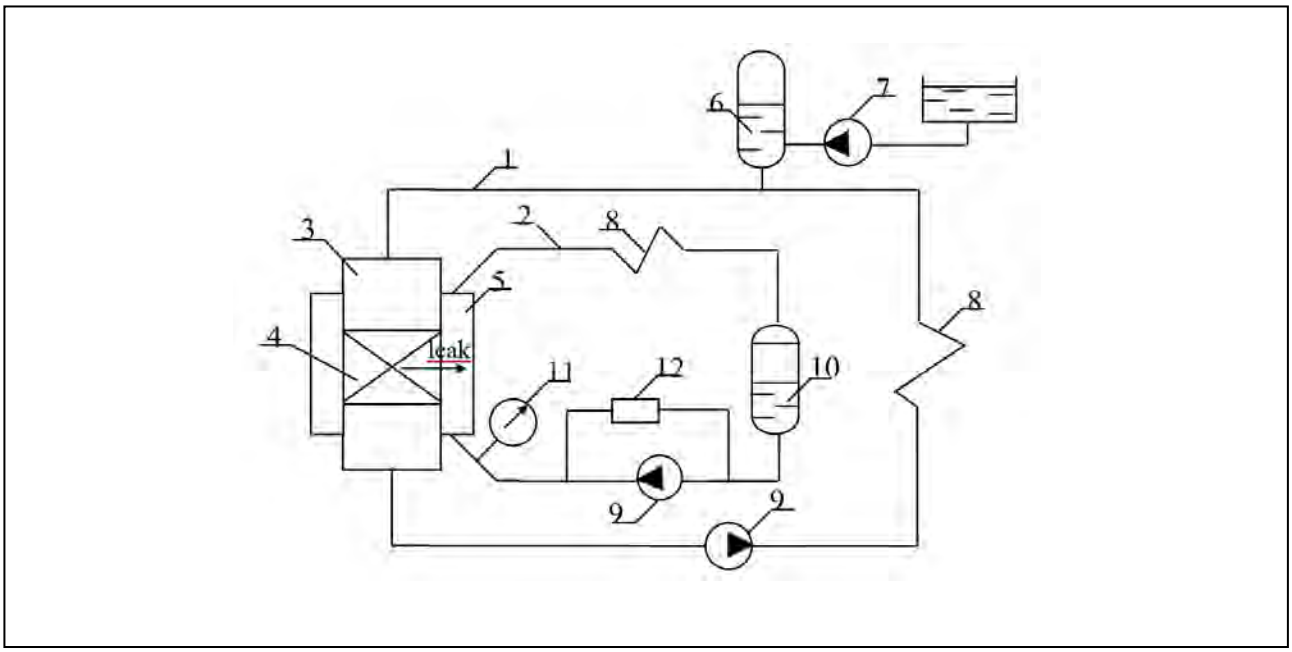

Scheme of the PIK reactor circuits (the primary cooling circuit and the liquid regulation cooling circuit) with the processing equipment for detection of the reactor vessel leak: 1 – primary cooling circuit; 2 – liquid regulation cooling circuit; 3 – reactor vessel; 4 – core; 5 – annular cavity; 6 – volume compensator of the primary cooling circuit; 7 – make-up pumps; 8 – heat exchangers; 9 – circuit pumps; 10 – degasser of the liquid regulation cooling circuit; 11 – pressure control instrument in the liquid regulation cooling circuit; 12 – analyzer Analysis-3 (room 022A, building 100A)

error is 0.002%, which is better than the graduation error of the old on-line detector Analysis-3 (0.01%). For the wide range of heavy water concentration, the graduation error is 0.01% which is also better than the graduation error of Analysis-3 (0.4%). Quality of calibration models was tested on independent heavy water samples. According to the results received, it is recommended to use the system packaging for on-line measurement of heavy water concentration in the LRCC.

The results of the work were reported at the VII Scientific and technical conference "Problems and Prospects of Development of Chemical and Radiochemical Control in the Nuclear-Power Engineering" (Atomenergoanalitika-2014) on September 15th–19th, 2014 in Russia.

Voronina T.V. // Mat. of VI Scientific and technical conf. "Problems and Prospects of Development of Chemical and Radiochemical Control in the Nuclear-Power Engineering" (Atomenergoanalitika-2011). Russia. 2011. P. 148–159.

Specific fuel costs for the PIK reactor as a function of thickness of a fuel element blade

A.N. Erykalov, E.G. Sakhnovsky
Theoretical Physics Division, PNPI NRC "Kurchatov Institute"

This work is the continuation of the study started in PNPI NRC "Kurchatov Institute" report ER-296 "Optimization of PIK fuel elements" (Gatchina, 2013). It presented considerations concerning the possible construction of the fuel elements for the PIK reactor that can reduce specific fuel costs. It was noted there that the process of slowing down the neutrons in the existing active zone of the reactor can be easily enhanced. Increase of the water fraction in the active zone will lead to a decrease of the neutron leakage and an increase of effective multiplication coefficient. This can be used to achieve a deeper burn-up and hence reduce specific fuel costs. In this paper we suggest to decrease the thickness of a fuel element blade in order to diminish its volume and, as a result, increase the fraction of the water in the active zone of the PIK reactor.

A fuel part of specific reactor costs is

$$S_f \sim \frac{agP}{yn\Phi},$$

where $a = 1.5 \cdot 10^{-5}$ g/MW · sec for ^{235}U thermal neutrons reactor, g – the cost of the fuel in fuel elements per 1 gram with account of the construction costs, P – the reactor power averaged over the period of reactor operation, y – the rate of burn-up in the fuel elements, n – the number of channels, Φ – the neutron flux averaged over the channels and the time of operation.

Curve 1 describes the relative specific fuel costs at standard load of 7.11 g ^{235}U per fuel element in a bronze mould. This curve demonstrates that a twofold decrease of the blade thickness reduces specific fuel costs of the reactor by a factor of two.

It was already noted that, in attempt to increase multiplication factor of High Flux Reseach Reactor SM, bronze mould in the core of its fuel elements were substituted with the silumin ones. Curve 2 refers to the case of the standard U load of 7.11 g ^{235}U per fuel element with silumin core. In this case, a twofold decrease of the core size reduces specific fuel costs only to 0.8. It is caused by the fact that neutron absorption in silumin is smaller than in bronze. If one compares specific fuel costs for silumin fuel elements with the costs for standard elements, it is obvious that in case of the fuel elements with the blade of the standard size equal to 1 mm, the fuel costs are 0.6 of the standard ones (see curve 3). Twofold reduction of the blade thickness smoothly decreases the fuel costs till 0.5. Obviously, the amount of burden for the thin blade (with thickness about 0.5 mm) is so small that extraneous absorption of the burden does not influence specific fuel costs that appear to be about 0.5 of the standard ones.

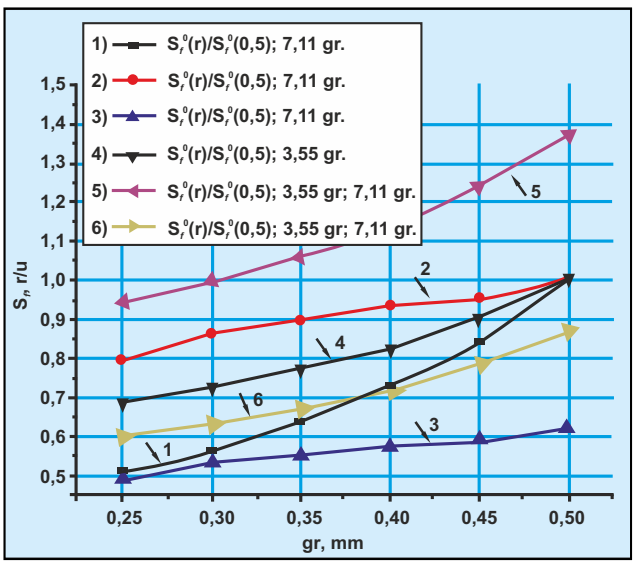

Specific fuel costs for the PIK reactor as a function of thickness of a fuel element blade

Reduction of thickness of a fuel element blade increases the concentration of the fuel in the burden if the load of the fuel element remains the same. This increases the probability of concentration of few fuel seeds at the border of fuel element. In this case the cover of fuel element can burn-out.

For this reason, one has to perform a complete technological investigation of this issue, which can suggest a use of copper plating of the inner surface of the fuel element However, we can avoid such a consideration if we assume that the uranium load of the fuel element is reduced simultaneously.

If we reduce ^{235}U load by a factor of two down to 3.55 g ^{235}U per fuel element with silumin core, then the change of thickness of the blade of fuel element from 1 mm to 0.5 mm will lead to diminishing of relative specific fuel costs from 1 to 0.7 (see curve 4). If one relates these costs to specific costs at standard load of 7.11 g ^{235}U per fuel element, it can be seen that as long as thickness of the blade is equal to 0.6 mm, specific costs would exceed costs with a standard load (see curve 5).

If specific costs for initial load of 3.55 g ^{235}U per fuel element with silumin core are related to specific costs of the standard fuel element with load of 7.11 g ^{235}U and bronze mould, then one can see that decrease of the blade thickness from 1 mm to 0.5 mm reduces relative fuel costs from 0.87 to 0.6 (see curve 6). Curves 2 and 3 demonstrate that at standard load of 7.11 g ^{235}U per fuel element with silumin core a change of the blade thickness in the interval from 1 mm to 0.6 mm leads to the reduction of fuel costs only by 15%. Thus, the decrease of the blade thickness is not very advantageous in this case.

According to the calculations, the concentration of fission products in the bronze burden of the fuel element with bronze core and blade thickness of 0.6 mm is equal to the concentration in the standard fuel element at burn-up of 0.8. It appeared that such a burn-up has already been achieved in fuel elements of SM reactors.

The results of this investigation were published, applications for two patents were sent and one patent license has already been obtained.

1. *Erykalov A.N., Sakhnovsky E.G.* Influence of the fuel element blade thickness on the specific fuel costs of the PIK reactor. PNPI report, ER-299. Gatchina, 2014. P. 6.
2. *Erykalov A.N., Sakhnovsky E.G.* Fuel element for PIK reactor. RF PATENT No. 145645, 20.08.14.

Upgrade of the high voltage generator for the neutron beam facilities at the PNPI 1 GeV synchrocyclotron

E.M. Ivanov, G.F. Mikheev, A.S. Pokrovsky, G.A. Riabov
Knowledge Transfer Division, PNPI NRC "Kurchatov Institute"

The PNPI NRC "Kurchatov Institute" synchrocyclotron possesses two operating neutron beam lines that use the system of fast one-turn deflection of 1 GeV proton beams to the internal neutron-producing target. The scheme of the cyclotron chamber arrangement is presented in Figure 1.

When a 1 GeV beam runs on the final orbit between deflector plates the generator feeds a high-voltage pulse on the deflector, which causes a proton beam vertical deflection, and the beam hits the neutron target on the second turn.

The requirements for the generator can be stated as follows: about 100 kV pulse voltage amplitude, the pulse current of $3 \cdot 10^3$ A, about 50 nsec pulse leading edge, about 1 nsec accuracy of the phase-lock with proton bunch.

The generator that have been used up to now was based on four TGI-700/25 type thyratrons connected in parallel and could not provide stability of synchronization of the set of four thyratrons, which resulted in unstable performance and difficulties with tuning the neutron beam.

The necessary accuracy and essential pulse parameters have been obtained after transition to two new TGI2-5k/50 type high power thyratrons produced by the "Pulse technology" company (Russia). This type of thyratrons demonstrates high reliability and precision of parameters, and is used in powerful pulse installations of various research centers in Russia and abroad.

Stable operation of the high voltage generator provides the stable and effective operation of both

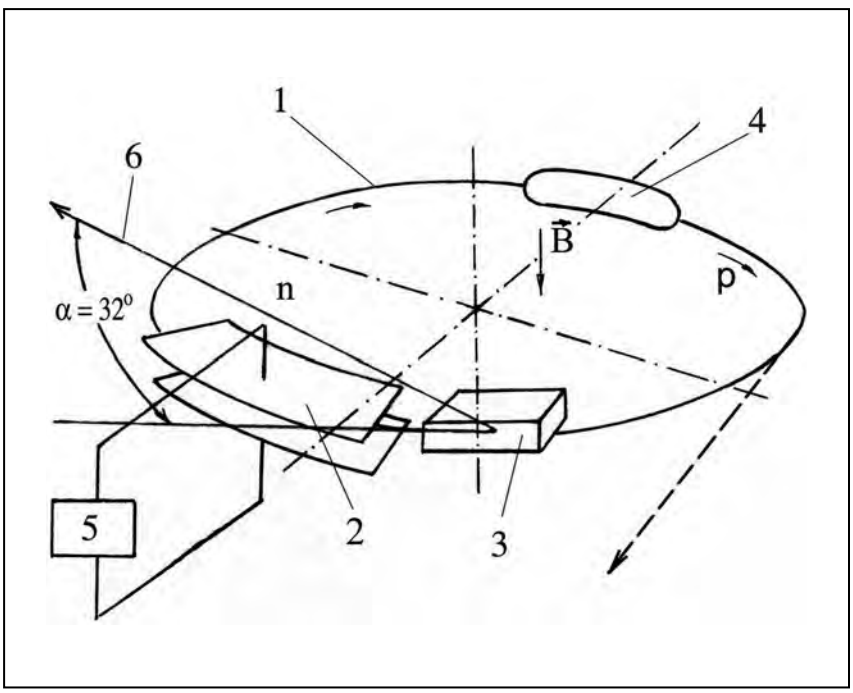

Fig. 1. Arrangement of a one-turn 1 GeV proton beam deflection to the internal target:
1 – final orbit of the 1 GeV proton beam;
2 – electrostatic deflector;
3 – neutron producing target;
4 – proton beam bunch;
5 – deflector power supply and control system;
6 – direction of the neutron beam

Fig. 2. The external view of the high voltage generator (final stage) after the upgrade

neutron facilities at 1 GeV synchrocyclotron. The first beam facility is a world-known GNEIS time-of-flight spectrometer designed to study neutron-nucleus interactions at neutron energies from 10^{-2} eV to several hundred MeV; the second beam line contains a unique beam with the atmosphere-like neutron spectrum, which is used for the accelerated testing of electronics for the aviation and space and has no equals in Europe. Both neutron beams share the same neutron producing target and deflector systems. GNEIS spectrometer uses the neutrons emerging from the polyethylene moderator, but the second beam utilizes neutrons coming immediately from the thick target. The atmosphere-like neutron spectrum can be received only when the selection angle is about 30 degrees. The external view of the high voltage generator after the upgrade is presented on Figure 2.

1. *Abrossimov N.K., Mikheev G.F.* Radio engineering systems of PNPI synchrocyclotron. Gatchina, 2012. P. 340.
2. *Ivanov E.M., Mikheev G.F., Pokrovsky A.S., Riabov G.A.* A device for stabilization of the proton beam pulse intensity with the use of *C*-electrode. RF PATENT No. 145675, 16.04.2014.

20
CKT
30
CKT

Applied Research and Developments

Determination of element composition of the Gd_2O_2S : Pr, Ce scintillation ceramics using neutron activation analysis

V.G. Zinovyev, Yu.E. Loginov, I.A. Mitropolsky, G.I. Shulyak, T.M. Tyukavina, S.L. Sakharov, S.V. Kosianenko et al.
Neutron Research Division, PNPI NRC "Kurchatov Institute"

X-ray luminescent ceramics based on Gd_2O_2S : Pr, Ce is used as a sensor of ionizing radiation, for example, in computer tomography. It combines high efficiency conversion with a short relaxation time. The concentration of the alloying element is changing from 0.1 to 1 000 ppm. Impurities have a negative effect on scintillation properties of ceramics.

The technique of neutron activation analysis of scintillation ceramics Gd_2O_2S : Pr, Ce was developed in this work. The concentrations of As, Ce, Co, Cr, Cs, Eu, Fe, La, Sc, Tb, Zn, Zr, Pr, Gd, Na in samples were

Table. Reactions, isotope abundance *p*, the cross-section σ_{th} of thermal neutron capture, energy E_γ of gamma radiation, half-life time $T_{1/2}$ and determination limits *DL*

Reaction	*p*, %	σ_{th}, bn	E_γ, keV	$T_{1/2}$, days	*DL*, %
$^{45}Sc(n, \gamma)^{46}Sc$	100	27.2 ± 0.2	1 120.92	83.8	$1.3 \cdot 10^{-8}$
$^{58}Fe(n, \gamma)^{59}Fe$	0.28	1.32 ± 0.03	1 099.45	44.5	$3.7 \cdot 10^{-5}$
$^{59}Co(n, \gamma)^{60}Co$	100	37.18 ± 0.06	1 173.52	1 925.3	$2.9 \cdot 10^{-7}$
$^{64}Zn(n, \gamma)^{65}Zn$	48.6	0.79 ± 0.02	1 115.55	243.9	$6.3 \cdot 10^{-6}$
$^{133}Cs(n, \gamma)^{134}Cs$	100	30.3 ± 1.1	796.09	754.3	$3.6 \cdot 10^{-7}$
$^{139}La(n, \gamma)^{140}La$	99.91	9.04 ± 0.04	1 596.65	1.68	$1.2 \cdot 10^{-7}$
$^{140}Ce(n, \gamma)^{141}Ce$	88.45	5.8 ± 0.02	145.44	32.5	$5.8 \cdot 10^{-5}$
$^{141}Pr(n, \gamma)^{142}Pr$	100	11.5 ± 0.3	1 575.6	0.80	$1.6 \cdot 10^{-4}$
$^{151}Eu(n, \gamma)^{152}Eu$	47.8	9 200 ± 100	1 408.3	4 944	$7.8 \cdot 10^{-8}$
$^{159}Tb(n, \gamma)^{160}Tb$	100	23.4 ± 0.4	966.42	72.3	$8.7 \cdot 10^{-8}$

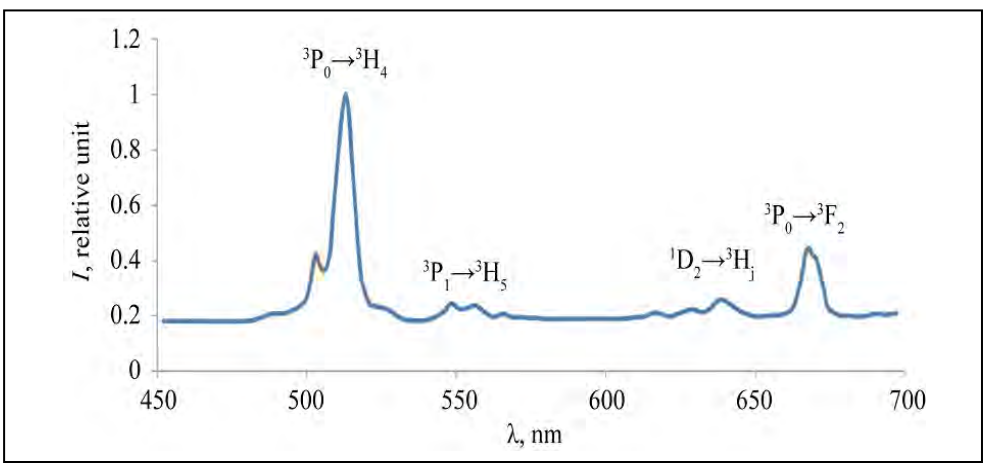

Fig. 1. Spectrum of luminescence of the Gd_2O_2S : Pr, Ce ceramics

measured in the range from $3 \cdot 10^{-8}$ to 2.0% of the mass. After the irradiation in a thermal neutron flux $f_{th} = 6.3 \cdot 10^{13}$ cm^{-2}s^{-1} for 2 hours, the determination limits of the elements were $(0.6–1.3) \cdot 10^{-8}$% (see Table).

It was established that the relative light yield (λ_{max} = 513 nm) decreases with the increase of the content of Ce in scintillation ceramics. The maximum value of the relative light yield of ~ 40% is obtained when the Ce content reaches ~ 10^{-5}%. It is shown that alloying of ceramics Tb (~ 10^{-6}%) leads to reduction of afterglow 0.045–0.055% after 5 ms and 0.001% after 500 ms.

From one to three hours long measurements of gamma spectra were conducted repeatedly. The time of exposure of the irradiated sample ranged from 3 to 40 days, which allowed us to separate the radiation of short-lived and long-lived nuclides, see spectra on Fig. 1 to 3, and to lower the corresponding content detection limits significantly.

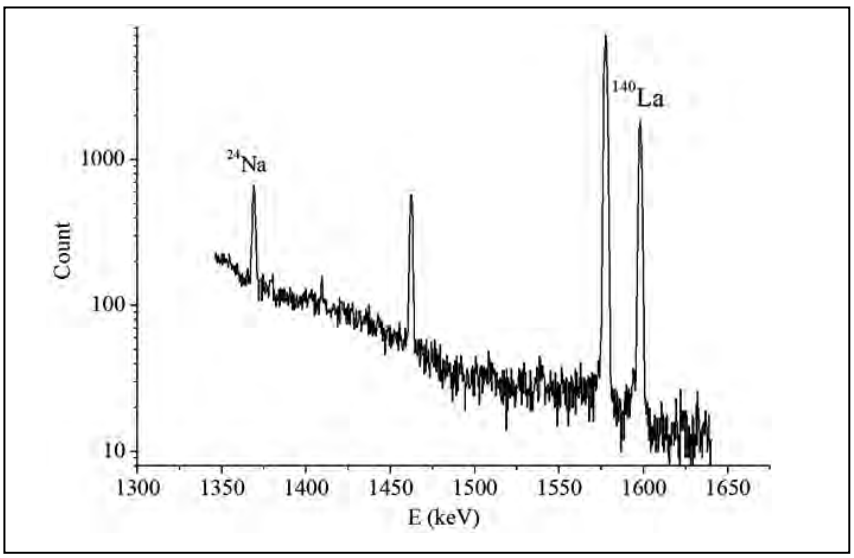

Fig. 2. Gamma spectrum of the Gd_2O_2S : Pr, Ce ceramics, 6 days after irradiation

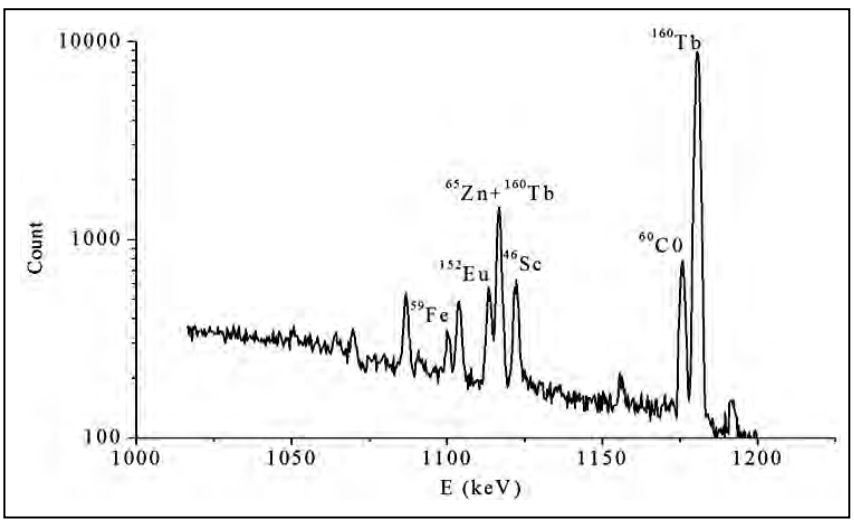

Fig. 3. Gamma spectrum of the Gd_2O_2S : Pr, Ce ceramics, 20 days after irradiation

Zinovyev V.G., Mitropolsky I.A., Loginov Yu.E., Shulyak G.I., Tykavina T.M., Sakharov S.L., Kosianenko S.V., Gorokhova E.I., Demidenko V.A. // World Journal of Nuclear Science and Technology. 2014. V. 4. P. 139–147.

Development and production of Gas Micro Pattern Detectors

L.G. Kudin
Knowledge Transfer Division, PNPI NRC "Kurchatov Institute"

The row of prototypes of Gas Micro Pattern Detectors, such as TGEM (Thick Gas Electron Multiplier), Monolithic TGEM, MICROMEGAS (Micro Mesh Gas System) (Figs. 1, 2) have been developed and produced by the Information Technologies and Automation Department in close collaboration with Relativistic Nuclear Physics Laboratory over the last few years. This engineering work was aimed at creation of the technological base for Gas Micro Pattern Detectors production.

The performance of these detectors and their combinations was subjected to laboratory tests and studied in the test beams of CERN and PNPI NRC "Kurchatov Institute" accelerators, which confirmed its compliance with requirements for the muon system of the CBM experiment (FAIR, GSI, Germany). The results of this work were presented at CBM collaboration meetings and PNPI seminars, and published in PNPI preprints. Four articles were prepared and sent for publication in "Instruments and Experimental Techniques" journal. Production of the TGEM and Monolithic TGEM was successfully implemented in industry.

The process of creating new Gas Micro Pattern Detectors is tightly connected to technology of their production and requires organization of special workshop equipped with clean areas, new equipment for prototyping, chemical processing and photo processing, and so on. Partly this job was done long time ago, but to the moment there is a strong need for subsequent innovations. Especial care should be devoted to attraction of young specialists to these investigations.

The experience accumulated in tasks mentioned above is also very important for its further application in experiments that will be carried out at the PIK reactor.

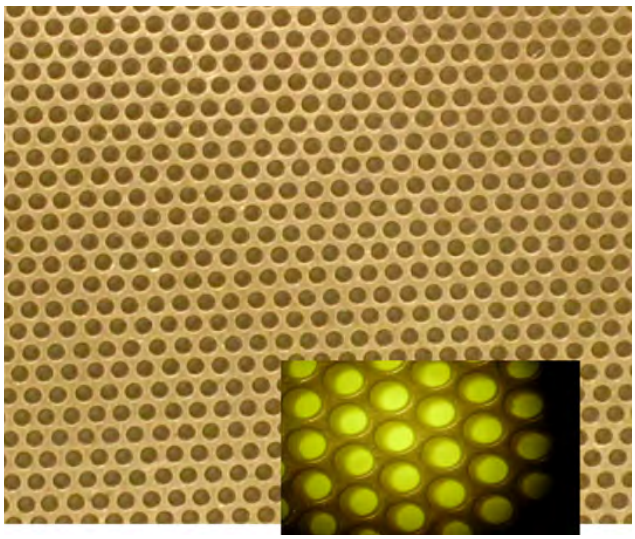

Fig. 1. TGEM, Monolithic TGEM

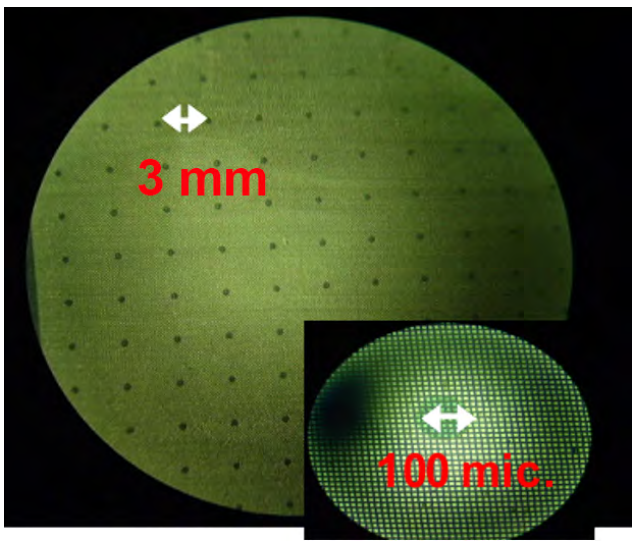

Fig. 2. MICROMEGAS

1. *Volkov S.S., Evseev V.A., Ivanov V.V., Komkov B.G., Kudin L.G., Nikulin V.N., Rostchin E.V., Rybakov G.V., Samsonov V.M., Tarasenkova O.P., Khanzadeev A.V., Chernysheva E.A.* // PNPI preprint 2929. Gatchina, 2013. P. 41.
2. *Volkov S.S., Zhdanov A.A., Ivanov V.V., Komkov B.G., Kudin L.G., Nikulin V.N., Rostchin E.V., Samsonov V.M., Khanzadeev A.V., Shvedchikov A.V.* // PNPI preprint 2935, Gatchina, 2013. P. 30.

Study of interaction of deuterium plasma with the first wall in spherical "Globus-M" tokamak

V.M. Lebedev, V.A. Smolin
Neutron Research Division and Knowledge Transfer Division, PNPI NRC "Kurchatov Institute"

"Globus-M" spherical tokamak, built at A.F. Ioffe Physical-Technical Institute in 1999, has the broad area of research in the field of thermonuclear synthesis. The big density of plasma current and the high relation of magnetic field to plasma radius allow one to work in the field of the big density of plasma ~ 10^{20} m^{-3}, which in conditions of a small backlash plasma-wall creates big loadings on the first wall. Almost 90% of the inner vacuum vessel (austenitic stainless steel) surface area, which faces the plasma directly is now covered by recrystallized graphite (RGTi) tiles with various additives (Ti, Si, B) (Fig. 1). Additionally, the inner surfaces of tokamak chamber were protected by B/C : H films using procedures of the boronization. After carrying out a long cycle of experiments (~ 10 000 plasma fluxes), a number of protective tiles have been subjected to the analysis. Tile material's (RGTi-91) ability to hold (collect) deuterium was analyzed. The migration of the deuterium and other elements inside the graphite tiles was studied. The element composition of the films deposited on the tiles was studied with the use of *X*-ray fluorescence analysis, Rutherford backscattering spectrometry and by nuclear reaction method with deuterons (see Table below).

During the research of protective properties of internal coverings (B/C : H films and carbon tiles) of the vacuum chamber of the "Globus-M" tokamak, it was established, that the mixed layers up to ~ 10^{19} at/cm^2 appear in them at interaction with deuterium plasma. The structure and thickness of these layers depend on the power allocated in these parts of the vacuum chamber. Layers consist basically of atoms of carbon and boron and are enriched by deuterium elements sprayed from tokamak details. Capture of deuterium occurs nonuniformly on the internal surface of tokamak and changes from < 0.01 at. % to 5 at. % in divertor tile of the vacuum chamber. Thus, deuterium does not get into volume of tiles and remains in the superficial mixed layer.

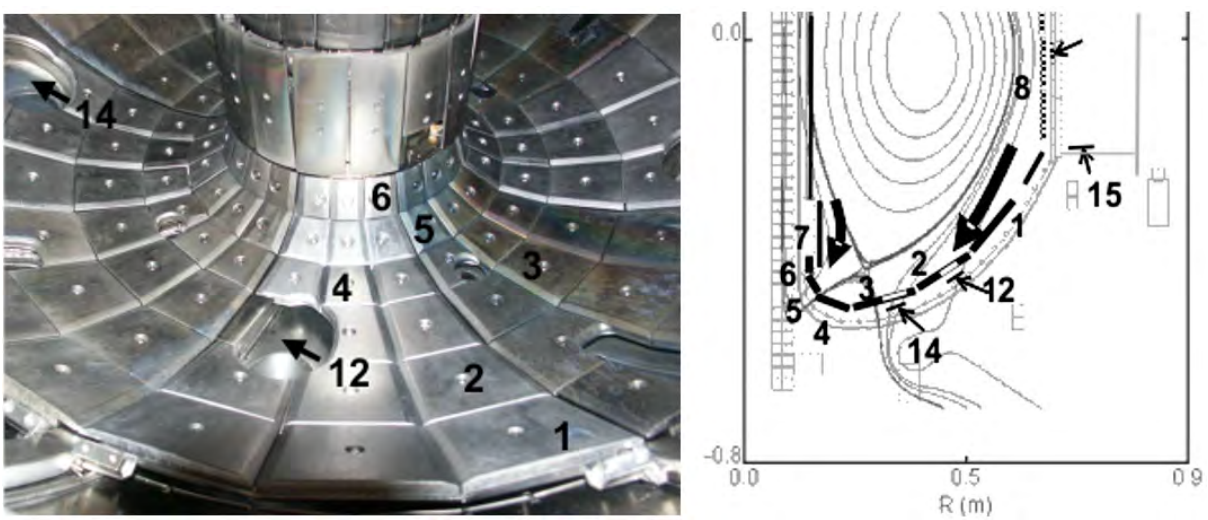

Fig. 1. The bottom part of the vacuum chamber of the "Globus-M" tokamak: divertor tiles and a section of the chamber with the magnetic configuration in it: 1–8 – graphite tiles; 12, 14, 15 – samples of 12X18H10T steel. The arrows indicate streams of particles and heat on the divertor tile

Table. Thickness of films of elements on various samples (· 10^{16} at/cm^2)

Sample	D	B	C	Si	Cr	Fe	Ni	Cu	W
1	36	83	–	6	17	44	5	1	4
2	56	63	–	1	30	75	9	3	6
3	79	660	–	0	45	112	13	3	7
4	82	650	–	2	53	139	18	7	6
5	100	200	–	8	39	102	13	4	2
6	120	94	–	0	45	120	15	5	7
7	~ 0.01	1	–	4	4	14	2	1	0
8	~ 0.01	0	–	2	2	7	0.3	0	0
12	32	5.4	90	–	–	–	–	–	–
14	31	15	80	–	–	–	–	–	–
15	19	16	28	–	–	–	–	–	–

After ~ 10 000 plasma fluxes, samples of dust from various places of the vacuum chamber of tokamak have been investigated – tiles, surfaces under bottom divertor plates and shutting flanges. Among these samples, it is possible to allocate several kinds of dust particles: rubble particles, large lamellar particles of the size from 10 to 1 000 μm, spherical particles with a smooth surface with diameter from 10 to 30 μm, spongy particles of the size up to 100 μm (Fig. 2). These particles are formed as a result of dispersion under the influence of powerful plasma streams of the reraised dust layers besieged on a surface of divertor plates. The dust contains basically the elements of metal, of which the vacuum chamber and the devices located in it are constructed. Atomic relations <boron/carbon> of the measured samples within an error of measurements are close: $(B/C)_{at} = 0.007 \pm 0.001$. The form and element structure of dust particles formed and collected in the vacuum chamber depend on a place of their formation and conditions of plasma fluxes.

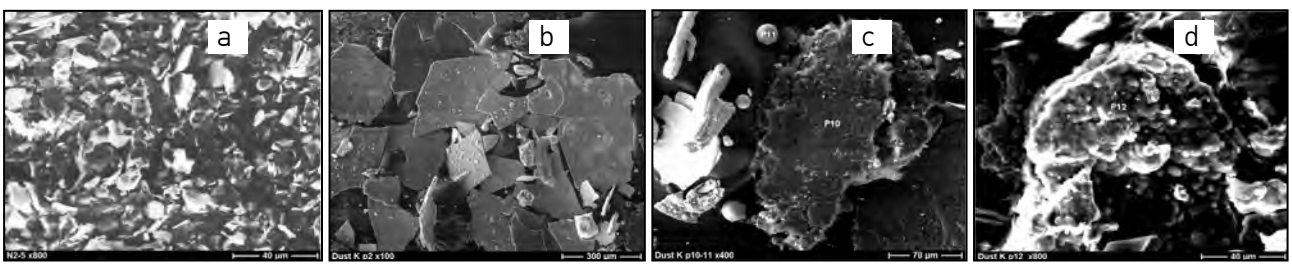

Fig. 2. SEM microphotos of dust particles collected in the vacuum chamber of "Globus-M" tokamak: rubble particles (a); lamellar particles of the size from 10 to 1 000 μm (b); spherical particles (c); spongy particles of the size up to 100 μm (d)

3D nano universal measuring microscope UIM-23

B.G. Turukhano, N. Turukhano, V.V. Dobyrn, S.N. Khanov, R.P. Sinelshchikova, O.G. Ermolenko, N.A. Schipunova, I.V. Ladatko, E.A. Vilkov
Holographic Information-Measuring Systems Laboratory, Knowledge Transfer Division, PNPI NRC "Kurchatov Institute"

The system "3D NANO UIM" (Fig. 1) uses linear holographic encoders (LHE) and is designed for high-precision 3-coordinate measurements (3D) in an orthogonal coordinate system. *X* and *Y* coordinates are operated manually and *Z* coordinate – with a pedal. The values of all coordinates, as well as the tables, are displayed digitally and can be reset at any point (Fig. 2).

Linear holographic encoder LHE-200/100/100 includes: a carriage guide, a laser module, a loop, protecting housing, photo detection units.

The guide way consists of a glass plate and the flatness of its surface provides a constant gap between the measuring and reference diffraction gratings, as well as a constant angle between their lines.

A measuring diffraction grating (MsDG) is located on a glass substrate, and a reference diffraction grating (R_FDG) – on the carriage rigidly mounted on the read head (RH). The laser and photo detector units are placed on the same carriage. The carriage is moving along the guide way on six ball bearings. Four magnets are mounted on the carriage and three metal strips are placed on the guide way. Signals are supplied via a ribbon cable 4 to the electrical "control unit *X*, *Y*, *Z*" and then through a loop system are received by the computer. The carriage has a lateral pin (Ø 2.44 mm), through which a movement is transmitted from an external device to the carriage.

The main window shows the resolution of all the encoders – 10 nm, the accuracy of all the encoders ±0.2 μm. Their maximum speed is 100 mm/s. All coordinates are read simultaneously. Thus, it was possible to establish on the basis of the standard device UIM-23 a three-coordinate (3D) universal measuring microscope, the accuracy of which is several times the accuracy of UIM-23. It should be noted that linear and radial HDG with unique precision (±0.4 μm/m and ±0.3 angl/s/2π) was developed at HIMSLabs. It allows one to obtain resolution of up to one nanometer and one-hundredth of arcsecond.

Fig. 1. 3D NANO UIM-23

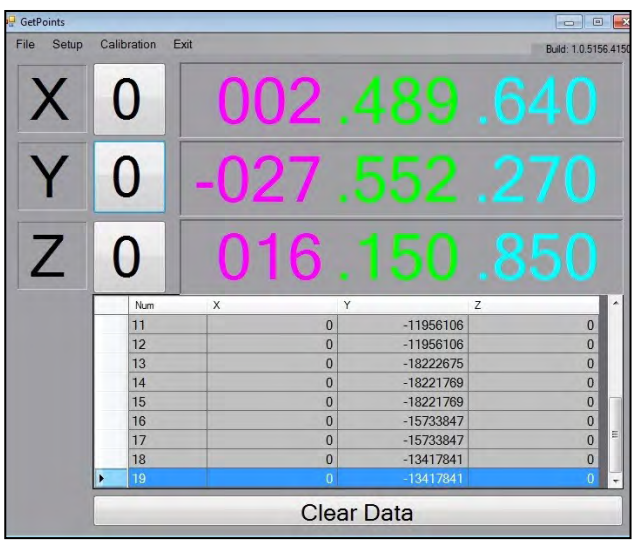

Fig. 2. The main window of the programm

Design and development of the complex for radiation testing of electronic components for aviation and space

S.A. Artamonov, G.F. Mikheev, G.A. Riabov, E.M. Ivanov, G.S. Lebedeva, D.A. Amerkanov, V.P. Gres, O.A. Shcherbakov, A.M. Gagarskii, L.A. Vaishnene, A.S. Vorobyev, G.I. Gorkin, S.V. Kosianenko, V.G. Muratov, V.V. Pashuk, V.A. Solovei
Knowledge Transfer Division, Neutron Research Division, High Energy Physics Division, PNPI NRC "Kurchatov Institute"

Space and aviation technology progress is largely associated with the use of modern micro- and nanoelectronics (electronic component base, ECB). One of the basic requirements for such systems is the ability to work in radiation fields in space and upper atmosphere. In Russia, as in all other countries, there are standards for mandatory radiation resistance testing of electronics used in space and aviation systems. In order to comply with these standards, a multipurpose Centre for radiation testing on proton and neutron beams was designed and developed on the basis of PNPI NRC "Kurchatov Institute" SC-1000 synchrocyclotron with maximum energy of accelerated protons of 1 000 MeV.

The use of 1 000 MeV proton beam for ECB testing

A stand for radiation testing was created on the P2 proton beam path (see Fig. 1). Modes of lens operation were defined to obtain narrow (26 mm diameter) and wide (230 mm) beams. The research team has designed and developed instruments for absolute measurements of the proton beam intensity at the energy of 1 000 MeV, and for measurements of the proton beam size and spatial distribution. The stand equipment allows one to install the ECB elements on the beam and move them along the beam, if necessary, and to conduct testing in a wide range of temperatures (up to 125 °C).

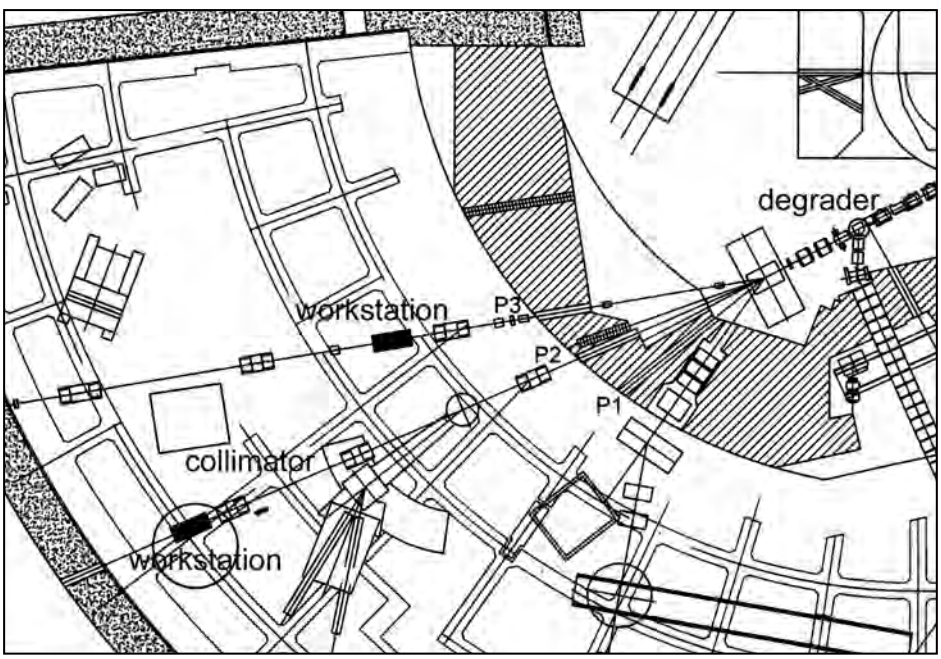

Fig. 1. A scheme of SC-1000 beams including those ones used for radiation tests on protons: P2 path is used to conduct tests on a beam with energy of 1 000 MeV, P3 path is used to conduct tests on a beam with variable energy

The use of proton beams of variable energy for ECB testing

The synchrocyclotron accelerates protons up to the fixed energy of 1 000 MeV. Therefore, a bremsstrahlung (slowing-down) of the original beam in the absorbing substance is used to create the beams of variable energy. A device for remote variation of the absorber length was designed, developed and manufactured, which greatly facilitates the transition from one beam energy to another, and reduces the radiation load on the staff. In the context of repeated measurements, this factor is very important. The beams emerging from the absorber are considered to be secondary beams. The calculations of the parameters of such beams of variable energy were carried out and optimal modes of lens usage on the P2 path were also determined through calculation (see Fig. 1). According to calculations one can obtain the beam energy in the range of 1 000–50 MeV with the intensity from $3 \cdot 10^{12}$ to ~ 10^{8} protons per second. A similar sequence of calculations was carried out for the P3 path.

Development and experimental study of the neutron beam used for testing the radiation resistance of electronics components

A neutron source with the spectrum resembling atmospheric neutrons, which is required for ECB testing and has no equals in Europe, was created at the PNPI SC-1000 synchrocyclotron. The works on improvement of the stand for radiation resistance testing on atmospheric-like neutrons in the energy range of 1–1 000 MeV (see Fig. 2) went on through 2014. All the units of the stand were completed and tested including the neutron beam monitor – fission ionization chamber (FIC); beam profilometer – multiwire proportional counter (MWPC); securing devices, movement and temperature control equipment for the device under test (DUT). Technical documentation and equipment were prepared for the complex testing and certification of the stand. Electronic products used in domestic space device engineering were tested on the stand in two sessions in cooperation with "United Rocket Space Corporation" JSC branch "Research Institute of Space Device Engineering" (Moscow).

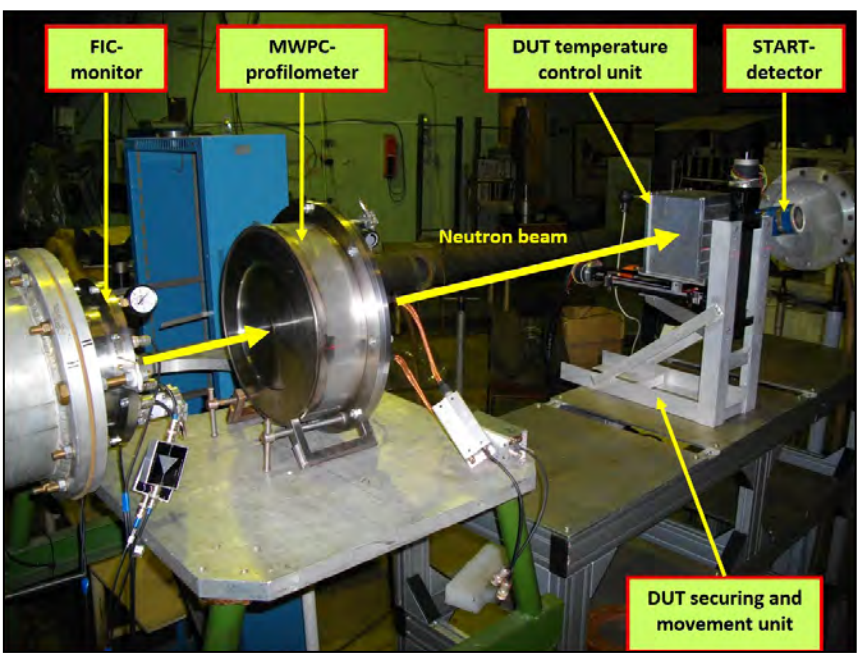

Fig. 2. Neutron/proton testing stand

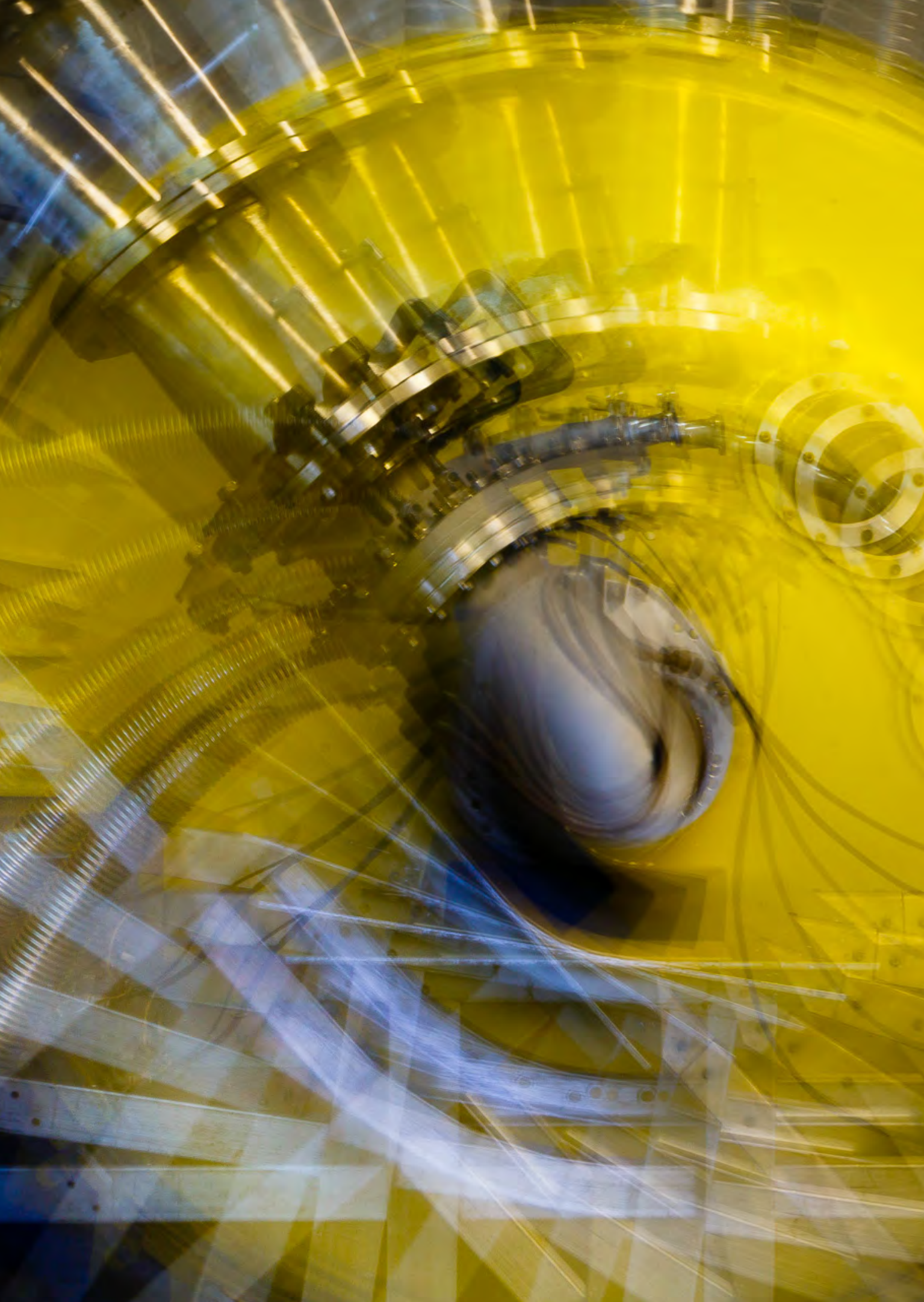

Basic Installations

WWR-M research reactor complex

V.A. Ilatovsky
Department of WWR-M Reactor Exploitation, PNPI NRC "Kurchatov Institute"

WWR-M research reactor complex (RRC) is one of the basic installations of PNPI, which is used to conduct the fundamental and applied research in fields of nuclear physics, condensed state physics, to develop the neutron methods for the study of matter, for radiation materials science, radiobiology, and production of radionuclides for medical purposes.

The WWR-M RRC has been operating stably for over 50 years. With account for its parameters, it is the best research steady state reactor in Russia. It offers a wide range of possibilities for research both in the reactor core and at experimental instruments located in the reactor hall, around the reactor.

More than 20 experimental works in fields of nuclear physics, condensed matter physics, and development of neutron methods for studying matter were performed in 2014.

Table 1. The main parameters of WWR-M

Title	Value
Thermal power	18 MW
Neutron flux	$4 \cdot 10^{14}$ sm$^{-2} \cdot$ s^{-1}
Number of horizontal channels	17
Number of vertical channels	15
Number of irradiation chambers in the core	6
Mean time of operation	3 600 hours per year
Mean energy production	2 500 MW · day a year
Operating personnel	85

Fig. 1. Experimental instruments at WWR-M reactor:
1A – Crystal-diffraction monochromator of polarized neutrons;
1B – 48-counters powder diffractometer;
2 – Installation for EDM-search by the crystal-diffraction method;
3 – Reflectometer of polarized neutrons with vertical plane of scattering (REVERANS);
4 – Small-angle scattering instrument of polarized neutrons "Vector";
5 – Small-angle scattering instrument "Membrana-2";
6 – Single-crystal diffractometer of polarized neutrons;
7 – "Neutrino-4" installation;
8 – Neutron radiation analysis;
9 – Powder diffractometer;
11 – Spin-echo spectrometer;
12 – Instrument for spin-echo small-angle neutron scattering – SESANS;
13 – Neutron Reflectometer NR-4M;
13A – Four-circle diffractometer;
14 – 3D analysis of polarization

Table 2. Short overview of WWR-M reactor operation in 2012–2014

No.	Key figures of the reactor operation at power	2012	2013	2014
1	Energy production (MW/day)	2 169.0	1 890.9	2 121
2	Number of hours of the reactor operation at power	3 123	2 685	3 162
3	Maximum power (MW)	17.0	17.0	17.0
4	Mean effective power (MW)	16.6	16.9	16.1
5	Time factor of the reactor use (%)	35.0	33.6	36.3
6	Number of irradiated ampoules and containers (units)	123	132	157

Irradiation of samples in the core and channels of the reactor reflector:

– Six export deliveries (about 100 kCi) of radionuclide Ir-192 with a high specific activity in agreement with the client's requirements;

– The production of isotopes for medical purposes:

• Mo-99 for production of Tc-99m with total activity of 200 Ci;

• I-125 with the total activity of 300 Ci;

– Irradiation of six ampoules with samples of structural materials and their welded junctions.

In 2014, the following groups of researchers used RRC WWR-M for their work:

– Employees of laboratories and groups of the Department of Condensed Matter Physics of the Neutron Research Division, PNPI;

– Students of the Department of Nuclear-Physics Research Methods (Faculty of Physics, St. Petersburg State University);

– Laboratory of Magnetic Sensors of National University "Politechnika Lwowska";

– Laboratory of Nanomaterials and Carbide Composites of Central Research Institute of Structural Materials;

– Laboratory of Strength of Materials, St. Petersburg State University;

– Laboratory of Physics of Plasticity and Strength, Siberian Physical-Technical Institute;

– Laboratory of Neutron Physical and Chemical Research, PNPI;

– St. Petersburg State University (Faculties of Physics and Chemistry), Institute of Macromolecular Compounds of the Russian Academy of Sciences, Central Research Institute of Structural Materials "Prometey";

– Boreskov Institute of Catalysis of the Siberian Branch of the Russian Academy of Sciences (St. Petersburg Division), the Ioffe Institute;

– Samara State University of Architecture and Civil Engineering, St. Petersburg State Technological Institute;

– the Ioffe Institute;

– Institute of Chemistry, St. Petersburg State University;

– Lomonosov Moscow State University, Faculty of Physics;

– Scientific and Practical Materials Research Centre of NAS of Belarus.

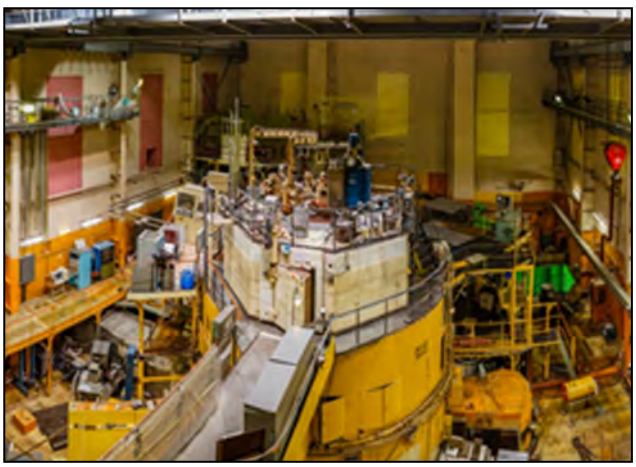

Fig. 2. General view of WWR-M reactor

The following publications were based on the work accomplished at WWR-M:

1. *Bolshakova I.A., Kulikov S.A., Konopleva R.F., Chekanov V.A., Vasilevskii I.S., Shurygin F.M., Makido E.Yu., Duran I., Moroz A.P., and Shtabalyuk A.P.* // Physics of Solid State. 2014. V. 56. No. 1. P. 157.
2. *Belyaev S.P., Gordeev S.K., Chekanov V.A., Konopleva R.F., Golosovsky I.V., Korchagina S.B., Denisov I.A. and Belobrov P.I.* // Physics of Solid State. 2014. V. 56. No. 1. P. 152.
3. *Belyaev S., Chekanov V., Kolobanov G., Konopleva R., Nakin A., Nazarkin I., Razov A., Resnina N., Volkov A.* Martensitic Transformation and Shape Memory Effect in TiNi-Based Alloys during Neutron Irradiation. *In* "Shape Memory Alloys: Properties, Technologies, Opportunities". 2015. Trans. Tech. Publications Inc. P. 429–456.
4. *Lebedev V.T., Török Gy., Vinogradova L.V.* // Physics of the Solid State. 2014. V. 56. No. 1. P. 183–189.
5. *Kulvelis Yu.V., Kononova S.V., Romashkova K.A., Lebedev V.T.* // Physics of the Solid State. 2014. V. 56. No. 1. P. 86–90.
6. *Lebedev V.T., Grushko Yu.S., Sedov V.P., Shikin V.A., Kozlov V.S., Orlov S.P., Sushkov P.A., Kolesnik S.G., Szhogina A.A., Shabalin V.V.* // Physics of the Solid State. 2014. V. 56. No. 1, P. 178–182.
7. *Lebedev V.T., Török Gy., Vinogradova L.V.* // Physics of the Solid State. 2014. V. 56. No. 1. P. 190–198.
8. *Lebedev V.M., Lebedev V.T., Orlov S.P., Margolin B.Z., Morozov A.M.* // Physics of the Solid State. 2014. V. 56. No. 1. P. 161–166.
9. *Lebedev V.M., Lebedev V.T., Orlova D.N., Tikhonov V.I.* // Journal of Surface Investigation. *X*-ray, Sinchrotron and Neutron Techniques. 2014. V. 8. No. 3. P. 411–417.
10. *Lebedev V.M., Lebedev V.T., Orlova D.N., Sovestnov A.E., Tikhonov V.I.* // Journal of Surface Investigation. *X*-ray, Synchrotron and Neutron Techniques. 2014. V. 8. No. 5. P. 1002–1009.
11. *Lebedev V.T., Kulvelis Yu.V., Runov V.V., Sedov V.P., and Szhogina A.A.* // Journal of Surface Investigation. *X*-ray, Synchrotron and Neutron Techniques. 2014. V. 8. No. 5. P. 1044–1054.
12. *Lebedev V.T., Kulvelis Yu.V., and Orlova D.N.* // Journal of Surface Investigation. *X*-ray, Synchrotron and Neutron Techniques. 2014. V. 8. No. 5. P. 1055–1062.
13. *Lebedev V.M., Lebedev V.T., Orlova D.N., Sovestnov A.E., Tikhonov V.I.* //Journal of Surface Investigation. *X*-ray, Synchrotron and Neutron Techniques. 2014. V. 8. No. 5. P. 1002–1009.
14. *Kozlov V.S., Suyasova M.V., Lebedev V.T.* // Russian Journal of Applied Chemistry. 2014. V. 87. No. 2. P. 121–127. ISSN 1070-4272. Pleiades Publishing. Ltd. 2014.
15. *Zobkalo I.A., Gavrilov S.V., SawNyi N.Z., Barilo S.N., Shiryaev S.V.* // J. Magn. Magn. Mater. 2014. V. 354. P. 85–89.
16. *Zobkalo I.A., Gavrilov S.V., Sanina V.A., and Golovenchits E.I.* // Physics of the Solid State. 2014. V. 56. No. 1. P. 51.
17. *Zinovyev V.G., Mitropolsky I.A., Loginov Yu.E., Schulyak G.I., Tyukavina T.M., Sushkov P.A.* // Journal of Atomic Energy. 2014. V. 116. No. 2. P. 89–94.
18. *Zinovyev V.G., Mitropolsky I.A., Loginov Yu.E., Schulyak G.I., Tyukavina T.M., Sakharov S.L., Kosianenko S.V., Gorokhova E.I., Demidenko V.A.* // Word Journal of Nuclear Science and Technology. 2014. V. 4, P. 139–147.
19. *Tikhonova A.E., Kozlov V.S.* // Physics of the Solid State. 2014. V. 56. No. 1. P. 17–19.
20. *Zinovyev V.G., Serebrov A.P., Mitropolsky I.A., Loginov Yu.E., Shulyak G.I., Tyukavina T.M., Sakharov S.L., Chernyj A.V.* // World Journal of Nuclear Science and Technology. 2015. V. 5. P. 43–56.
21. *Gerashchenko O.V., Matveev V.A., Pleshanov N.K., Bairamukov V.Yu.* // Physics of the Solid State. July 2014. V. 56. Iss. 7. P. 1438–1442.
22. *Matveev V.A., Pleshanov N.K., Gerashchenko O.V., Bairamukov V.Yu.* // Journal of Surface Investigation. *X*-ray, Synchrotron and Neutron Techniques. 2014. V. 8. No. 5. P. 991–996.
23. *Pleshanov N.K.* // Technical Physics. 2014. V. 59. No. 2. P. 275–282.
24. *Syromyatnikov V.G., Ulyanov V.A., Lauter V., Pusenkov V.M., Ambaye H., Goyette R., Hoffmann M., Bulkin A.P., Kuznetsov I.N. and Medvedev E.N.* // J. Phys.: Conf. Ser. 528. 2014. 012021 (1–7).
25. *Zabenkin V.N., Aksel'rod L.A., Didenko G.P., Sumbatyan A.A., Gordeev G.P., Lazebnik I.M., Syromyatnikov V.G.* // Technical Physics. 2014. V. 59. Iss. 2. P. 287–290.

Applications, patents, etc.

1. *Sedov V.P., Szhogina A.A.* Means of production of water-soluble derived fullerenes: invention application No. 2014113248 / Sedov V.P., Szhogina A.A.; priority of 26.05.14.
2. *Kabina L.P., Lisin S.S., Mitropolsky I.A.* Computer code ELENA – radiation properties of elements and isotope for purposes of the neutron analysis of materials. Certificate of State Registration of computer code 2014611564, Rospatent, 2014.
3. *Zakharov A.A.* A device for loading and testing samples in channel of a nuclear reactor. RF PATENT 2507497, 20.02.2014.

PIK research reactor complex

V.L. Aksenov
Director of PNPI NRC "Kurchatov Institute"

M.V. Kovalchuk
Director of NRC "Kurchatov Institute"

The PIK neutron research reactor (Russian abbreviation for a high-beam research shell-type reactor) is to become a base for the modern research centre capable of coping with national and international demand for the use of neutron beams for research purposes in the coming decades.

Currently, the PIK research reactor complex (RRC PIK), Fig. 1, consists of 38 buildings with the total area of 65 000 m^2. As a result of realization of projects on modernization of engineering systems and reconstruction of a laboratory complex planned to be implemented in 2015–2020, 13 additional buildings and constructions with the total area of 50 000 m^2 will be added to the RRC PIK.

The PIK reactor is a compact neutron source with the volume of the core of ~ 50 l surrounded by a heavy-water reflector (Figs. 2–4). Maximum undisturbed density of the thermal neutron flux reaches the value of $5 \cdot 10^{15}$ $cm^{-2} \cdot sec^{-1}$ in the central water cavity and $1.2 \cdot 10^{15}$ $cm^{-2} \cdot sec^{-1}$ in the reflector at reactor thermal power of 100 MW (Tab. 1).

Despite the fact that the PIK reactor concept was formed in the end of 1960s, it still determines modern trends of reactor engineering.

The basic conception of the reactor design, namely a light water cooled core and a heavy water reflector, which was applied for the first time in the PIK reactor project (protected by the inventor's certificate of 1976), is now recognized as the most efficient and technological.

Fig. 1. Overall view of the PIK reactor complex

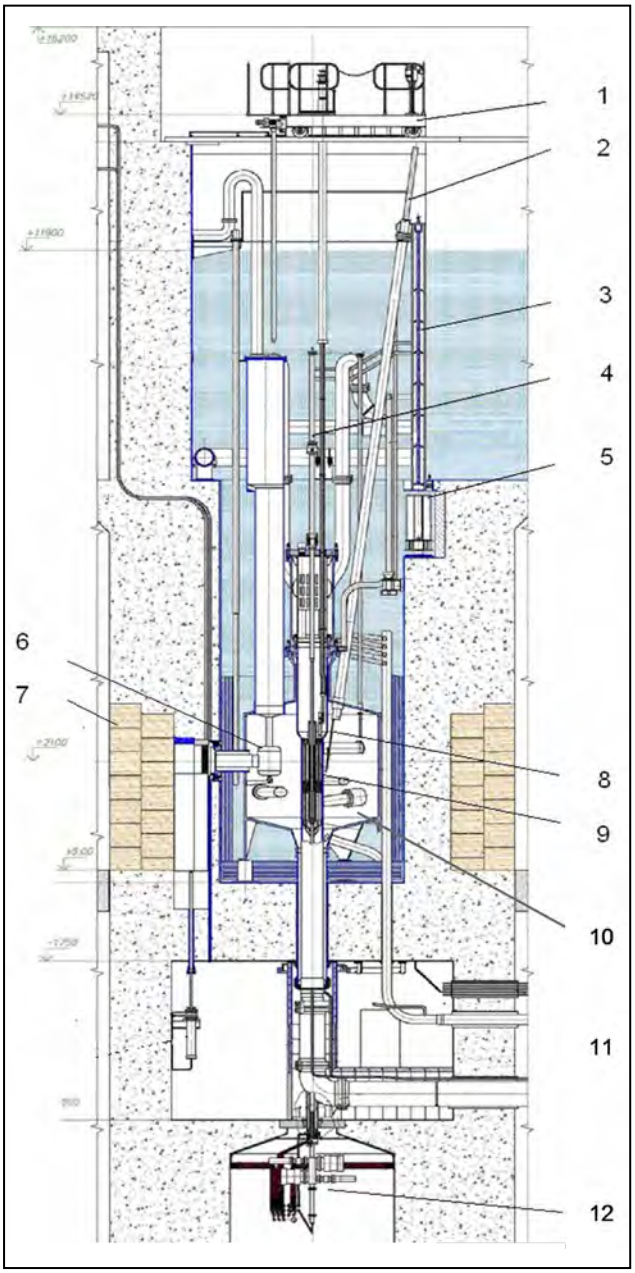

Fig. 2. Vertical cross-section of the PIK reactor:
1 – refueling machine;
2 – control rod drive;
3 – hydro lock;
4 – central experimental channel;
5 – reloading cylinder;
6 – UCN source;
7 – dismountable shielding;
8 – absorber;
9 – reactor vessel with the core;
10 – heavy water reflector;
11 – horizontal experimental channel (HEC);
12 – shutters drive

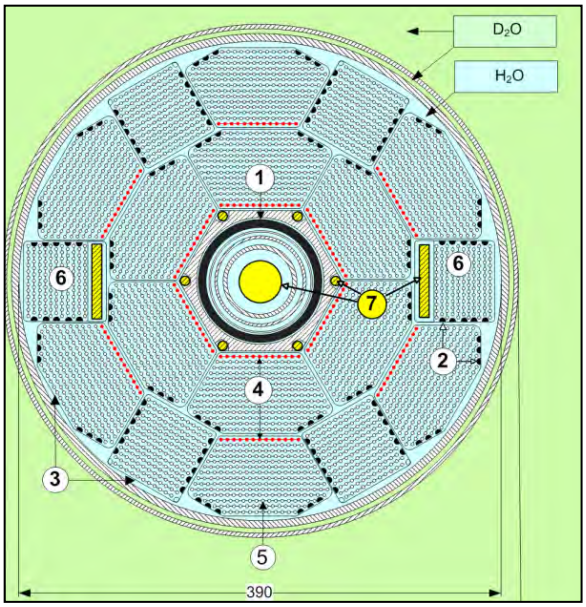

Fig. 3. Core of the PIK reactor
(with operation fuel assembly package):
1 – Hf absorbing shutters;
2 – burnable absorber rods Gd_2O_3+ZrO_2;
3 – Zr casings tubes of fuel assemblies;
4 – fuel elements with reduced fuel content
(0.48 of nominal);
5 – fuel elements with nominal fuel content;
6 – fuel assemblies with irradiated samples;
7 – irradiated samples

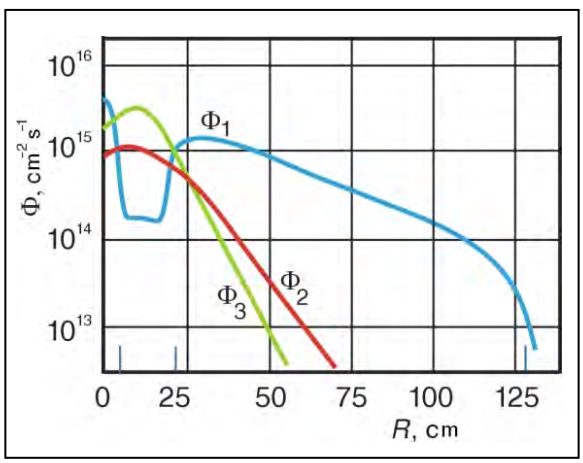

Fig. 4. Distribution of the neutron flux in the reflector:
Φ1 < thermal neutron flux,
E < 0.6 keV;
Φ2 < epithermal neutron flux,
0.6 keV < E < 5 keV;
Φ3 < fast neutron flux,
E > 5 keV

Table 1. The PIK reactor design parameters

Title	Value
Thermal power	100 MW
Volume of the core	50 l
Type of fuel elements	rod-shaped
Fuel	UO_2 + Be Bronze
Fuel enrichment	90%
Content of ^{235}U in the core	27.2 kg
Number of fuel assemblies in the core	18
The core height	500 mm
The moderator / coolant	H_2O distillate
Reflector • Side reflector • End reflector	 D_2O H_2O
Maximum density of thermal neutron flux in reflector	$1.3 \cdot 10^{15}$ cm$^{-2} \cdot$ s^{-1}
Maximum density of thermal neutron flux in a trap	$5.0 \cdot 10^{15}$ cm$^{-2} \cdot$ s^{-1}
Reactor cycle length	≤ 30 days
Water flow in the primary circuit through the core	2 400 m^3/h
The pressure in the primary circuit	5.0 MPa
The temperature of the primary circuit moderator: • Inlet • Outlet	 50 °C 86 °C
Experimental channels: • Central • Horizontal • Inclined • Vertical	 1 10 6 6

The PIK reactor construction, its physical and technical characteristics have no analogs in reactor engineering. After the start-up, it will become a unique Russian research base. The experimental possibilities of the PIK reactor are determined not only by the high intensity of neutron beams but also by the availability of sources of cold and ultra-cold neutrons. Therefore, in comparison to the existing reactors, the PIK reactor opens up unique possibilities both for on-going in-depth research based on neutrons, which is now being conducted in Russia, and for the new research, which is now unavailable at Russian reactors.

With regard to the PIK reactor parameters and experimental possibilities, it can be said that it surpasses all the operating research reactors (Tab. 2) including its closes analogue – reactor HFR at the Institute of Laue–Langevin (Grenoble, France).

The PIK reactor has one central, ten horizontal, six inclined and six vertical channels for beam ejection and irradiation of samples. Neutron guide systems allow one to transport neutrons to experimental installations located in the Neutron guide hall under zero-background conditions. Up to 50 experimental installations are planned to be equipped in three experimental halls of the complex, which will allow different research groups to work simultaneously. A scheme of experimental channels of the PIK reactor is presented in Figs. 5–7 demonstrate the view of the experimental hall of horizontal channels and a neutron guide hall respectively.

Location of the main buildings of the RRC PIK is shown in Fig. 8. The start-up complex No. 1 is marked with green filling, start-up complexes No. 2 and 3 – with blue filling.

Description of the existing buildings and the ones under construction within the project on "Modernization of technological systems for exploitation of the PIK reactor and its research stations" is presented in Table 3.

The modernization project workscope (the type of construction – reconstruction with the complex extension) includes both existing, operating or constructed buildings and the new ones. The majority of existing buildings was constructed and equipped with utility systems. The main areas of modernization are:

– Further equipment of the RRC PIK with modern technologies;

Table 2. Comparison of characteristics of high-flux nuclear reactors

Installation, location	Start-up year	Thermal power, MW	Maximum thermal neutron flux density, $cm^{-2} \cdot sec^{-1}$	Number of stations at neutron beams
PIK Gatchina, Russia	2018 (planned)	100	$5.0 \cdot 10^{15}$	50
HFR Grenoble, France	1971	58	$1.5 \cdot 10^{15}$	40
HFIR Oak Ridge, USA	1965 (2007 – after modernization)	85	$3.0 \cdot 10^{15}$	15
FRM-II Munich, Germany	2005	20	$0.8 \cdot 10^{15}$	27
CARR Beijing, China	2010	60	$0.8 \cdot 10^{15}$	6
CMRR Minyan, China	2004	20	$0.3 \cdot 10^{15}$	15
OPAL Sidney, Australlia	2006	20	$0.4 \cdot 10^{15}$	10
WWR-M Gatchina, Russia	1959	18	$0.4 \cdot 10^{15}$	16

– Reaching the requirements of modern safety regulations with regard to the value of technical tasks;

– Replacement of worn out and outdated equipment (assembled more than 15 years ago), which does not comply with federal regulations on the use of atomic energy based on the results of technical inspections held by specialized organizations together with the general design engineer in 2010–2012.

The modernization project cost is 89.0 million Euro; the structure of expenses is presented in Table 4.

In accordance with all the federal norms and regulations on the use of atomic energy, the RCC PIK is classified as a complex with a research nuclear facility.

OJSC SPII "VNIPIET" (Sosnovy Bor, Leningrad region) is the company responsible for the RCC PIK project development, general design and engineering. JSC "NIKIET" (Moscow) is the organization responsible for general construction of the reactor facility. General contractor organization at the construction of RCC PIK start-up complexes No. 1, 2 and 3 is the "Holding TITAN-2" (Sosnovy Bor, Leningrad region).

CJSC "Alliance Gamma" (Pavlov Posad, Moscow region) is responsible for general design and engineering of the modernization project. PNPI is the project owner, technical customer and coordinator, operating organization; NRC "Kurchatov Institute" is a state customer and a budget holder.

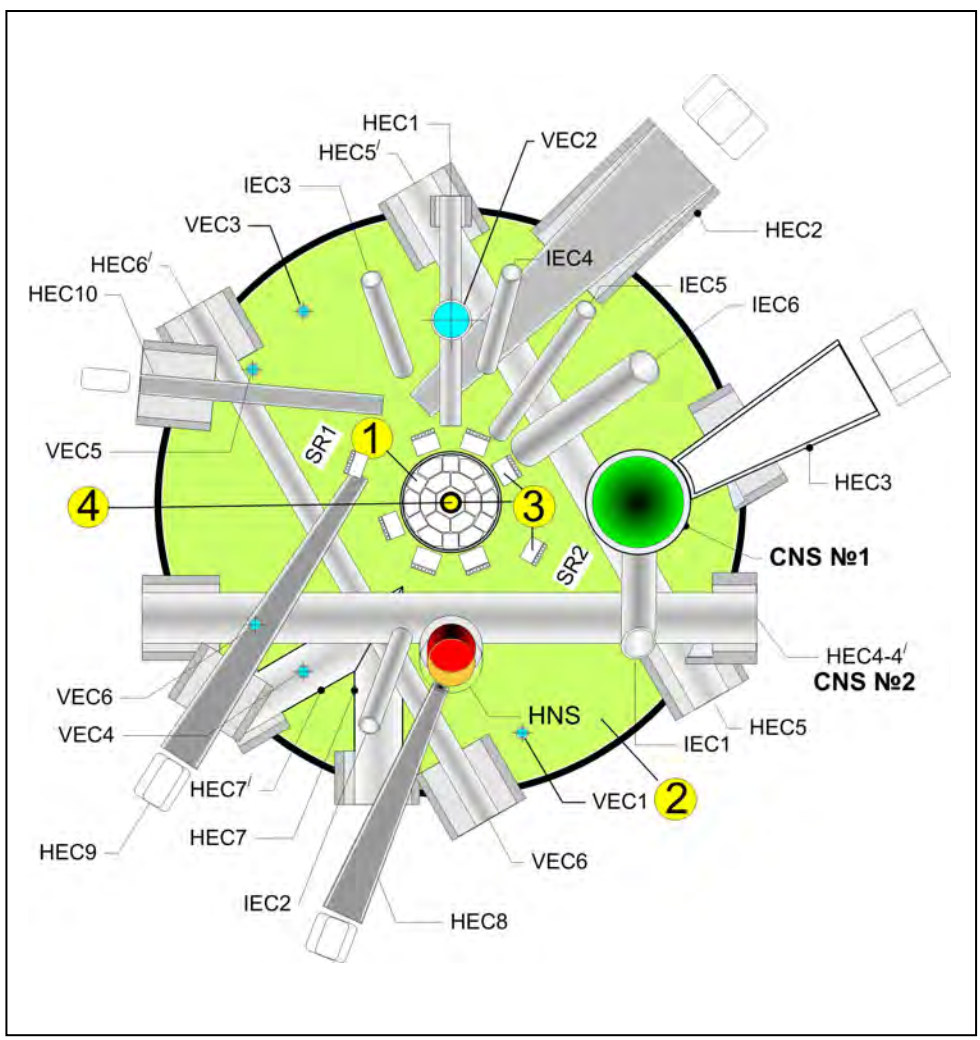

Fig. 5. Scheme of the experimental channels (HEC –horizontal, IEC – inclined, and VEC – vertical channels; CNS – cold neutron source; HNS – hot neutron source): 1 – reactor core; 2 – D_2O reflector; 3 – control rods; 4 – central experimental channel (CEC)

Fig. 6. The experimental hall of horizontal channels

Fig. 7. In the framework of cooperation with GKSS Research Centre in Geesthacht, the SANS-2 installation is delivered to the location of its destination – the neutron guide hall of the RRC PIK

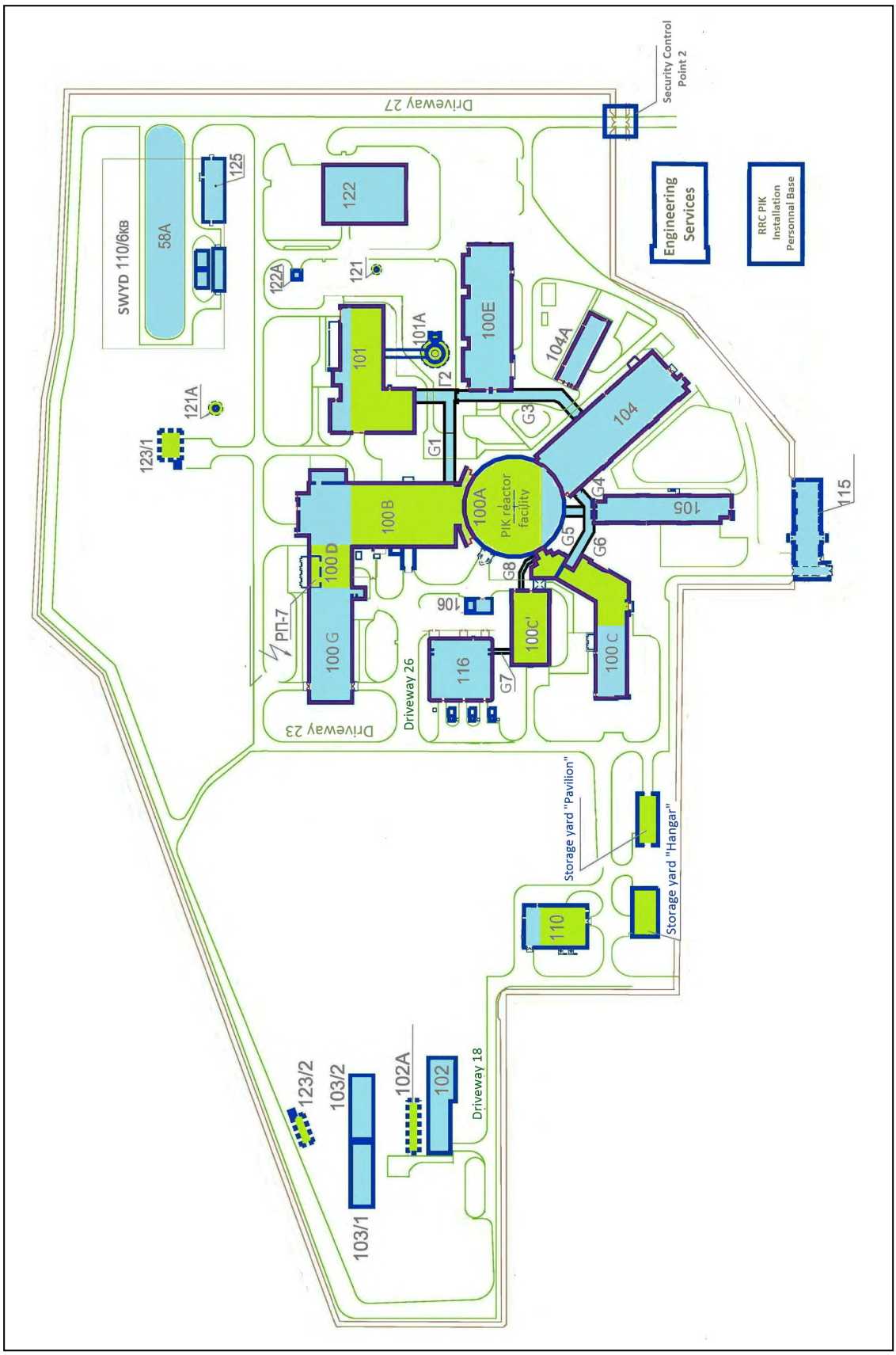

Fig. 8. Research and technological ground of the RRC PIK

Table 3. Discription of buildings and constructions of the modernized RRC PIK

Buildings	Purpose of the structure	Constructional characteristics	Comments
100A	Building 100 block "A" (reactor facility) with an underground floor	Structural volume – 89 686.0 m^3, including the underground area – 22 760 m^3; building area – 2 706.8 m^2; total area – 12 796.9 m^2	
100B	Building 100 block "B" (pumping block of the primary circuit)	Structural volume – 105 600 m^3; building area – 3 228.1 m^2; total area – 11 535.1 m^2	
100C	Building 100 block "C" (decontamination building) with underground floors and a tower	Total structural volume – 21 630 m^3; total building area – 1 510.2 m^2; total area – 5 970.6 m^2	
100C'	Building 100 block "C" (input ventilation)	Structural volume – 9 202 m^3; total building area – 970.5 m^2; total area – 1 646.0 m^2	
100D	Building 100 block "D" (power supply building)	Structural volume – 15 618 m^3; Building area – 816.4 m^2; total area – 2 151.7 m^2	
100G	Building 100 block "G" (pumping block of the intermediate circuit)	Structural volume – 29 376 m^3; building area – 1 422.4 m^2	
101, G1, G2	Building 101 (ventilation centre) with an underground floor, an adjacent building and passages	Total structural volume – 40 713 m^3; building area – 2 572.3 m^2; total area – 4 938.8 m^2	
101A	Building 101A (ventilation pipe)	Structural volume – 3 346 m^3; total building area – 62.5 m^2	
102	Building 102 (reverse water supply pumping station with cold water chamber (building 102A))	102 building area – 787.2 m^2; 102A building area – 213.2 m^2; total structural volume – 8 431 m^3	
103/1,2	Building 103/1,2 (water-cooling tower)	103/1 building area – 481 m^2; 103/2 building area – 481 m^2	
110	Building 110 (low and high pressure compressed air station)	Total structural volume – 10 028 m^3; building area – 902.7 m^2; total area – 965.9 m^2	
121A,123/1	Purification complex: building 121A – an underground construction; building 123/1 – regulating reservoir, decanter, desander, petrol-and-oil separator	Building 121A – an underground construction d = 4.0 m, h = 8.1 m; building 123/1 total structural volume – 658 m^3; building area – 212.1 m^2	
123/2	Building 123/2 (station 2 for rainfall discharge cleaning)	Building 123/2 – total structural volume – 357 m^3; building area – 176.7 m^2	
122/1	Building 122/1 (tritium extraction facility)	Total structural volume – 19 120 m^3 including a subsurface part – 4 190 m^3; building area – 995 m^2	New construction
116	Building 116 (backup diesel power station, backup control panel, training and modeling complex) with a passage (G8)	Total structural volume – 24 336 m^3; building area – 1 299.7 m^2; total area – 4 599.8 m^2	

Table 3 continues

Buildings	Purpose of the structure	Constructional characteristics	Comments
122	Building 122 (emergency storage of liquid radioactive waste with a modular transformer substation 122A)	Total structural volume – 18 428 m^3; building area – 1 067.7 m^2; total area – 2 823.8 m^2	
122B	Transformer substation of 122B UIT unit	Total area – 61 m^2	New construction
122/2	Construction 122/2 (a ground for four recievers and a gasifier for UIT unit)	Building area – 75 m^2	New construction
G-9, G-10	Passages between buildings 122, 122/1 and 100E (G-9, G-10)	Passage G-9: total area – 24.0 m^2; building area – 27.0 m^2; total structural volume – 114.48 m^3. Passage G-10: total area – 67.05 m^2; building area – 74.76 m^2; total structural volume – 313.56 m^3	
Monitoring wells	Monitoring wells	Five units, d = 89 mm, each 8 m deep	
Outdoor networks and structures	Outdoor networks and structures	Utility and drinking-water fire-fighting pipeline – 908 m; RRC PIK heating system– 708.4 m; telephone conduit – 1 054 m; wastewater sewerage – 2 062.2 m; storm-water drainage – 4 884.9 m; external cable nets and lighting – 24 461 m; active drainage pipework – 1 098 m; traffic roads, driveways and parking grounds – 40 501 m^2	Partially new construction
Closed equipment storage yard “Hangar”	Closed equipment storage yard “Hangar”	Total area – 355.5 m^2	
Closed equipment storage yard “Pavilion”	Closed equipment storage yard “Pavilion”	Total area – 508.2 m^2	

The PIK modernization project consists of the following areas of its implementation:

– Safety systems (SS) – upgrade of the technological systems of the reactor in order to comply with modern safety regulations (15.0 million Euro);

– Systems of handling radioactive materials (RM) and radioactive waste (RW) – modernization of systems of handling radioactive materials and radioactive waste produced during the normal reactor operation and abnormal incidents, including design basis accidents (3.1 million Euro);

– Systems of handling spent nuclear fuel (SNF), fresh nuclear fuel (FNF), solid radioactive waste (SRW), modernization of shielding “hot” chambers, tube transfer system and hoisting mechanisms (27.4 million Euro);

– Networks of monitoring of engineering systems (NMES) of buildings and constructions, reactor technologies (RAKURS), local computer networks (LCN) (9.4 million Euro);

– Tritium Extraction System (TES) – newly built installation for tritium and protium extraction from the heavy water reflector of the PIK reactor (34.1 million Euro).

Table 4. The structure of expenses for modernization project

Types of expenses	Summary construction cost estimate, thousands rubles (prices of the third quarter of 2014)	Expenses, EUR (at the rate of the third quarter of 2014)
Construction works	172 710	3 598 127
Electrical wiring	681 526	14 166 530
Plumbing	92 317	1 923 275
Technological installation	3 294 307	68 664 155
Start-up works (idle)	29 027	604 728
Total	**4 269 887**	**88 956 815**

In May 2013, the president of the Russian Federation V.V. Putin supported a proposal of NRC "Kurchatov Institute" to create the instrumentation base of the PIK reactor (Fig. 9). The concept of a complex of experimental stations and its engineering infrastructure started to be developed in June 2013.

12 working groups of employees from NRC "Kurchatov institute" and our colleagues from research centres in Russia and Europe were established. 12 national and international workshops on the concept were held. The activity of the working groups spread in the following areas.

1. Experimental stations for condensed matter physics and molecular biology.

1.1. Diffractometers;

1.2. Inelastic scattering spectrometer;

1.3. Small-angle scattering installation;

1.4. Reflectometers.

2. Experimental stations for particle physics and fundamental interactions.

2.1. Ultra cold neutrons researches installation;

2.2. Cold neutrons researches installation;

2.3. Stations for nuclear spectroscopy.

3. Infrastructure for experiments.

3.1. Creation of neutron guide complexes;

3.2. Ultra-cold neutron sources of the second priority;

3.3. Detector technology;

3.4. Sample environment system and molecular biology laboratory.

In accordance to the general concept, the groups worked out guidelines for the modernization of 12 available experimental installations and technological recommendations for project works, construction and creation of 20 experimental stations in the framework of the investment project on "the creation of instrumentation base of the RIK reactor".

International Centre for Neutron Research (ICNR) is planned to be established on the basis of the RRC PIK.

Germany is our strategic partner in ICNR establishment. In 2010, an agreement on cooperation with the Helmholtz Centre Geesthacht was signed; in 2014, we signed an agreement with the Jülich Research Centre, which is the coordinator of the participation of German research centres in ICNR establishment in Gatchina. The PIK reactor, along with the ILL reactor (Grenoble, France) and the spallation source ESS (Lund, Sweden), is included as a research base in strategies of neutron science development in Europe. The cooperation with German research centres was discussed at the workshop in Gatchina in October 2013.

The scientific program and the agenda for the creation of the PIK reactor instrumentation base are developed in coordination with other neutron centres, primarily with the JINR (Dubna), the Jülich Research Centre based at the Research Reactor Munich (Germany),

Fig. 9. The president of the Russian Federation V.V. Putin visits the RRC PIK in April 2013

FRAMEWORK COOPERATION AGREEMENT

between

Forschungszentrum Jülich GmbH
52425 Jülich
Federal Republic of Germany
- hereinafter referred to as „*Forschungszentrum Jülich*" -

and

National Research Centre "Kurchatov Institute"
Moscow
Russia
- hereinafter referred to as "NRC Kurchatov Institute" -

Fig. 10. A framework cooperation agreement was signed between NRC "Kurchatov Institute" and Jülich Research Centre. Prof. M.V. Kovalchuk and Prof. S. Shmidt at the signing ceremony

ILL and ESS. We expect the participation of European physicists, especially from Germany and Hungary, in further development of the concept of experimental stations and their further design and construction.

In June 2013, a workshop of NRC "Kurchatov Institute" – ILL was held in Gatchina, as a result of which the agreement on cooperation in research, creation of the instrumentation base for the PIK reactor and on the scientific examination of projects of experimental stations was signed between PNPI and ILL. ILL agreed to take on the role of the international expert organization.

The International Advisory Committee for Photon and Neutron Sciences of NRC "Kurchatov Institute" will act as an international expert council, co-chaired by Professor H. Dosh (DESY, Germany), and the Corresponding Member of the Russian Academy of Sciences M.V. Kovalchuk (NRC "Kurchatov Institute"). Professor S. Shmidt (FZ Jülich, Germany) was elected a chairman of Subcommittee for Neutron Sciences. The next stage is the discussion of experimental stations proposed and their location on neutron channels. First public discussions took place at PNPI Scientific Council in October 2014 and at the Session on the use of neutron scattering and synchrotron radiation for condensed matter studies (October 27–31, 2014, Peterhof). After several discussion sessions, final materials will be considered by the International Advisory Committee for Photon and Neutron Sciences of NRC "Kurchatov Institute". The first meeting of the Subcommittee for Neutron Sciences was planned to be held in the beginning of March 2015.

1. *Aksenov V.L., Kovalchuk M.V.* (scientific editors). The PIK reactor complex (in 4 volumes). PNPI NRC "Kurchatov Institute". Gatchina, 2014.
2. *Aksenov V.L., Kovalchuk M.V.* // Mat. of the conf. "Innovation projects and technologies of nuclear-power engineering". 2014. JSC "NIKIET". V. 1. P. 103–113.

The 1 GeV proton synchrocyclotron (SC-1000)

E.M. Ivanov, S.A. Artamonov, G.A. Riabov, G.F. Mikheev
Knowledge Transfer Division, PNPI NRC "Kurchatov Institute"

The proton synchrocyclotron SC-1000 (Fig. 1) with the proton energy of 1 GeV and the intensity of an extracted proton beam of 1 μA is one of the basic installations of PNPI NRC "Kurchatov Institute".

It is in operation since 1970. During its exploitation, it was significantly modernized. The experimental complex of the SC-1000 is used for investigations in fields of elementary particle physics, atomic nucleus structure and mechanisms of nuclear reactions, solid state physics and for the purposes of applied physics and nuclear medicine.

In 2014, the SC-1000 has been in operation for 2 784 hours. The list of works conducted at the SC-1000 in 2014 is as follows:

– Investigation of new materials by the muon spin rotation technique (μSR-method) – 20%;

– Investigation of short-lived isotopes (Short-Lived Nuclei Laboratory) – 14%;

– Commercial contracts – 19%;

– Modernization of the accelerator and its beam lines – 14%;

– Investigation of a nuclear matter on the MAP spectrometer – 10%;

– Proton channeling – 7%.

The generator used for the production of neutron beams was upgraded in 2014. PNPI synchrocyclotron possesses two operating neutron beams that use a fast one-turn deflection of the 1 GeV proton beam on the internal neutron producing target.

When the 1 GeV beam runs along the last orbits between the deflector plates, the generator feeds an operating voltage on deflector. As a result, the proton beam is deflected in the vertical direction and one turn later, it hits the neutron target.

Technical parameters of the SC-1000 synchrocyclotron

Energy of accelerated protons	1000 MeV
Number of proton beams	3
Intensity of proton beams	up to $6 \cdot 10^{12}$ p/s
Secondary particle beams	neutrons, pi mesons, muons
Induction in the magnet centre	1,9 T
Magnet weight	7 800 tons
Operating time of a physical experiment	up to 3 600 hours per year
Operation personnel	70 people

Fig. 1. General view of the 1 GeV proton synchrocyclotron (SC-1000)

Fig. 2. The external view of the high voltage generator after the upgrade

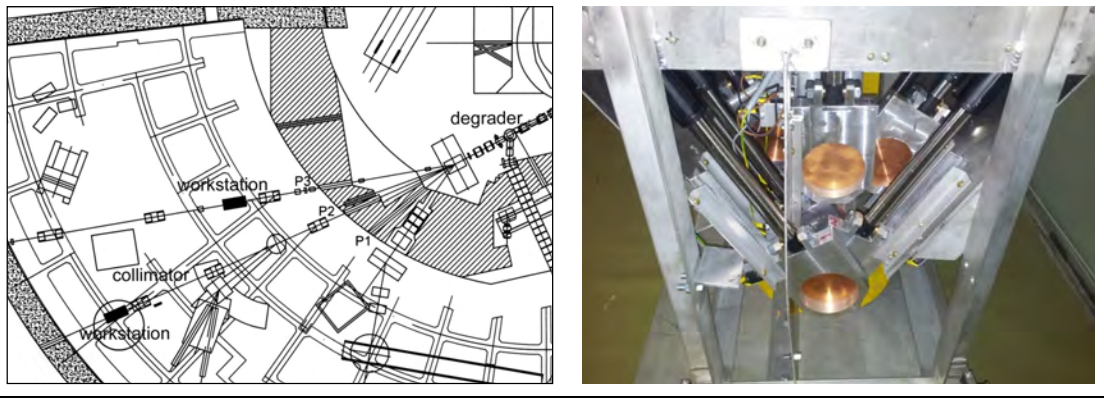

Fig. 3. Proton beam lines: P2 – with the energy of 1 000 MeV, P3 – for beams with variable energy of 40–1 000 MeV; and the device for remote variation of the absorber length and the proton energy

The requirements to the generator can be formulated as follows: the pulse voltage amplitude of about 100 kV, the pulse current of $3 \cdot 10^3$ A, the pulse leading edge of about 50 nsec, the accuracy of the phase-lock with a proton burst of about 1 nsec.

Four connected in parallel thyratron of TGI-700/25 type have been used in the generator up to now. However, the synchronization set of four thyratrons could not be kept stable. As a result, it was challenging to stabilize the performance and tune the neutron beam.

The necessary accuracy and pulse parameters have been obtained by the introduction of two new high power thyratrons of TGI 2-5k/50 type, produced by the company "Pulse technology" (Russia). This type of thyratrons demonstrates a high reliability and precision of parameters. It is used in many scientific centres of Russia and abroad.

A stable operation of the high voltage generator provides a stable and effective operation of both neutron facilities of the 1 GeV synchrocyclotron. The first one is the beam of the well-known in the world TOF spectrometer GNEIS designed to study neutron-nucleons interactions at neutron energies from 10^{-2} eV to several hundred MeV. The second beam with the atmosphere-like neutron spectrum is used for the accelerated testing of electronics for the aviation and space and has no analogs in Europe. Both neutron beams share the same neutron producing target and deflector systems. However, GNEIS uses neutrons after polyethylene moderator, and the second beam utilizes neutrons immediately from the thick target. The necessary atmosphere – like neutron spectrum is received under condition of the selection angle equal to about 30 degrees. The external view of the high voltage generator after the upgrade is presented in Fig. 2.

The proton therapy complex at the 1 GeV beam is now being modernized.

Serious efforts were made to organize the universal facility for radiation resistance testing of electronics components (EC Radiation Test Centre). The Centre is based on the 1 000 MeV proton test bench, the variable 40–1 000 MeV proton energy stand, and the neutron beam stand with atmosphere-like neutron spectrum. The parameters of variable energy beams were calculated and optimized for P2 and P3 beam lines with a copper absorber at the energy range of 40, 100–1 000 MeV with one step equal to 100 MeV.

Two stands for ECB radiation testing equipped with the beam diagnostics and monitoring systems were created on neutron and proton beams.

A special device for remote variation of the absorber length was created for the quick transition from one beam energy to another in order to avoid personal irradiation (Fig. 3, right).

Eight commercial contracts on ECB radiation testing were performed in 2014.

1. *Artamonov S.A., Amerkanov D.A., Gorkin G.I., Gres V.P., Ivanov E.M., Riabov G.A.* // Proc. of XX Intern. Conf. Beam Dynamics & Optimization, BDO-2014. Saint Petersburg. Russia. June 30 – July 04. 2014. P. 18–19.
2. *Veresov O.L., Gavrish Yu.N., Galchuk A.V., Grigorenko S.V., Grigoriev V.I., Korolev L.E., Kuzhlev A.N., Mudrolyubov V.G., Strokach A.P., Tsygankov S.S.* (Efremov Scientific Research Institute of Electrophysical Apparatus, Saint Petersburg); *Artamonov S.A., Ivanov E.M., Ryabov G.A.* (PNPI NRC "Kurchatov Institute", Gatchina) // Problems of Atomic Science and Technology. No. 3 (91). 2014. P. 3–7.

The 80 MeV H^- cyclotron (C-80)

E.M. Ivanov, S.A. Artamonov, G.A. Riabov, G.F. Mikheev
Knowledge Transfer Division, PNPI NRC "Kurchatov Institute"

For several years PNPI NRC "Kurchatov Institute" has been developing and building an isochronous cyclotron for acceleration of H^--ions up to 80 MeV with the beam current up to 200 μA.

The Accelerator Department proposed the construction of the 80 MeV cyclotron (the C-80) at PNPI in 1990, and its project was for the first time reported at the International Particle Accelerator Conference in Vancouver (Canada, 1992).

The main characteristics of the C-80 are as follows:

– The fast-spiral magnetic field structure allows one to accelerate H^--ions up to the energy of 80 MeV at the pole diameter of merely 2 m;

– In order to provide a good vacuum condition under acceleration of H^--ions, the pole tips and magnetic shims are located outside the vacuum chamber and upper and lower lids of the chamber are attached to the poles of a magnet;

– The external injection system consists of a plasma ion source with electrostatic optics, a beam line with two focusing lenses and two correcting electromagnets, inflector and diagnostics units. The system is located under the magnet;

– The high-frequency accelerating system consists of two symmetrical 60° dees working at the second harmonic f_0 = 20.6 MHz;

Fig. 1. General view of the C-80 cyclotron

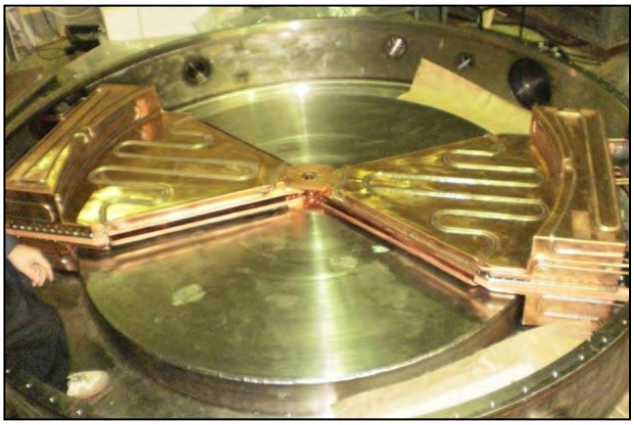

Fig. 2. A vacuum chamber and a high-frequency accelerating system with two dees

Fig. 3. PNPI director V.L. Aksenov and NIIEFA director O.G. Philatov

– Acceleration of H^--ions has obvious advantages: a possibility for 100% extraction of the beam with high intensity and variable energy. The extraction system is based on the H^--ions stripping using the carbon foil. The stripping device is equipped with a mechanism for adjustment of radial and angular positions of the carbon foil in order to provide a required range of ion energies from 40 to 80 MeV;

– To gain access to the inner chamber mechanisms, the upper beam of the magnet can be lifted using four pairs of ball bearings and screws equipped with servomechanisms and position sensors. The height of the half-yoke lifting is no less than 600 mm, the setting accuracy is no worse than 50 μm;

– Graphitic protective baffles arranged circumferentially inside the vacuum chamber protect the walls of the chamber from the proton radiation damage;

– Management and control over the C-80 is fully computerized.

PNPI Accelerator Department was responsible for the design, 3D calculation, measurements and forming a necessary magnetic field on the full-scale magnet. The problem of purchase of industrially and commercially produced equipment was solved in the framework of the nuclear medicine program of National Research Centre "Kurchatov Institute" in 2010. All cyclotron subsystems have been installed and tested in cooperation with NIIEFA.

The first criticality was gained by C-80 on December 5th, 2014. The beam of accelerated H^--ions was obtained up to the radius of 30 cm with intensity of 30 μA and the energy of 10 MeV, which proves the operation capacity of the cyclotron (Figs. 3–4). The continuation of the experimental work will require the license for the work with C-80 as with the source of ionizing radiation.

The main function of the C-80 cyclotron is the production of generator radioisotopes. For this purpose the RIC project, radioactive isotopes at the C-80 cyclotron, is being implemented on the basement level under the cyclotron. Cyclotron beam can be used as a host for creation of an eye melanoma treatment facility. Radiation resistance testing of the electronic component base (ECB) for aviation and space will be conducted at the C-80 cyclotron as well.

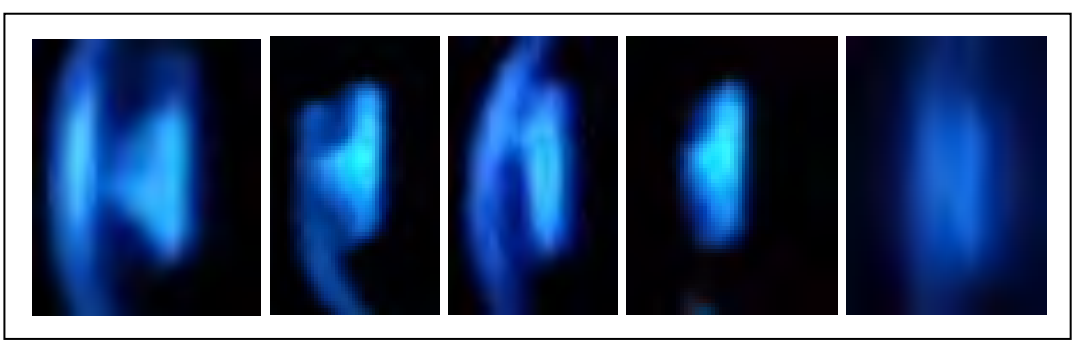

Fig. 4. Images of the beam of H^--ions on the quartz glass inside the chamber, obtained on December 17, 2014


ЛИК

Management and Research

PNPI NRC “Kurchatov Institute” management structure

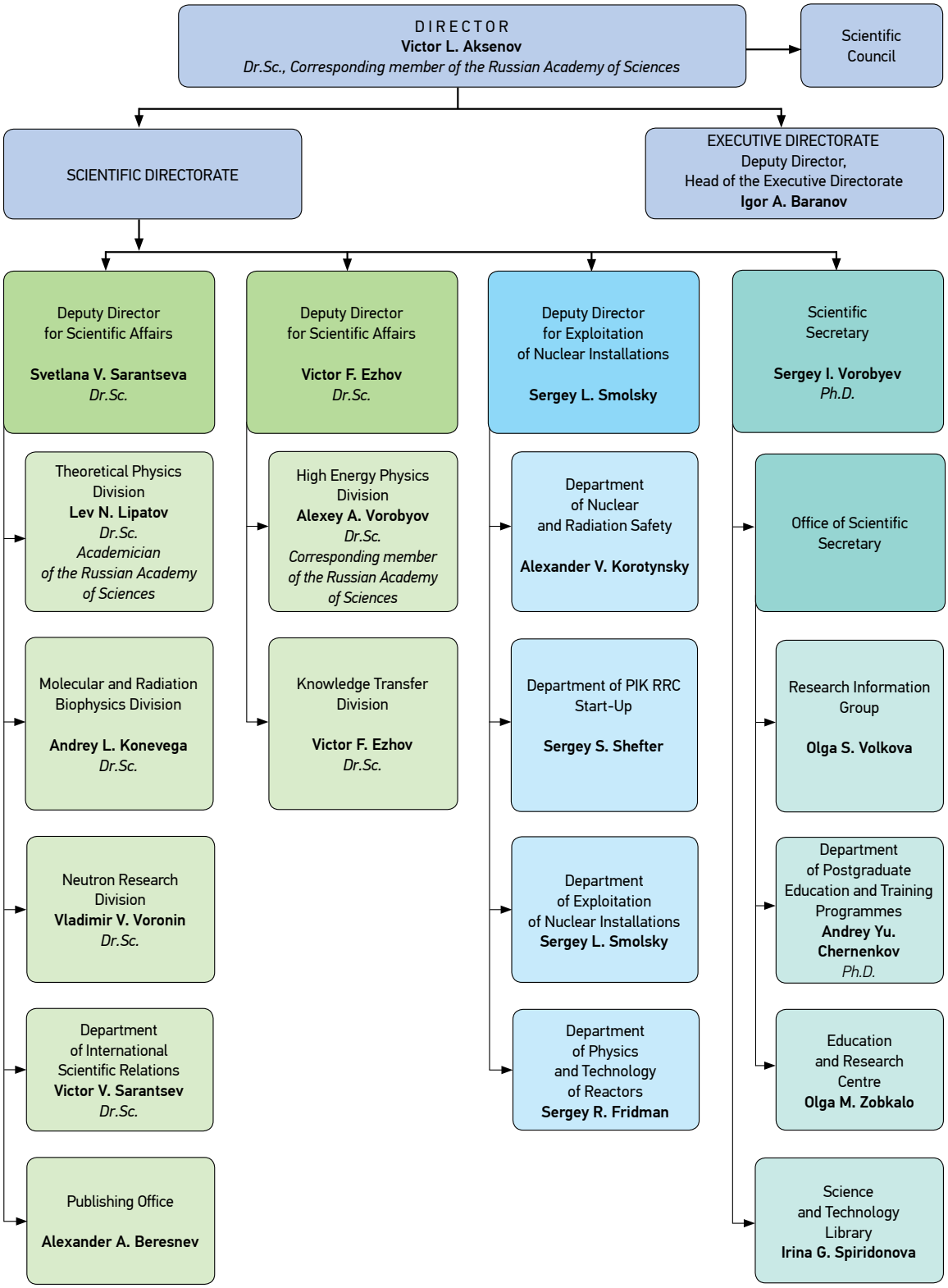

Research results in figures

PNPI NRC “Kurchatov Institute” conducts more than 70 works supported by grants of the Russian Scientific Foundation, the Russian Foundation for Basic Research, grants of the government of the Russian Federation, etc.

Number of grants

Grants	2014
RFBR	56
RSF	5
President of the RF	2
Government of the RF	
Other grants	10

Number of publications

Publications	2014
In russian editions	116
In foreign editions	403
Monographies	2

Eight doctoral theses were defended in 2014.

Patents

In 2014, 13 patents were received including four patents on an invention, six patents on a useful model, and three certificates of the state registration of the computer programme.

Ten patent applications were filed, including one application for the patent on invention, eight applications for the patent on a useful model and one application for the state registration of the computer programme.

Honors and awards

The whole Institute is proud of the works accomplished within the study of the subglacial lake Vostok, which gained interest and support of the Russian Federation. Such interest is proved by the state honors (Order of Honor) awarded to the leaders and participants of the project by the president of the Russian Federation V.V. Putin personally. One of the PNPI employees was honored with such award – deputy director for scientific work, the head of the Knowledge Transfer Division V.F. Ezhov.

In 2014, the administration of the Leningrad region continued to support 15 works, which were earlier honored with awards and scientific scholarships of the governor of the Leningrad region. Three new works have been awarded in 2014:

1. The paper "Chemistry of elements from the island of stability" (Neutron Research Division employee Yu.A. Demidov) was awarded with the Prize of the governor of the Leningrad region of the 1st Order for the best research paper among the young scientists;
2. The work "Aggregation of α-synuclein as a possible molecular link of lysosomal storage disorder and synucleinopathy" (leading researcher S.N. Pchelina, Dr.Sc., Molecular and Radiation Biophysics Division) was awarded with the scientific scholarship;
3. The work "A complex superconformal string and its application to the description of meson spectrum" (junior researcher A.N. Semenova, Theoretical Physics Division) was awarded with the scientific scholarship of the governor of the Leningrad region.

Each year the works of PNPI researchers cover the wider range of research, combining and applying their experience and knowledge in new areas, building innovative solutions for modern scientific and technological challenges. In 2014, the HI-TECH competition considered the work of B.G. Turukhano to be one of such innovative solutions and he was awarded with two silver medals for the best innovative invention. The young PNPI employee O.S. Vityuk has also placed innovations in the centre of his interests – he became a winner of the programme "Member of the Youth Research and Innovation Competition" for 2013–2014.

The photo of B.G. Turukhano

I.S. Dupnitskiy, postgraduate student of the PNPI base department in Saint Petersburg State University (Department of Nuclear Physics Methods of Research) was awarded with the scholarship of the government of the Russian Federation for the works accomplished at PNPI in the framework of his thesis "Behavior of a local magnetism in a structured network of ferromagnetic nano-knots: numerical simulation and experiment".

Science and technology councils (active in 2014)

Advisory bodies of the directorate

	Scientific Council	Presidium of Scientific Council
Chief councilor	V.L. Aksenov	V.L. Aksenov
Deputy chief councilor	S.V. Sarantseva	S.V. Sarantseva
Secretary	I.A. Zobkalo	I.A. Zobkalo
	S&T Council of the Complex of Nuclear Accelerators	S&T Council on Information Technologies
Chief councilor	S.L. Smolsky	V.F. Ezhov
Deputy chief councilor	K.A. Konoplev	Yu.F. Riabov
Deputy chief councilor	A.V. Korotynsky	
Secretary	S.R. Friedmann	S.B. Oleshko
	Editorial Board	Library Board
Chief councilor	V.L. Aksenov	S.V. Sarantseva
Secretary	S.V. Sarantseva	
	Council of Young Scientists and Specialists	Engineering Centre for Technological Re-equipment of Pilot Production
Chief councilor	N.M. Chubova	The conceptual idea of the centre organization is being developed by a specially created working group headed by A.P. Bulkin
Deputy chief councilor	S.I. Vorobyov	
Deputy chief councilor	A.A. Dzuba	
Secretary	O.S. Volkova	

Recommendations of the Science and Education Council under the President of the Russian Federation (V.L. Aksenov is one of its members) and the International Advisory Committee for Photon and Neutron Sciences of NRC "Kurchatov Institute" are taken into account upon the strategic decision making.

The International Advisory Committee for Photon and Neutron Sciences of NRC "Kurchatov Institute"

Co-chairs: The Corresponding member of the Russian Academy of Sciences M.V. Kovalchuk (NRC "Kurchatov Institute"); Professor H. Dosh (DESY, Germany)	
Committee for Photon Sciences	Committee for Neutron Sciences
Francesco Sette (European Synchrotron Radiation Facility, France) Jean Daillant (Synchrotron SOLEIL, France) Miguel Angel García Aranda (ALBA-CELLS synchrotron, Spain) Rafael Abela (Paul Scherrer Institut, Switzerland) Christoph Quitmann (Max IV Laboratory, Sweden) Franz Pfeiffer (Technische Universität München, Germany) Vaclav Holy (Charles University in Prague, Czech Republic) Natalia Novikova (Institute of Crystallography, Russia) Serguei Molodtsov (European XFEL, Russia – Germany) Dmitri Novikov (Deutsches Elektronen-Synchrotron DESY, Russia – Germany) Robert Feidenhans'l (University of Copenhagen, Denmark) Marek Stankiewicz (National Synchrotron Radiation Centre SOLARIS, Poland)	The Chair – Sebastian M. Schmidt (Jülich Forschungzentrum, Germany) The Secretary – Sergey Grigoriev (PNPI NRC "Kurchatov Institute", Russia) Anatoly Balagurov (Joint Institute for Nuclear Research, Russia) Olwyn Byron (University of Glasgow, UK) Andrew Harrison (Diamond Light Source, UK) Valery Nesvizhevsky (L'Institut Laue–Langevin, France) Winfried Petry (Technische Universität München, FRM-II and MLZ, Germany) Dieter Richter (Jülich Forschungzentrum, Germany) Mikhail Rychev (NRC "Kurchatov Institute", Russia) Helmut Schober (L'Institut Laue–Langevin, France) Andreas Schreyer (Helmholtz-Zentrum Geesthacht, Germany) Yaroslav Shtrombakh (NRC "Kurchatov Institute", Russia) James Yeck (European Spallation Source, Sweden) Hartmut Zabel (Ruhr-Universität Bochum, Germany)

Conferences

PNPI NRC "Kurchatov Institute" acts as a host for conferences, lections and workshops within the wide range of its research fields. Leading Russian and foreign research centres are active participants of such events.

In 2014, 15 scientific events were organized with PNPI participation (meetings, conferences and scientific schools). More than 1 500 participants took part in these events including 500 representatives of the world scientific community (from Germany, Sweden, USA, Switzerland, Japan, China, Netherlands, Italy, Belgium, Ireland, etc.)


ПИК
РЕАКТОР

The list of scientific events organized in 2014

1. 48th PNPI Winter School on Nuclear and Particle Physics, Theoretical Physics, Nuclear Reactor Physics, **February 24 – March 1**;
2. PNPI Winter School on Condensed State Physics, **March 10–15**;
3. "Neutron Diffraction" Discussion, **February 20–21**;
4. Discussion session on inelastic neutron scattering "NeRoN-2014", **June 19–20**;
5. International Conference "NanoPiter-2014", **June 21–27**;
6. International Conference "Hadron Structure and QCD: HSQCD'2014", **June 30 – July 4**;
7. Discussion session on Small-Angle Neutron Scattering "Muromets-2014", **September 19–20**;
8. XI International Conference "Quark Confinement and Hadron Spectrum", **September 8–12**;
9. XXIII Session on the use of neutron scattering and synchrotron radiation for condensed matter studies (NSSR-CM -2014), **October 27–31**;
10. Youth conference in the framework of XXIII Session on the use of neutron scattering and synchrotron radiation for condensed matter studies (NSSR-CM -2014), **October 27–31**;
11. International workshop within PolFusion project (polarized fusion), **November**;
12. Seminar in memory of academicians V.F. Nazarenko and V.M. Lobashov, **November 10**;
13. Conference of Young Scientists, PNPI-CYSS-2014, **November 13–14**;
14. Seminar devoted to 50th anniversary of the Radiation and Molecular Biophysics Division, **December 9**;
15. Discussion session "School of Polarized Neutrons in Gatchina" (PN School-2014), **December 22–23**.

In 2014, PNPI employees presented their works and papers at 44 international and 127 national conferences.

Visits

PNPI development is closely connected to the cooperation with other research institutions, organizations and committees. For this purpose, a series of meetings took place in 2014, with PNPI acting both as a guest and as a host.

March 25th. Session of the Board of Directors of Industrial Organizations and Entrepreneurs of Gatchina Region. A central topic of the meeting was the discussion of the concept of "Emperor's Ring" investment project. The aim of the project is to create the first Russian city with postindustrial economy based on the model of the best small historical and innovative centres of the world. The board had also discussed the current issues of the project on creation of North-Western nanotechnological centre in Gatchina in partnership with PNPI.

April 9th. The visit of the current ESS (European Spallation Source) Machine Director, Ferenc Mezei, who held a workshop devoted to the future neutron source and its current state.

May 23rd. The visit of Prof. Jochen Schneider, Director for research of DESY Research Centre. In the framework of this visit, the issues of international expertise of project of PIK RRC experimental stations were discussed.

June 10th. The visit of Alexis Michel, a Councilor for Science of the French Embassy in Russia, which was devoted to the discussion of a possible collaboration of PNPI with research institutions of France.

September 25th. The visit of Tord Ekelöf, Director of Accelerator Development Division of Uppsala University (Sweden), with the proposal of the neutrino long base-line project aimed at detection of failure of combined *SR*-parity in lepton sector and neutrino mass hierarchy.

October 16th. A meeting of Youth Department of Nuclear Society of Russia (YDRNS) with PNPI Council of Young Scientist and Specialists. Participants shared ideas and experience on organization of the work with the youth at the nuclear establishments and research institutes, discussed the possibilities of further cooperation.

More than a dozen meetings with Russian and foreign representatives of science were organized in 2014. Colleagues from JINR, ILL, Rogante Engineering Office, München University of Technology, CERN, University of Groningen, SPbU, Institute of Cytology RAS and other institutions presented their research results to PNPI employees.

Education

Cooperation with the Faculty of Physics, St. Petersburg State University

Dean of SPbU Faculty of Physics, Corresponding member of the Russian Academy of Sciences M.V. Kovalchuk

PNPI NRC "Kurchatov Institute" developed a long-standing close cooperation with one of the leading universities of Russia – St. Petersburg State University (SPbU). SPbU Faculty of Physics plays an important role in this collaboration, being a constant participant of joint scientific events. Postgraduate students of the Faculty conduct research works coordinated by PNPI researchers and PNPI employees hold lections for the students of field specific departments of the Faculty. Thus, the PNPI base department in St. Petersburg State University (Department of Nuclear Physics Methods of Research) trains physicists for research work in neutron and synchrotron centres of Russia and Europe.

Examples of events organized in cooperation with SPbU in 2014 are listed below.

March 19th, Gatchina. The visit of employees and heads of all the degree-granting departments of SPbU Faculty of Physics, heads of the resource centres and students. The guests participated in the overview excursion to the RRC PIK and met PNPI director and heads of divisions.

March 27th, Gatchina. A workshop organized by a postgraduate student of the Quantum Mechanics Department of the Faculty of Physics, TPD employee E.A. Mistonova. The topic of the workshop was "Quantum electrodynamic theory of electron capture by multi-charged ions" (the thesis topic of E.A. Mistonova).

June 10th, Peterhof. Defense of Master theses of the first class of graduates of the PNPI base department – Department of Nuclear Physics Methods of Research (SPbU, Faculty of Physics). Seven Master theses were presented for defense.

October 27–31, Peterhof. The Session on the use of neutron scattering and synchrotron radiation for condensed matter studies (NSSR-CM-2014), a joint scientific event organized by PNPI NRC "Kurchatov Institute", SPbU Faculty of Physics and the Shubnikov Institute of Crystallography of the Russian Academy of Sciences.

Working with schools

With the aim to raise the interest of the youth in the science in general and in gaining a higher education in fields of physics and biology in particular, PNPI is organizing guided excursions to the Institute (in particular, to the accelerator complex, PIK and WWR-M reactor complexes) and takes part in the process of occupational guidance of perspective students.

17 excursions were organized in 2014; more than 360 school children from the following educational institutions took part in these excursions:

- No. 9 Gatchina School of Secondary General Education with advanced studies of specific subjects;
- No. 9 Gatchina School of Secondary General Education;
- SPbU Academic Gymnasium;
- V.G. Khlopin Radium Institute, OJSC;
- K.D. Ushinsky Gymnasium, Gatchina;
- Vyritsa Town School, Gatchina district;
- Kommunar Town School;
- No. 2 Gatchina School of Secondary General Education;
- No. 8 Lyceum, Tikhvin;
- No. 6 Lyceum, Tikhvin.

Excursions were organized not only for school children, but also for veterans, school directors of Gatchina district and the Council of Young Scientists of the Institute of Problems on Atomic Energy Safe Development, the Russian Academy of Sciences.

Among the events aimed at occupational guidance of school children organized by PNPI, the following are the most prominent:

– **Participation in the project "Open Government. Youth Employment Assistance"** (Oreol 47 TV-channel);

– **Participation of the Council of Young Scientists and Specialists in the Career and Recruitment Fair**; 39 schools of secondary general education of Gatchina and Gatchina district took part in this fair;

– **Teaching classes in "Gatchina Evening (Shift-Type) School of Secondary General Education"**.

PNPI employees teach physics, informatics and such elective subjects as "Applied Physics", "Applied Mathematics" and "Research Activity". All elective courses are approved by the Methodology Centre of the Faculty of Natural Sciences and Mathematics of Leningrad Regional Institute of Education Development (LIIRO) and by the Education Committee of Gatchina Municipal District. Extracurricular courses and clubs are organized as well: "The physics experiment", "Preparation to the State Unified Examination in Physics", "3D-simulation", "Web-design", etc. All the courses are included in the curriculum and school schedule. "Scientific Club of Senior School Students" (SCSS) is meeting regularly. It helps the school students to develop their creative potential, to advance the knowledge in specific fields of science, to widen their horizons. "Scientific Fridays" lections are being held in framework of SCSS, which allow school students, teachers and parents to learn about achievements of modern science.

In memory of colleagues deceased in 2014

Gilyari M. Drabkin, Dr.Sc., USSR State Prize winner, passed away on **June 27th**. He was the founder of Soviet–Russian school of polarized neutrons who organized a neutron research on condensed state at PNPI NRC "Kurchatov Institute".

Prof. Boris G. Erozolimsky, Dr.Sc., USSR State Prize winner, senior researcher of the Neutron Research Laboratory of Leningrad Nuclear Physics Institute (1982–1990), passed away on **August 26th**.

Vladimir I. Medvedev, senior researcher of Cryogenic and Superconductive Techniques Laboratory of PNPI High Energy Physics Division, the head of the trade-union committee, passed away on **October 26th**.